Evaluation of brain permeability and neuroprotection of novel 3-hydroxy-4-pyridinone bidentate iron chelators for the treatment of parkinson's disease

Azizi, Juzaili Bin

Awarding institution:
King's College London

EVALUATION OF BRAIN PERMEABILITY AND NEUROPROTECTION OF NOVEL 3-HYDROXY-4-PYRIDINONE BIDENTATE IRON CHELATORS FOR THE TREATMENT OF PARKINSON'S DISEASE

by

JUZAILI AZIZI

A thesis submitted to King's College London for the degree of

Doctor of Philosophy

February 2018

DECLARATION

This thesis submitted for the degree of Ph.D. entitled **"Evaluation of brain permeability and neuroprotection of novel 3-hydroxy-4-pyridinone bidentate iron chelators for the treatment of Parkinson's disease"** is based upon work conducted by the author at the Institute of Pharmaceutical Science, King's college London between January 2013 and May 2017. All the work described herein is original unless otherwise acknowledged in the text or by references. None of the work has been submitted for another degree in this or any other university.

JUZAILI AZIZI

February 2018

TABLE OF CONTENTS

ABSTRACT

Iron has been linked with the neurodegenerative process in Parkinson's disease (PD) as autopsied Parkinsonian showed increases in iron level in the brain, especially in the basal ganglia. Treatment with the blood-brain barrier (BBB) permeable iron chelator, deferiprone (CP20) shows improvement in motor symptoms among PD patients possibly by neuroprotective mechanism. However, serious side effects such as agranulocytosis and neutrocytopenia limit its use especially for the elderly PD patients that are more prone such toxicity. A series of CP20 derivatives with chiral functional group have been developed by chemical modification and showed better toxicity profiles than CP20 when tested in rodents. However, the structural modifications of CP20 might change their brain permeability profile and reduce their effectiveness as neuroprotective agents. For this reason, the aim of the studies reported in this thesis was to investigate the brain permeability of CP20 derivatives by *in situ* brain perfusion. In addition, a CP20 derivative that is conjugated with glucose was also investigated as a strategy to improve BBB permeation. This was followed by investigation of the neuroprotective capability on dopaminergic cell death in *in vitro* and in *vivo* models of cell death in PD. The effect of functional group chirality on the biological experiments were also evaluated.

Seven out of eight of the CP20 derivatives tested showed successful brain penetration as assessed by *in situ* brain perfusion. From these seven brain penetrant CP20 derivatives, one (CP84) show superior brain uptake, three CN128, CN226 and CN228) showed comparable brain uptake, and three (CN116, CN118 and CN126) showed lower brain uptake than CP20. Glucose conjugated CP20 derivative failed to cross the BBB. The *in vitro* neuroprotection study in SH-SY5Y neuroblastoma cells revealed neuroprotective effect of the brain penetrant CP20 derivatives against H_2O_{2-}, 6-OHDA-, and FeNTA- but not MG-132-induced cell death. Some of the CP20 derivatives showed better neuroprotection at equimolar concentration of CP20. In both studies, molecules chirality did not have effect on *in situ* brain permeability or *in vitro* neuroprotection. One CP20 derivative (CN128) was selected for *in vivo* neuroprotection study with 6-OHDA rat model of PD. CN128 showed comparable neuroprotection of dopaminergic neurons in the nigro-striatal dopamine pathway. In conclusion, these studies showed that all but the glucose-conjugated derivative of CP20 can permeate the BBB and are neuroprotective in

experimental models of PD suggesting these novel iron chelators may be used as potential neuroprotective agent in the treatment of PD.

LIST OF FIGURES

LIST OF TABLES

LIST OF ABBREVIATIONS

^{3}H-OMG	^{3}H-O-methyl-D-glucose
6-OHDA	6-hydroxydopamine
ATP	Adenosine triphosphate
BBB	Blood-brain barrier
BCEC	Brain capillary endothelial cells
BCH	2-amino-2-norbornanecarboxylic
BSA	Bovine serum albumin
cLogP	Lipophilicity
CNS	Central nervous system
CP20	Deferiprone
CSF	Cerebrospinal fluid
DFO	Deferrioxamine
DFX	Deferasirox
DNA	Deoxyribonucleic acid
DOPAC	3,4-dihydroxyphenylacetic acid
DPM	Disintegration per minute
ETC	Electron-transport chain
Fe^{2+}	Ferrous iron
Fe^{3+}	Ferric ion
FeNTA	Ferric nitrolotriacetoacetate
GLUT1	Glucose transporter 1
GLUTs	Glucose transporters
GSH	Glutathione
HEPES	4-(2-hydroxyethyl)-1-piperazineethanesulfonic acid
HPLC	High performance liquid chromatography
HPO	3-hydroxy-4-pyridinone
HVA	Homovanilic acid
i.p.	Intraperitoneal
ID	Internal diameter
ISF	Interstitial fluid
LAT1	Large neutral amino acid transporter 1

LB	Lewy bodies
LIP	Labile iron pool
LPS	Lipopolysaccharide
LSS	Liquid scintillation spectroscopy
MAO-B	Monoamine-oxidase B
MPTP	1-methyl-4-phenyl-1,2,3,6- tetrahydropyridine
mRNA	Messenger RNA
mtDNA	Mitochondrial DNA
MTT	3-(4,5-dimethylthiazol-2-yl)-2,5-diphenyltetrazolium
NMDA	N-methyl-D-aspartate
NRS	Normal Ringer's solution
OD	Outer diameter
PCO_2	CO_2 partial pressure
PD	Parkinson's disease
PE	Polyethylene
$p\mathrm{Fe}^3$	Iron affinity constant
P-gp	P-glycoprotein
PhyBS	Physiological buffer solution
PO_2	O_2 partial pressure
PTFE	Polytetrafluoroethylene
RBC	Red blood cells
ROS	Reactive oxygen species
SNPc	Substantia nigra *pars compacta*
TFA	Trifluoroacetic acid
UPS	Ubiquitin proteasome system

LIST OF CONTRIBUTIONS

KCL IPS Postgraduate Research Symposium	Poster	London, UK	May 2014
4th UK and Ireland Blood-Brain Barrier Symposium	Oral	London, UK	November 2014
KCL IPS Postgraduate Research Symposium	Oral	London, UK	May 2015
American Association of Pharmaceutical Scientists (AAPS) Annual Meeting and Exposition	Poster	Florida, USA	October 2015

ACKNOWLEDGEMENT

With boundless love and appreciation, I would like to extend my heartfelt gratitude and appreciation to the people who help me bring this study into reality. I would like to extend my profound gratitude to the following: My supervisors, Dr Sarah Salvage, Dr Jane Preston and Dr David Begley whom expertise, consistent guidance, ample time spent and consistent advices that help me bring this study into success. I would also like to express my appreciation to Professor Robert Hider to provide the compounds for this study and for technical advices. My deepest gratitude and appreciation to Dr Atsuko Hikima for her invaluable advice, support and assistance in the laboratory.

To my best friend, Awis Sabere, who have been by my side through thick and thin of my PhD journey. Without his moral support, this journey would be harder to traverse. Not to forget my PhD friends: Asyura Amdan, Fauzi Jalil, Goh Choon Fu, Hazeeq Azman Muzamir Mahat and Norzawani Buang whom have been facing the same hurdle. The journey felt livelier when surrounding with friends whom understand your struggles. My utmost gratitude to Louis Porta, whom allows me to stay in his flat in the last year of my PhD and helping me with the proof-reading of the thesis. To my past and present colleagues whom have been helping me with my study, especially Ana Georgian, Dominika Klisko, Ferdinand Fuchs, Jaewon Lee and Louise Lincoln.

Finally, my greatest gratitude and love to my family especially my father, the late Azizi Buyong and my mother, Khadijah Elias for their love, support and encouragement. This project was supported financially by The Ministry of Higher Education Malaysia and Universiti Sains Malaysia (USM) Penang, for which I am indebted.

CHAPTER 1

GENERAL INTRODUCTION

1 General Introduction

1.1 *Parkinson's disease (PD)*

Parkinson's disease (PD) is the second most common neurodegenerative disease after Alzheimer's disease which affects 1% of the population over 60 years of age and the incidence increases with age (de Lau and Breteler, 2006). The disease is characterised by progressive cardinal motor symptom which include bradykinesia, rigidity, resting tremor, gait dysfunction and postural instability (Jankovic, 2008). Non-motor symptoms can also occur including depression, anxiety, autonomic dysfunction, cognitive impairment, and sleep disturbance (Jankovic, 2008). With increasing life expectancy, it is estimated that the world-wide population of PD patients will double by 2050 (Schapira and Jenner, 2011). Current therapy focuses on symptomatic management of the motor symptoms, however, there is currently no available treatment to prevent the progress of the disease, and this remains a serious unmet clinical need.

1.1.1 *Aetiology of PD*

PD is a multifactorial neurodegenerative disease that involves genetic, environmental or combination of both factors in inducing cell death (Warner and Schapira, 2003). Extensive years of research has unveiled mutated genes and environmental toxins that could cause PD. Familial-type of PD which involves genetic mutations only account for less than 10% of PD cases and is normally characterised by early age of onset (<40 years old) (Gasser, 2009). The rest of the reported cases of PD is sporadic without definite causes (>90%) which usually affect population of age more than 40 years old (de Lau and Breteler, 2006). The cases of sporadic PD also corroborate the theory that aging as an important risk factor in developing PD (Zhang et al., 2000).

Although familial-type of PD only accounts for less than 10% of PD population, the discovery of mutated-genes identified by genetic linkage analysis and genome wide association studies is an important breakthrough and provide explanation of the molecular mechanism underlying the pathogenesis of PD (Klein and Westenberger, 2012). These genes express proteins that are involved in cell regulation and protection which include protein degradation, antioxidant and mitochondria homeostasis. To date, 28 genes associated with PD have been identified with five of them are the most studied (Lin and

Farrer, 2014, Pankratz and Foroud, 2007). These genes are *SNCA* (encode for α-synuclein), *LRRK2* (encode for leucine-rich repeat kinase-2), *parkin* (encode for parkin), *PINK1* (encode for phosphatise and tensin homologue induced putative kinase-1) and *DJ-1* (encode for DJ-1).

SNCA is the first PD-associated gene that was identified in 'Contursi kindred' of Italian descent (Golbe et al., 1999). Mutation in this gene lead to accumulation and aggregation of fibrillar α-synuclein as a major component of LB, a signature and a post-mortem diagnostic criterion for familial and sporadic PD (Chai and Lim, 2013). Remarkably, cytosolic dopamine can form an adduct with α-synuclein protofibril, stabilise it and inhibit conversion to α-synuclein fibril (Conway et al., 2001). Although this may seem as neuroprotective, the dopamine-α-synuclein protofibril adduct is capable of disrupting the cellular membrane by forming pore-like structure which might suggest the selective dopaminergic neuron loss in PD (Tosatto et al., 2012). This finding also provides the role of α-synuclein not only in familial-PD, but also in sporadic-PD.

Mutation in *LRRK2* is the most common cause of familial PD in the world characterised by hyper-phosphorylation activity of mutated LRRK2, a tyrosine kinase like protein (Chai and Lim, 2013). Elevated phosphorylation of LRKK2 substrates which include MAP kinase and peroxiredoxin underlies the pathogenesis of LRRK2 mutation (Boon et al., 2014).

Parkin function as E3 ligase associated with the ubiquitin-proteasome system which degrades unwanted proteins (Riley et al., 2013). Mice expressing mutant parkin and parkin knock-out mice have been shown to exhibit features of PD pathology and symptom such as mitochondrial dysfunction, age-dependent hypokinetic motor deficits and dopaminergic neuron degeneration (Lu et al., 2009, Palacino et al., 2004).

PINK-1 mutations are prevalent in PD patients of Asian descent by 20-fold than European descent (Kilarski et al., 2012). This gene encodes for mitochondrial membrane-bound serine/threonine kinase that involves in the recruitments of protein for mitophagy (Zhou et al., 2008). Study of PD-related PINK-1 mutant expressed in human neuroblastoma cell line revealed dysfunction of mitophagy as the cause of apoptosis while overexpression of wild-type PINK-1 was found to be neuroprotective (Petit et al., 2005).

DJ1 encodes for peroxiredoxin-like peroxidase that is localised in mitochondria and capable to scavenge mitochondrial H_2O_2 (Andres-Mateos et al., 2007). Base on the fact that DJ1 protein involve as a mitochondrial antioxidant, it can be deduced that mutation of DJ*1* could predispose dopaminergic neurons to oxidative stress, consistent with finding observed in MPTP treated DJ1-deficient mice (Kim et al., 2005).

Although genetic mutations have contributed greatly to the understanding of pathogenesis of PD, they do not explain most sporadic PD cases. Therefore, some suggest that environmental agents are the main causal factor, and this is supported with the following evidence. The notion that environmental toxins could induce PD come from the observation of four young drug abusers that developed chronic Parkinsonism. This chronic Parkinsonism was later revealed to be cause by the contamination with the meperidine analogue, 1-methyl-4-phenyl-1,2,3,6- tetrahydropyridine (MPTP) after using illicit drugs intravenously. The ability of MPTP to induce neurochemical, pathological and clinical features of PD suggest that other toxins could also induce PD (Dick et al., 2007). Indeed, epidemiological studies reveal the positive correlation between exposure to pesticides with developing PD (Gorell et al., 1998, Petrovitch et al., 2002, Semchuk et al., 1992). This has been confirmed in the laboratory whereby injection of pesticides such as rotenone and paraquat into rodents induce loss of nigral dopaminergic neurons (Greenamyre et al., 2003, Peng et al., 2004). Consumption of well water by rural population associated with agricultural industry have also been linked to an increased risk of PD (Gatto et al., 2009, Priyadarshi et al., 2001). The involvement of metals in the aetiology of PD has been demonstrated from epidemiological studies. It is evident that people chronically exposed to welding manganese fumes exhibited PD-like clinical features (Jankovic, 2008). Indeed, metals such as iron and copper has been reported to accumulate within the SNPc of autopsied Parkinsonian brain. These metals contribute to the production of H_2O_2 during the non-enzymatic oxidation of dopamine and the conversion of H_2O_2 to $OH^{\bullet -}$ by Fenton reaction (Dexter et al., 1989, Earle, 1968). Based on the epidemiological data, there is a clear link between environmental factors with PD. Nevertheless, some people may be more prone to developing PD when expose to toxins than the other. This might suggest that both genetics and environmental factors could be the plausible explanation for idiopathic PD. Although the causal factors are still not fully understood, PD has well defined pathological features that is discussed next.

1.1.2 *Pathology of PD*

Two important pathological features characterise PD in autopsied brains namely the loss of dopaminergic neurons within SNPc and accumulation of intracellular inclusions within the cell body of surviving neurons termed as Lewy bodies (LBs) (Antony et al., 2013).

Loss of dopaminergic neurons within SNPc occurs progressively without causing the cardinal motor symptoms of PD until approximately 50% of nigral dopaminergic cell bodies have degenerated and about 70% of striatal dopamine content has depleted (Cheng et al., 2010, Delaville et al., 2011). This is because, normal function of nigro-striatal pathway in controlling voluntary movement is maintain by compensatory mechanisms which include increase dopamine turnover and increase in post-synaptic dopamine D_2 receptors in the striatum (Navntoft and Dreyer, 2016). In addition to the loss of nigral dopaminergic neurons that defines the motor symptom in PD, loss of noradrenaline neurones in locus coeruleus (LC), serotonin neurones in the dorsal raphe nuclei (RN) and cholinergic neurones in nucleus basalis of Meynert (NBM) which causes non-motor symptoms to occur (Ferrer, 2011, Olanow et al., 2009a). Non-motor symptoms associated with neurodegeneration in these areas include anxiety and depression that are related to the loss of noradrenergic and serotonergic neurons while dementia is linked to the degeneration of the cholinergic neurons (Calabresi et al., 2006, Hanagasi and Emre, 2005). Neuron loss is also found in areas some distance from SNPc such as the olfactory system, the dorsal motor nucleus of the vagus (DMNV) and the peripheral nervous system (PNS) although to a lesser extent (Visanji et al., 2013).

The second pathological feature of PD is the accumulation of globular LBs in surviving neurons within SNPc (Antony et al., 2013). LBs are eosinophilic proteinaceous cytoplasmic inclusions mainly compose of α-synuclein aggregates as well as ubiquitin, neurofilaments and parkin (Wakabayashi et al., 2013). Besides SNPc, LBs are also found in other brain areas that experience degeneration (Braak et al., 2003, Olanow and Prusiner, 2009b). The role of LBs in pathology of PD is remained elusive. LBs are initially thought to be toxic to the neurons since they are related to neuronal loss (Wakabayashi et al., 2006). However, later discoveries suggest that α-synuclein oligomers and protofibrils are cytotoxic, while the formation of fibrillar LBs containing α-synuclein aggregates may be cytoprotective (Wakabayashi et al., 2013). Therefore, although LBs may serve as the pathological marker of PD, it does not necessarily indicate that the

inclusions are the cause of cell death. Nevertheless, LBs are clearly associated with the progressive cell death in the basal ganglia. Having said this, the mechanism of cell death in PD brain is described in the following section.

1.1.3 *Cell death mechanism in PD*

Neurodegeneration in PD started with neuronal cell death. There are two type of neuronal cell death mechanism namely apoptosis and necrosis that are mainly differentiate by their morphology (Nikoletopoulou et al., 2013). Cells undergo apoptosis morphologically exhibit shrinkage, chromatin and cytoplasmic condensation**,** nuclear fragmentation and budding of the plasma membrane forming smaller apoptotic bodies (Elmore, 2007). Membrane-bound apoptotic bodies are destructed by controlled phagocytosis which does not induce inflammatory reaction. Changes in cell morphologies and cell destruction are regulated genetically by pro-apoptotic molecules such as caspases which requires ATP-dependent steps for activation (Tsujimoto, 1997, Zamaraeva et al., 2005). On the contrary, cells undergo necrosis show extensive cytoplasmic vacuolisation and swelling. Cell are destructed by spontaneous ruptures of cell membrane and releases of cell's content that initiate inflammatory response (Nikoletopoulou et al., 2013). Necrosis is a passive form of cell death which does not require ATP and occurs in response to toxic insults or spontaneous insults such as stroke or trauma (Stoica and Faden, 2010).

Evidence from *in vitro* and *in vivo* studies, as well as post-mortem on Parkinsonian brains lean towards apoptosis as the primary mechanism of cell death in PD. However, necrosis is also suggested as a possible mechanism of cell death although there has not been sufficient evidence supporting this view (Jellinger, 2000). *In vitro* studies using primary rat ventral mesencephalic cultures, and rat pheochromocytoma PC-12 and SH-SY5Y cell lines expose to MPP^+, the toxic metabolite of MPTP, induce morphological and biochemical hallmarks of apoptosis (Walkinshaw and Waters, 1994, Blum et al., 1997, Lotharius et al., 1999, Viswanath et al., 2001). Similarly, dopamine and 6-OHDA also induces morphological and biochemical changes in PC12 cell line with characteristics of that apoptosis. The protection conferred by overexpression of antiapoptotic protein Bcl-2 and pre-treatment with caspase in this toxins-induced cell death further support apoptosis as the chief mechanism of cell death (Offen et al., 1997, Takai et al., 1998).

In addition to the *in vitro* studies, data from *in vivo* PD models strongly suggest the involvement of apoptosis in dopaminergic cell death in SNPc. Mice treated with MPTP exhibits increased number of apoptotic markers such as DNA fragmentation, caspases and JNK activation, and upregulation of bax mRNA (Saporito et al., 2000, Tatton and Kish, 1997, Vila et al., 2001). Inhibition of caspase-3 substrate and JNK ablation of the pro-apoptotic Bax gene as well as overexpression of Bcl-2 protein appears to be protective against MPTP-induced cell death in mice (Wang et al., 2004, Cosi et al., 1996, Vila et al., 2001, Offen et al., 1997, Yang et al., 1998). Likewise, studies from 6-OHDA-lesioned rats also display a typical morphology of cells undergoing apoptosis in basal ganglia which was confirmed by terminal deoxynucleotidyl transferase-mediated dUTP nick-end labelling (TUNEL) staining (He et al., 2000, Marti et al., 2002). Interestingly, the dose of 6-OHDA use to induce lesion seem to determine the preferred cell death pathway, where high concentration of 6-OHDA exclusively causes cell necrosis (Jeon et al., 1995). This support the theory that cells can decide which appropriate route of cell death mechanism depending on the specific situation (Nikoletopoulou et al., 2013).

Finally, evidence from autopsies performed on brain tissue of PD patients reveal the presence of apoptotic neurons in SNPc, morphologically characterised by chromatin condensation, cell shrinkage and DNA fragmentation in dying neurones (Mochizuki et al., 1996, Anglade et al., 1997, Tatton et al., 1998). In addition to the well-defined morphology characteristics of apoptosis, molecular markers of apoptosis such as Bax and caspase-3 have been reported to increase (Anglade et al., 1997, Tatton, 2000, Hartmann, 2004). Besides apoptosis, the presence of necrotic neurons was also evidence in the post-mortem brain suggesting involvement of more than one type of cell death mechanism in PD brain (Anglade et al., 1997).

To conclude, evidence from *in vitro* and *in vivo* studies as well as from brain autopsies support apoptosis as the primary mechanism of cell death neuronal degeneration of PD, although necrosis could also occur depending on the specific situation. The exact cause of apoptosis in PD brain is remain elusive but oxidative stress, mitochondrial dysfunction, ubiquitin proteasome system impairment and inflammation might partly contribute to the process.

1.1.4 *Pathogenesis of cell death in PD*

Many factors are implicated in the neuronal cell death cascade observed in PD. The initiator of the cascade is unknown, but they are deleterious and potential targets for disease-modifying agents. For this reason, it is essential to fully understand the mechanisms associated with cell death. These mechanisms described in detail below include the dysfunctions in the protein degradation systems: oxidative stress, mitochondrial dysfunction, ubiquitin proteasome system impairment and inflammation.

a) Oxidative stress

Oxidative stress is defined as the imbalance between reactive oxygen species (ROS) production and endogenous anti-oxidant systems. ROS such as superoxide anions (O_2^-), hydrogen peroxide (H_2O_2), hydroxyl radicals ($OH^{\bullet -}$) and peroxy radicals (O_2^{-2}) are continuously produce as by-products of the of mitochondrial electron-transport chain (ETC). Under normal physiological condition, ROS participates in the immunity and autophagy processes in cells (Sena and Chandel, 2012). A defence mechanism consisting of enzymes such as superoxide dismutase (SOD), catalase, glutathione (GSH) and glutathione proxidae (GPx) convert these radicals into harmless molecules (Turrens, 2003). Excessive ROS production causes oxidation of cellular macromolecules such as proteins, DNA and lipids which results in their damage and loss of membrane integrity (Popa-Wagner et al., 2013). Remarkably, aging process appears to increase the incidence of oxidative stress as shown by elevated level of oxidised proteins (carboxyls and nitro-protein adducts), DNA (8-Hydroxy-2-guanosine) and lipid (4-hydroxynonenal and malondialdehyde) in PD brain suggesting age as one of the risk factor in neurodegeneration process (Mariani et al., 2005, Dexter et al., 1994, Cardoso et al., 2005).

Abnormal activity of antioxidant defence mechanism such as GSH appears to play a role in precipitating oxidative stress in PD. Evidence from post mortem brain of PD patients showed simultaneous increased level of SOD but reduced levels of GSH within the SNPc suggesting accumulation of H_2O_2 due to inability of GPx to reduce H_2O_2 to H_2O (Jenner and Olanow, 1996, Sian et al., 1994, Sofic et al., 1992, Perry and Yong, 1986). Similarly, the reduction of GSH levels was also seen in the autopsied brain of incidental Lewy body disease (ILBD) patients which are considered to represent the early-stage PD, thus suggesting oxidative stress might occur earlier before PD develop (DelleDonne et al.,

2008). Increase ROS production due to abnormal antidefense mechanism impaired Complex I of ETC due to thiol oxidation of critical residues (Genestra, 2007). Conversely, impairment of Complex I by neurotoxins such as rotenone also reduce GSH production by inhibition of glutathione reductase also by thiol oxidation (Chinta and Andersen, 2008, Li et al., 2003). Either way, this imbalance results in mitochondrial dysfunction and eventually cell death (Dias et al., 2013).

Dopaminergic neurons in the basal ganglia are inherently prone to oxidative stress due to the nature of dopamine metabolism in generating ROS. Spontaneous auto-oxidation of dopamine creates O_2^-, H_2O_2 and reactive quinone (Izumi et al., 2005). Additionally, enzymatic conversion of dopamine to 3,4-dihydroxyphenylacetic acid (DOPAC) and homovanilic acid (HVA) by monoamine-oxidase B (MAO-B) generates H_2O_2 (Meiser et al., 2013). Nevertheless, dopamine metabolism alone cannot explain neurodegeneration in PD since other non-dopaminergic neurons in brain also undergo degeneration (Braak et al., 2003). Increase of iron as well as decrease iron storage protein, ferritin level seen in basal ganglia exacerbates oxidative stress by undergo Fenton reaction with H_2O_2 generates highly reactive $OH^{\bullet-}$ (Dexter et al., 1987, Dexter et al., 1989, Sofic et al., 1992, Sofic et al., 1988).

b) Mitochondrial dysfunction

Mitochondria serve the role as the energy factory for cells by producing the adenosine triphosphate (ATP) molecules, the primary energy source that facilitates many of the energy-dependent biochemical reactions within cells. Accumulating lines of evidence has shown abnormalities of the mitochondrial respiratory chain in PD. Production of ATP involves series of electrons transport and oxidative phosphorylation through Complex I-IV of mitochondrial ETC, which finally end up with reduction of O_2 to H_2O. Impairment of electrons transfer along ETC such as inhibition of Complex I by environmental toxins MPP^+ and rotenone cause oxidative stress due to increase of electrons leakage and deficiency in ATP production (Keane et al., 2011, Betarbet et al., 2000). Indeed, early evidence of mitochondrial dysfunction in PD come from investigation of drug users and farmers inflicted with MPP^+ and rotenone toxicity respectively. Besides increase in ROS production, inhibition or impairment of mitochondrial ETC causes inability of Na^+/K^+ ATPase pumps to maintain membrane potential due to inadequate ATP production

(Sherer et al., 2003). This lead to partial depolarisation of neurons and increase sensitivity of excitatory N-methyl-D-aspartate (NMDA) receptor to glutamate resulting in excitotoxicity by accumulation of intracellular Ca^{2+}. Furthermore, firing of glutamate from subthalamic nucleus to SNPc in PD further exacerbate the condition and lead to cell death (Keane et al., 2011).

Reduction in activity and reduce amount of mitochondrial Complex I in the SNPc and frontal cortex of autopsied PD patient brain have been reported (Mizuno et al., 1989, Schapira et al., 1990). Interestingly, mitochondria isolated from PD patients' platelet also showed a reduction in Complex I activity. Formation of cybrid cell line containing the isolated mitochondria was more prone to MPP^+-induced cell loss suggesting a widespread pathology of mitochondrial dysfunction (Schapira et al., 1990, Parker et al., 2008). Indeed, genetic factors may contribute to the impairment of mitochondrial function as exemplified by increased levels of mitochondrial DNA (mtDNA) deletions in the striatum of PD patients (Ikebe et al., 1990)

Studies on transgenic mouse model further support the role play by genetic factors such as gene mutations in mitochondrial dysfunction. Evidence from mitochondrial transcription factor (Tfam) knock-out mouse reveal progressive degeneration of dopaminergic neurons and progressive motor deficits (Ekstrand et al., 2007). Gene mutation in PINK1 that encodes for mitochondrial membrane kinase is associated with autosomal recessive forms of PD (Gandhi et al., 2006). This is supported by PINK1 knock-out mice that exhibit impairment in dopamine release mitochondrial respiration, as well as increased sensitivity to oxidative stress (Gautier et al., 2008, Kitada et al., 2007).

c) Ubiquitin proteasome system (UPS) impairment

The ubiquitin proteasome system (UPS) is an ATP-dependant protein degradation pathways for unwanted intracellular proteins that are misfolded, mutated and damaged to smaller peptides. Degradation of unwanted proteins is important for maintaining cell homeostasis (Wang and Maldonado, 2006). Additionally, UPS is involved in the regulation of many cellular processes such as cell cycle and division, development and differentiation, apoptosis, cell trafficking and morphogenesis of neuronal networks

(Ciechanover, 1998). Besides protein, UPS also play a role in degradation of defective mitochondria.

The mechanism of protein degradation by UPS involve two separate but related components. Protein for degradation is firstly marked with ubiquitin (Ub) with a series of Ub activating, conjugating and ligating enzymes (Glickman and Ciechanover, 2002). Poly-ubiquited protein is a substrate for multisubunit tubular proteasome, the second components of UPS that function to digest the tagged protein into smaller peptides. Poly-ubiquitination only serve to mark unwanted protein for recognition by proteasome, that is later release into cytoplasm and hydrolysed to ubiquitin monomers (Gong and Leznik, 2007). Therefore, dysfunction of the UPS including poly-ubiquitin hydrolysis are implicated in degeneration of dopaminergic neurons in PD.

Defect in one or both components of UPS machinery lead to accumulation of tagged and un-tagged unwanted proteins that are toxic to the cells by forming insoluble aggregates. Indeed, fail in UPS system might be related to the presence of inclusion body such as LBs that contain ubiquitinated α-synuclein (McNaught et al., 2004, McNaught et al., 2002a, Olanow et al., 2004). This hypothesis is confirmed in *in vitro* studies whereby inhibition of UPS with inhibitors such epoxomicin and lactacystin in neuronal cells result in accumulation of ubiquitinated proteins. Additionally, this cell exhibit increases in inflammatory markers such as cyclooxygenase-2 (COX_2) and prostaglandin-E_2 (PGE_2) (Rockwell et al., 2000), that activate cell death mechanism (McNaught et al., 2002b). Similar observation is replicated in *in vivo* study in which case administration of N-benzyloxy-carbonyl-Ile-Glu(*O*-t-butyl)-Ala-leucinal (PSI) and epoxomicin to rodents caused nigrostriatal degeneration with simultaneous formation of LB inclusions consisting of ubiquitin and α- synuclein (McNaught et al., 2004, Zeng et al., 2006, Bukhatwa et al., 2009)

Mutation of genes that encodes for component in UPS system also play a role in impairment of protein degradation. Mutation in parkin and UCHL1 genes that encode for ubiquitin ligase and ubiquitin hydrolase cause familial forms of PD (Cordato and Chan, 2004). In addition, UPS activity appears to decrease in autopsied brain of sporadic PD patients which may suggest contribution of environmental factors in UPS dysfunction (McNaught and Jenner, 2000, McNaught et al., 2003).

To conclude, impairment of UPS by proteasomes inhibitors and gene mutations that encode for UPS components promote the accumulation of misfolded or damaged proteins, as well as the formation of Lbs. This evidence supports the role of UPS impairment in the pathogenesis of dopaminergic cell death in PD.

d) Inflammation

Evidence from post mortem brain of PD patient reveal increase level of inflammatory markers and mediators in SNPc as assessed by immunohistochemical technique. The type of inflammatory markers and mediators present at raised levels include interleukin-1β (IL-1β), interleukin-6 (IL-6), tumour necrosis factor-α (TNFα), interferon-γ (IFNγ) and prostaglandin-E_2 (PGE_2) (Wu et al., 2008, Teismann and Schulz, 2004, Long-Smith et al., 2009, Hirsch and Hunot, 2009). The presence of raised inflammatory markers are not restricted in brain parenchyma, but also in cerebrospinal fluid (CSF) of PD patients suggesting that this could serve as a biomarker as part of diagnosis of PD (Dobbs et al., 1999, Nagatsu et al., 2000). Additionally, there is a consistent and substantial increase in the number of activated resident immune cells of the brain in the SN of post-mortem PD brains when compared to control which suggest their involvement in neuroinflammatory-induced nigrostriatal dopamine neurone degeneration (Wu et al., 2002).

Studies in animal model of PD involving inflammation has given more insight into the involvement of microglia in PD brain. Lipopolysaccharide (LPS), a pro-inflammatory endotoxin from Gram-negative bacteria induce inflammation by interacting with Toll-like receptor 4 (TLR-4) expressed on cell surface (Pålsson-McDermott and O'Neill, 2004). Injection of this endotoxin into rodents SNPc lead to dopaminergic cell death through the reaction with inflammatory insults. The inflammation response to LPS is mediated by microglia, a resident macrophage in the CNS because neurons do not express TLR-4 (Liu and Bing, 2011, Castano et al., 1998). The mechanism of inflammation generated by microglia upon LPS exposure is unclear, but is thought to involve increase production of pro-inflammatory cytokines (TNF-α, IL-1β, IL-2 and IL-6), proteinases, eicosanoids and nitric oxide (NO) to the site of injection that is toxic to the cells and promote persistent degeneration (Knott et al., 2000, Czlonkowska et al., 2002, Zhang et al., 2005, Beal, 2003, Long-Smith et al., 2009). For example, inhibition of inducible NO synthase (iNOS) activity in microglia attenuate LPS induce inflammation in rats (Iravani et al., 2005, Iravani et al.,

2002, Dutta et al., 2008, Arimoto and Bing, 2003). This is because, excessive NO is capable to react with superoxide radicals to produce highly reactive peroxynitrite radicals, which damage cellular proteins and DNA by forming adducts with them (Hald and Lotharius, 2005). To summarise, post mortem on human brain and studies on animal model of PD support the damaging role of glial cell in mediating inflammation that lead to dopaminergic cell death in SNPc.

1.1.5 *Irons and their role in PD*

Excessive iron accumulation by two-fold of age-matched normal brain, has been observed within the SNPc of Parkinsonian brain (Sofic et al., 1988, Dexter et al., 1987). Although iron does accumulate progressively in SNPc as people aged, this iron is tightly regulated by intracellular iron storage protein, ferritin and therefore confer little or no toxicity (Daugherty and Raz, 2015, Zecca et al., 2004). The reason why SNPc is prone to iron accumulation remain unclear. Dopamine oxidation product (neuromelanin) (Zecca et al., 2001), neuroinflammation (Ward et al., 2009, Frank-Cannon et al., 2009), changes in BBB permeability (Mills et al., 2010, Gerlach et al., 2006) and malfunction of iron homeostasis (Mills et al., 2010) have all been proposed to be the contributing factors. The toxicity of iron in PD is central on the ability of iron to undergo Fenton reaction with H_2O_2 to produce $OH^{\bullet -}$, the most harmful ROS because of its high reactivity with biomolecules such as protein, lipid and DNA (Sharma et al., 2012). Unlike O_2^- and H_2O_2 that are converted to O_2 and H_2O by antioxidant enzymes (catalase, glutathione peroxidase and superoxide dismutase), no enzymes exist to scavenge $OH^{\bullet -}$ (Rosario de la Torre et al., 1996). Therefore, excess accumulation of $OH^{\bullet -}$ due to iron-catalyse Fenton reaction causes cellular death (Pinto et al., 2003). The excessive production of $OH^{\bullet -}$ could contribute to the pathogenesis of PD by causing sequence of pathogenic events such as oxidative stress, mitochondrial dysfunction, ubiquitin proteasome system (UPS) impairment and inflammation as described in **Section 1.1.4** (Mounsey and Teismann, 2012). For example, oxidative stress confers by excessive $OH^{\bullet -}$ production through iron-catalysed Fenton reaction may cause mitochondrial membrane oxidation. This leads to mitochondrial dysfunction and reduction of ATP synthesis. This would implicate cellular protein degradation that requires energy in the form of ATP causing UPS impairment and followed by cell death (Mounsey and Teismann, 2012).

1.1.6 *Iron chelators*

Intracellularly iron is stored by sequestering into ferritin (Ponka et al., 1998). Ferritin is an oligomeric protein composed of an apoprotein shell of 24 subunits that forms a hollow protein shell which capable of storing up to 4500 iron atoms (Pan et al., 2009). The 24 subunits are heteropolymers of light (L) and heavy (H) chain subunits. Both H and L subunits cooperate for the iron mineral core formation (Sammarco et al., 2008, Boyd et al., 1985). The H subunit of ferritin has ferroxidase activity for oxidation of Fe^{2+} to Fe^{3+} as iron is internalised and packed into the ferritin mineral core. On the other hand, L subunits enhance oxidation activity by increasing the binding affinity of ferric iron at the nucleation sites of the iron core (Levi and Rovida, 2015, Pfaffen et al., 2013). Not all intracellular iron is stored within ferritin. About 5% of intracellular iron is available in cytoplasm and form a complex with various population of ligands such as glutathione, ascorbate and citrate. Iron bound to these ligands is not properly co-ordinated and therefore is redox active. This chelatable intracellular redox-active iron complex is widely known as the cellular labile iron pool (LIP) (Kruszewski, 2003, Kakhlon and Cabantchik, 2002, Cabantchik, 2014). LIP play an important role as an immediate transitory pool for the biosynthesis of iron-associated protein such as mitochondrial iron-sulfur-cluster and metalloenzymes (Cabantchik, 2014). The level of LIP is normally under tight control because non-coordinated free iron can generate oxygen derived free radicals and render tissue damage as in extreme cases of iron overload (Halliwell and Gutteridge, 1984). However, in extreme cases of iron overload, the changes might exceed the cell homeostatic capacity, thus compromising its integrity. In this situation, the oxidative stress impose by excessive LIP could be minimise by administration of iron chelators (Glickstein et al., 2005, Kakhlon and Cabantchik, 2002).

Iron chelators are primarily indicated for the treatment of systemic iron-overload as seen in Thalassemia patient due to chronic blood transfusion (Saliba et al., 2015, Cianciulli, 2008). Introduction of the first iron chelators in the market in 1960 significantly improve the quality of life and life expectancy of Thalassemia patients (Chaston and Richardson, 2003). Before the first iron chelation therapy is available, most chronically transfused patients died in their teens and twenties due to toxicity associated with iron overload (Sheth, 2014, Poggiali et al., 2012). Since the first introduction of iron chelators for clinical use, researchers have successfully developed much better iron chelators molecules that use in clinics. Nowadays, there are three options for iron chelation therapy available for

the treatment of iron overload which is discussed below (Poggiali et al., 2012, Sheth, 2014).

a) Deferrioxamine (DFO)

Deferrioxamine (DFO, Desferal®) is a microbial siderophore derived from *Streptomyces pilosus* and show selectivity towards ferric ion (Fe^{3+}) (Zhou et al., 2012). DFO has high iron affinity constant (pFe^{3+}=26.6) and chelates iron in a hexadentate fashion [FeIII$(DFO)_1^{+1}$ iron complex]. Ferrioxamine, the 1:1 iron complex of DFO has net positive charge (+1) and does not permeate plasma membrane due to its low lipophilicity ($logD_{7.4}$ = -2). DFO enter the liver via carrier-mediated transport and interacts with both hepatocelluar and reticuloendothelial iron stores which later promote both biliary and urinary iron excretion (Hershko, 1978). DFO is a complex molecule and therefore has a large molecular weight (560 Da) which render it orally inactive due to limited gastrointestinal tract permeability. DFO is the first authorised iron chelator for the treatment of iron overload in Thalassemia patient in 1960. It is developed and marketed by Ciba-Geigy and has been extensively use in the clinics before the emergence of orally active iron chelators (Bernhardt, 2007). Due to lack of oral permeability, DFO is administered by intravenous or subcutaneous routes. Unfortunately, DFO has an extremely short half-life in the plasma (~10 minutes) due to extensive metabolism and rapid renal clearance. Because of this, DFO is continuously infuse systematically for 8-12h per day, 5-7 days per week at a standard dose of 40 mg/kg/day to achieve body iron homeostasis. Some major side effects that are associated with DFO infusion are depletion of body iron stores, neurotoxicity and abnormalities of cartilage formation (Porter et al., 1989). Because of its administration route, longer treatment time, high cost and severe side effects patient compliance is often poor (Porter et al., 1989).

b) Deferasirox (DFX)

Deferasirox (DFX, Exjade®, ICL670) is a triazole iron chelator. DFX prefer trivalent ion such as Fe^{3+} over divalent ions. DFX has pFe^{3+} that is comparable to deferoxamine (22.5) and chelates iron in a tridentate fashion [FeIII$(DFX)_2]^{3-}$ iron complex]. The 1:2 iron complex of DFX has a net -3 charge under physiological condition and can permeates plasma membranes easily due to its high lipophilicity ($logD_{7.4}$ = 1.0) (Zhou et al., 2012). The low molecular weight of DFX (373 Da) facilitates its absorption from the gastrointestinal tract

which makes it orally active. Indeed, DFX is the second orally active iron chelator use in the clinic for removal of excessive iron accumulation in Thalassemia patient due to routine blood transfusions and the first orally active iron chelators approved worldwide. DFX promotes iron excretion approximately four to five times more effective than DFO in hypertransfused rat model. Furthermore, the pattern of iron excretion produced by DFX is distinct from DFO. A substantial proportion of DFO-chelated iron derived from reticuloendothelial (RE) cells is excreted in the urine. On the other hand, DFX-chelated iron excretion is limited to the bile regardless of whether it is derived from RE or hepatocellular stores (Hershko et al., 2001). DFX was approved for human use in 2005 by FDA and marketed by Novartis (Zhou et al., 2012). DFX has long plasma half-life upon oral consumption and therefore is taken only once daily. DFX has been demonstrated to be efficient in removing liver iron from regularly transfused patients but appear to be less effective in removing cardiac iron (Wood et al., 2010, Cappellini et al., 2010). High lipophilicity of DFX contributes to great affinity towards plasma albumin (>98%) and therefore is less toxic by limiting its distribution to peripheral tissues (Weiss et al., 2006). Kidney toxicity is the prevalent side effect of this chelator (Rafat et al., 2009).

c) Deferiprone (CP20)

Deferiprone (CP20) is 1, 2-dimethyl derivative of 3-hydroxypyridin-4-ones (HPOs) iron chelator. HPOs like CP20 prefer trivalent ions such as Fe^{3+} and not physiologically important divalent ions such as Zn^{2+}, Cu^{2+}, Mn^{2+} and Co^{2+} (Hider et al., 2000). However, although CP20 shows very high affinity towards Fe^{3+}, it still can bind to Fe^{2+} under aerobic conditions and autoxidise them to Fe^{3+} (Harris, 1977). CP20 has pFe^{3+} that is comparable to deferoxamine (20.5) and chelates iron in a bidentate fashion [$FeIII(CP20)_3$ iron complex]. In contrast to ferrioxamine, the 1:3 iron complex of CP20 is neutral in charge and therefore can permeate plasma membrane to removes potentially toxic iron such as in iron-loaded liver, cardiac and brain tissues (Hider et al., 2000, Jamuar and Lai, 2012). CP20 is relatively hydrophilic ($LogD_{7.4}$=-0.77) in comparison to DFO and DFX. The low molecular weight of CP20 (139 Da) facilitates its absorption from the gastrointestinal tract which makes it orally active. Indeed, CP20 is the first orally active iron chelator use in the clinic for removal of excessive iron accumulation in Thalassemia patient due to routine blood transfusions. CP20 was authorised to enter the European Union and Canadian markets by European Medicines in 2002 and was approved by the FDA in 2011. It is

marketed by Apotex Inc. Toronto, Canada as Ferriprox™ (Zhou et al., 2012). Despite all the advantages, CP20 suffered from extensive glucuronidation at the 3-hydroxyl in the liver after oral consumption, and therefore has lower bioavailability and short half-life (3-4 hours) in the plasma. Because of this, large dose of CP20 is required to achieve body iron homeostasis which is 75 mg/kg/day. Consequently, some major side effects are associated with the use of CP20 which includes musculoskeletal and joint pains, neutropenia, agranulocytosis and gastric intolerance (Fisher et al., 2013, Kontoghiorghes, 1995, Hoffbrand, 2005, Hoffbrand et al., 2003).

1.1.7 *Novel HPO iron chelators as potential treatment for PD*

One noticeable effect of CP20 is the improvement of motor symptom and slower disease progression in Parkinson's disease (PD) patients (Devos et al., 2014, Abbruzzese et al., 2011). It is established that interruption of iron homeostasis in the basal ganglia of PD patients contribute to the progression of the disease (Griffiths et al., 1999, Hopes et al., 2012, Hopes et al., 2016). Indeed, iron dysregulation in the substantia nigra is hypothesised to be the primary or secondary factor that initiate or exacerbate the death of dopaminergic neurons in this brain region (Liddell, 2015, Munoz et al., 2016, Urrutia et al., 2014). This is because, iron-binding protein such as transferrin and ferritin cannot keep up with the excess influx of iron into the mitochondrial matrix and therefore increase the reduction-oxidation (redox) reaction of ferrous iron (Fe^{2+}) with hydrogen peroxide (H_2O_2) which is abundant in mitochondria as a by-product of oxidative respiration (Kudin et al., 2004). The redox reaction coined as Fenton reaction produce the mischievous hydroxyl radicals ($OH^{\bullet-}$) that initiate the chain of radical reaction which ultimately lead to cell death (Liddell, 2015, Munoz et al., 2016, Urrutia et al., 2014)

This positive effect of CP20 in PD patients undoubtedly due to the ability of CP20 to enter the brain via passive membrane diffusion in addition to their ability to chelate labile iron in brain (Glickstein et al., 2005, Hider et al., 2011a). In fact, CP20 has been reported to not only chelate excess iron in the brain region, the CP20-iron complex formed in the brain was also able to permeate out and redistribute iron the circulated transferrin in plasma (Evans et al., 2012, Abbruzzese et al., 2011, Ayton et al., 2016, Cabantchik et al., 2013). Furthermore, CP20 at the dose indicated for PD patients did not interfere with normal systemic iron balance (Abbruzzese et al., 2011, Ayton et al., 2016, Cabantchik et al., 2013).

However, CP20 suffered from extensive first-pass metabolism in the liver on its 3-hydroxyl (3-OH) group to glucuronidation (45% in rat and 85% in man) lead to a very low bioavalaibility in plasma upon oral dosing (Singh et al., 1992). The 3-OH group on the HPO molecule is important for the iron chelation activity of CP20, therefore extensive glucuronidation at this site render it inactive **Figure 1.1.1** (Hider, 2014).

a) **b)**

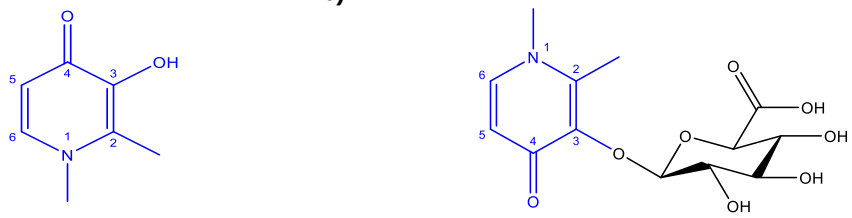

Figure 1.1.1: a) CP20 molecular structure with oxygen ligand (3-OH) available to form bond with iron b) CP20 glucuronide structure which is pharmacologically inactive.

Thus, very large and frequent oral doses (75 mg/kg daily) was needed to keep the iron-overload patients in the negative-iron state albeit CP20 route of administration was more feasible than desferioxamine. Although the aim of treatment with CP20 in PD patients was slightly different and therefore lower dosage was indicated (30 mg/kg daily), it was still considered as high (Devos et al., 2014, Abbruzzese et al., 2011). Moreover, due to the prevalence of PD in the elderly, the high and frequent doses are inconvenience, and this contribute to the low compliance among patients, and thus reducing the success rate of the treatment (Hirsch et al., 2016).

Concerted efforts have been taken to minimise or eliminate the metabolism of CP20 by modification of CP20 structure. The approached involved the functionalisation of the pyridinone ring with bulkier alkyl side chains with the aims to hinder or limit the access of drug metabolising enzymes active site to the labile 3-OH group (Li et al., 2015, Novakovic et al., 2004). One of the molecules, CP94 showed a promising result in rats with lower glucuronidation at the 3-OH side (Porter et al., 1990). Unfortunately, the result did not translate into man where 85% of the administrated dose was recovered in the urine as a 3-OH glucuronide metabolite (Porter et al., 1993, Porter et al., 1994). Another promising molecule, CP40 and CP41 were synthesised by adding OH functional group to N1 (Hider and Liu, 2003). However, this approach cause reduction in lipophilicity, and thus contribute

to lower absorption from GIT and possibly not efficient to get into the brain (Fredenburg et al., 1996, Singh et al., 1996).

Recently, a range of novel HPO iron chelators were synthesised by alteration of CP20 structure by adding substituent at the N1 and/or C2 of HPO ring in the Professor Robert C. Hider laboratory at King's College London in collaboration with Zhejiang University China (Hider et al., 2011a). The HPO were designed to minimise the glucuronidation reaction by adding chiral alkyl substituent containing -OH functional group at N1. The strategy to add substituent containing -OH with chiral centre to the N1 is due to the observation that drug metabolising enzymes are stereo-specific in which one strereosiomer would be more susceptible to metabolism than the other (Molenda et al., 1994, Nguyen et al., 2006). In contrast to CP40 and CP41, this structural modification did not lead to lower lipophilicity, but rather increase in lipophilicity due to additional alkyl group. At the same time, the modification of the structure does not cause signification alteration of the ferric ion (Fe^{3+}) affinity constant, pFe^{3+} compared to CP20. Therefore, it was expected to be more efficacious than CP20 in removing iron upon oral dosing at the same dose. Indeed, a preliminary study with rats has showed increased bioavailability and efficacy of these compounds to remove excess iron compared to CP20 due to reduction in the first-pass metabolism upon oral dosing (Lu, 2016, Hider et al., 2011a).

Remarkably, the lethal dose for these novel iron chelators obtained from acute toxicities study performed on mice were found to be higher than CP20 (Hider et al., 2011a). This also negates the claimed of Kontoghiorghes et al. (1993) that increasing HPO lipophilicity lowered the LD_{50}. These findings lead to the potential development of these set of compounds as a clinical drug better than CP20. Moreover, higher efficacy means lower doses and frequency are required to give to patients, therefore increase patients' compliance and saving cost. As mentioned earlier, CP20 has been demonstrated to improved symptoms in PD patient. Therefore, one potential future application of this new set of compounds is for the treatment of PD that is better than CP20 in term of efficacy for chelating iron, high in potency and possibly fewer side effects. Theoretically, in order for a drug to elicit it effect in the brain, it must able to cross the blood-brain barrier (BBB) (Abbott et al., 2010).

1.1.8 *The blood-brain barrier (BBB)*

The brain is the integration centre of communicating neurons that make up the nervous system (Abbott et al., 2010, Bundgaard and Abbott, 2008b). The nature of neuronal communications via ion propagation along the axons is achieve by differences in ionic concentration between interstitial fluid and intracellular fluid which warrant a delicate control (Kress and Mennerick, 2009, Holcman and Yuste, 2015). Disturbance with the ionic balance between interstitial fluid and intracellular fluid is therefore catastrophic as it affects the body universally. To prevent this to happen, the brain is protected with three levels of protective barrier which are arachnoid membrane-cerebrospinal fluid barrier (ACSFB), blood-cerebrospinal fluid barrier (BCSFB) and blood-brain barrier (BBB) (Abbott et al., 2010, Liddelow, 2011, Abbott, 2005, Engelhardt and Sorokin, 2009). ACSFB and BCSFB barrier sites are located at the level of the epithelial cells that make up the arachnoid membrane and choroid plexus. On the other hand, BBB barrier site is at the level of endothelial cells brain capillary that make up brain capillary. These sites share the same characteristics such as complex tight junctions that seal the paracellular route and expression of transporters to transport nutrients, electrolytes and metabolites into or out of the brain (Luissint et al., 2012, Tietz and Engelhardt, 2015, Upadhyay, 2014b, Abbott et al., 2010).

Although these three levels of protective barrier share the same characteristics as mentioned, the degree of the restrictiveness was different. BBB showed the most restrictive barrier with transendothelial resistance (TEER) reaching up to 2000 Ω.cm *in vivo* (Wong et al., 2013, Wang et al., 2017, Srinivasan et al., 2015). TEER is a measure of differences in electrolytes concentration between blood and interstitial fluid (ISF) which indicates the junction tightness in allowing electrolytes movements between compartment. In perspective, peripheral TEER is just below 10 Ω.cm. On the other hand, TEER for A-CSFB and CP-CSFB are less than BBB but higher than the peripheral epithelial membrane (Srinivasan et al., 2015). The variation of barrier restriction with BBB at the level of brain capillary endothelial cells (BCEC) having the highest restriction is an evolutionary process that mainly to protect the brain parenchyma from the fluctuation of electrolytes in brain ISF as explained earlier (Bundgaard and Abbott, 2008a, Mayer et al., 2009).

The brain arteries on the surface of meningeal layer penetrate deeper brain tissue and braches into smaller capillaries (Cipolla, 2009). The capillary branches are so extensive

with a surface area of 15 m^2 per kg brain (Pardridge, 2002b, Hitchcock and Pennington, 2006). One capillary branch at least serves 1 neuron with proximity between capillaries and neuron is 8-13 µm (Cipolla, 2009). In addition to that, 30% of systemic blood perfused to the brain despite its weight being just 0.02% of the weight in 70 kg man (Cipolla, 2009). To put this in perspective, the liver, which is 0.07% of body weight, receives only 5% of systemic blood (Abbott et al., 2010). The total length of brain capillaries is 450 km (Cipolla, 2009). The extensive blood perfusion into the brain reflect it high metabolic demand for nutrients suited with the active physiological functions in integrating the neuronal communications (Raichle and Gusnard, 2002, Bélanger et al., 2011, Mergenthaler et al., 2013). At the same time, the compensatory mechanism to maintain ISF homeostasis such as active efflux pump requiring energy. Therefore, it is understood why brain need a huge blood perfusion to get the nutrients it needs for neurons and for maintaining the barrier functions.

Taking into account the total length of brain capillaries, and the fact that a large proportion of circulating blood is directed to these blood vessels, and that the BBB has a large surface area and is at close proximity to the individual neurons, there is significant interest in developing CNS drugs that have improved BBB penetration (Hitchcock and Pennington, 2006). Since BBB equipped with multitude transporters and receptors with overlap specificity for micro- and macromolecules, this can be an advantage to manipulate the transport systems into transporting CNS-active drug (Pardridge, 2005, Pulicherla and Verma, 2015, Banks, 2016, Pardridge, 2002a, Upadhyay, 2014a). The research into circumventing BBB by various approach has become an area of active research (Papademetriou and Porter, 2015, Hendricks et al., 2015, Misra et al., 2003). This is because, up to 90% of CNS-drug in the initial stage of development failed to get into the brain despite showing promising pharmacological effect in *in vitro* studies (Misra et al., 2003, Pardridge, 2005, Basavaraj and Betageri, 2014). If this could be rectified earlier during the drug discovery and development process, other approach can be taken for example by converted into prodrugs, encapsulation with nanoparticles or changing the drug molecular structure. This can save the cost later when it reaches the pre-clinical stage (Papademetriou and Porter, 2015, Hendricks et al., 2015, Misra et al., 2003).

1.1.9 *Overcoming the BBB*

The major problem that hinders delivery of drug molecules to brain is the presence of the BBB which limit the movement of water and lipid soluble molecules from blood to brain. Therefore, molecules that are targeted against diseases in the CNS must be effectively passing the BBB to reach the brain via the blood compartment. Paracellular diffusion is a non-saturable and noncompetitive movement of molecules such as water between cells (O'Donnell and Maddrell, 1983, Pantzar et al., 2006). However, it is absence at the BBB, due to the presence of complex tight junctions. The following briefly described the available transport mechanism for molecules brain uptake:

- Passive membrane diffusion is a non-saturable and noncompetitive movement across cells that utilise by lipophilic molecules such as ethanol.

- Carrier-mediated transporters are expressed on BCEC to facilitate the entry of essential polar metabolites, such as glucose and amino acids due to the tightness of brain endothelial cells (Begley and Brightman, 2003). The expression of these carriers is often polarized which mean they are co-localized on both the luminal and abluminal membranes of the brain capillary endothelium to optimize substrates transport into the brain (Begley, 2004). Carrier-mediated transport utilise membrane protein carriers that recognise specific solute molecule. Solute like glucose bind to carrier triggers a conformational change of the carrier; which results in uptake (Egleton and Davis, 2005).

- Endocytosis can be isolated into bulk-phase (pinocytosis) endocytosis and mediated endocytosis (receptor and absorptive mediated) (Pardridge, 2005). Pinocytosis is the noncompetitive, non-saturable, temperature and energy dependent non-specific uptake of extracellular fluids. It occurs to a very limited degree in the endothelial cells of the cerebral microvasculature (Pardridge, 1995). Receptor-mediated endocytosis provides a means for selective uptake of high molecular weight molecules by specific type receptors present on the luminal membrane (Nicholson and Sykova, 1998). Cells have different receptors for the uptake of many different types of ligands, including hormones, growth factors, enzymes, and plasma proteins (Pardridge, 2007, Duffy et al., 1988). Absorptive-mediated endocytosis is triggered by an electrostatic interaction between a

positively charged substance (charge moiety of a peptide) and the negatively charged plasma membrane surface such as glycocalyx. It has a lower affinity and higher capacity than receptor-mediated endocytosis (Bickel et al., 2001).

Multiple strategies have been reported to overcome the BBB for successful brain uptake such as direct injection of drugs into the CNS (intrathecal), nanoparticle carrier systems for large drug delivery, and chemical modification of drugs to improve small drug delivery (Pardridge, 2005, Pulicherla and Verma, 2015, Banks, 2016, Pardridge, 2002a, Upadhyay, 2014a). One of the best strategies for improving brain uptake for low molecular weight molecule such as CP20 (139.1 Da) is by alteration of the chemical structure to increase the lipophilicity, so that its propensity to cross the brain via passive membrane diffusion would also increase. Alternatively, CP20 attaches with endogenous substrate for carrier-mediated transporter such as glucose or amino acid is also possible.

a) Passive membrane diffusion

Passive membrane diffusion at BBB is driven by the gradient between the extracellular and intracellular concentration of molecules (Avdeef, 2011, Sugano et al., 2010, Avdeef, 2001). The ability of small molecules to permeate through the membrane lipid bilayer is governed by their physicochemical properties such as lipophilicity, polarity and size. (Lipinski et al., 2001) had proposed a range of optimum physicochemical properties termed the 'Rule of Five' as guidelines for discovery and development of drug-like molecules. A molecule is more likely to be successfully developing into drug if it has the following properties namely a molecular weight smaller than 500 Da, a lipophilicity (logP) smaller than 5, 5 or fewer hydrogen bond donors and 10 or fewer hydrogen bond acceptors (Lipinski et al., 2001, Lipinski et al., 1997).

Molecular weight smaller than 500 Da: Large molecules that have a cross sectional area (CSA) more than 80A is energetically unfavourable due to the need to displace large number of lipid molecules in the biological membrane (Fischer et al., 1998). Indeed, the diffusion of molecules across biological membrane is inversely related with their CSA. Since CSA need to be determined experimentally or using specific software for estimation, approximation to molecular weight is often use due to ease of getting the value by a simple calculation. It has been estimated that molecular weight between 300 to 400Da

correspond to be around 80A (Fischer et al., 1998, Pardridge, 2003). This mark the rationale of the maximum limit of molecular weight for drug-like molecules as suggested by Lipinski et al. (2001).

Lipophilicity (logP) smaller than 5: A good balance between solubility in water or lipid is paramount in development of drug-like molecules. Due to the nature of biological membranes which compose of lipid bilayer, molecules with low lipophilicity would have low level of partition into the membrane and therefore slow down the diffusion processes (Smith et al., 2014, Tsinman et al., 2011). Conversely, highly lipophilic molecules would have difficulty to dissolve in aqueous media and may precipitate out from the solution. Furthermore, lipophilic molecules tend to trap within the biological membrane and thus would not reach the target site across the cell membranes. The systemic distribution of lipophilic molecules would also be limited due to their high affinity toward plasma protein especially albumin (Smith et al., 2014, Tsinman et al., 2011, Lipinski et al., 2001).

Polarity (5 or fewer hydrogen bond donors and 10 or fewer hydrogen bond acceptors): The sums of the surface of all polar atoms in a molecule dictate the overall polarity of a molecule. Hydrogen bond donor (HBD) and acceptor (HBA) play an important role in determining the overall polarity. High polarity would increase molecules solubility in water but solubility in lipid would be limited, and vice versa. Therefore, it is suggested that the cut off point for polarity would be 5 or fewer HBD and 10 or fewer HBA (Lipinski et al., 2001).

The ‘Rule of Five Guidelines’ is originally devise to assist in the discovery and development of drug-like molecules that would be likely to permeate gastrointestinal tract (GIT) after oral administration (Lipinski et al., 2001). However, due to it is the first comprehensive guidelines in the field pharmaceutical research, it is also widely used as a guide for discovery of new molecules intended for BBB permeation with some success (Pajouhesh and Lenz, 2005, Banks, 2009). However, the lipid composition and packing in the plasma membrane in addition to expression of multitudes of transport mechanism at BBB call for more stringent guidelines for drug-like molecules targeting the brain. The modification of Lipinski rule of 5 with more stringent parameters has been devised by Hitchcock and Pennington (2006), **Table 1.1.1**.

Table 1.1.1: Physicochemical property ranges. Suggested for increased CNS permeability.

Property	(Lipinski et al., 2001)	(Hitchcock and Pennington, 2006)
MW	≤500	<500
LogP	≤5	2-5
HBA	≤10	-
HBD	≤5	<3
TPSA	-	<90

Alkylated HPO uptake into the brain by membrane diffusion has been shown to increase as the alkyl group is getting longer, due to increase in lipophilicity. By contrast, addition of hydroxyl group into HPO molecules lower the lipophilicity and their entry into the brain is almost entirely abolished in comparison to their non-hydroxylated derivatives (Habgood et al., 1999). Nevertheless, it is important to highlight that breaking one of the suggested cut-offs point in these guidelines would not necessarily lead to unsuccessful brain permeation by passive membrane diffusion.

b) Transporter systems

Due to the presence of complex tight junction that form continuous belt along the perimeter of BCEC, the paracellular diffusion of small molecules through the intercellular space is completely absent. Furthermore, passive membrane diffusion for hydrophilic molecules is very limited due to the lipidic nature of biological membranes. Because of these reasons, multitude of different transport systems are expressed at the BBB to assist with nutrients uptake and metabolites removal (carrier-mediated uptake). Additionally, a specific transport system with broad substrate specificity is aimed for preventing the entry of xenobiotics, toxins and potentially harmful molecules into the brain (efflux pump) (Zlokovic, 2008, Abbott et al., 2010, Pardridge, 2012). Utilization of these carrier systems expressed at the BBB might be an attractive strategy for improve delivery of therapeutics such as iron chelators that would otherwise have minimal access to the CNS (Pardridge, 2012, Lee et al., 2001, Qin et al., 2010).

Carrier mediated transport (CMT). The brain requires many hydrophilic biomolecules as nutrients to support normal biochemical and physiological functions. Access of these molecules to the brain from blood circulation via paracellular route are completely absent,

and therefore is entirely rely on carrier-mediated transport. BBB express many specialise carriers to transport these biomolecules which include glucose, amino acids, nucleotides and choline (Lee et al., 2001, Pardridge, 2012, Abbott et al., 2010). Mechanisms of CMT could be passive (uniporter) or secondary-active (symporter and antiporter). Many drugs are known to take the advantage of these CMT to get into the brain. These include L-DOPA, valproic acid, gabapentin, lidocaine and morphine glucuronide (Begley, 2004, Tamai and Tsuji, 2000, Anderson, 1996).

One of the CMT at BBB that has successfully been employed for drug delivery is the large neutral amino acid transporter 1 (LAT1). LAT1 is an amino acid exchanger (antiporter) expressed on the apical (blood side) and basolateral (brain side) of BCEC. This transporter recognises and transport for large L-α-amino acids such as tyrosine, phenylalanine and leucine (Ylikangas et al., 2014, Pavan et al., 2008, Abbott et al., 2010). Similarly, drugs that are transported by LAT1 such as L-DOPA (Gomes and Soares-da-Silva, 1999), melphalan (Cornford et al., 1992) and 4-chlorokynurenine (Hokari et al., 1996) are L-α-amino acids derivatives which resembles their natural substrates. On the contrary, gabapentin does not show structural similarity with L-α-amino, however, its cyclic structure and restricted conformation bring the amino and carboxy groups in close proximity allowing recognition and transport by LAT1 (Pardridge, 2012). Other CMTs have also been suggested as facilitators of brain-directed drug delivery (Pardridge, 2012, Begley, 2004, Tamai and Tsuji, 2000, DiNunzio and Williams, 2008). A good example in this respect is the glucose transporters (GLUTs) at BBB. Because brain neurons are unable to synthesize or store glucose, they are fully dependent on glucose transport across the BBB, which is facilitated by glucose transporters. In mammalian brain, GLUT1 and GLUT3 are the predominant GLUTs responsible for glucose transport (McEwen and Reagan, 2004). GLUT1 is highly expressed in the brain capillary endothelial cells and is responsible for transporting glucose from blood into the extracellular space of the brain (Qutub and Hunt, 2005). GLUT3 is the major neuronal GLUT and helps transport glucose from the extracellular space into the neurons (Dwyer et al., 2002). In addition, GLUT2 is expressed in astrocytes of the brain. The GLUT1 is located in the membrane of brain capillary endothelial cells composing the BBB (Choeiri et al., 2002). Furthermore, the glucose consumption of the brain amounts to about 30% of the total body glucose consumption (Dick et al., 1984). This high level of cerebral glucose uptake suggests that the facilitative transporter by GLUTs might be a useful carrier for efficient and selective glucose-targeted

drug delivery to the brain. Glucose analogues are theoretically good candidates for drug transport through the BBB (Qin et al., 2010).

Currently, there are no available clinical drugs that target GLUT transporter at BBB. The idea of conjugating CNS-targeted drugs with glucose is based on the observation that GLUT1 transporters are highly expressed on brain capillary endothelial cells, increasing the chances of glucose-conjugated drugs to cross the BBB via GLUT1 transporters. However, due to the widespread expression of other isoforms of GLUTs, severe side effects might arise since the glucose-conjugated drugs can be distributed all over the body. Potential side effects can be minimised when GLUT1 is selected as a targeted transporter, taking advantage of different regulation of GLUT1 in comparison with other GLUTs. GLUT1 is a non-insulin dependent glucose transporter in which it is continuously expressed on brain capillary endothelial cell membrane regardless of the blood insulin level (Gould and Holman, 1993). Other types of GLUTs are transiently stored in cytoplasmic vesicles and expressed only on cell membrane upon rising of blood insulin level after food intake. Therefore, side effects could be set to minimum if glucose-conjugated drugs are taken during low blood insulin level for example in between meals or patients required to fast prior to drugs intake (Calvaresi and Hergenrother, 2013). In previous studies, different glycoconjugates used as candidates for the treatment of CNS diseases have been synthesized, which could increase the BBB permeability by carrier-mediated transport, such as 7-chlorokynurenic acid (Bonina et al., 2000b), dopamine (Francesco et al., 2003), glycosyl derivatives of ibuprofen (Chen et al., 2009).

Efflux-pump. BBB is armed with efflux pumps to export potentially toxic molecules out from the brain. Efflux pump exclusively requires ATP regardless of the concentration gradient of the molecules between extracellular (blood) and intracellular (cytoplasm) space. Notable examples of efflux pumps that are express at BBB are P-glycoprotein (P-gp), breast cancer resistance protein (BCRP) and the multidrug resistance-associated proteins (MRP) (DiNunzio and Williams, 2008, Löscher and Potschka, 2005). These efflux pumps have broad substrate specificity but they share one common characteristic, that is lipophilic molecules as their primary substrates (Rautio et al., 2008a, Jong and Huang, 2005). Therefore, although having the range of optimum lipophilicity for drug molecules appear to be important for passive membrane diffusion at BBB, it does not confirm successful brain penetration. Co-administration of drug molecule that is a substrate for

efflux-pump with efflux pump inhibitor have been shown to effective to increase brain uptake in *in vitro* and *in vivo* model (Hoosain et al., 2015, Amin, 2013). However, translation into the clinic was unsuccessful due to the effective dose for efflux-pump inhibitor to allow brain penetration of efflux-pump substrate, is associated with toxicity (Amin, 2013). Recognising contribution of efflux pumps in brain uptake at the early stage of drug discovery and development is important to avoid failure or inefficient brain permeability in the later clinical stage. Clinical example of drug that has low brain permeability due to efflux pump is the antiretroviral, zidovudine for AIDS treatment (Pan et al., 2007, Ene et al., 2011, Fox et al., 2002). Although zidovudine helps to slow down HIV replication and thus delay disease progression, it does not effectively reduce neurological symptoms associated with HIV virus. It was later found out that zidovudine is a substrate for BCRP efflux pump that was discovered in 1998 (Pan et al., 2008, Ni et al., 2010).

Having said this, increase in lipophilicity of the novel CP20 derivatives with chiral substituent containing -OH functional group (cLogP=-0.496 to 1.130) may increase brain uptake compare to CP20 (cLogP=-0.903) as described in **Section 1.1.7**. However, this may at the same time increase the potential of the compounds to be a substrate for efflux pumps which counteract the increase partition in cell membrane (Banks, 2009). Additionally, conjugating CP20 derivatives with molecules that are known to be carried by specific transporters at BBB may also be one of the strategy to circumvent BBB. The glucose conjugated compound was very likely to exhibit increase brain uptake due to possible interaction of glucose moiety with GLUT that facilitated uptake into the brain (Rautio et al., 2008b, Devraj et al., 2011).

1.2 *General hypothesis and aims*

Accumulating evidence has shown that loss of dopaminergic neurones in the substantia nigra *pars compacta* in Parkinson's disease (PD) patients are exacerbated by the presence of excess iron which contribute to the generation of reactive oxygen species (ROS), leading to oxidative stress and eventually, cell death (Mochizuki and Yasuda, 2012, Ayton et al., 2014).

Deferiprone (CP20) is the only orally active 3-hydroxy-4-pyridinone (HPO) iron chelator used in clinic, mainly to treat Thalassemia, sickle cell anaemia and Friedrich's ataxia.

CP20 crosses the blood-brain barrier (BBB), and is effective in improving motor symptoms in PD patients (Mounsey and Teismann, 2012, Abbruzzese et al., 2011). However, high dose of CP20 need to be administered due to low oral bioavailability as a result of extensive glucuronidation in the liver (Singh et al., 1992). Additionally, CP20 can cause severe side effects due to the iron chelation property such as agranulocytosis and cytopenia (Henter and Karlen, 2007). As a potential future treatment for PD patients and to outweigh the therapeutic ability over side effects, novel iron chelators have been developed to overcome this problem.

A series of novel bidentate HPO iron chelators synthesised base on CP20 structure was designed to resist glucuronidation in the liver by adding chiral hydroxyalkyl group but maintain the affinity towards iron at least comparable to CP20 (Hider et al., 2011). Despite structural alteration, the novel HPOs still exhibit physicochemical properties that favour brain penetration.

It is hypothesised that the novel HPO iron chelators based on the CP20 structure are able to cross the BBB and show neuroprotection in PD**.**

The aims of these studies were to investigate whether the novel iron chelators can cross the BBB and are protective against dopaminergic neurons from toxin-induced cell death. Specifically, these studies had the following objectives:

a) The determination of the BBB permeability of novel HPO bidentate iron chelators by using *in situ* brain perfusion technique in rats.

b) Determination of the neuroprotective properties of the novel iron chelators against Parkinson's disease (PD)-related toxins *in vitro* using neuroblastoma cell line (SH-SY5Y).

c) The evaluation of the pharmacokinetic distribution of selected novel iron chelators upon intraperitoneal (*i.p.)* injection in plasma and brain to determine dose and frequency for *in vivo* studies.

d) The evaluation of the neuroprotective effect of selected novel iron chelators *in vivo* using the 6-hydroxydopamine (6-OHDA) rat model of PD.

CHAPTER 2

MATERIALS AND METHODS

2 Materials and Methods

In order to test the hypothesis that the novel HPO iron chelators based on the CP20 structure are able to cross the BBB and show neuroprotection in PD the following studies were performed:

- Six novel HPO bidentate iron chelators (CN116, CN118, CN126, CN128, CN226 and CN228) were evaluated for brain penetration by using *in situ* brain perfusion in male Wistar rat. In addition, CP84 and its glucose conjugate (FCF132) were also evaluated to determine whether transport via the glucose transporter (GLUT) would enhance brain delivery. The brain permeability results were compared with the parent molecule, CP20. This study addressed the first aim in order to determine the BBB permeability of novel HPO bidentate iron chelators.

- The novel HPO bidentate iron chelators which crossed the BBB (CP84, CN116, CN118, CN126, CN128, CN226 and CN228) were then evaluated for thir ability to protect SH-SY5Y neuroblastoma cell lines against toxins that are relevant to the mechanism of induction of cell death in PD (H_2O_2, 6-OHDA and Fe^{3+}). The cell viability was assessed with 3-(4,5-dimethylthiazol-2-yl)-2,5-diphenyltetrazolium bromide (MTT) assay. This addressed the second aim determine the neuroprotective properties of the novel iron chelators against Parkinson's disease (PD)-related toxins *in vitro*,

- Selected novel HPO bidentate iron chelators that showed brain permeation *in situ* and neuroprotective *in vitro* (CP84, CN128 and CN226) were then assessed for distribution in plasma and brain of male Wistar rat after an *i.p.* injection. CP20 was used as a reference drug in this study. A validated HPLC assay was used to quantify the concentration of HPO in plasma and brain. This addressed the third aim to evaluate of the pharmacokinetic distribution of selected novel iron chelators upon intraperitoneal (*i.p.)* injection in plasma and brain to determine dose and frequency for *in vivo* studies.

- Finally, selected novel HPO bidentate iron chelators that showed brain permeation *in situ,* neuroprotection *in vitro* and brain permeation *in vivo* were assessed for neuroprotective effect by *i.p.* injection on 6-OHDA striatal lesioned male Wistar rat.

The neuroprotective effect was compared to lesioned rat treated with CP20.This chapter describes in detail the methodologies that were used in these studies which includes method optimisation and validation for each results chapter. This addressed the final aim to evaluate of the neuroprotective effect of selected novel iron chelators *in vivo* using the 6-hydroxydopamine (6-OHDA) rat model of PD.

The material and methods required to perform these studies are described in this chapter.

2.1 *Evaluation of the blood-brain barrier permeability of iron chelators using in situ brain perfusion*

2.1.1 *Introduction*

In situ brain perfusion technique involves direct insertion of cannula into the common carotid arteries that bring oxygenated blood and nutrients to the brain. The inserted cannula allows perfusion with oxygenated buffers (normal Ringer's buffer) and studied compounds replacing the circulating blood. The jugular veins are severed, making the system open, and thus avoiding re-circulation of perfusate. This technique is used at the initial stage of drug discovery and development to determine the brain permeability of compounds of interest. The compounds are perfused into the brain *in situ* bypassing the systemic circulation, thus, avoiding systemic drug metabolism not only in the liver, but also in other metabolically active organs such as spleen and kidney that render the compound intact (Preston et al., 1995). Besides circumventing systemic metabolism, this technique also restricts peripheral distribution, making sure that the studied compound is primarily distributed to the brain (Smith, 2003). Having said this, metabolism in brain tissue, if any, is unavoidable. Although direct systemic injection of a drug of interest is considered as a 'gold standard' in BBB permeability study, data derived from this technique need to be carefully interpreted and are not straightforward as it involves systemic metabolism and distribution to other tissues (Takasato et al., 1984, Bickel, 2005, Mensch et al., 2009). The perfusion was terminated during predominantly influx and unidirectional transports process at the BBB, allowing determination of both brain uptake and rate of brain uptake (Smith, 2003, Takasato et al., 1984).

Total brain uptake and rate over time can be determined from the drug concentration in brain and perfusate at terminal time point. In addition, brain homogenate devoid of brain

capillary endothelial cells (BCEC) can be prepared from brain homogenate by differential density centrifugation using concentrated dextran, which has a density in between brain capillary endothelial cells and the rest of brain tissue. The so called 'capillary depleted brain' will correct for compound that adhere to endothelial cells and trapped intracellularly (Triguero et al., 1990).

In situ brain perfusion was performed by a modified version of Preston et al. (1995). Detailed methodology is described below.

2.1.2 *Animals*

Male Wistar rats weighing between 250-300 g (Harlan UK Ltd) were housed between 2-4 rats per cage in the Biological Service Unit (BSU), King's College London. Temperature and humidity were maintained at 21-24 ºC and 55-65% respectively with 12h light/dark cycle. The rats had accessed to standard food pellet and tap water *ad libitum*. The rats were allowed an acclimatisation period of at least one day after arrival at BSU before the perfusion experiment commence. The experiments were approved under Animal (Scientific Procedure Act) 1986 and conducted under project license number 70/0688.

2.1.3 *Preparation of buffers*

a) Normal Ringer's solution

The perfusion fluid was a normal Ringer's solution (NRS), **Table 2.2.1**, containing bovine serum albumin (BSA; representing physiological concentration of plasma proteins) with traces of Evan's blue for visualisation of vessels (Triguero et al., 1990). NRS was kept warm at 37 °C, and continuously bubbled with 5% CO_2/95% O_2 during *in situ* brain perfusion. The NRS was initially allowed to equilibrate with 5% CO_2/95% O_2 for at least 20 minutes. The pH of the solution was evaluated after equilibrium and within the range of 7.35 to 7.45. After equilibration with O_2, NRS pH deviating from the aforementioned ranges was adjusted using 2 N NaOH or 2 N HCl. Prior to perfusion, oxygen equilibrated NRS was pumped into the *in situ* brain perfusion surgical set up by peristaltic pump (505S; Watson Marlow, UK), passing through all the connecting tubing to terminal polyethylene (PE) cannula. Prepared NRS (without glucose, BSA and Evan's blue) was stored at 4 °C and used within 4 weeks of preparation.

Table 2.1.1: Chemical constituent of normal Ringer's solution and their concentration.

Chemicals	Concentration (g/L)	Concentration (mM)
NaCl	6.90	118.0
KCl	0.35	4.7
$CaCl_2$	0.37	2.5
$MgSO_4$	0.30	1.2
$NaHCO_3$	2.10	25.0
KH_2PO_4	0.16	1.2
HEPES	2.38	10.0
Glucose*****	1.80	10.0
BSA*****	40.00	-
Evan's blue*****	0.0011	-

*******Glucose, BSA and Evan's blue were added on the day of the experiment to avoid microbial growth.*

b) Physiological buffer

Physiological buffer solution (PhyBS), **Table 2.2.2** (Triguero et al., 1990), was used during the brain homogenisation process to maintain the pH and physiological environment of brain tissue. PhyBS pH was adjusted using 2 N NaOH or 2 N HCl to be within the range of pH 7.35 to pH 7.45.

Table 2.1.2: Chemicals constituents of physiological buffer solution and their concentration.

Chemicals	Concentration (g/L)	Concentration (mM)
NaCl	8.24	141.0
KCl	0.30	4.0
$CaCl_2.2H_2O$	0.41	2.8
$MgSO_4.7H_2O$	0.25	1.0
$NaH_2PO_4.H_2O$	0.14	1.0
HEPES	2.38	10.0
Glucose*	1.80	10.0

**Glucose was added on the day of the experiment to avoid microbial growth.*

2.1.4 *In situ brain perfusion*

The perfusion set up is portrayed in **Figure 2.1.1**. This system was made ready before surgery by filling all connected tubing with oxygen equilibrated NRS. HPO and radiolabelled compounds were filled into two 20 mL syringes and secure on slow-drive Harvard Type 22 syringe pump (Harvard Apparatus, USA) and primed into the flowing NRS to make sure all air bubbles are removed. The connecting tubing was then clamped, and NRS was allowed to flow for another 2 minutes to wash out all traces of compounds.

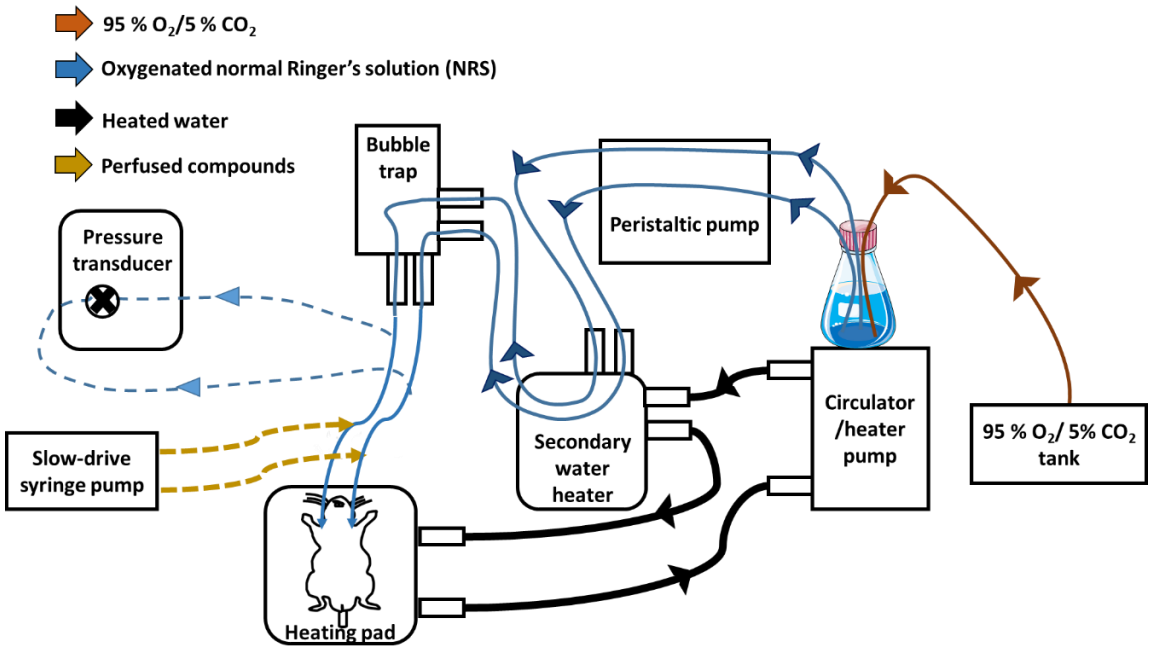

Figure 2.1.1: **Schematic diagram of *in situ* brain perfusion set up.**

The *in situ* brain perfusion technique in this study involves perfusion of both hemispheres of the brain in the absence of the systemic circulation as a modification of the unilateral perfusion described by Takasato et al. (1984), and modified to bilateral perfusion by Preston et al. (1995). Rats were anaesthetised with 50 mg/kg ketamine (Vetalar^{TM}V; Pfizer, USA) and 0.2 mg/kg medetomidine (Domitor®; Orion Pharma, UK) intraperitoneally (*i.p.*), and maintained at 37 °C using a heating pad. Whilst in a supine position, rats were injected with 100,000 U/kg heparin (*i.p.*; Wockhardt UK Ltd, UK) to prevent blood clotting. Local anaesthetic, lignocaine/adrenaline (Norbrook, UK) was then injected subcutaneously (*s.c.*) at five multiple sites (total dose was 20 and 12.5 mg/kg) on the chest.

An incision was made posterior to the chest and going upward to the chin. Muscles that covered the trachea were slowly detached to the sides to expose the trachea. Carotid arteries were located beneath the muscle layers under trachea. The common carotid arteries were exposed and cleaned from fat tissues with forceps. Two pairs of surgical cotton threads were loosely ligated posterior and anterior to the exposed arteries.

In all of the experiments, tubing made from silicone was used to reduce drug or protein binding in the tube lumen (**Figure 2.1.2**). NRS was passed through a heat exchanger, then a double chamber filter and bubble trap filled with polymer wool to the silicone tubing (internal diameter, ID=1 mm, outer diameter, OD=1.5 mm, length=420 mm; Altec, UK) connected to bevelled PE tubing cannula (ID=0.58 mm, OD=0.96 mm, length=20 mm; Carl Stuart UK Ltd., UK) through PE tubing fitting (ID=0.86 mm, OD=1.27 mm, length=10 mm; Carl Stuart UK Ltd., UK).

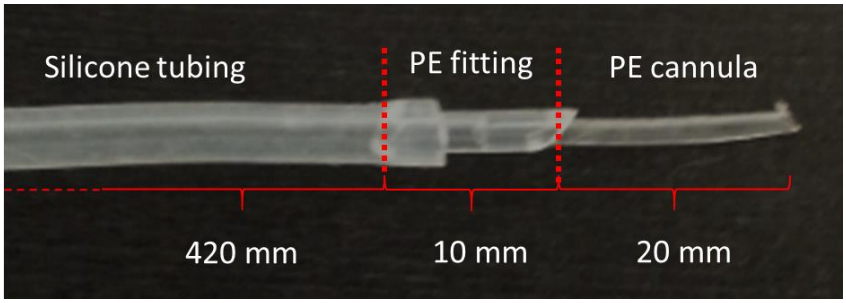

Figure 2.1.2: The tubing and cannula for *in situ* brain perfusion.

NRS was infused at 90% (1.44 mL/min) of the total flow rate (1.60 mL/min in total) to each brain hemisphere. The posterior ligation of the artery was tightened to halt blood flow and a small hole was made in each carotid artery with Vanna scissors. The PE cannulas connected to the NRS perfusion system were inserted into the hole for perfusate inflow and held in place by tightening the anterior ligature (**Figure 2.1.3**). The jugular veins on both sides were exposed and severed for perfusate drainage out from the brain just after the insertion of cannula. Brain was allowed to perfuse with NRS for at least one minute to wash out the blood.

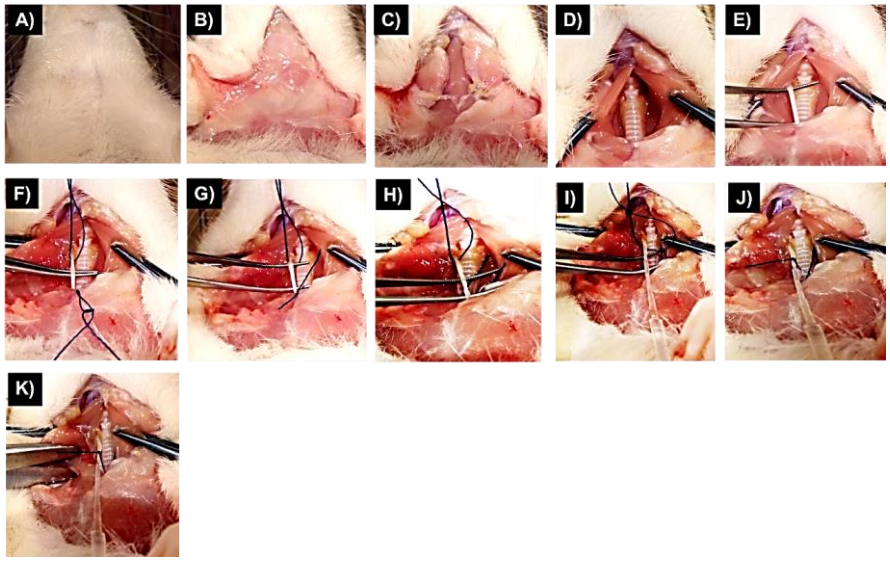

Figure 2.1.3: Step by step procedures of carotid artery cannulation.

***A**) The neck area was exposed and injected with local anaesthetic, lignocaine and adrenaline (s.c.) **B**) An incision was made vertically on the neck **C**) The fats and muscles covering the neck was pulled away until the tissue covering the trachea is visible **D**) The tissue covering the trachea was pulled away with haemostat **E**) Carotid artery was located beneath the tissue covering the trachea. A pair of forceps were used to isolate the carotid artery from the tissue. The carotid artery was cleaned from fats and associated tissues **F**) A pair of cotton thread was loosely ligated on the anterior and posterior part of the artery **G**) The ventral ligation was tightened **H**) Small hole was made above the tightened posterior ligation with Vanna scissors **I**) A cannula with flowing NRS was slowly inserted into the pre-made hole **J**) The anterior ligation was tightened to hold the cannula in place **K**) The jugular vein on the ipsilateral side was cut-off to allow the perfused NRS to flow out. The same steps were repeated on the contralateral side of carotid artery.*

Compounds for study were filled into a 20 mL syringe powered by slow-drive syringe pump (22-5555, Harvard Apparatus, USA). The perfusion rate of slow drive syringe pump was 10% (0.16 mL/min) of the overall flow rate (1.60 mL/min in total). Ninety percent of the perfusate came from the oxygenated/proteinaceous NRS to support normal brain physiology. Brain perfusion with compounds of interest began at least 3 minutes after both of the cannulas were inserted into right and left common carotid arteries in order to allow removal of blood from brain capillaries (Smith and Allen, 2003). The perfusion pressure was monitored constantly by a pressure transducer and fell between 30 mmHg to 50 mmHg in this setup. Pressure deviating from this range may indicate improper perfusion.

2.1.5 *Measurement of pH, gases and ions in whole blood and perfusate*

In situ brain perfusion was performed for 5, 10, 20, 40 and 60 minutes to evaluate the physiological parameters of the perfused NRS to support normal brain function during long duration of perfusion, the perfusate was sampled before beginning of perfusion and after it has passed the brain and flow out through the jugular vein. Additionally, whole blood was also sampled from the anaesthetised rat before the start of the perfusion so that comparison can be made with the NRS perfusate.

The arterial blood was sampled via tail ventral artery with 23G winged needle (Hospira, USA) connected to 1 mL syringe (Terumo, Japan) with 25G needle (Terumo, Japan) before start of perfusion. Rat jugular vein on the left side was made visible with a pair of forceps from surrounding muscle tissues and fats. Surgical cotton thread was loosely ligated anterior to the incision site. Isolated jugular vein was held in place with forceps and small incision was made on the vein with Vanna scissors. Bevelled PE cannula (internal diameter, ID=0.58 mm, outer diameter, OD=0.96 mm, length=20 mm; Carl Stuart UK Ltd., UK) connected to silicone tubing (ID=0.5 mm, OD=0.75 mm, length=120 mm; Altec, UK) was inserted and the cotton thread was tightened to secure the cannula in place. Flowing venous blood was collected into 1 mL syringe (Terumo, Japan) attached to 25G needle (Terumo, Japan).

Additionally, the perfusion fluid (oxygenated NRS) was sampled from the tip of the perfusion cannula before carotid artery cannulation. After the perfusion started, venous perfusate was sampled from the cannulated jugular vein at 10, 20, 40 and 60 minutes.

The collected whole blood and perfusate samples were immediately pipetted into a $CG8^{+}$ cartridge (Abbott, USA) and analysed for O_2, CO_2, glucose, pH and physiological ions [Na^{+}, K^{+}, HCO_3^{-} and ionised Ca^{2+} (iCa^{2+})] level with an iSTAT portable blood analyser (Abbott, USA). **Figure 2.1.4** shows the results obtained from whole blood and perfusate using iSTAT portable blood analyser.

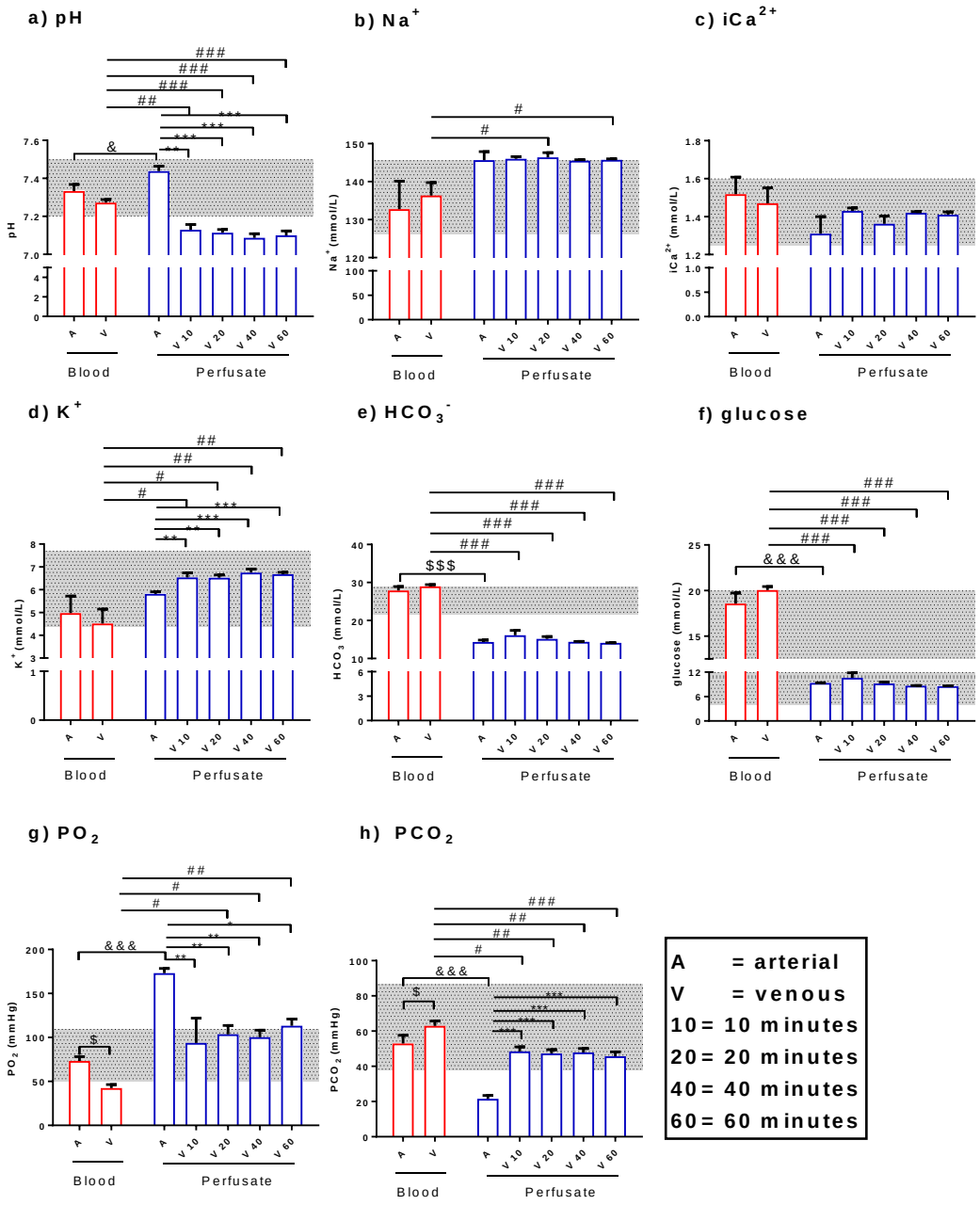

Figure 2.1.4: **pH, ions and blood gaseous in arterial and venous of whole blood (naïve rats) or perfusate (perfused rats).**

The whole blood and perfusate samples were analysed by iSTAT portable blood analyser using CG8+ cartridge for simultaneous analysis of pH, ions and blood gaseous ***(Graph a-h)****. Red bars denote data for whole blood and blue bars denote data for perfusate. The grey shaded area showed the normal physiogical range of pH, gases and ions in blood. Data are expressed as mean+SEM (n=3-6 rats). $ p<0.05 (arterial blood vs venous blood; paired t-test, two-tailed); & p<0.05, &&& p<0.001 (arterial blood vs arterial perfusate; unpaired t-test, two-tailed); * P<0.05, ** p<0.01, *** p<0.001 (arterial perfusate vs venous perfusate; one-way ANOVA followed by Holm-Šídák multiple comparison test); # p<0.05, ## p<0.01, ### p<0.001 (venous blood vs venous perfusate; one-way ANOVA followed by Holm-Šídák multiple comparison test).*

The pH between arterial and venous blood was not different from each other and was within the reported physiological range (**Figure 2.1.4a**; Subramanian et al., 2013, Guyenet et al., 2005). Arterial perfusate pH was within the physiological pH although the pH was slightly higher. In contrast to the venous blood, pH of venous perfusate dropped at all perfusion time end-point, with the average pH was 0.1 unit lower than the reported physiological range (physiological range pH=7.20-7.50; Subramanian et al., 2013, Guyenet et al., 2005**)**.

Na^+, ionised Ca^{2+} (iCa^{2+}) and K^+ concentration in whole blood fall within the physiological range (**Figure 2.1.4b, c & d**; Giknis and Clifford, 2008, Hemmingsen et al., 1998). There was no different in Na^+, iCa^{2+} and K^+ level between arterial and venous blood. Similarly, no different was observed in Na^+, iCa^{2+} and K^+ level between arterial blood and arterial perfusate. Comparison between venous blood and venous perfusate showed no different in iCa^{2+} level. In contrast, Na^+ and K^+ level in venous perfusate were higher than venous blood, although they still fall within the reported physiological range (Giknis and Clifford, 2008, Hemmingsen et al., 1998).

HCO_3^- level in arterial and venous blood were within reported physiological pH (**Figure 2.1.4e**; Giknis and Clifford, 2008). However, HCO_3^- showed unexpected lower concentration (2-fold lower) in arterial perfusate although during preparation of the NRS perfusion fluid, $NaHCO_3$ salt amounting to 25 mM that mimics physiological condition was added. One possible explanation for this observation is that continuous and extensive oxygenation of the perfusion fluid caused displacement of CO_2 in the solution, thus the reaction showed in **Equation 2.1.1** move to the left (Swietach et al., 2010).

$$H_2O + CO_2 \leftrightarrow H_2CO_3 \leftrightarrow HCO_3^- + H^+ \qquad \textbf{Equation 2.1.1}$$

Similar observation has been reported in hyperventilated rat whereby the HCO_3^- level in blood dropped 2-fold to 11.5 mmol/L (Weyne et al., 1970). As the reaction shifted to the left, the bicarbonate buffering system was less able to maintain the perfusion fluid pH within the physiological range as described above. Thus, addition of 10 mM 4-(2-hydroxyethyl)-1-piperazineethanesulfonic acid (HEPES) into the perfusion fluid helped to maintain the pH (Choi and Zheng, 2009).

Glucose concentration in whole blood was higher (18-20 mmol/L) than the reported physiological range (3.9-11.6 mmol/L; **Figure 2.1.4f**; Giknis and Clifford, 2008, Subramanian et al., 2013). However, this is expected as rats anaesthetised with general anaesthesia and muscle relaxant such as ketamine and xylazine have been shown to exhibit higher level of blood glucose up to 19.4 mmol/L **(**Brăslaşu et al., 2007, Saha et al., 2005). Therefore, the accepted physiological range became widened in this study to include range of blood glucose in anaesthtised rats (3.9-20 mmol/L). Arterial and venous perfusate level were within physiological range correspond to the 10 mM glucose added into the perfusion fluid.

O_2 partial pressure (PO_2) in arterial blood was within physiological range (**Figure 2.1.4g**; Giknis and Clifford, 2008). Venous blood PO_2 dropped 1.7-fold as would be expected for jugular venous blood (Duong et al., 2001). Arterial perfusate PO_2 was 2.4-fold higher than arterial blood PO_2 as the NRS perfusion fluid was continously bubble with 95% O_2/5% CO_2. Similar observation has been reported where hyperventilation in living rats caused 1.3-fold increase in arterial PO_2 (Duong et al., 2001).The continous and extensive oxygenation of the NRS was important to supply the perfused brain with sufficient O_2 to support brain metabolism. Venous perfusate PO_2 was 2.4-fold higher than venous blood PO_2. However, venous perfusate PO_2 was 1.7-fold lower than arterial perfusate PO_2 which corresponds to venous PO_2 dropped in whole blood. This suggest that the brain was metabolically active as in living rat when perfused for up to 60 minutes.

CO_2 partial pressure (PCO_2) in whole blood was within physiological range. PCO_2 in venous blood increase by 1.2-fold as reported (**Figure 2.1.4h**; Dauchy et al., 2000). Arterial perfusate CO_2 was 2.4-fold lower than arterial blood PCO_2 as should be expected for continuously oxygenated perfusate (Duong et al., 2001, Weyne et al., 1970). Venous perfusate PCO_2 was 1.3-fold lower than venous blood PCO_2. However, venous perfusate PCO_2 was increase by 2.2-fold compared to arterial perfusate PCO_2. This suggest that the brain actively remove metabolic waste for up to 60 minute perfusion. The absence of red blood cells (RBC) in the perfusate might explain the higher PCO_2 in venous perfusate as carbonic anhydrous in RBC helps in reducing the level of post-capillary CO_2. The higher PCO_2 in venous perfusate might also explain the slight dropped in pH in venous perfusate as incresased soluble CO_2 in solution contributed to decrease in pH (Motais et al., 1989).

The concentration of dissolved O_2 and CO_2 in blood and perfusate were calculated by multiplying the PO_2 and PCO_2 with 0.0031 mL O_2/mmHg O_2/dL and 0.067 mL CO_2/mmHg CO_2/dL respectively as described by Henry's Law (Bacher, 2005). The difference of O_2 and CO_2 concentration in arterial and venous samples were calculated. Arterial-venous (A-V) difference of soluble O_2 in whole blood and perfusate were within the physiological range (**Figure 2.1.5**). Similarly, venous-arterial (V-A) difference of soluble CO_2 in whole blood was also within the reported physiological range (Giknis and Clifford, 2008, Duong et al., 2001).

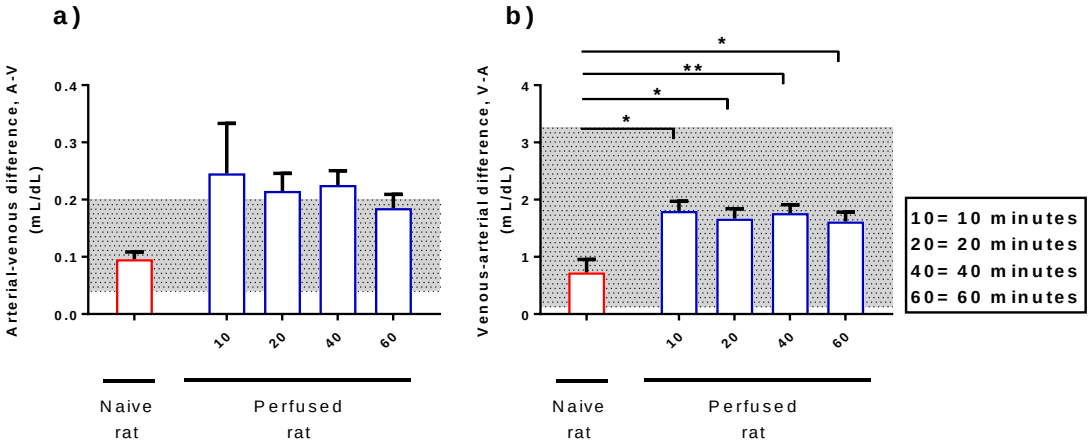

Figure 2.1.5: Arterial-venous O_2 (A-V) and venous-arterial (V-A) CO_2 diferences in rats.

a) *The O_2 concentration difference between arterial and venous blood/perfusate in naïve and perfused rats.* ***b)*** *The CO_2 concentration difference between venous and arterial blood/perfusate in naïve and perfused rats. The grey shaded area showed the normal physiogical range. Data are expressed as mean+SEM (n=3-6 rats).* P<0.05, ** P<0.01 (naïve rat vs perfused rat; one-way ANOVA followed by Holm-Šídák multiple comparison test).*

Physiologically reported arterial-venous difference of glucose was very low (0.06-1.11 mmol/L (Somogyi, 1948). Thus, negative A-V values can easily be obtained due to slight analytical error (**Figure 2.1.6**). Nevertheless, the positive A-V of glucose obtained in this study was within the reported physiological range. This observation suggested that the brain was metabolically active up to 60-minute perfusion.

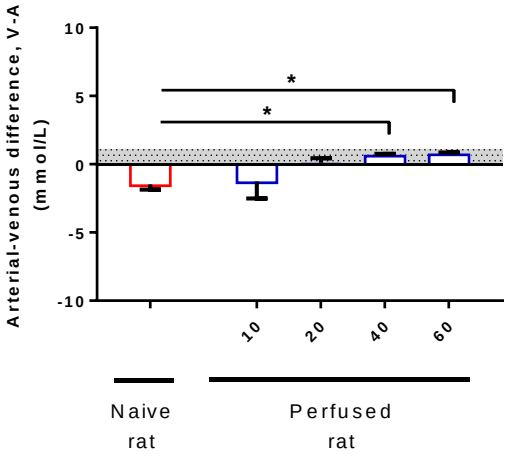

Figure 2.1.6: Arterial-venous (A-V) glucose diference in rats.

*Glucose concentration difference between arterial and venous blood/perfusate in naïve and perfused rats. The grey shaded area showed the normal physiogical range. Data are expressed as mean+SEM (n=3-6 rats). * P<0.05 (naïve rat vs perfused rat; one-way ANOVA followed by Holm-Šídák multiple comparison test).*

In summary, the pH, electrolytes and blood gases in the arterial perfusate generally agreed with the accepted physiological range in whole blood. Although some parameters showed deviation from physiological range, this is expected and explainable as the perfusion fluid was continously and extensively gas with O_2, and lacked RBC that help buffering pH and ion levels.

2.1.6 *Validation of in situ brain perfusion*

It has been shown in previous section (**Section 2.1.5**) that the NRS perfusate physiological parameters were within the blood physiological range for up to 60-minutes perfusion. In this section, details of the experiment conducted to determine the linearity of HPO brain uptake for up to 60-minute perfusion using CP20 as the prototype HPO was described. ^{14}C-sucrose and ^{3}H-O-methyl-D-glucose (^{3}H-OMG) were simultaneously measured to determine the integrity and functionality of BBB.

In situ brain perfusion was validated by using deferiprone (CP20, MW=139.15 g/mol; Sigma-Aldrich, USA) as a model drug of HPO bidentate iron chelators, ^{3}H-O-methyl-D-glucose (^{3}H-OMG, MW=194.2 g/mol; Perkin Elmer, USA) and ^{14}C-sucrose (MW=342.3 g/mol; Perkin Elmer, USA). CP20 crosses the BBB through passive diffusion and was used as prototype drug to evaluate the brain penetration of novel HPO (Hider et al., 2011,

Habgood et al., 1999). ^{3}H-OMG was transported across the BBB via GLUT-1 transporter (Reyes et al., 2002). ^{14}C-sucrose was used as a vascular space marker and negative control since it does not crossed BBB (Ennis and Betz, 1986).

CP20 (500 µM), ^{3}H-OMG [(296 kBq/rat (8 µCi/rat)] and ^{14}C-sucrose [185 kBq/rat (5 µCi/rat)] in NRS were filled in a 20 mL syringe. The specific activity and amount of ^{3}H-OMG and ^{14}C-sucrose were summarised in **Table 2.1.3**. The carotid arteries were isolated as described earlier in **Section 2.1.4**.

Table 2.1.3: Specific activity of radionuclides and amount perfused.

Radionuclide	Specific activity (Ci/mmol)	Purity (%)	Molecular weight (g/mol)	Amount perfused per rat (nmol)
^{3}H-OMG	80	>97	194.2	0.100
^{14}C-sucrose	0.432	>97	342.3	12

These compounds were perfused simultaneously to the brain for 5, 10, 20, 40 and 60 minutes. At each of the perfusion time point, the perfusion was stopped and the head was decapitated.

2.1.7 *Preparation of in situ brain perfusion samples for quantification analysis*

At the end of perfusion, the rats were decapitated and the brain was removed immediately for sample processing. Additionally, sample of flowing perfusate was taken from the end of the PE cannula. Brain hemispheres were cleaned with cotton bud moistened with PhyBS to remove pial layer followed by dissection to remove the cerebellum and choroid plexus. Cerebellum is mainly supplied by a vertebral artery and therefore was not included in the brain uptake measurement (Yao et al., 1990, Preston et al., 1995). Additionally, choroid plexus, a highly vascularise brain structure found at the lateral, third and fourth ventricles was also removed because of the leaky capillaries in this region (Liddelow, 2015, Preston et al., 1995). The brain was homogenised in PhyBS. ^{14}C-sucrose perfused along with ^{3}H-OMG and CP20 work as a vascular marker so that ^{3}H-OMG and CP20 in capillary lumen leaked during the homogenisation process can be estimated and corrected (Triguero et al., 1990, Preston et al., 1995). Processed whole brain homogenate represent

the uptake of ^{3}H-OMG and CP20 in BCEC and brain parenchyma. As BCEC is the barrier component of BBB, the uptake of ^{3}H-OMG and CP20 in BCEC and brain parenchyma must be differentiated. Differential centrifugation with concentrated dextran that has a density in between BCEC and brain parenchyma helps to physically separate these two compartments, thus allowing measurement of ^{3}H-OMG and CP20 in brain parenchyma only (Triguero et al., 1990). This section explained in detail the method used in preparation of the samples for quantification analysis.

The brain was weighed and homogenise in PhyBS [1:1 (w/v) dilutions, ten strokes homogenisation in a Potter-Elvehjem borosilicate glass homogeniser, 150 mm x 10 mL; Jencons, England]. Sequentially, the same volume of 30% (w/v) dextran [(final concentration 15% (w/v)] was added and briefly homogenised for four strokes with the homogeniser producing whole brain homogenate. Total dilution of brain at this point was 1:3 (w/v).

a) Sample preparation for ^{3}H-OMG and ^{14}C-sucrose measurement

i) **Perfusate**

Perfusate sample (100 µL) taken from the end of polyethylene cannula upon termination of *in situ* brain perfusion was pipetted into 7 mL scintillation vial. Tissue solubiliser (0.5 mL, Soluene; Canberra-Packard, UK) was added and mix with a mixer (Vortex-Genie2; Scientific Industries, USA). The samples were incubated at room temperature for 24 h. Five millilitre of scintillation cocktail (Ultima Gold XR; Perkin Elmer, USA) was added, mixed with a mixer and incubated for 30 minutes before analysis by liquid scintillation spectroscopy (LSS) counter. Vehicle (NRS) was processed the same way as a blank. Samples preparation was performed in duplicate.

ii) **Whole brain fraction**

Five hundred microliters of whole brain homogenate were pipetted into a 7 mL scintillation vial. Tissue solubiliser (0.5 mL) was added and mixed with a mixer. The samples were incubated at room temperature for 24 h to allow tissue solubilisation. Scintillation cocktail (5 mL) was added, vortex and incubated for 30 minutes before analysis by LSS counter. Vehicle (PhyBS and dextran mixture) was processed in the same way forming blank controls. Sample preparation was performed in duplicate.

iii) Capillary depleted brain fraction

Seven hundred microliters of whole brain homogenate were pipetted into 1.5 mL microcentrifuge tube and spun at 5400 *g* for 20 minutes at 4 ºC (Triguero et al., 1990). Three layers of separation were formed upon centrifugation (**Figure 2.1.7**).

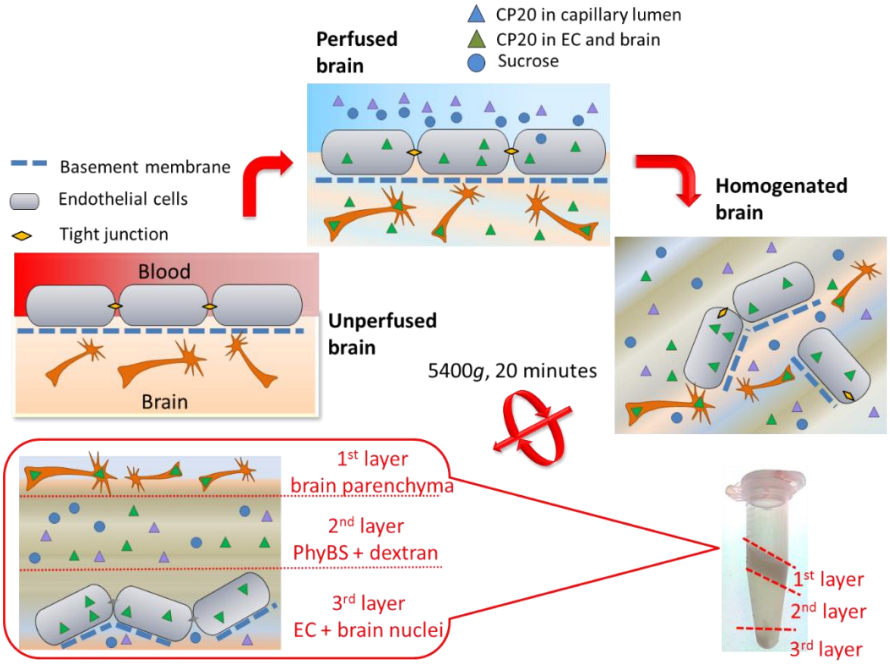

Figure 2.1.7: **Illustration of capillary depleted brain preparation.**

First layer from the top was brain parenchyma, second layer was mixture of physiological buffer and dextran, and third layer was capillary rich brain tissue pellet. Capillary depleted brain parenchyma (1st layer) was carefully loosened by small spatula from the microcentrifuge wall before decanted into other microcentrifuge tube together with the 2nd layer and subsequently vortexed to evenly distribute the supernatant. PhyBS= physiological buffer saline; EC=endothelial cells.

Tissue solubiliser (0.5 mL) was added to 500 µL of capillary depleted brain homogenate and mixed by a mixer. The samples were incubated at room temperature for 24 h. Five millilitre of scintillation cocktail was added, vortexed and incubated for 30 minutes before analysis by LSS counter (**Figure 2.1.8**). Vehicle (PhyBS and dextran mixture) was processed in the same way as blank controls.

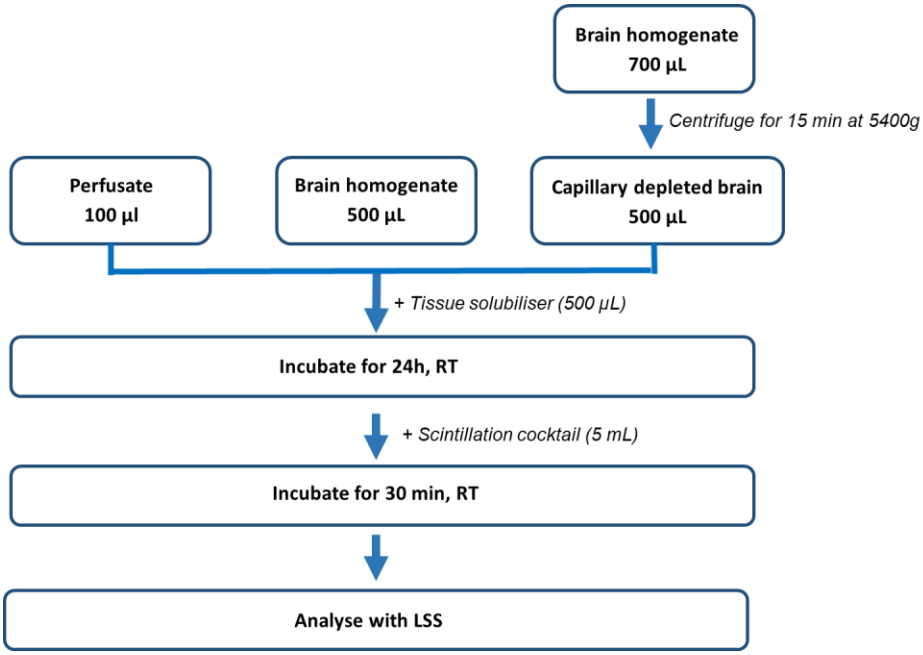

Figure 2.1.8: **Sample preparation for LSS analysis.**

b) Sample preparation for HPO iron chelators measurement

i) Perfusate

Perfusate sample (300 µL) taken from the end of polyethylene cannula upon termination of *in situ* brain perfusion was diluted 1:4 (v/v) with NRS. Three hundred microliter of diluted perfusate was pipetted into 1.5 mL microcentrifuge tube and 30 µL of trifluoroacetic acid (TFA; Sigma-Aldrich, USA) was added to denature the proteins. After a brief mixed with a mixer, the samples were centrifuged at 20800 *g* for 45 minutes to precipitate the protein. One hundred microliters of supernatant were taken and pipetted into 0.3 mL conical crimp vial (Kinesis, UK), seal with 8 mm polytetrafluoroethylene (PTFE) crimp cap (Kinesis, UK) sealed with a crimper. Thirty microliters was injected into high performance liquid chromatography (HPLC) system (**Figure 2.1.9**). Samples preparation was performed in duplicate.

ii) Whole brain fraction

Five hundred microliters of whole brain homogenate were pipetted into 1.5 mL microcentrifuge tube and 50 µL of TFA was added to denature the proteins. After a brief mixed with a mixer, the samples were centrifuged at 20800 *g* for 45 minutes to precipitate

the protein. One hundred microliters of supernatant were taken and pipetted into HPLC vial and seal with crimper. Samples preparation was performed in duplicate.

iii) Capillary depleted brain fraction

Capillary depleted brain was prepared as described in **Section 2.1.6.a.iii**. Capillary depleted brain homogenate (500 uL) was pipetted into 1.5 mL microcentrifuge tube and 50 µL of TFA was added to denature proteins. After a brief mixed by a mixer, the samples were centrifuged at 20800 *g* for 45 minutes to precipitate the protein. One hundred microliters of supernatant were taken and pipetted into 0.3 mL conical HPLC vial. Samples preparation was performed in duplicate.

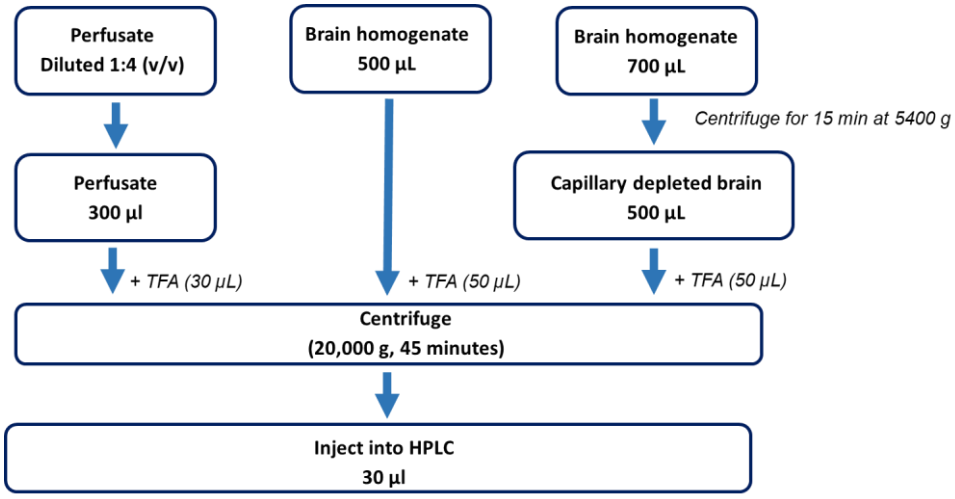

Figure 2.1.9: Sample preparation for HPLC analysis by gradient reversed-phase ion-pair method.

2.1.8 *Validation of capillary depleted brain preparation*

Alkaline phosphatase is a water-soluble enzyme abundantly present in brain capillary endothelial cells but not in brain parenchyma. Therefore, alkaline phosphatase enzyme activity was assayed in capillary-depleted brain parenchyma and capillary enriched pellet to asses for effective separation (Triguero et al., 1990, Williams et al. 1980). *p*-nitrophenyl phosphate (*p*NPP) was used as a probe substrate in the reaction. Alkaline phosphatase catalysed dephosphorylation of *p*NPP to *p*-nitrophenol (*p*NP), a product that turn yellow in alkaline condition and shows maximal absorption at 405 nm **(Figure 2.1.10)**.

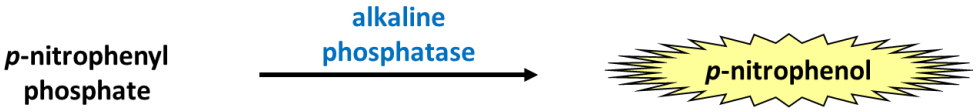

Figure 2.1.10: Conversion of *p*-nitrophenyl phosphate, a probe substrate for alkaline phosphatase to formed yellowish hue product in alkaline condition, *p*-nitrophenol, which has maximal absorption at 405 nm.

The amount of *p*NP formation is proportional to the amount of alkaline phosphatase present in the brain homogenate, and therefore the activity of the enzyme can be calculated.

a) Determination of protein concentration

Prior to alkaline phosphatase assay, protein concentration of capillary depleted brain and capillary enriched tissues were determined with a commercial Pierce™ bicinchoninic acid (BCA) Protein Assay Kit (Thermo Fisher, UK). A set of known concentrations of bovine serum albumin (BSA) in 0.9 % NaCl were prepared and the absorbance of each sample was read on a microplate reader (540 nm). A standard curve of absorbance against BSA concentration was constructed just prior to measurements of samples (**Figure 2.1.11).** Capillary depleted brain and capillary enriched tissues (25 µL) were pipetted into a 96-well microplate. Reaction reagent (200 µL) composed of reagent A and reagent B at 50 to 1 ratio was added to each well and the plate was mix thoroughly on a plate shaker for 30 seconds. The plate was covered and incubated at 37 °C for 30 minutes and the absorbance was measured at 540 nm on a plate reader. The amount of protein in brain samples was calculated based on linear equation derived from BSA standard curve.

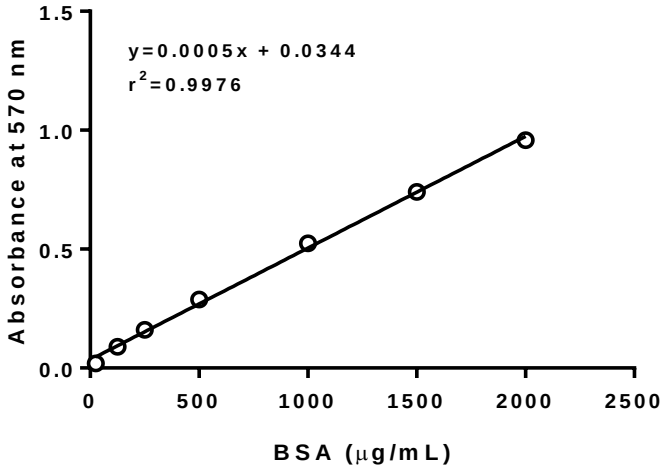

Figure 2.1.11: Typical BSA standard curve obtained from BCA protein assay.

Data analysed by least-square regression analysis (GraphPad Prism 7 Software).

b) Alkaline phosphatase assay

Reaction mixture (500 µL) contained 50 mM $MgCl_2$, 5 mM $CaCl_2$, 100 mM KCl, 100 mM Tris (pH 9) and 5 mM *p*NPP. The reaction was initiated by adding 50 µL of capillary depleted brain or capillary enriched tissues (0.5 mg/mL final concentration) and incubated at 37 ºC for 30 minutes. At the end of the incubation time, the reaction was terminated with 500 µL NaOH (1 M) and put on ice for 10 minutes. The absorbance was taken at 405 nm in a final volume of 300 µL against a blank (reaction mixture with capillary depleted brain/capillary rich fraction was replaced with water).

The concentration of *p*NP formed in the reaction mixture was determined by substituting the absorbance in the linear equation obtained from *p*NP standard curve (**Figure 2.1.12**) constructed from absorbance reading at 405 nm of *p*NP concentration between 0.04 to 0.7 mM.

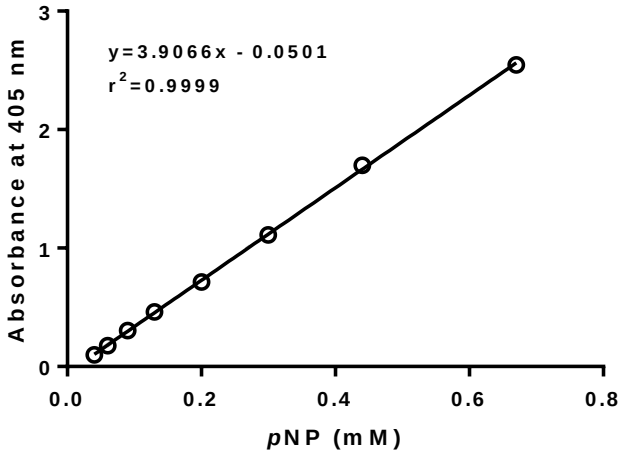

Figure 2.1.12: Typical *p*NP standard curve obtained from alkaline phosphatase enzyme assay.

Data analysed by least-square regression analysis (GraphPad Prism 7 Software).

The alkaline phosphatase specific activity was calculated as followed:

$$AP\ (nmol/min/g) = \frac{pNP\ (uM)}{t\ (\text{min})\ \text{X protein (mg/mL)}}\ X\ 1000 \qquad \textbf{Equation 2.2.2}$$

Alkaline phosphatase specific activity in capillary enriched pellet was greater than capillary depleted brain by 37-fold (**Figure 2.1.13**). The percentage purity of capillary separation from brain homogenate was 96.68 % based on alkaline phosphatase specific activity, thus confirming the separation using dextran density differential centrifugation (Moos and Morgan, 2001, Triguero et al., 1990).

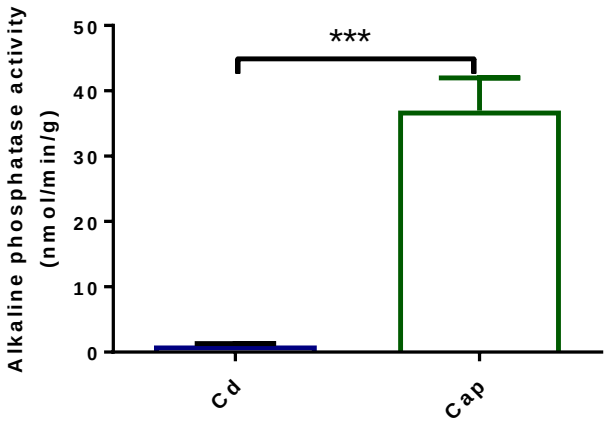

Figure 2.1.13: Alkaline phosphatase specific activity in capillary depleted brain (Cd) and capillary enriched pellet (Cap).

*Individual brain was taken from in situ brain perfused rats. Capillary enriched pellet (Cap) shows higher alkaline phospatase activity compared to capillary depleted brain (Cd). Data are expressed as mean+SEM (n=6 rats). *** P<0.001 (paired t-test, one-tailed).*

2.1.9 *Quantification analysis of in situ brain perfusion samples*

Samples prepared after *in situ* brain perfusion were analysed by liquid scintillation spectroscopy (LSS) counter and high-performance liquid chromatography (HPLC) to quantify HPO and radiolabelled compounds.

a) Liquid-scintillation spectroscopy (LSS)

^{3}H-OMG and ^{14}C-sucrose (Perkin Elmer®, USA) activity were counted on a LSS counter (LKB Wallac 1219 Rackbeta, Wallac, USA). The LSS counter was pre-programmed in the computer memory to correct automatically the preparation errors for newly quenched samples. The radioactivity was expressed as disintegration per minute (DPM).

b) High-performance liquid chromatograpy (HPLC)

i) Calibration curve

Standard solutions of HPOs ranging from 5 to 1000 µM were prepared by serial dilution from a 5000 µM stock dissolved in HPLC water**.**

ii) Quantification of hydroxypyridinones (HPOs) by HPLC

HPOs concentrations were evaluated by a gradient ion-pair HPLC method. The quantification method was provided by Dr Sukhvinder Bansal from Institute of Pharmaceutical Science, King's College London. Two mobile phase systems compose of 10% (v/v) acetonitrile in water (mobile phase A) and 90% (v/v) acetonitrile in water (mobile phase B) with 1 g/L pentadecafluorooctanoic acid as the ion-pair reagent in each mobile phase were used to separate the HPOs.

The quantification was performed on an Ultimate 3000 Standard LC Systems equipped with quaternary pump delivery system (LPG-3400SD), autosampler (WPS-3000(T)SL Analytical) and multi-wavelength detector (3000 VWD).

Thirty microliters (30 µL) of each sample was injected into Poroshell 120 EC-C18 reversed-phase column, 2.7 µm particle size, 2.1 x 50 mm diameter and length manufactured by Agilent (Cat no. 699775-902). The pump flow rate was set at 0.2 mL/min and HPO separation was obtained with a mobile phase B gradient starting at 10% B, rising

to 90% over 10mins, held for 3 mins and falling back to 10% over 2 mins **(Figure 2.1.14**). The total running time was 25 minutes including equilibration time for the column at 10 % B 10 minutes before the next injection. HPOs eluted from the column were detected at 280 nm wavelength.

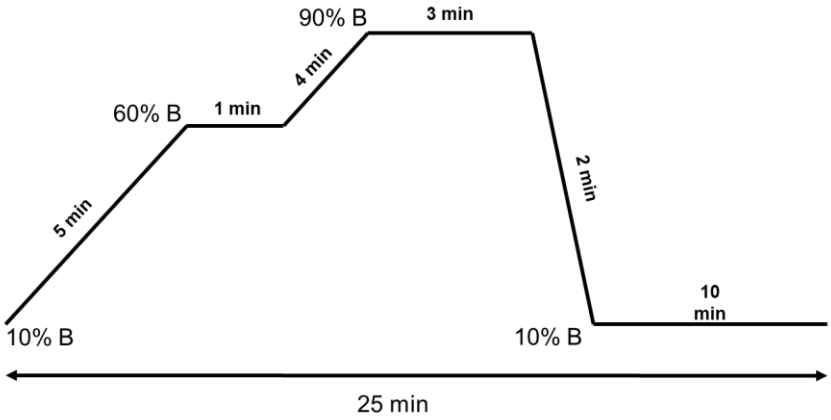

Figure 2.1.14: HPLC gradient method for a successful separation of HPOs. Mobile phase B contained 90 % (v/v) acetonitrile in water with 1 g/L pentadecafluorooctanoic and 0.01 % (v/v) formic acid.

The peak integrations and data analysis were performed using Chromeleon 6.8 Chromatography Data System **(Figure 2.1.15).** The peak height (H) signal of concentration-known HPO chromatogram was used to construct the calibration curve (**Figure 2.1.16**). The peak height (H) signal of HPO chromatogram for in perfusate, brain homogenate and capillary depleted brain was multiplied with the dilution factor **(Table 2.1.4).** The corrected value was converted to concentration in µM based on the constructed calibration curve.

Table 2.1.4:Total dilution of *in situ* brain perfusion samples before injected into HPLC

Samples	**Dilution factor (DF)**
Perfusate	5.5
Brain homogenate	4.4
Capillary depleted brain	4.4

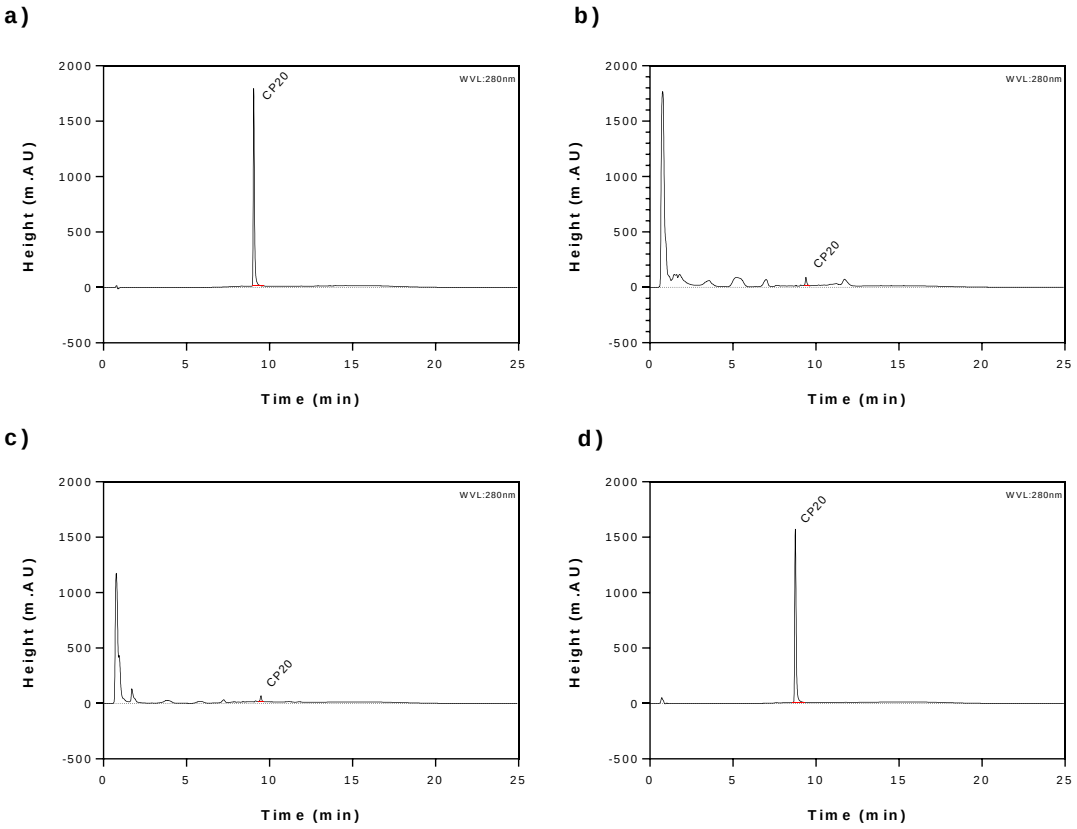

Figure 2.1.15: Representative chromatogram for CP20.

a) *500 µM standard* ***b)*** *brain homogenate* ***c)*** *capillary depleted brain and* ***d)*** *perfusion fluid from rat perfused with 500 µM CP20 for 20 minutes. CP20 retention time was ~8.3 minute. m.AU: mili-absorption unit.*

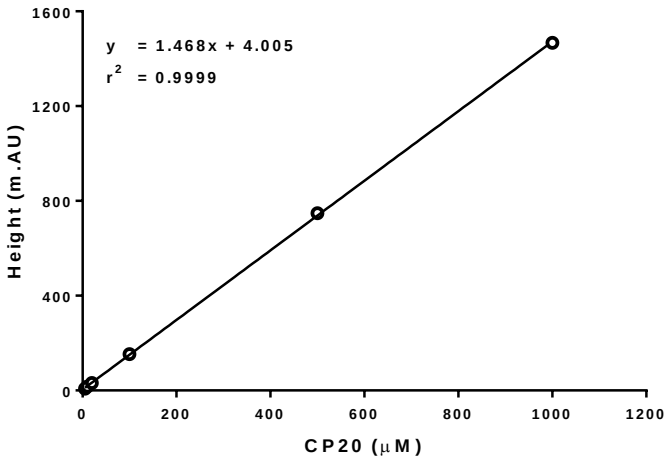

Figure 2.1.16: Representative calibration curve for CP20 prepared in HPLC water.
m.AU: mili-absorption unit. Data was analysed by least-square linear regression analysis (GraphPad Prism 7 Software).

iii) Recovery study for HPOs

Recovery studies of HPOs from brain tissues and perfusion fluid was performed since the standard calibration curve was prepared in HPLC water. HPOs working stock (450 µM) were prepared in water. The working stock was spiked into HPLC water, pooled brain homogenate or perfusate in triplicate at 1:14 (v/v) dilution (final = 30 µM). TFA was added so that its final concentration in the solution was 10% (v/v). All of the samples were mixed and centrifuged at 20800 *g* for 45 minutes. The supernatant was taken and analysed by HPLC as described in **Section 2.1.7a ii**. Percentage recovery was calculated as showed in **Equation 2.1.3**.

$$Recovery\ (\%) = \frac{H_{Br}\ or\ H_{Pf}}{H_{water}}\ X\ 100 \qquad \textbf{Equation 2.1.3}$$

Where H_{Br} is the peak height of HPO chromatogram in brain homogenate, H_{Pf} is the peak height of HPO chromatogram in perfusion fluid and H_{water} peak height of HPO chromatogram in water.

The sample extraction step was a crucial part in HPLC analysis of biological samples to precipitate proteins and release HPO from the association of biological matrices protein and lipid into the solution (Alshammari et al., 2015). CP20, FCF132, CN116 and CN118 in perfusion fluid and brain samples showed between 88-100% recovery (**Table 2.1.5**). CN126 and CN128 were showed 80-86 % recovery from perfusate and 64-70% from brain. CP84, CN226 and CN228 showed the least recovery among all of the HPOs tested (61-65% recovered). As showed in **Table 2.1.5**, recovery from perfusion fluid was equal to or higher than recovery from brain homogenate. The percentage recovery for all of the HPOs were corrected when the peak height signal of HPO chromatograms was converted to concentration using a constructed standard calibration curve.

Table 2.1.5: Percentage (%) recovery of HPOs extracted with 10% (v/v) TFA from spiked perfusion fluid and brain homogenate.

HPOs	% Recovery	
	Perfusion fluid	Brain
CP20	95.3±2.8	87.7±1.2
CP84	68.7±4.6	62.0±12.7
FCF132	104.0±3.5	104.7±3.3
CN116	104.7±0.9	102.3±0.9
CN118	94.0±3.6	95.3±0.3
CN126	79.7±2.3	64.3±3.2
CN128	85.6±5.8	70.7±4.2
CN226	65.0±4.0	50.7±2.3
CN228	60.7±3.7	50.7±0.7

Data are expressed as mean±SEM (n=3 independent samples).

2.1.10 *Determination of unbound HPO in brain, plasma and perfusion fluid*

The NRS perfusion fluid contained the physiological concentration of bovine serum albumin (40 g/L BSA; **Section 2.1.3**). Therefore, it is imperative to determine the extent of HPO binding to BSA as only unbound HPO would be able to cross the BBB (Hammarlund-Udenaes et al., 2008, Friden et al., 2007). In addition, HPO binding in brain tissue was also evaluated.

The method reported by Summerfield et al. (2007) was followed to determine the fraction of HPO unbound in brain, plasma and perfusion fluid. Evaluation of unbound HPO was performed in a separate *in vitro* experiment, as the bound HPO releases during sample processing and extraction with TFA due to protein denaturation (**Section 2.1.7**). ^{3}H-OMG and ^{14}C-sucrose has been reported to not significantly bind to plasma protein at low concentrations (Mereish et al., 1982, Chinachoti and Steinberg, 1988). Brain from control rats were used to prepare a whole brain homogenate at 1:3, 1:7 and 1:15 (w/v) dilutions. Degree of dilutions did not affect the degree of HPOs binding to protein; therefore, brain diluted 1:3 (w/v) was used for all experiments (**Table 2.1.6**).

Table 2.1.6: Effects of brain homogenate dilution on the detection of free, unbound CP20 in brain tissue

Brain dilution factor (w:v)	CP20
	% unbound
1:3	103.1±0.7
1:7	104.3±1.8
1:15	104.0±3.5

CP20 was spiked into a diluted pooled brain homogenate. Data are expressed as mean±SEM (n= 3 tubes). Statistical analysis using one way ANOVA showed no significant different.

Blood was collected from control rats by cardiac puncture with 21G needle attached to 5 mL syringe. The collected whole blood was transferred into heparinised tube and spun at 5400 *g* for 20 minutes; the supernatant which is the plasma was isolated and kept frozen until use. Perfusion fluid was prepared by supplementing NRS with 10 mM glucose and 40 g/L BSA as described in **Section 2.1.3**. HPO stock solution (1800 µM) was spiked into whole brain homogenate, plasma, perfusion fluid and distilled H_2O (as a control) in a ratio of 1:10 to give a final HPO concentration of 180 µM. The tubes were mixed with vortex mixer and incubated in a shaking water bath at 37 °C for 20 minutes before transferred into Vivaspin® tubes (2 kDa MWCO; GE Healthcare Life Sciences, UK**)**. Vivaspin® tubes were spun at 3000 *g* for 20 minutes and the filtrate collected at the bottom collector of Vivaspin® tube was analysed by HPLC. The percentage of HPO unbound to protein in brain homogenate, plasma and perfusate, was calculated as showed in **Equation 2.1.4**.

$$\%\, unbound = \frac{C_f}{C_c}\, X\, 100 \qquad \textbf{Equation 2.1.4}$$

Where C_f = concentration of HPO in filtrate (µM) and C_c = concentration of HPO for control (µM).

The extent of unbound HPO in perfusion fluid was compared with pooled rat plasma as showed in **Figure 2.1.17**. There was no difference between plasma and perfusion fluid unbound concentration for all of the HPOs tested. Indeed, it has generally been accepted that plasma albumin primarily governs the binding of drug in blood circulation (Gurevich, 2013, Weiss et al., 2006, Smith et al., 2010, Bohnert and Gan, 2013). This justifies the addition of physiological concentration of BSA (40 g/L) into the normal Ringer's solution for brain perfusion to mimic *in vivo* plasma content (**Table 2.1.1**). FCF132, CN116 and CN118 showed no or limited binding in plasma and perfusion fluid (86–100% unbound

concentration). CP84, CN126, CN128 and CN228 were between 54–69% unbound in plasma and perfusion fluid. CN228 and CP20 have 50% or less in unbound state in plasma and perfusion fluid with CP20 in perfusion fluid showed the least unbound (45%). For all of the HPOs evaluated, percentage unbound in perfusion fluid was always less than percentage unbound in plasma although this was not significantly different.

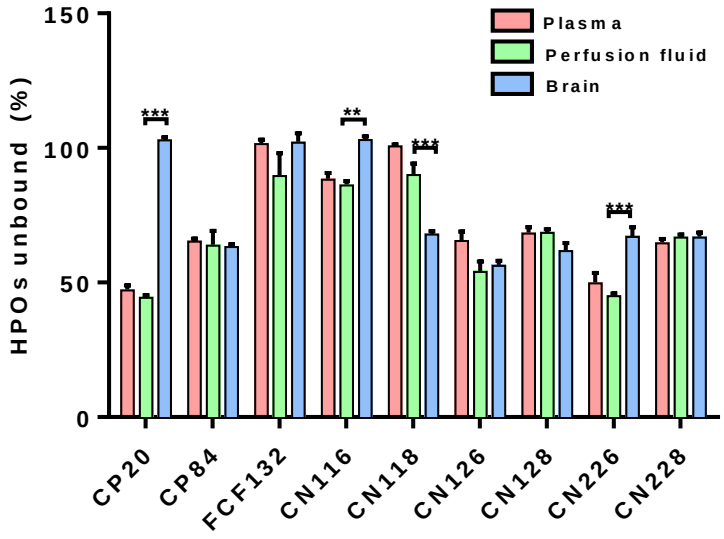

Figure 2.1.17: Percentage of free-unbound HPOs in perfusate, plasma and brain homogenate.

*HPO were spiked into pooled diluted [1:3 (w/v) dilution] brain homogenate. Data are expressed as mean+SEM. n=3 different determinations. No significant different P> 0.05 (plasma vs perfusion fluid; unpaired t-test, two-tailed),** P< 0.01, *** P< 0.001 (perfusion fluid vs brain; unpaired t-test, two-tailed).*

CP20, FCF132 and CN116 showed 100% unbound in the brain (**Figure 2.1.17**). CP84, CN118, CN128, CN226 and CN228 were moderately unbound in brain (62–68%). CN126 showed the least unbound among all other HPO in the brain (57%). As opposed to drug binding to albumin in blood, drug binding in brain is primarily governed by the lipid constituent of brain tissues. This is because, brain has a lower composition of protein (8% vs 18%) and higher lipid composition than blood (11% vs 0.7%; Jeffrey and Summerfield, 2007). CP20, CN116 and CN226 unbound concentration in brain was higher by 2-fold, 1.2-fold and 1.4-fold respectively than perfusion fluid. In contrast, CN118 unbound in brain was 1.3-fold lower than in perfusion fluid. Other HPO (CP84, FCF132, CN126, CN128 and CN228) showed the same degree of binding in perfusion fluid and brain. The fraction of

HPO unbound was taken into account during brain uptake calculation as was described in **Section 2.1.10**.

In order to see any relationship between free, unbound HPO with lipophilicity (cLogP), regression analysis was performed on the unbound HPO against cLogP plot. The percentage unbound HPO in plasma, perfusion fluid and brain homogenate were less as the lipophilicity constant (cLogP) increased (**Figure 2.1.18**).

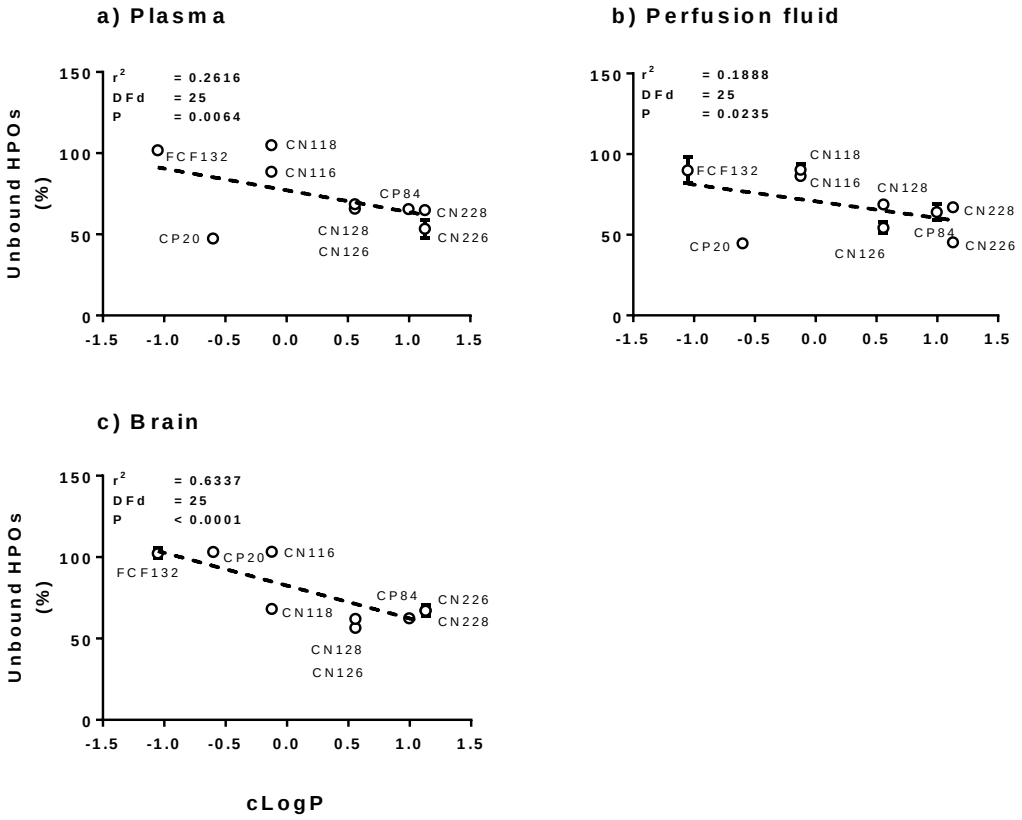

Figure 2.1.18: Relationship between free unbound HPO with HPO cLogP.

*Unbound HPO were plotted against HPO lipophilicity (cLogP). **Black circle** (○) represents unbound HPO in graphs **a)** pooled plasma, **b)** perfusion fluid and **c)** pooled brain homogenate. **Black dotted line (…)** represents best-fit line for regression analysed on compounds represented by **black circle** (○) in graph **a)**, **b)** and **c)**. HPO cLogP were obtained using a ChemDraw Software version 15.1. Data are expressed as mean±SEM (n=3 tubes). Significant difference for linear regression analysis was set at P<0.05. Co-efficient of variation (r^2), degree of freedom (df; 25) and P values were calculated using linear-regression analysis (GraphPad Prism 7 Software).*

The relationship was strongest in the brain followed by plasma while perfusion fluid showed the weakest relationship with cLogP. In plasma and perfusion fluid, unbound CP20 was the outlier that contributed to a weaker relationship with cLogP. cLogP has been

shown to be the dominant factor in determining the brain tissue binding due to its higher lipid content than blood (Wan et al., 2007, Jeffrey and Summerfield, 2007).

In summary, it can be concluded that there was a significant inverse relationship between the degree of HPO cLogP and unbound HPO in plasma, perfusion fluid and brain homogenate that was going to influence the total uptake of HPO into the brain.

2.1.11 *Brain uptake calculation*

a) ^{3}H-OMG and ^{14}C-sucrose

Disintegration per minute (DPM) was taken to show the rate of radioactive decay. Total brain uptake (R_{total}) of ^{14}C-sucrose and ^{3}H-OMG was calculated by finding a ratio between concentration in whole brain (C_{Br}) or capillary depleted brain (C_{Cd}) (DPM/g) and concentration in perfusate, C_{Pf} (DPM/mL), **Equation 2.1.5**.

$$R_{Br,total}\ or\ R_{Cd,total}\ (mL/g) = \frac{C_{Br}\ or\ C_{Cd}\ (DPM/g)}{C_{Pf}\ (DPM/mL)} \qquad \textbf{Equation 2.1.5}$$

Similarly, ^{14}C-sucrose confined in vasculature was also calculated, **Equation 2.1.6.**

$$R_{sucrose}(mL/g) = \frac{C_{sucrose}\ (DPM/g)}{C_{Pf}\ (DPM/mL)} \qquad \textbf{Equation 2.1.6}$$

$R_{sucrose}$ were subtracted from $R_{Br,total}$ and $R_{Cd,total}$ to give a net brain uptake, R_{Br} or R_{Cd}, **Equation 2.1.7**.

$$R_{Br}\ or\ R_{Cd}(mL/g) = R_{Br,\ total}\ or\ R_{Cd,\ total} - R_{sucrose} \qquad \textbf{Equation 2.1.7}$$

The rate of brain uptake $K_{in,}$ was calculated only for capillary depleted brain dividing with total perfusion time in minute (*t*), **Equation 2.1.8**.

$$K_{in,Cd}\ (mL/g/min) = \frac{R_{Cd}\ (mL/g)}{t\ (min)} \qquad \textbf{Equation 2.1.8}$$

Figure 2.1.19 showed the example of brain uptake calculation for ^{3}H-OMG.

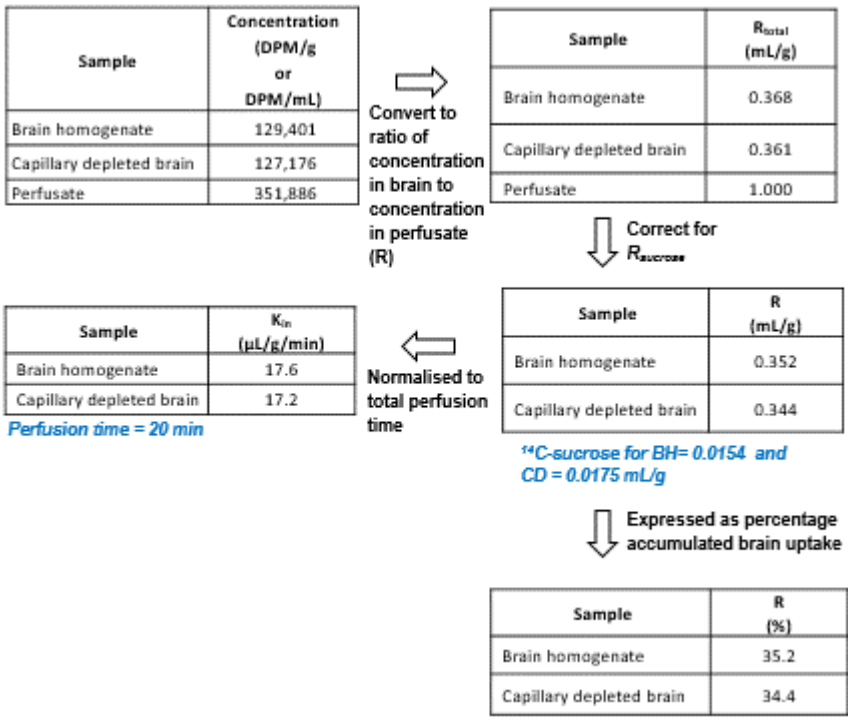

Figure 2.1.19: Example of calculation for ^{3}H-OMG R_{Cd} and $K_{in,Cd}$.

b) HPO

HPO percentage unbound in perfusion fluid and brain was determined *in vitro* as described in **Section 2.1.10**. Total brain uptake ($R_{Br,\ total}$ and $R_{Cd,\ total}$) was calculated by finding a ratio between concentration in whole brain (C_{Br}) or capillary depleted brain (C_{Cd}) (nmol/g) and concentration in perfusate (C_{Pf}) (nmol/mL).

$$R_{Br,\ total}\ or\ R_{Cd,\ total}\ (mL/g) = \frac{C_{Br}\ or\ C_{Cd}\ (nmol/g)}{C_{Pf}\ (nmol/mL)} \qquad \textbf{Equation 2.1.9}$$

$R_{sucrose}$ were subtracted from $R_{Br,total}$ and $R_{Cd,total}$ to give a net brain uptake, R_{Br} or R_{Cd}, as described in **Equation 2.1.7**.

HPO concentration in perfusion fluid were corrected for percentage unbound as only free HPO were able to cross the BBB. Net brain uptake corrected for HPO unbound in perfusate ($R_{Br,u}$ and $R_{Cd,u}$) was calculated by dividing with percentage HPO unbound in perfusate (Pf_u).

$$R_{Br,u}\ or\ R_{Cd,u}\ (mL/g) = \frac{R_{Br}\ or\ R_{Cd}\ (mL/g)}{Pf_u} \qquad \textbf{Equation 2.1.10}$$

$R_{Br,u}$ and $R_{Cd,u}$ described the transport properties at BBB and brain affinity towards HPO. $R_{Cd,u}$ was used to calculate the rate of brain uptake, $K_{in,Cd,u}$ by dividing with the total perfusion time in minute (*t*) as described by **Equation 2.1.11**.

$$K_{in,Cd,u}\ (mL/g/min) = \frac{R_{Cd,\ u}\ (mL/g)}{t\ (min)} \qquad \textbf{Equation 2.1.11}$$

Additionally, both HPO concentration in perfusate and capillary depleted brain were corrected for percentage unbound and described as $R_{Cd,uu}$ (**Equation 2.1.12**).

$$R_{Cd,uu}\ (mL/g) = R_{Cd}\ X\ \frac{Br_u}{Pf_u} \qquad \textbf{Equation 2.1.12}$$

$R_{Cd,\ uu}$ was used to describe the extent of distribution of unbound HPO in brain tissue. $R_{Cd,\ uu}$ was used to calculate the rate of brain uptake, $K_{in,cd,uu}$ by dividing with the total perfusion time in minute (*t*) as described by **Equation 2.1.13**.

$$K_{in,Cd,uu}\ (mL/g/min) = \frac{R_{Cd,\ uu}\ (mL/g)}{t\ (min)} \qquad \textbf{Equation 2.1.13}$$

The concepts of these brain uptake parameters are explained in more detailed in the following Section (**Section 2.1.11**). **Figure 2.1.20** showed the example of brain uptake calculation for CP20.

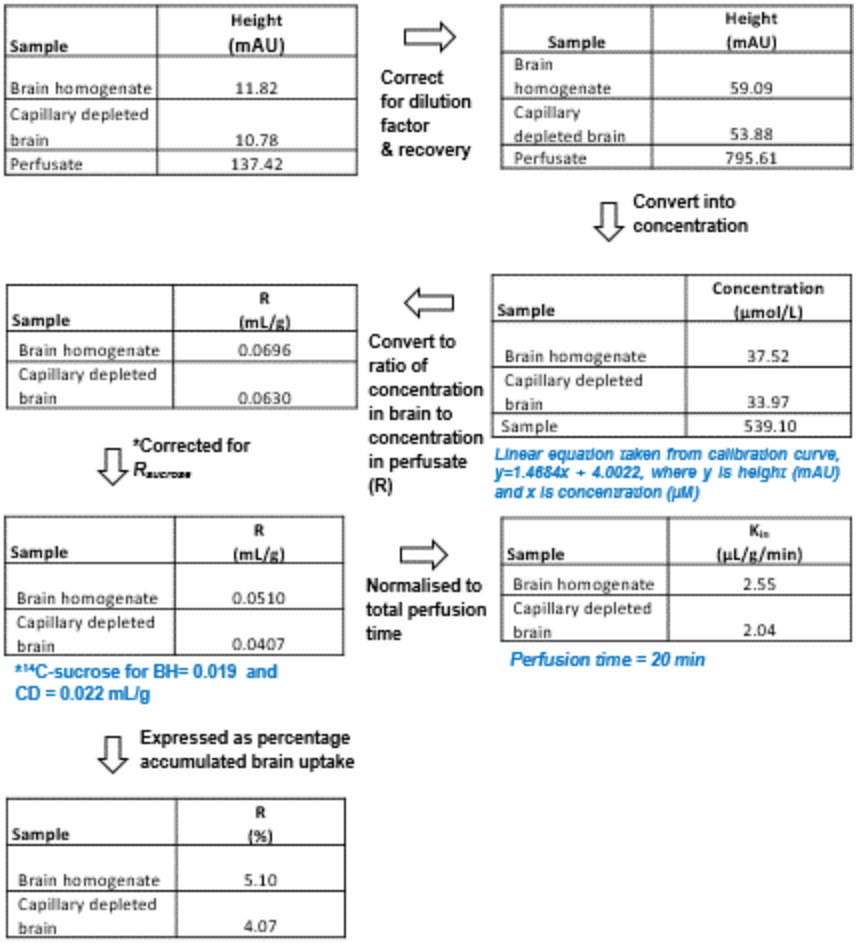

Figure 2.1.20: Example of calculation for CP20 $R_{Cd,u}$ and $K_{in,Cd,u}$

2.1.12 *Concepts and description of brain uptake parameters*

Two main brain uptake parameters arises from the brain uptake calculation for HPO (**Section 2.1.11**) namely brain uptake from unbound compound in perfusate, in whole brain ($R_{Br,u}$) and in capillary depleted brain ($R_{Cd,u}$). $R_{Br,u}$ includes total brain uptake in brain capillary endothelial cells (BCEC) and brain parenchyma. $R_{Cd,u}$ is total brain uptake in brain parenchyma only since BCEC was removed through differential centrifugation with 15% (w/v) dextran (**Section 2.1.7**). Differences between $R_{Br,u}$ and $R_{Cd,u}$ showed the degree of trapping of compound in BCEC (Triguero et al., 1990). Compounds trapped in BCEC were not considered as to have crossed the BBB since BCEC is the component of the BBB itself. Therefore, it was important to evaluate this phenomenon to avoid false positive results.

$R_{Cd,u}$ describes the transport properties at BBB and the affinity of brain for HPO (Loryan et al., 2016, Hammarlund-Udenaes et al., 2008, Friden et al., 2007). Correction for HPO

unbound in both perfusate and in capillary depleted brain give rise to another parameter, $R_{Cd,uu}$ that is independent of binding to protein and lipid. This parameter describes the distribution of unbound HPO in brain tissue at the terminal perfusion time point. Therefore, this parameter is useful in describing the level of pharmacologically unbound (presumed to be active) HPO in brain tissue (Loryan et al., 2016, Hammarlund-Udenaes et al., 2008, Friden et al., 2007). In summary, $R_{Cd,u}$ and $R_{Cd,uu}$ parameters were used in this thesis to describe the brain uptake at the BBB and to calculate the rate of brain uptake ($K_{in,Cd,u}$ and $K_{in,Cd,uu}$).

2.1.13 *Patlak plot*

$R_{Br,\ u\ total}$ and $R_{Cd,\ u\ total}$ was plotted against multiple terminal perfusion times to determine the linearity of brain uptake as described by Patlak (Patlak et al., 1983, Patlak and Blasberg, 1985). Linear regression analysis was performed on the linear portion of the points and the linear equation, $y = mx + C$ was expressed as:

$$R_t = K_{in}\,(t) + V_{Vas} \qquad \textbf{Equation 2.1.13}$$

Where R_t is the total brain uptake at time t, K_{in} is the unidirectional rate constant, t is the perfusion time and V_{vas} is the vascular luminal space of brain capillaries. **Figure 2.1.21** showed a Patlak plot for CP20. CP20 showed a linear brain uptake up to 60-minute perfusion. Linear regression analysis using all the point gives a linear equation $y = 1.265x + 2.819$. This showed that K_{in} and vascular space expressed respectively as mass/volume/time and volume/mass were 12.65 µL/min/g and 0.028 mL/g.

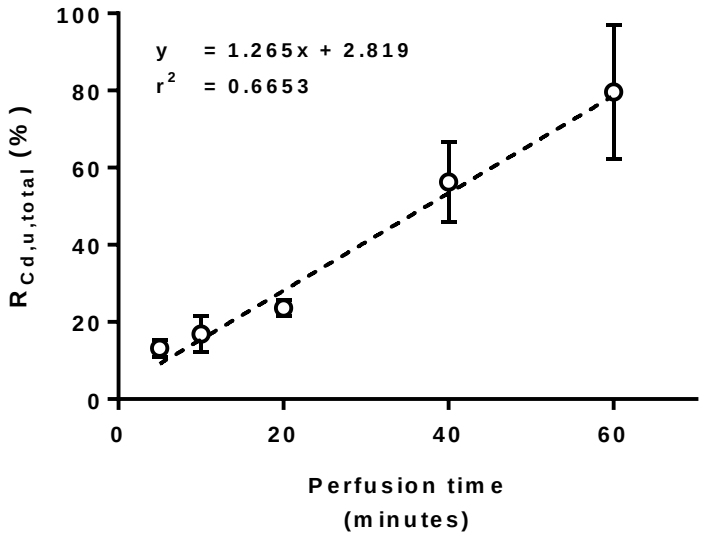

Figure 2.1.21: Example of Patlak plot for CP20 in rat brain.

Each point represents $R_{Cd,\,u}$ for CP20 plotted against respective terminal perfusion time. The data was not corrected for $R_{sucrose}$. Each point represents the mean±SEM (n=3-10 rats). Data was analysed by least square regression analysis (GraphPad Prism 7 Software). Degrees of freedom (Df; n-2) = 26.

2.1.14 *Linearity of brain uptake*

It is important to determine the linearity of brain uptake especially for HPO since the rate of brain uptake can only be reliably measured before HPO reaching the steady-state (SS) concentration in the brain. $R_{Br,u,total}$ and $R_{Cd,u,total}$ for 5, 10, 20, 40 and 60 minutes were plotted as a Patlak plot as showed in **Figure 2.1.22.** Both brain uptake profiles are not significantly different from each other, which indicate no significant trapping of HPO in the BCEC (Triguero et al., 1990). $R_{Cd,u}$ showed brain uptake beyond the BBB, and thus was explained further in the following paragraph.

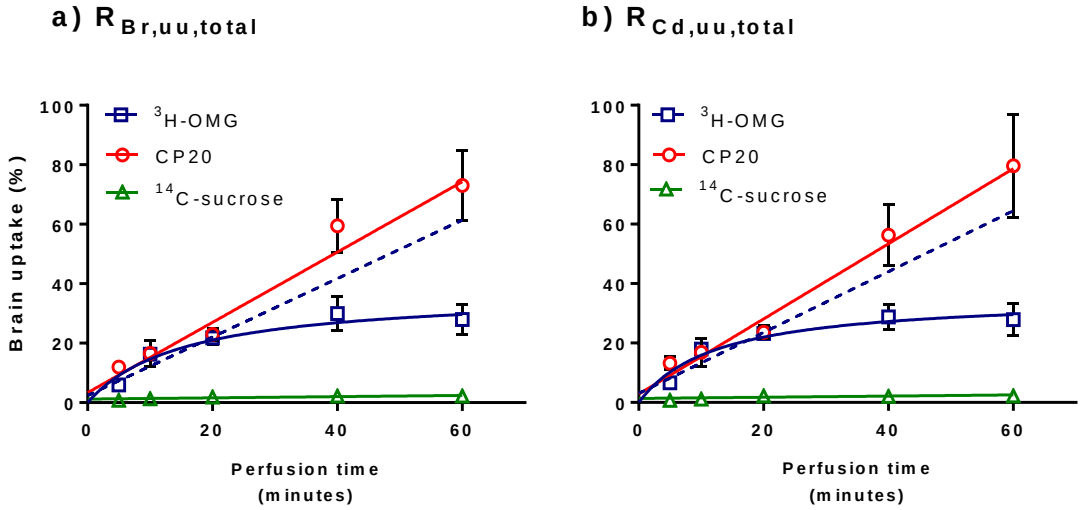

Figure 2.1.22: Patlak plot for ^{3}H-OMG, CP20 and ^{14}C-sucrose in rat brain.

a) *$R_{Br,u,total}$ for ^{3}H-OMG, CP20 and ^{14}C-sucrose was plotted against multiple perfusion times.* ***b)*** *$R_{Cd,u,total}$ for ^{3}H-OMG, CP20 and ^{14}C-sucrose was plotted against multiple perfusion times.* ***Blue square*** *(□) represents brain uptake for ^{3}H-OMG.* ***Red circle*** *(○) represents brain uptake for CP20.* ***Green triangle*** *(△) represents brain uptake for ^{14}C-sucrose. Data are expressed as mean±SEM (n=3-18 rats). The* ***blue line*** *represent best-fit of data at multiple perfusion time (5, 10 and 20 minutes) while the* ***red*** ***and*** ***green*** ***lines*** *represent best-fit of data at multiple perfusion time (5, 10, 20, 40 and 60 minutes) analysed by linear regression analysis (GraphPad Prism 7 Software). The* ***dotted blue line*** *represent the best-fit of data at multiple perfusion time analysed by non-linear fit analysis (competitive inhibition, GraphPad Prism 7 Software).*

a) ^{14}C-sucrose

The range of vascular space values during 5 to 60 minutes *in situ* brain perfusion were between 0.01-0.02 mL/g. This correspond with previously reported studies which showed ^{14}C-sucrose vascular space fell between 0.01-0.04 mL/g (Triguero et al., 1990, Zlokovic et al., 1994, Pardridge et al., 1990).^{14}C-sucrose was used as a negative control to confirm the integrity of the BBB because of it hydrophilicity and the lack of specific carrier at the BBB which render it to confine only in the vascular space (Ennis and Betz, 1986). Additionally, ^{14}C-sucrose was also employed as a vascular space marker to differentiate between brain capillary lumen space and brain parenchyma space after brain homogenisation take place (Triguero et al., 1990, Lockman et al., 2003). Selection of vascular space marker with suitable molecular weight is important to represent the vascular space of co-administered HPO. ^{14}C-sucrose has a molecular weight of 342.3 g/mol. The molecular weight falls within the range of tested compounds [^{3}H-OMG (194

g/mol) and hydroxypyridinones (139 to 363 g/mol)] making ^{14}C-sucrose appropriate as a vascular space marker in this study.

b) ^{3}H-OMG

^{3}H-OMG showed a linear uptake up to 20-minutes perfusion before reaching plateau afterwards. Maximum ^{3}H-OMG accumulated uptake was approximately 29**%** of the concentration perfused (**Figure 2.1.22b**). ^{3}H-OMG is a substrate for glucose transporter (GLUT1) and was employed as a positive control and as a functional indicator of intact BBB in respect of carrier-mediated transporter. As with the ^{14}C-sucrose, ^{3}H-OMG is a hydrophilic compound which would not crossed the BBB. However, GLUT1 carrier was expressed at the BBB to transport glucose from blood to brain down the concentration gradient (Reyes et al., 2002). ^{3}H-OMG is a non-metabolised derivative of glucose, thus make it suitable for quantification for brain uptake via GLUT1 transporter (Jay et al., 1990).

c) CP20

Since the novel HPO were designed based on CP20 structure, it was used as a model of HPO brain uptake. CP20 uptake was linear for up to 60-minutes perfusion time. Maximum accumulated brain uptake at the terminal time point (60 minutes) was approximately 80% of the concentration perfused (**Figure 2.1.22b**). CP20 showed increase accumulation in the brain over the perfusion time (5 to 60 minutes) confirming the linearity of the brain uptake for reliable determination of K_{in}. CP20 has been previously reported to penetrate the brain (Fredenburg et al., 1996, Roy et al., 2010)**.** Indeed, a ground-breaking pilot clinical study in Parkinson's disease patients that were administered with 30 mg/kg/day for 36 months attenuates disease symptoms and analysis with T* MRI showed a reduction of iron in basal ganglia, demonstrating that deferiprone entered the brain to chelate and re-distributed iron (Abbruzzese et al., 2011).

Regression analysis performed on ^{3}H-OMG and CP20 Patlak plot revealed that the rate of uptake in the capillary depleted brain were 10.2 and 12.7 µL/min/g respectively (**Table 2.1.7**). The vascular space (V_{vas}) obtained from the *y*-intercept of least-square linear regression analysis for ^{3}H-OMG and CP20 agreed with the published data (Roy et al., 2010, Triguero et al., 1990, Zlokovic et al., 1994, Pardridge et al., 1990).

Table 2.1.7:Rate of brain uptake in capillary depleted brain for ^{3}H-OMG and CP20, and the respective brain vascular space derived from linear regression analysis on Patlak plot (Figure 2.23b).

	^{14}C-sucrose	^{3}H-OMG	CP20
$K_{in,Cd,u}$ (µL/min/g)	0.2±0.1	10.2±1.9 ***	12.7±1.8 ***
V_{vas} (mL/g)	0.01±0.38	0.03±0.06	0.03±0.02
V_{vas} (%)	1.0	3.0	3.0
r^2	0.0671	0.5835	0.6653
p	0.1216	< 0.0001	< 0.0001
df (n-2)	35	20	26

*Least-square linear regression analysis was performed on the linear portion of Patlak plot in **Figure 2.2.22b**. Linear portion for ^{3}H-OMG was from 5 to 20 minutes perfusion. Linear portion for CP20 and ^{14}C-sucrose was from 5 to 60 minutes perfusion. ^{14}C-sucrose $K_{in,Cd,u}$ showed rate of distribution in brain capillary lumen rather than brain uptake. Data are expressed as mean±SEM (n=22-37 rats). p< 0.001 compared to CP20 (one-way ANOVA followed by Tukey's multiple comparison test). Significant difference for linear regression analysis was set at P<0.05. Co-efficient of variation (r^2), degree of freedom (df: n-2) and p values were calculated using linear-regression analysis (GraphPad Prism 7 Software).*

Base on multiple times point uptake presented in **Figure 2.1.22b**, 20 minutes was selected as the terminal perfusion time point for other novel HPO iron chelators. This is because, at 20 minutes, the brain uptake was still in the linear portion for a reliable estimation of K_{in}. Furthermore, HPO accumulated in the brain at 20-minute time point give enough sensitivity to be detected by HPLC-UV analysis. What most important is the vascular space showed by ^{14}C-sucrose and uptake of ^{3}H-OMG at 20 minutes strongly suggest that the BBB was physiologically intact and functional.

$R_{Cd,\ u,\ total}$ for 20-minutes perfusion for ^{3}H-OMG, CP20 and ^{14}C-sucrose depicted in **Figure 2.1.22b** was extracted and plotted into bar graph as shown in **Figure 2.1.23**. The $R_{sucrose}$ that represent the capillary space was subtracted from ^{3}H-OMG and CP20 $R_{Cd,\ u,\ total}$.

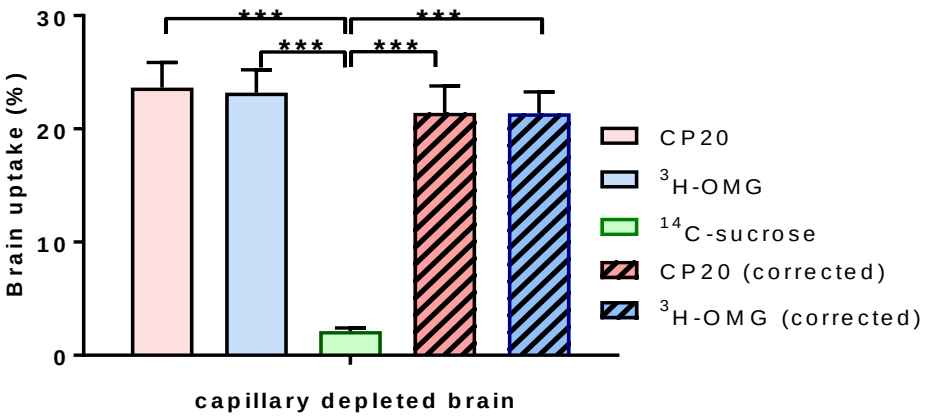

Figure 2.1.23: Brain uptake at 20-minutes perfusion time for ^{3}H-OMG and CP20 in capillary depleted brain before ($R_{Cd,u,total}$) and after ($R_{Cd,u}$) correction with ^{14}C-sucrose vascular space.

*Striped bar graphs depict brain uptake that was corrected for ^{14}C-sucrose vascular space. Data are expressed as mean±SEM (n=10-18 rats). ** P< 0.01, *** P< 0.001 compared to CP20 (corrected) (one-way ANOVA followed by Dunnett's test).*

The initial rate of uptake ($K_{in,Cd,u}$) for 20 minutes was calculated as described in **Section 2.1.11**. The $K_{in,Cd,u}$ obtained from 20-minute perfusion showed no different from the results obtained from linear regression analysis of Patlak plot (**Table 2.1.8**). This strongly suggests that the methods and analysis used in this study were validated where the $R_{sucrose}$ value reflecting the vascular space (V_{vas}) for CP20 derived from Patlak plot.

Table 2.1.8: Comparison between $K_{in,Cd,u}$ for ^{3}H-OMG and CP20 calculated by single-time point (20 minutes) or regression analysis on Patlak plot (Figure 2.23b).

$K_{in,Cd,u}$ (µL/min/g)	^{3}HOMG	CP20
Patlak plot	10.2±1.9	12.7±1.8
Single-time point	10.7±1.0	10.7±1.2

Data are expressed as mean±SEM (n=10-36 rats). Statistical analysis using showed no significant different, p> 0.05 (unpaired t-test,two-tailed).

To summarise, *in situ* brain perfusion was validated prior to brain permeability evaluation of novel HPO. These include measurement of pH, gas and ions in whole blood and perfusate in rats. After *in situ* brain perfusion, brain was taken out and the blood capillary associated with brain tissues was separated by density centrifugation with 15% (w/v) dextran. Following this, alkaline phosphatase specific activity was assessed in some of

the capillary depleted brain to confirm the success of separation. HPO that get into the brain after perfusion was extracted with 10 % (v/v) TFA. Recovery of HPO after extraction with TFA in brain and perfusate samples was measured with HPLC quantification method. Free-unbound concentration of HPO in perfusate and brain homogenate was evaluated in separate *in vitro* experiment whereby HPO were incubated with perfusate (NRS) or naïve rat brain homogenate followed by membrane-ultrafiltration. Results from this experiment were used to correct for unbound HPO in perfusate and brain.

Experiment performed with CP20 at 5, 10, 20, 40 and 60 minutes showed linear uptake with tight and functional BBB (**Figure 2.1.22**). Following this, *in situ* brain perfusion were conducted in Male Wistar rats to evaluate permeability of novel HPO iron chelators using 20 minutes as the optimum perfusion time due to linearity of brain uptake and adequate sensitivity for HPO measurement by HPLC-UV analysis.

2.1.15 *Optimised and validated protocol for in situ brain perfusion*

This section explained the final protocol used for *in situ* brain perfusion for evaluation of novel HPO iron chelators, after optimisation and validation processes. Rats were anaesthetised with 50 mg/kg ketamine and 0.2 mg/kg medetomidine, *i.p.*, and maintained at 37 °C using a heating pad (**Figure 2.1.1**). Whilst in a supine position, rats were injected with 100,000 U/kg heparin (*i.p)*. Local anaesthetic, lignocaine/adrenaline was then injected subcutaneously (*s.c.*) at five multiple sites (total dose was 20 and 12.5 mg/kg) on the area of the chest. Common carotid arteries on the left and right sides were isolated one at a time. Two loose ligatures on the anterior and posterior part of each common carotid artery were added. Sequentially, jugular veins on both sides were isolated with a pair of forceps (**Figure 2.1.2**). Posterior loose ligature was tightened and a small incision with Vanna scissors was performed just above the tightened ligation. Cannula with flowing oxygenated NRS at 1.44 mL/min rate was inserted through the incision. At the same time, the jugular vein was severed to allow the drainage of the perfusate. The anterior ligature was tightened to secure the cannula in place. The NRS was allowed to perfuse for at least three minutes to wash out the blood. The same procedure was repeated for the contralateral common carotid artery.

Infusion of novel HPO iron chelators was started when both common carotid arteries were cannulated with slow drive syringe pump that joined the main NRS circulation at 0.16

mL/min rate. The total flow rate that reach the end of the cannula was 1.6 mL/min. *In situ* brain perfusion with iron chelators were performed for 20 minutes after which the cannulas were removed from the arteries. Perfusate flowing out from the end of the cannulas were collected every time after completion of brain perfusion. Following this the rats were decapitated, and the brain was removed immediately for sample processing and analysis as described previously in **Section 2.1.7** and **Section 2.1.8.**

2.2 *Determination of neurotoxins IC_{50} and HPO toxicity for neuroprotection studies using neuroblastoma cell lines (SH-SY5Y)*

2.2.1 *Introduction*

In vitro models of Parkinson's disease (PD) are often used as a preliminary tool in the discovery of neuroprotection agents. The most utilised *in vitro* model of PD is the dopaminergic neuroblastoma cell line, SH-SY5Y (Xicoy et al., 2017). It is widely employed due to its catecholaminergic nature, which is relevant to the pathogenesis of PD in the general population of PD patients (Hasegawa et al., 2003, West et al., 1977). Historically, the SH-SY5Y cell line was derived from a third successive sub-clone (SH-SY → SH-SY5 → SH-SY5Y) of metastatic bone tumour biopsy (SK-SN-SH) of a 4-year old female with a neuroblastoma in 1973 (Kovalevich and Langford, 2013a). The SH-SY5Y cell line was preferred as an *in vitro* tool in neuroprotection study over neuronal primary culture such as primary mesencephalic cell or primary cortical neuron because of its ease of growing in the laboratory, stability for higher passage number and with limited contamination with glial cells (Xicoy et al., 2017). Furthermore, due to its wide acceptance and extensive use among the research community, comparison and reference with other similar types of work are possible.

Typically, in the *in vitro* PD model for neuroprotection study using SH-SY5Y, cells were exposed to several different types of toxin to mimic the pathological event *in vivo* that lead to cell death. Each toxin is unique in terms of mechanism that causes the cell death. Therefore, selection of different types of toxins would give an insight into the way the neuroprotective agents work. The current study employed hydrogen peroxide (H_2O_2), 6-hydroxydopamine (6-OHDA), MG132 and iron [ferric nitrolotriacetate (FeNTA)] as neurotoxins. This introduction section described the mechanism on how these neurotoxins cause cell death.

a) H_2O_2

H_2O_2 is the most commonly used toxin to create oxidative stress in *in vitro* research. H_2O_2 is a ubiquitous molecule that is continuously produced during mitochondria respiration (Giorgio et al., 2007). It is soluble in water and readily permeate biological membranes. In

the cell, H_2O_2 is produced either spontaneously or catalytically by superoxide dismutase (SOD) from the superoxide radical ($O_2^{\bullet-}$) that is released specifically from the Complex I or Complex III of the mitochondria respiratory chain. This endogenous molecule is metabolised immediately after production by enzyme catalase, glutathione peroxidase (GPx) or peroxiredoxin to water and/or molecular oxygen (Rocha et al., 2015). H_2O_2 *per se* is mildly toxic relative to other neurotoxins, however, during oxidative stress, production of H_2O_2 increases as catalase fails to inactivate H_2O_2 efficiently due to saturation of the active site. In this situation, probability for H_2O_2 to react with endogenous iron via Fenton reaction also increases (**Reaction 2.2.1**). The Fenton reaction occurs spontaneously to produce highly reactive hydroxyl radical ($OH^{\bullet-}$). In the presence of $O_2^{\bullet-}$ that was concomitantly produced as a by-product of mitochondria respiration, Fe^{3+} is reduced to Fe^{2+} by Heber-Weiss reaction (**Reaction 2.2.2**). In this condition, a vicious cycle of $OH^{\bullet-}$ production occurs.

$$H_2O_2 + Fe^{2+} \longrightarrow OH^{\cdot-} + OH^- + Fe^{3+} \qquad \textbf{Reaction 2.2.1}$$

$$O_2^{\cdot-} + Fe^{3+} \longrightarrow O_2 + Fe^{2+} \qquad \textbf{Reaction 2.2.2}$$

$OH^{\bullet-}$ species primarily contributes to cell death by membrane lipid peroxidation that cause disintegration of cells and by interaction with DNA that interrupts the production of essential proteins. Loss of membrane integration disrupts the homeostatic balance of physiological ions. In the case of mitochondria as the production site of the $OH^{\bullet-}$, disruption of mitochondrial membrane induces releases of mitochondrial Ca^{2+} into cytoplasm that leads to activation of cell death. Similarly, the proximity of $OH^{\bullet-}$ production to mitochondrial DNA might interfere with the expression of mitochondrial respiratory chain proteins that exacerbates oxidative stress (Chinnery and Hudson, 2013). Besides the production of $OH^{\bullet-}$ from H_2O_2 degradation, H_2O_2 on its own stimulates activation of intracellular signalling pathways for cell death (Marinho et al., 2014). The combination of these cellular events eventually leads to cell death.

b) 6-OHDA

6-OHDA is a classical tool to model Parkinson's disease pathology and was initially thought to be a non-endogenous metabolite of dopamine (Jellinger et al., 1995). Interestingly, it was later found in the brain and urine of Parkinsonian patients and is

believed to form by non-enzymatic hydroxylation of endogenous dopamine in the presence of Fe^{2+} and H_2O_2; **Reaction 2.2.3** (Andrew et al., 1993, Curtius et al., 1974).

$$Dopamine \xrightarrow{H_2O_2 + Fe^{2+}} 6-OHDA \qquad \textbf{Reaction 2.2.3}$$

6-OHDA is a metabolite of dopamine that is toxic to the dopaminergic cells by two distinct but related mechanisms. The first mechanism directly generates ROS by auto-oxidation with O_2 forming *p*-quinone and O_2^- (**Reaction 2.2.4**) or through enzymatic conversion by monoamine oxidase (MAO) forming H_2O_2 (**Reaction 2.2.5**) (Soto-Otero et al., 2000, Izumi et al., 2005).

$$6-OHDA \xrightarrow{O_2} p-quinone + O_2^{\cdot -} \qquad \textbf{Reaction 2.2.4}$$

$$6-OHDA \xrightarrow{MAO} DOPAC + H_2O_2 \qquad \textbf{Reaction 2.2.5}$$

The second mechanism is by direct inhibition of electron transport chain (ETC) in mitochondrial (Glinka and Youdim, 1995, Glinka et al., 1998). Extracellular toxicity occurs primarily by ROS generation through 6-OHDA metabolism, while intracellular toxicity occurs by both ROS generation and ETC inhibition. Preliminary step of intracellular toxicity relies on the expression of dopamine transporters (DAT) express on the axon terminal of dopaminergic neurons (Lehmensiek et al., 2006, Storch et al., 2004). Inside the neuron, 6-OHDA either undergoes oxidative metabolism or directly inhibits Complex I and Complex IV of mitochondrial respiratory chain (Glinka and Youdim, 1995). Inhibition of the mitochondrial complexes generate more ROS that further exacerbates oxidative stress. Several studies revealed that *p*-quinone, an electrophile formed from 6-OHDA auto-oxidation (**Reaction 2.2.4**) might be the primary species that confers 6-OHDA toxicity (Izumi et al., 2005, Villa et al., 2013). *p*-Quinone generated extracellularly can readily penetrate the cell membrane and exert toxicity by forming protein-adduct with intracellular proteins (Miyazaki et al., 2007). Furthermore, generation of *p*-quinone causes oxidative stress through depletion of GSH and ATP levels (Villa et al., 2013). 6-OHDA can also induce the release of iron bound to ferritin, which can induce the formation of dopamine toxic metabolite, 6-OHDA, *in vivo;* **Reaction 2.2.3** (Jameson et al., 2004, Double et al., 1998). Furthermore, 6-OHDA can also modulate several proteins for intracellular iron uptake such as Nedd4 family-interacting protein 1 (Ndfip1); an adaptor protein for the

Nedd4 family of ubiquitin ligases, hepcidin; an iron binding protein and divalent-metal transporter 1 (DMT1); an iron transporter that raised the level of intracellular iron (Jia et al., 2015, Xu et al., 2016). All these cellular events lead to decrease in cell protective mechanism which results in cellular degeneration (Glinka & Youdim, 1995).

c) MG132

MG132 is a peptide-aldehyde that inhibits proteasomes enzymes complex responsible for intracellular protein degradation. As part of the ubiquitin-proteasomes system (UPS), this enzymes complex degrades intracellular proteins that are tagged with ubiquitin to smaller peptides for further degradation to amino acids and re-cycling for the synthesis of intracellular proteins. MG132 is relevant to model the pathogenesis of PD *in vitro* as mutant α-synuclein expressed in familial PD patients which tend to self-aggregate forming Lewy bodies also inhibit the proteasome (Kim et al., 2014). It has been shown that transfected cells overexpressing mutant α-synuclein were sensitised to cell death compared to non-transfected cells after exposure to MG132 (Petrucelli et al., 2002). Inhibition of proteasomes enzymes complex initiate ROS productions presumably by decreasing the turnover rate of mitochondria and thus decreasing the capacity of electron transport chain (ETC) (Sullivan et al., 2004). Increase in ROS generates more misfolded protein by oxidation with some misfolded proteins forming fibrils that can increase mitochondria membrane permeability through pore formation. These can activate another pathway for ROS generations by releasing Ca^{2+} and cytochrome *c* to the cytosol (He and Lemasters, 2002). Apart from ROS production, inhibition of the proteasome raises the level of intracellular proteins, most of which are important in intracellular signalling involving cell survival. One mechanism of MG132 that lead to cell death is by increasing the level of the short-lived tumour-suppressor protein, p53 which mediate apoptosis by decreasing its degradation (Nakaso et al., 2004). Besides tumour-suppressor proteins, other proteins involved in intracellular cell signalling such as transcription factors [e.g. nuclear factor-kappa B (NF-kB)] and cell cycle protein [e.g. cyclin A] are also modulated which favour towards activation of cell death machineries (Guo and Peng, 2013). In summary, proteasomes inhibition caused accumulation of intracellular signalling proteins and generations of free-radicals that induce cell death.

This section described the method used to grow the SH-SY5Y cells and the determination of toxins and HPOs toxicity.

2.2.2 *Human neuroblastoma cell lines (SH-SY5Y)*

Human neuroblastoma cell line (SH-SY5Y) was obtained from the European Collection of Cell Cultures (ECCC). The cells were arrived in dry ice and were grown in serum-supplemented cell culture medium, complete-DMEM (**Table 2.2.1**) on the day of arrival. SH-SY5Y cells used in this study were initially at passage 18.

Table 2.2.1: Complete cell culture medium (complete-DMEM) constituents

Component	Volume (mL)	Supplier
Dulbecco's Modified Eagle Medium (DMEM)	500	Life Technologies, UK
Fetal bovine serum (FBS)	50	Life Technologies, UK
Penicillin-Streptomycin-Neomycin (PSN) antibiotic mixture [0.5% P, 0.5% S, 0.5% N in 0.85% (w/v) saline]	6	Life Technologies, UK

To grow the cells, the cryovial containing cells suspension was thawed quickly in a water bath (Grant Instruments Ltd, UK) pre-set at 37 °C. Cell handling after this step was performed in sterile condition under a Grade II biosafety cabinet (Envair Ltd, UK). The commercially obtained SH-SY5Y cell suspension was slowly added into 10 mL complete-DMEM in a Falcon tube followed by centrifugation (ThermoFisher, UK) at 200 g for 5 minutes.

Subsequently, supernatant was removed, and the cell pellet was reconstituted in 1 mL complete-DMEM. The cells suspension was briefly triturated and added to 25 cm^2 (T25) flask coated with Nunclon Delta Surface (Nunc®; ThermoFisher, UK) containing 10 mL complete-DMEM followed by gentle shaking to distribute the cells. The cells were grown in an incubator (Panasonic Corporation, Japan) with humidified carbogen (5% CO_2 and 95% O_2), and the cells were observed under an inverted optical light microscope (Nikon TMS) at 5X magnification the following day to confirm cell attachment to flask. Medium was replaced once or twice every week with fresh complete-DMEM.

2.2.3 *Sub-culturing SH-SY5Y*

When the cells have covered approximately 80% of the surface area of the T25 flask (i.e. reaching 80% confluence) by checking under the optical light microscope at 5X magnification (**Figure 2.2.1**), they were washed with 5 mL DPBS followed by 2 mL 0.05% trypsin-EDTA in phosphate buffer (Life Technologies, UK) for 6 minutes at 37 °C in CO_2 incubator. The cell suspension was centrifuged at 200 xg for 5 minutes. The cell pellet was re-suspended with 1 mL complete DMEM after the supernatant has been discarded. After a short trituration, the cells were passage into a 75 cm^2 (T75) Nunc ® Nunclon Delta Surface flask (ThermoFisher, UK) containing 15 mL complete-DMEM.

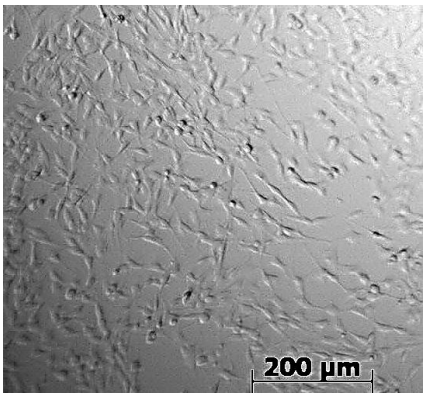

Figure 2.2.1: SH-SY5Y cells grown at approximately 80% confluence (5X magnification).

Upon reaching 80% confluence in T75 flask, the same steps of medium removal, cells trypsinisation and passaging were repeated, except that the 175 cm^2 (T175) flask with 20 mL complete-DMEM was used. After 2-3 passages, the cells grown in 175 cm^2, they were ready for use in experiments.

2.2.4 *Cells storage*

Some of the cells that were grown after receiving from commercial suppliers were stored in 1 mL cryovials (Starlab Group, UK) for future use. The storage of the cells maintained the lowest passage number relative to their sub-cultured counterparts.

For storage, cells that reached 80% confluence in T175 flask were washed with 5 mL DPBS followed by 6 mL 0.05% trypsin-EDTA for 6 minutes at 37 °C. The cell suspension was centrifuged at 200 *xg* for 5 minutes. Cells number was counted as described in detail in **Section 2.2.6** with improved Neubaeuer Brightline® 1mm deep haematocytometer

(Reichert Tecnologies, USA). The optimum cells number (3 X 10^6 cells/mL) was prepared in storage medium (40% DMEM, 40% FBS and 20% DMSO) and aliquoted (1 mL) to cryovials. The cryovials containing cells were frozen at -20 ºC (12 h), and finally stored at -70 ºC.

2.2.5 *Growing cells from storage*

Two 1 mL cryovials containing cells were removed from the -70 ºC freezer and thawed quickly in a waterbath at 37 ºC. The cells were grown in T25 flask and sub-cultured to larger flask before use in experiments as described in **Section 2.2.2** and **Section 2.2.3**.

2.2.6 *Counting cells with hematocytometer*

SH-SY5Y cells grown in T175 flask were washed when the cells reached 80% confluence with 5 mL DPBS followed by incubation with 6 mL 0.05% trypsin for 5 minutes at 37 °C. The cell suspension was centrifuged at 200 xg for 5 minutes. The cell pellet was re-suspended with 1 mL complete DMEM after the supernatant has been discarded. The cells suspension was diluted 1:49 (v/v) with 0.4% trypan blue solution prepared in 0.81% (w/v) NaCl and 0.06% (w/v) K_2HPO_4 (Sigma-Aldrich, UK). Two microliter of diluted cells-trypan blue suspension was loading at the edge of a glass coverslip on a haemocytometer. Haemocytometer contains a grid of four identical squares on each corner with 16 smaller boxes with each square can occupy 0.0001 mL cell suspension. The average of cells from the four corner squares was taken and the cells number was calculated as the following:

$$\boldsymbol{Cells\ number}\ (\boldsymbol{cells/mL}) = average\ of\ 4\ corner\ boxes \times DF \times 10^4$$ **Equation 2.2.1**

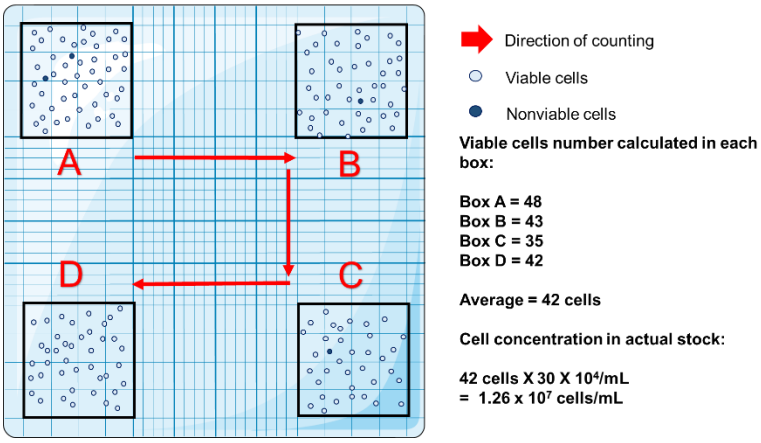

Figure 2.2.2: Example of cells number calculation with haemocytometer.

2.2.7 *Plating SH-SY5Y cells to 96-well plates*

Passage number (P) of SH-SY5Y used in this study were between P20 to P40. Whenever the cells show increase in the growth rate and resistance towards toxins, cells with lower passage number were used. Cells were diluted into several concentrations from the main cell suspension with complete-DMEM and were plated in a volume of 100 µL per well. The cells were allowed to attach to the surface of 96-well plate for at least 12 h after plating before use for experiment. The remaining stock of cells suspension was passaged to a new T175 cm^2 for the next experiments.

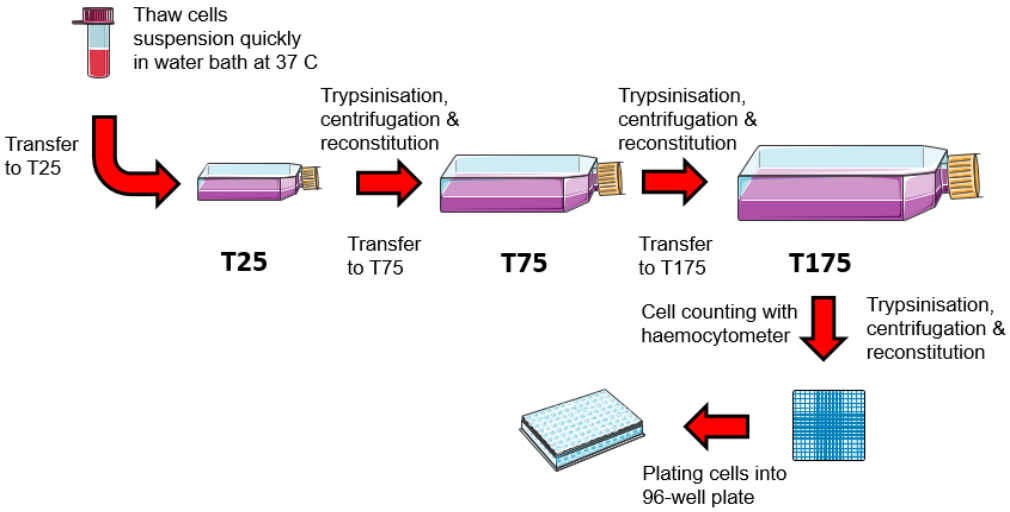

Figure 2.2.3: Schematic diagram showing steps from cells thawing, growing in flask, counting and plating into 96-well plates.

2.2.8 *Estimation of cell viability*

Cells viability was estimated with 3-(4,5-dimethylthiazol-2-yl)-2,5-diphenyltetrazolium (MTT) assay. The assay was based on the principle that viable cells could take up MTT intracellularly and reduce to insoluble purple formazan crystal by mitochondria reductase (van Meerloo et al., 2011). The formazan crystal was solubilised with dimethyl sulfoxide (DMSO) after the incubation medium removed and has a maximum absorption at 570 nm which correspond to the viable cells and mitochondrial enzyme activity (**Figure 2.2.4**).

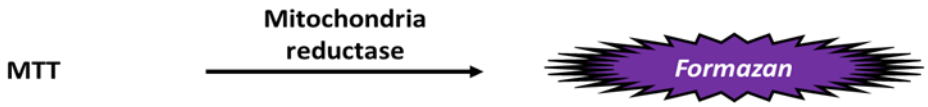

Figure 2.2.4: Schematic diagram for conversion of mitochondria reductase substrate, MTT to purple formazan that has maximal absorption at 570 nm.

MTT main stock solution (5.5 mg/mL) was prepared by dissolving in distilled water and was sonicated for 30 minutes, protected from light. The MTT main stock solution was sterile filtered using a 0.45 µm membrane with a 20 mL syringe under the biosafety cabinet. The filtered MTT main stock solution was aliquoted into microcentrifuge tubes and stored at -20 ˚C until use.

On the day of the assay, the MTT stock solution was thawed in a water bath at 37 ˚C and MTT working stock solution (0.5 mg/mL), prepared in serum-free DMEM was added to the cells in 96-well plate. The plate was then incubated for 4h in CO_2 incubator at 37 ˚C after incubation medium was removed. At the end of the incubation time, the culture medium with MTT was removed by quick inversion into a sink and slowly tapped into tissue to remove excess liquid (Morgan, 1998). DMSO (100 µL) was added into the 96-well, and lightly tapped to assist solubilisation. Absorbance at 570 nm was taken immediately and the percentage of viable cells calculated as follows:

$$Viable\ cells\ (\%) = \frac{Treated_{570nm} - Blank_{DMSO,570nm}}{Control_{570nm} - Blank_{DMSO,570nm}}\ X\ 100 \qquad \textbf{Equation 2.2.2}$$

The formation of formazan crystals as detected at 570 nm shows linear positive correlation with SH-SY5Y densities in the 96-well plates (**Figure 2.2.5**). Base on this observation, SH-SY5Y density at $1X10^5$ cells/mL was selected to be sufficient for toxicity and neuroprotection studies. The selected density was also widely reported by other literatures which makes comparison between studies feasible.

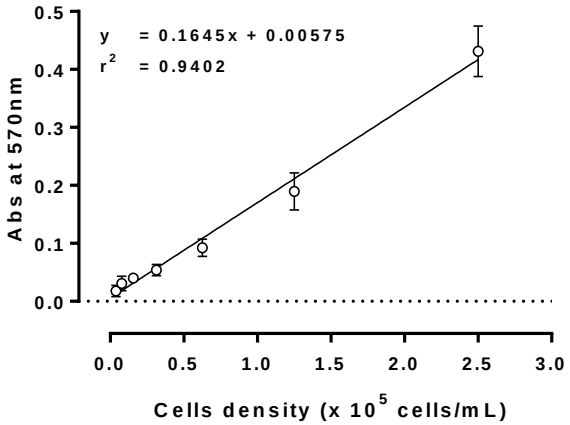

Figure 2.2.5: **Linearity of MTT absorbance at 570 nm with different cell density.**

Data are expressed as mean±SEM (n=3). Data was analysed by least-square regression analysis (GraphPad Prism 7 Software). Degrees of freedom (df) = 19.

2.2.9 *Neurotoxins*

Selected neurotoxins were used to induce SH-SY5Y cells death. The death of SH-SY5Y cells mimicked the dying dopaminergic neurons, the pathological hallmark of Parkinson's disease. Series of concentrations range were prepared for determination of concentration that caused 50% cell death (IC_{50}) by MTT assay described in **Section 2.2.8**. The IC_{50} concentration obtained were used in the neuroprotection studies.

a) Hydrogen peroxide (H_2O_2)

Working stock solution (2000 µM) for H_2O_2 was prepared from the 30% (w/v) H_2O_2 main stock solution (Sigma-Aldrich, UK) in serum-free DMEM. A series of H_2O_2 concentrations ranging from 16-1000 µM were prepared in serum-free DMEM using the H_2O_2 working stock solution and were added (100 µL) into the 96-well plate containing $1x10^5$ SH-SY5Y cells/mL. The cells were exposed to the various concentration of H_2O_2 (16-2000 µM) for 20 h in a CO_2 incubator. Cells incubated with serum-free DMEM were served as a control. After 20 h exposure to H_2O_2, the medium was removed and replaced with serum-free DMEM containing 0.5 mg/mL MTT and further incubated in the CO_2 incubators for 4 h. At the end of the incubation, the medium was removed followed by cells lysis with 100% (v/v) DMSO and the absorbance was taken at 570 nm as described in **Section 2.2.8**.

H_2O_2 started to show a concentration dependent reduction in cell viability at 125 µM and above (**Figure 2.2.6**). The IC_{50} value for H_2O_2 obtained by non-linear regression analysis was 222±33 µM which is within the range of reported values (Yeon and Kim, 2010, Ismail et al., 2012).

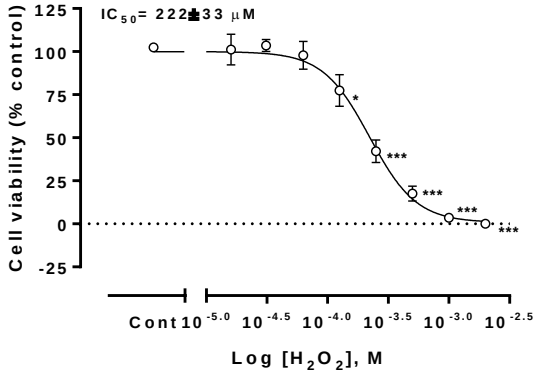

Figure 2.2.6: **Cell death of SH-SY5Y cells following exposure to H_2O_2.**

*SH-SY5Y cells were exposed to H_2O_2 (16-2000 µM) for 20h. Cell viability was assesed by the MTT assay, where untreated cells was recorded as ~100% viable and served as a control. Data are expressed as mean±SEM (n=5). Non-linear regression analysis [log(toxin) vs. response -- Variable slope (four parameters)] was performed to calculate the IC_{50} (GraphPad Prism 7 Software). Degrees of freedom (df) = 42. * p <0.05, *** p <0.001 compared to control cells (one-way ANOVA followed by Dunnett's test).*

b) 6-Hydroxydopamine (6-OHDA)

Main stock solution (50 mM) for 6-OHDA (Sigma-Aldrich, UK) was prepared in 0.3% (w/v) ascorbic acid as sodium ascorbate (Sigma-Aldrich, UK) dissolved in serum-free DMEM. 6-OHDA working stock solution (1000 µM) was prepared from the 6-OHDA main stock solution by 1:49 (v/v) dilution in serum-free DMEM. A series of 6-OHDA concentrations ranging from 4-250 µM were prepared in 0.006% (w/v) ascorbic acid in serum-free DMEM from the 6-OHDA working stock solution and were added (100 µL) into the 96-well plate containing $1x10^5$ SH-SY5Y cells/mL. The cells were exposed to the various concentration of 6-OHDA (4-250 µM) for 20 h in a CO_2 incubator. Cells incubated with 0.006% (w/v) ascorbic acid in serum-free DMEM was served as a control. After 20 h exposure to 6-OHDA, the medium was removed and replaced with free-medium containing 0.5 mg/mL MTT and further incubated in the CO_2 incubators for 4 h. At the end of the incubation, the medium removed followed by cells lysis with 100% (v/v) DMSO and the absorbance was taken at 570 nm as described in **Section 2.2.8**.

6-OHDA showed a concentration dependent reduction in cell viability at 31 µM and above (**Figure 2.2.7a**). The IC_{50} value for 6-OHDA obtained by non-linear regression analysis was 39.5±5.8 µM which is within the range of reported values (Ryu et al., 2013, Storch et

al., 2000, Shi et al., 2013, Silva et al., 2016). The final concentration of ascorbic acid added into serum-free DMEM to reduce the rate of 6-OHDA oxidation was 0.006% (w/v) chosen based on the cell viability-ascorbic acid concentration response curve, which did not cause significant cell death (**Figure 2.2.7b**). Indeed, sodium ascorbate has been reported to induce apoptosis in neuroblastoma cell lines by interfering with iron uptake (Carosio et al., 2007). In addition, report on protective effect of ascorbate on amyloid beta-exposed SH-SY5Y cells used much lower concentration of ascorbate, 0.001% (w/v) than that was used in the current study (Huang and May, 2006).

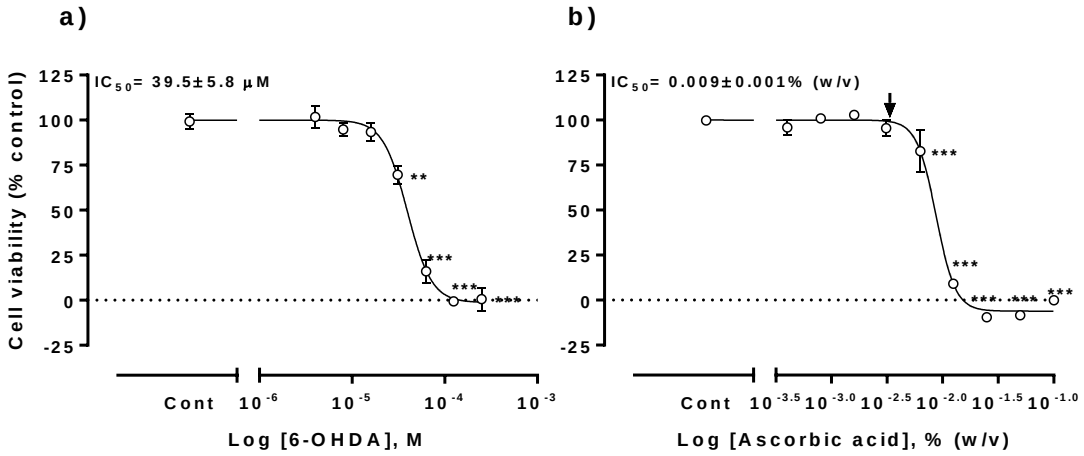

Figure 2.2.7: **Cell death of SH-SY5Y cells following exposure to 6-OHDA and L-ascorbic acid.**

SH-SY5Y cells were exposed to ***a)*** *6-OHDA (4-250 µM) and* ***b)*** *L-ascorbic acid [(0.0004-0.1% (w/v)] for 20 hours. Cell viability was assesed by the MTT assay, where* ***a)*** *cells treated with 0.006 % (w/v) ascorbic acid* ***b)*** *untreated cells were recorded as ~100% viable and served as controls. Arrowhead indicates the final L-ascorbic acid concentration chosen to protect 6-OHDA from rapid oxidation. Data are expressed as mean±SEM* ***a)*** *n=4,* ***b)*** *n=5. Non-linear regression analysis [log(toxin) vs. response-variable slope (four parameters)] was performed to calculate the* IC_{50} *(GraphPad Prism 7 Software). Degrees of freedom (df)=* ***a)*** *36 and* ***b)*** *26. ** p <0.05, *** p <0.001 compared to control cells (one-way ANOVA followed by Dunnett's test).*

c) MG132

MG132 main stock solution (1 mM) was prepared in 100% DMSO (Fisher Scientific, UK). MG132 working stock solution (10 µM) was prepared from the MG132 main stock solution by 1:9999 (v/v) dilution in serum-free DMEM. A series of MG132 concentrations ranging from 5 pM - 5 µM were prepared in 0.001% (v/v) DMSO in serum-free DMEM from the MG132 working stock solution and were added (100 µL) into the 96-well plate containing

$1x10^5$ SH-SY5Y cells/mL. The cells were exposed to the various concentration of MG132 (5 pM -10 µM) for 20 h in a CO_2 incubator. Cells incubated with 0.001% (w/v) DMSO in serum-free DMEM served as a control. After 20 h exposure to MG132, the medium was removed and replaced with free-medium containing 0.5 mg/mL MTT and further incubated in the CO_2 incubators for 4 h. At the end of the incubation, the medium removed followed by cells lysis with 100% (v/v) DMSO and the absorbance was taken at 570 nm as described in **Section 2.2.8**.

MG132 showed a concentration dependent reduction in cell viability at 0.0005 µM and above (**Figure 2.2.8a**). The IC_{50} value for MG132 obtained by non-linear regression analysis was 352±0.05 pM which is rather lower than the reported values. The reported IC_{50} values for MG132 were between 0.5 to 10 µM (Yamada et al., 2011, Nakaso et al., 2004). The higher IC_{50} values in those reports probably due to the used of cells at higher passage number as they tend to be resistant toward toxins. Unfortunately, for most reported studies employing SH-SY5Y, details on the passage number used were not provided and therefore this is not conclusive. Another possible explanation was that, repeated freezing and thawing of MG132 main stock solution may contributed to the significant loss of MG132 potency due to the fact that MG132 is a small peptide. It is believed that small peptides are prone to misconfiguration after a freezing-thawing cycles which reduced its potency (Prasad et al., 2013, Turner et al., 2011). The final concentration of 0.001% (v/v) DMSO did not significantly cause cell death (**Figure 2.2.8b**).

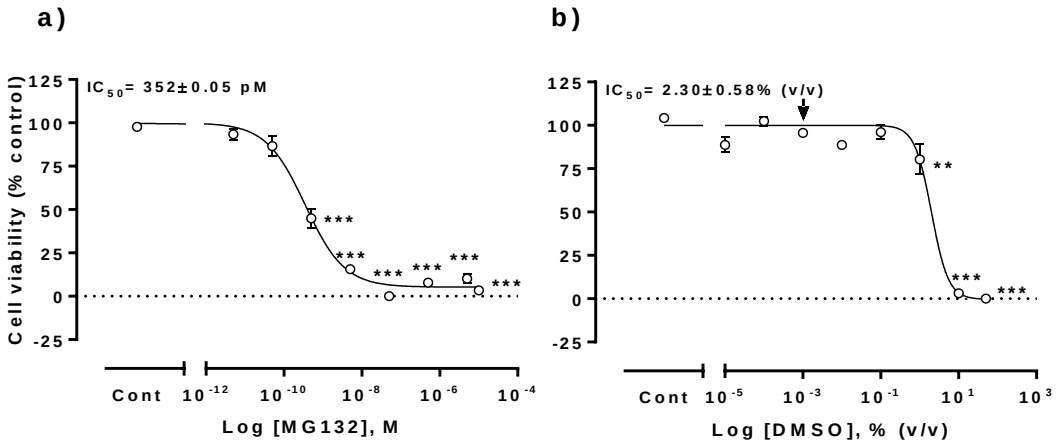

Figure 2.2.8: Cell death of SH-SY5Y cells following exposure to MG132.

SH-SY5Y cells were exposed to ***a)*** *MG132 (5 pM – 10 µM) and* ***b)*** *DMSO [0.0001-50% (v/v)] for 20 hours. Cell viability was assesed by the MTT assay, where* ***a)*** *cells treated with 0.001 % (v/v) DMSO* ***b)*** *untreated cells were recorded as ~100% viable and served as controls. Arrowhead indicates the final DMSO concentration chosen to not significantly cause cell death. Data are expressed as mean±SEM* ***a)*** *n=4 &* ***b)*** *n=3. Non-linear regression analysis [log(toxin) vs. response-variable slope (four parameters)] was performed to calculate the* IC_{50} *(GraphPad Prism 7 Software). Degrees of freedom (df)=* ***a)*** *33 &* ***b)*** *24. ** p <0.05, *** p <0.001 compared to control cells (one-way ANOVA followed by Dunnett's test).*

d) Ferric nitrolotriacetoacetate (FeNTA)

Main stock solution (12.5 mM) for ferric nitrolotriacetoacetate (FeNTA) was prepared from a combination of $FeNO_3.9H_2O$ (Sigma-Aldrich, UK) and sodium nitrilotriacaetace (NaNTA) (Santa Cruz Biotechnelogy, USA) in a 1 to 5 molar ratio (FeNTA 1:5) in 10 mM HEPES (Sigma-Aldrich, UK) according to a method described by Molina-Holgado et al. (2008). The pH of the main stock solution was adjusted to pH 7.4 with 5 M NaOH and sterile filtered (0.45 µm filter; ThermoFisher, UK) under the biosafety cabinet. The working stock solution for FeNTA (1:5; 5000 µM) was prepared in serum-free DMEM from the main stock solution. A series of FeNTA (1:5) concentrations ranging from 40-2500 µM were prepared in in serum-free DMEM from the FeNTA (1:5) working stock solution and were added (100 µL) into the 96-well plate containing $1x10^5$ SH-SY5Y cells/mL. The cells were exposed to the various concentration of FeNTA (1:5) (40-5000 µM) for 20 h in a CO_2 incubator. Cells incubated with serum-free DMEM was served as a control. After 20 h exposure to FeNTA (1:5) the medium was removed and replaced with serum-free DMEM containing 0.5 mg/mL MTT and further incubated in the CO_2 incubators for 4 h. At the end of the

incubation, the medium removed followed by cells lysis with 100% (v/v) DMSO and the absorbance was taken at 570 nm as described in **Section 2.2.8**.

FeNTA (1:5) showed a concentration dependent reduction in cell viability at 1250 µM and above (**Figure 2.2.9a**). SH-SY5Y is relatively resistance towards FeNTA (1:5) compared to other neurotoxins used in this study with an IC_{50} value obtained by non-linear regression analysis was 1082±125 µM. No reported IC_{50} values available for FeNTA (1:5) with SH-SY5Y cells. IC_{50} for FeNTA (1:5) on primary cells of mouse cortical neurons was low, 10 µM, relative to the IC_{50} obtained in this study (Molina-Holgado et al., 2008). In the same report, SH-SY5Y was also employed, however, FeNTA was not used as a toxin for SH-SY5Y cells probably because of its marked resistance towards cell death. Furthermore, IC_{50} for NaNTA derived from exposure of comparable NaNTA concentration over Fe^{3+} concentration (5 to 1 ratio) showed approximately 5-fold the IC_{50} of FeNTA (1:5) (**Figure 2.2.9b**). It can be concluded that the IC_{50} value from FeNTA was primarily due to the NTA toxicity rather than Fe^{3+} itself. NTA is a tripodal chelator for Fe^{3+} that requires 3 molecules of NTA to act as a bidentate chelator to completely chelate 1 molecule of iron (Gabričević and Crumbliss, 2003). It is possible that the interaction of NTA as a ligand for Fe^{3+} is so strong that Fe^{3+} was not available for chemical reactions. Alternatively, due to the excess molecules of NTA, availability of Fe^{3+} was limited due to efficient chelation. $Fe(NO)_3$ on its own did not kill the cells because of precipitation to form inactive $Fe(OH)_3$ at physiological pH which limit the use by its own in this study (**Figure 2.2.9c**).

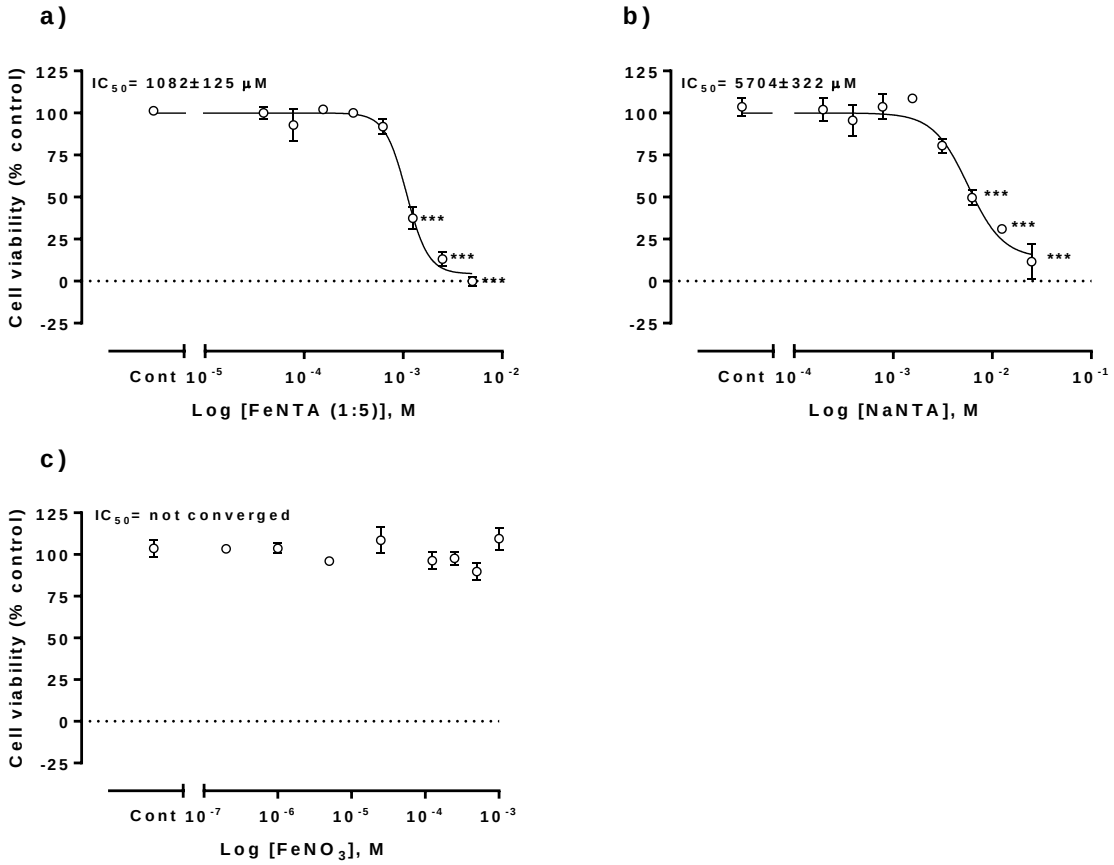

Figure 2.2.9: **Cell death of SH-SY5Y cells following exposure to FeNTA (1:5).**

SH-SY5Y cells were exposed to ***a)*** *FeNTA (1:5) (40 - 5000 µM),* ***b)*** *NaNTA (20 - 25000 µM) &* ***c)*** *$FeNO_3$ (4 - 5000 µM) for 20 hours. Cell viability was assesed by the MTT assay, where untreated cells was recorded as ~100% viable and served as a control. Data are expressed as mean±SEM* ***a)*** *n=4 ,* ***b)*** *&* ***c)*** *n=3. Non-linear regression analysis [log(toxin) vs. response-variable slope (four parameters)] was performed to calculate the IC_{50} (GraphPad Prism 7 Software). Degrees of freedom (df) =* ***a)*** *33 &* ***b)*** *24. *** p <0.001 compared to control cells (one-way ANOVA followed by Dunnett's test).*

In an attempt to lower the NTA concentration for every mole of Fe^{3+}, FeNTA was prepared as above, however by a combination of 1 to 3 molar ratio of $FeNO_3.9H_2O$ and NaNTA as reported by Iqbal et al. (2003). Several concentrations of FeNTA (1:3) were prepared and exposed to SH-SY5Y cells as described above. After 20 h exposure with FeNTA, the medium was removed and replaced with serum-free DMEM containing 0.5 mg/mL MTT and further incubated in the CO_2 incubators for 4 h. At the end of the incubation, the medium was removed followed by cells lysis with 100% (v/v) DMSO and the absorbance was taken at 570 nm as described in **Section 2.2.8**.

FeNTA (1:3) showed a concentration dependent reduction in cell viability at 625 µM and above (**Figure 2.2.10a**). The IC_{50} value for FeNTA (1:3) obtained by non-linear regression analysis was 457±32 µM. At this FeNTA (1:3) concentration, the equivalent NTA concentration is 1371 µM. The IC_{50} value derived from cell viability-NTA concentration response curve for each equivalent concentration of FeNTA (1:3) was 6383±308 µM with reduction of cells viability started at 3750 µM and above (**Figure 2.2.10b**). Exposure of 500 µM FeNTA (1:3) on hepatoma cell lines, HepG2, only killed approximately 20% of the cells population (Sakurai and Cederbaum, 1998).

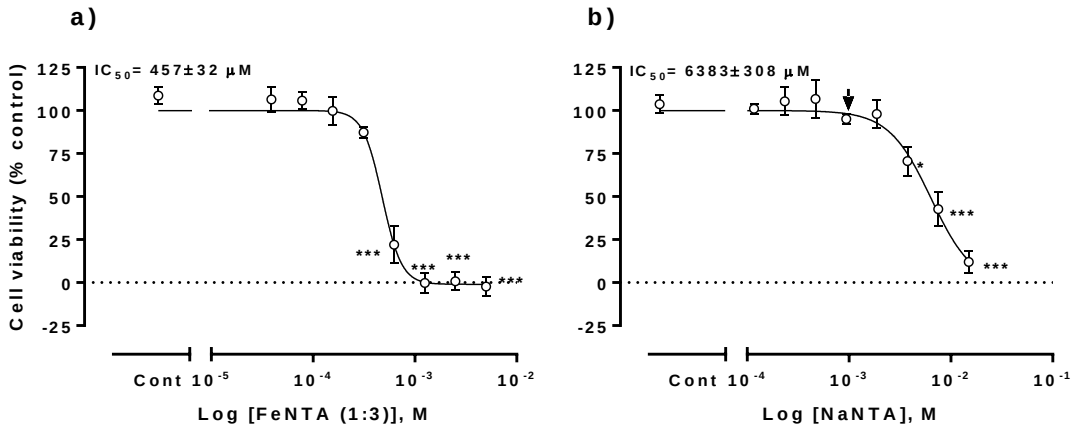

Figure 2.2.10: **Cell death of SH-SY5Y cells following exposure to FeNTA (1:3).**

SH-SY5Y cells were exposed to ***a)*** *FeNTA (1:3) (4-5000 µM) and* ***b)*** *NaNTA (12-15000 µM) for 20 hours. Cell viability was assesed by the MTT assay, where untreated cells was recorded as ~100% viable and served as a control. Arrowhead indicates the final NaNTA concentration for the FeNTA (1:3) complex. Data are expressed as mean±SEM (n=3). Non-linear regression analysis [log(inhibitor) vs. response-variable slope (four parameters)] was performed to calculate the IC_{50} (GraphPad Prism 7 Software). Degrees of freedom (df) =* ***24****. * p <0.05, *** p <0.001 compared to control cells (one-way ANOVA followed by Dunnett's test).*

To summarise, MG132 was the most toxic to SH-SY5Y as evaluated by MTT assay with IC_{50} value of 352 pM. This was followed by 6-OHDA (IC_{50} = 39 µM) and H_2O_2 (IC_{50} = 222 µM). FeNTA was the least toxic of all toxicants with IC_{50} value of 457 µM. The IC_{50} concentrations for toxins were rounded up to the nearest whole number and was used as final IC_{50} concentrations in the neuroprotection study (**Table 2.2.2**).

Table 2.2.2: Summary of the toxin with their IC_{50} use in the *in vitro* neuroprotection study.

Toxins	IC_{50}
Hydrogen peroxide (H_2O_2)	220 µM
6-Hydroxydopamine	40 µM
MG132	350 pM
FeNTA (1:3)	460 µM

2.2.10 *3-hydroxy-4-pyridinones*

Several concentrations of HPOs (5, 50, 100, 500, 1250, 2500 and 5000 µM) were tested for their toxicity against SH-SY5Y cells and the cell viability was measured with MTT assay. Main stock solution for CP20 and novel HPOs (50 mM) were prepared in sterile distilled water except for CP84 that was dissolved in 100% (v/v) DMSO. The working stock solution for HPOs (5000 µM) was prepared in serum-free DMEM from the main stock solution. A series of HPOs concentrations ranging from 5 to 5000 µM were prepared in serum-free DMEM from the HPOs working stock solution and were added (100 µL) into the 96-well plate containing $1x10^5$ SH-SY5Y cells/mL. The cells were exposed to the various concentration of HPOs for 20 h in a CO_2 incubator. Cells incubated with serum-free DMEM was served as a control. After 20h exposure to HPOs, the medium was removed and replaced with free-medium containing 0.5 mg/mL MTT and further incubated in the CO_2 incubators for 4 h. At the end of the incubation, the medium was removed followed by cells lysis with 100% (v/v) DMSO and the absorbance was taken at 570 nm as described in **Section 2.2.8**.

CP20 did not cause significant cell death when compared to control group for all of the concentrations tested (**Figure 2.2.11a**). Similarly, CN116 and CN118 also did not cause cell death up to the highest concentration (5000 µM) tested when compared to control (**Figure 2.2.11c**). CN126 and CN128 caused significant cell death when compared to control at the highest concentration tested (5000 µM; **Figure 2.2.11d**). Conversely, CN226 and CN228 started to lower the cell viability at 2500 µM compared to control with almost complete cell death following 5000 µM (**Figure 2.2.11e**). Among all HPOs, only CP84 significantly killed the cells at 500 µM and above suggesting that it is relatively toxic compare to other HPOs (**Figure 2.2.11b**).

Comparison between equimolar concentrations of CP20 with novel HPOs revealed that treatment with CN126 and CN128 significantly lowered cell viability at 5000 µM. On the other hand, treatment with CN226 and CN228 significantly lowered cell viability at 2500 and 5000 µM compared to equimolar concentration of CP20. Additionally, CP84 lowered the cell viability in a concentration-dependant manner starting at 500 µM when compared with equimolar concentration of CP20.

SH-SY5Y cells have been shown to be resistance towards toxicity of deferioxamine, a hexadentate iron chelator due to higher level of ferritin expressed in SH-SY5Y compared to non-cancerous cells (Castino et al., 2011, Selig et al., 1998). In this situation, the intracellular iron was sequestered and tightly bound within ferritin complex and was released as intracellular free-iron as needed for cellular functions. Because of the high number of ferritins in SH-SY5Y cells, more iron chelators are needed to compete with ferritin to bind iron until free-irons are depleted and causing cell death.

The IC_{50} values for HPOs rounded up to the nearest whole number were listed in **Table 2.2.3.** The selected concentration of HPOs used for *in vitro* neuroprotection study were 50, 100 and 500 µM which have been shown to be sufficient to protect SH-SY5Y cells from toxin-induced cell death (Selig et al., 1998). In neuroprotection study employing FeNTA (1:3), HPOs concentrations for up to 1250 µM were used to show neuroprotection due to the nature of co-ordination chemistry for iron chelation. For CP84, the concentration employed was limited for up to 100 µM due to its marked toxicity at 500 µM (**Figure 2.2.11b**).

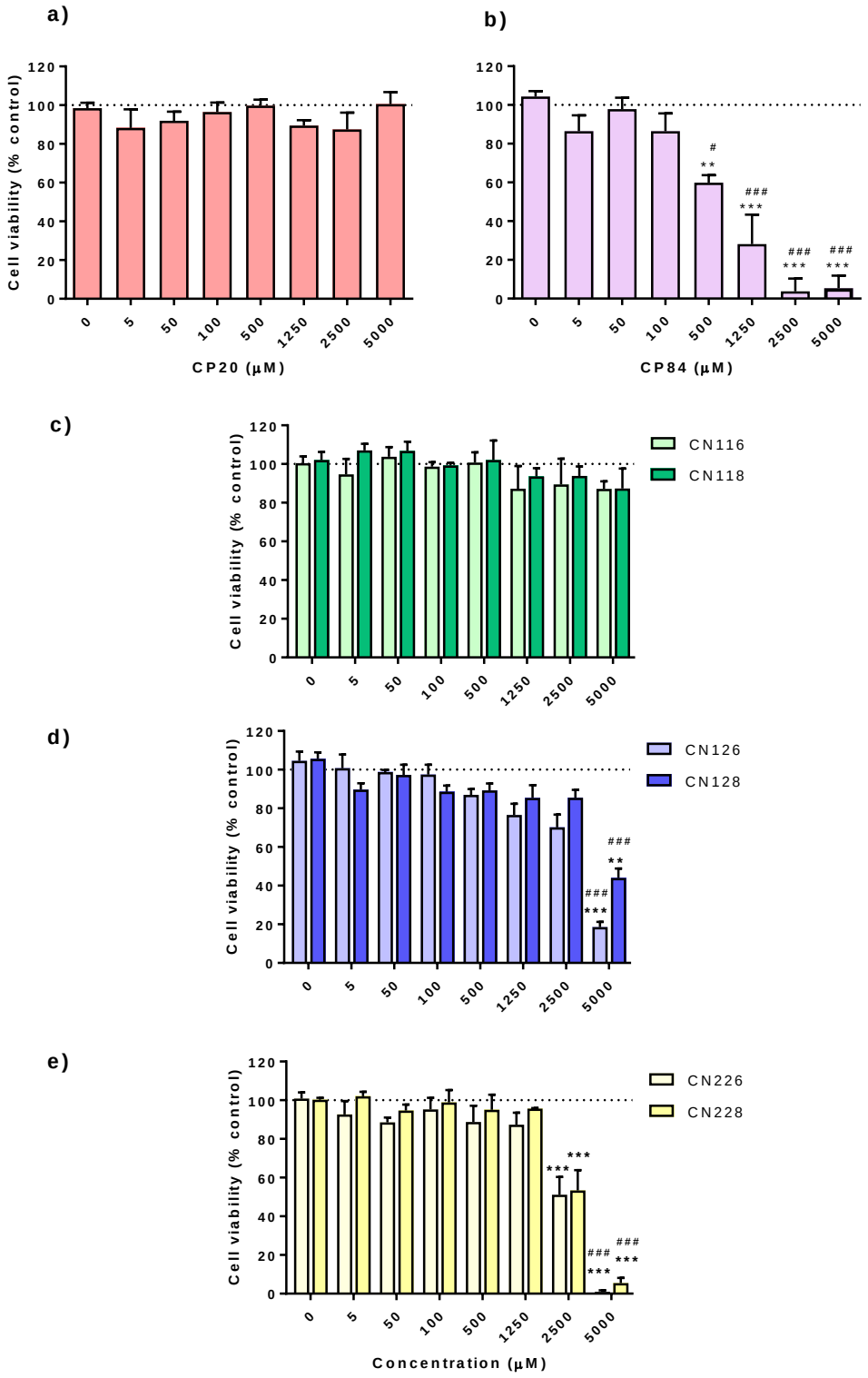

Figure 2.2.11: **Effect of CP20 and novel HPOs on SH-SY5Y cells viability.**

*SH-SY5Y cells were exposed to HPOs (5-5000 µM) for 24 hours. Cell viability was assesed by the MTT assay, where untreated cells was recorded as ~100% viable and served as a control. Data are expressed as mean±SEM (n=3). *** p <0.001 compared to control group; ### p <0.001 compared to CP20 (one-way ANOVA followed by Holm-Šídák multiple comparison test)*

Table 2.2.3: IC_{50} values for HPOs assessed by MTT assay.

HPOs	IC_{50} (μM)
CP20	na
CP84	690
CN116	na
CN118	na
CN126	na
CN128	na
CN226	2590
CN228	2550

na = not applicable; for this HPOs, an accurate IC_{50} value cannot be determined due to absence of inflection point in the log(toxin) vs. response-variable slope. Data are expressed as mean±SEM (n=3). Non-linear regression analysis [log(toxin) vs. response-variable slope (four parameters)] was performed to calculate the IC_{50} (GraphPad Prism 7 Software).

2.3 *HPLC method validation for evaluation of selected novel 3-hydroxy-4-pyridinone iron chelators in rat brain and plasma for pharmacokinetics application.*

2.3.1 *Introduction*

Biological fluid or matrix such as urine, plasma, milk and brain homogenate often contained analytes inherent to the matrix that might interfere with the separation and efficiency of drug extraction (Siddiqui et al., 2017). In addition, recovery of HPOs spiked into NRS supplemented with BSA and brain homogenate were less than 100 percent for some HPOs when extracted with TFA (**Section 2.1.9b iii**), which requires correction for recovery during HPLC data analysis. The Food and Drug Administration, USA (US-FDA) had released guidelines for analysis of analytes in biological matrices (US-FDA, 2001). The guidelines suggested preparation of standard calibration curve by spiking a standard analyte into the relevant biological matrix rather that water, followed by extraction procedures similar to the actual biological samples so that preparation error could be minimised. Additionally, a second standard (internal standard) preferably with the same physicochemical properties of the main standard but with different retention time was also added at a constant concentration prior to the extraction (Pitt, 2009). The HPLC response was taken as the ratio of area under the curve (AUC) or height of the peaks for the main standard and internal standard. This step could minimise the error that might be introduced during sample preparation such as during pipetting or during sample injection into HPLC. To ensure accuracy and reproducibility (precision) of the HPLC analysis within day (intraday) or between days (interday), concentrations of standard that covers the low, middle and high concentration were selected as quality controls to be run along the standard calibration curve (US-FDA, 2001). Accuracy is defined as the closeness of the obtained response to the expected response. On the other hand, precision measures the reproducibility of HPLC response in between analysis (Kadian et al., 2016).

This section described the improved sample preparation method for HPO analysis in matrix other than water according to the guidelines provided by the US-FDA (2001). This step was taken to minimise error that might be introduced during sample preparation and/or flaws in the HPLC machinery for application in the pharmacokinetic study.

2.3.2 *Experimental animals*

Male Wistar rats weighing between 300-350 g (Harlan UK Ltd) and were housed between 2-4 rats per cage in the Biological Service Unit (BSU), King's College London. The conditions of the holding unit at BSU and rat diet were described previously in **Section 2.1.2**. The experiments were approved under Animal (Scientific Procedure Act) 1986 and performed under the project license number 70/0688.

2.3.3 *HPLC method validation in plasma and brain*

The method validation for HPOs determination in plasma and brain was performed according to the US-FDA Bioanalytical Method Validation Guidance for Industry (US-FDA, 2001) with CP20 was used as an HPO prototype. Blanked plasma and brain were obtained from naïve rats. Upon confirmation of loss of reflex by toe pinching, the rats were terminally anaesthetised with 600 mg/kg pentobarbital sodium (Merial Animal Health Ltd, UK) by *i.p.* injection, the chest was open with a pair of scissors to expose the heart. Whole blood was collected by cardiac puncture using 21G needle attached to a 5 mL syringe and transferred into a heparinised tube. Whole blood was centrifuged at 5400 g, 4 ºC for 20 minutes and plasma removed and stored at -20º C until analysis. The brain was removed and homogenised in PhyBS in 1:3 (w/v) dilution and stored in -20º C.

2.3.4 *HPOs solution preparation*

CP20 and CN226 were dissolved in HPLC water at a concentration of 50 mM which was used as main stock solution. Dilutions of CP20 (20 to 1250 µM) were prepared from the CP20 stock solution in HPLC water for calibration curve and quality control (QC) preparation. CN226 working stock solution at 200 µM was prepared from the CN226 main stock solution and was used as an internal standard (IS).

2.3.5 *Standard calibration curve*

CP20 calibration curve with concentrations ranging from 2 to 125 µM were prepared in blank plasma and brain from naïve rats. CP20 (20-1250 µM; 20 µL) was spiked into 180 µL blank matrices (plasma or brain) followed by 22 µL internal standard (CN226) working solution. TFA (22 µL) was added to the spiked matrices so that the final concentration of TFA was 9.1% (v/v). The mixture was vortexed and centrifuged at 20800 *g*, 4º C for 45

minutes. Clear supernatant was taken and injected (30 µL) into HPLC for analysis. The method for analysis of HPOs in the plasma and brain was performed as described in **Section 2.1.9b.** The ratio of the CP20 and CN226 peak height was calculated and plotted for linear regression analysis.

$$HPLC\ signal = \frac{Peak\ height\ of\ CP20}{Peak\ height\ of\ CN226} \qquad \textbf{Equation 2.3.1}$$

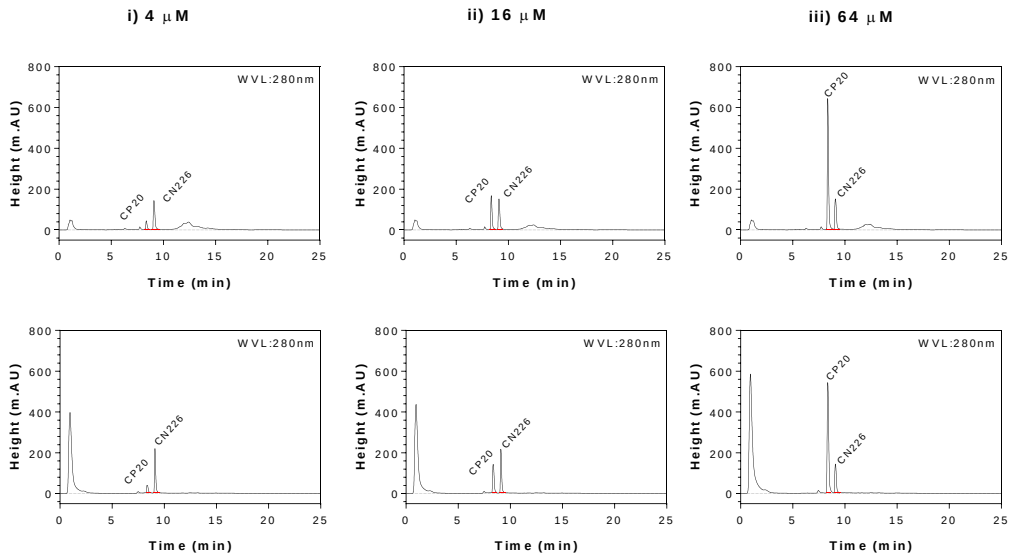

Figure 2.3.1: **Representative chromatogram for CP20 and CN226 spiked into rat plasma or brain homogenate.**

CP20 and CN226 retention times were ~8.3 minute and ~9.1 minute respectively.

Linear regression analysis was performed on the linear plot of CP20 to CN226 height ratio against CP20 concentrations to obtain the linear equation y = mx + C.

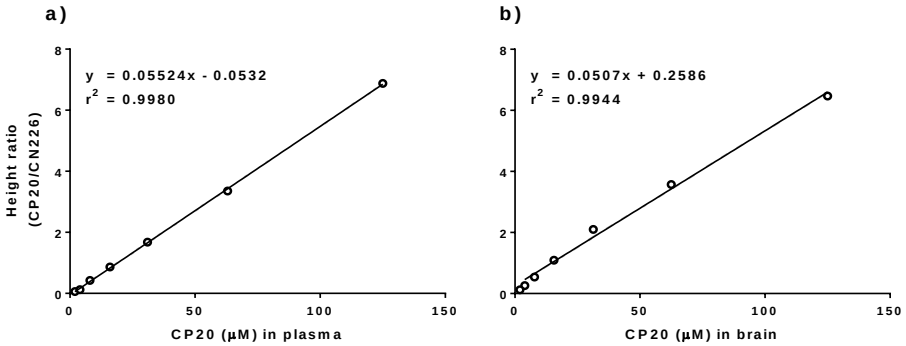

Figure 2.3.2: **Representative standard calibration curve of CP20 spiked into blanked plasma and brain.** *Data was analysed by least-square linear regression analysis (GraphPad Prism 7 Software).*

Lower limit of detection (LOD) is defined as the lowest concentration in the standard curve that can be detected by the HPLC system, but cannot be accurately quantify (Armbruster and Pry, 2008). LOD was calculated following this formula:

$$LOD = \frac{3\,\sigma}{m}$$ **Equation 2.3.2**

Where, σ is standard deviation of the residuals of the calibration curve linear equation, y = mx + C, and m is the slope of the line.

Lower limit of quantification (LOQ) is defined as the lowest concentration in the standard curve that can be accurately quantify (Armbruster and Pry, 2008). LOQ was calculated using the following formula:

$$LOQ = \frac{10\,\sigma}{m}$$ **Equation 2.3.3**

Where, σ is standard deviation of the residuals of the calibration curve linear equation, y = mx + C, and m is the slope of the line.

LOD and LOQ for CP20 spiked into blanked plasma were approximately 0.5 and 2 µM (**Table 2.3.1**). On the other hand, LOD and LOQ for CP20 spiked into brain homogenate were about twice the value in plasma (Armbruster and Pry, 2008). Therefore 2 µM and 4 µM were selected as the minimum concentration to construct standard calibration curves for CP20 spiked into plasma and brain respectively.

Table 2.3.1: LOD and LOQ of CP20 spiked into rat brain and plasma.

Matrices	LOD (µM)	LOQ (µM)
Plasma	0.55±0.14	1.82±0.46
Brain	1.19±0.14	3.95±0.8

Data are expressed as mean±SEM (n=3 independent standard calibration curve).

2.3.6 *Quality control*

Three quality controls (QC) that covers low (4 µM), middle (16 µM) and high (64 µM) concentrations were prepared from the CP20 working solution in 3 different vials for each concentration. QC samples were prepared by spiking CP20 into blank plasma or brain homogenate, extracted and analysed by one working day for intraday analysis or by 3 consecutive days for interday analysis. Accuracy gives an information on how far the obtained concentration derived from the standard calibration curve deviate from the expected concentration.

$$\%\ Accuracy = \frac{[Obtained]}{[Expected]}\ X\ 100 \qquad \textbf{Equation 2.3.4}$$

Precision gives an information on how close the similarity of the obtained concentration derived from standard calibration curve.

$$\%\ Precision = \frac{Mean\ [Obtained]}{SD}\ X\ 100 \qquad \textbf{Equation 2.3.5}$$

Based on the guidelines provided by the US-FDA Bioanalytical Method Validation Guidance for Industry (2001), accuracy and precision for intraday and interday analysis should be within ±15-20% from the expected concentration. Intraday and interday analysis revealed that both accuracy and precision for CP20 spiked into blanked plasma or brain were within the accepted range as suggested by the guidelines (**Table 2.3.2 and Table 2.3.3**).

Table 2.3.2: Intraday assay precision and accuracy for CP20 in rat plasma and brain

Matrices	Concentration	Accuracy (%)	Precision (%)
Plasma	**4**	92.3	3.5
	16	109.7	7.5
	64	107.3	1.5
Brain	**4**	84.3	2.5
	16	98.2	1.7
	64	95.1	2.2

Accuracy represent the mean values (n=3 injection in one day).

Table 2.3.3: Interday assay precision and accuracy for CP20 in rat plasma and brain

Matrices	Concentration	Accuracy (%)	Precision (%)
Plasma	**4**	92.6	7.1
	16	106.8	3.0
	64	103.9	2.8
Brain	**4**	90.8	14.2
	16	96.3	3.8
	64	92.5	7.7

Accuracy represent the mean values (n=3 days).

2.4 *Determination of optimum 6-OHDA dose for striatal injection in rat*

2.4.1 *Introduction*

PD is pathologically characterised by loss of dopaminergic neurons in basal ganglia specifically the neurons that made up the nigro-striatal pathway in the midbrain area, with the cell bodies located within the substantia nigra pars compacta (SNPc) region and the axons projection terminate in the striatum (Alexander, 2004). In an animal model of PD, the loss of dopaminergic neurons was induced by injection of toxins either systematically or directly to the area associated with the nigro-striatal dopaminergic tract (Tieu, 2011, Bové et al., 2005, Duty and Jenner, 2011). Specific areas in this tract namely striatum, medial forebrain bundle (MFB) and SNPc have been targeted for induction of cell death depending on the aim of study (Duty and Jenner, 2011)**.**

Unilateral 6-OHDA rat model is extensively use during the early stage of drug discovery and development due to the model mirror some of the important aspect of pathogenesis and biochemistry of PD such as oxidative stress and reduced level of striatal dopamine and tyrosine hydroxylase (TH) (Duty and Jenner, 2011). 6-OHDA is the metabolite of dopamine that can generates oxidative stress via mechanism explained in detail in **Section 2.2.1b**. One main drawback of the 6-OHDA model is the need of substantial surgical training to administer the 6-OHDA into the brain using a stereotaxic technique due to the inability of 6-OHDA to cross the BBB in contrast to other toxins such as 1-methyl-4-phenyl-1,2,3,6-tetrahydropyridine (MPTP) that can be administered systematically creating bilateral lesion (Kostrzewa and Jacobowitz, 1974, Duty and Jenner, 2011). On the other hand, unilateral lesions by stereotaxic technique allow the use of the contralateral hemisphere as an internal control of cell loss measurement (Duty and Jenner, 2011). Furthermore, the unilateral 6-OHDA-lesion model shows a rotational pattern ipsiversive or contraversive to the lesion site when injected with amphetamine or apomorphine respectively, that can be used as an indicator of lesion severity (Torres and Dunnett, 2007, Jerussi and Glick, 1975).

For neuroprotection studies, partial unilateral 6-OHDA lesions (40% to 60% cell loss in SNPc) are often generated to allow the assessment of efficacy of potential disease modifying agents. By contrast, full lesion (>90% cell loss in SNPc) are more appropriate

to assess drug that is intended for symptomatic relief such as L-DOPA (Duty and Jenner, 2011). This is because, partial lesion represents the early stage of PD where the cardinal motor symptoms are absent contrary to the full lesion that represents the late stage of PD where the cardinal motor symptoms are visible. Generation of partial or full lesion of 6-OHDA model is largely depending on the doses used to create the lesions. Moreover, the location of the 6-OHDA injection for partial lesion dictate the rate of progression of the nigral cell loss with striatal injection showing slower progress (maximal cell loss within 3 weeks after lesion) compared to injection into SNPc or MFB that have maximal cell loss within 2 weeks after the 6-OHDA treatment (Duty and Jenner, 2011).

This section described the method used to create a partial unilateral 6-OHDA-lesioned rat model of Parkinson's disease and the subsequent techniques to determine the extent of cell death. Three doses of 6-OHDA were employed to determine the optimum dose for 6-OHDA that will be used in *in vivo* neuroprotection study.

2.4.2 *Animals*

Male Wistar rats weighing between 225-250 g (Harlan UK Ltd) and were housed between 2-4 rats per cage in the Biological Service Unit (BSU), King's College London. The rats were allowed to acclimatise for at least a week after arrival at BSU before the striatal lesion. Only rats that reached the weight between 250 to 300 g after a week of acclimatisation were used for the lesion. The conditions of the holding unit at BSU and rat diet were described in **Section 2.1.2**. The experiments were approved under Animal (Scientific Procedure Act) 1986 and performed under the project license number 70/7977.

2.4.3 *6-Hydroxydopamine (6-OHDA) preparation*

The concentration of 6-OHDA HCl (Sigma-Aldrich, UK) was calculated as a free base and dissolved in 0.9% (w/v) NaCl (Sigma-Aldrich, UK) containing 0.1% (w/v) L-ascorbic acid (Sigma-Aldrich, UK) on the day of surgery. Concentrations of 6-OHDA prepared for striatal injection were 1 mg/mL, 2 mg/mL or 3 mg/mL. Aliquots of 6-OHDA (1000 µL) were wrapped with aluminium foil to protect from light and was kept on ice. The prepared 6-OHDA aliquots were used within 6 hours of preparation.

2.4.4 *Intrastriatal injection of 6-OHDA*

The aliquot of 6-OHDA (1 mg/mL, 2 mg/mL or 3 mg/mL) in a total volume of 4 µL was injected using a microsyringe into striatum to develop a unilateral lesioned of rat PD model. The dose for each concentration was listed in **Table 2.4.1**. The details of the surgical procedures performed under a sterile condition were outlined below.

Table 2.4.1: The concentrations and doses of 6-OHDA injected into the rat left striatum.

Concentration	Dose injected
1 mg/mL	4 µg
2 mg/mL	8 µg
3 mg/mL	12 µg

6-OHDA was prepared in in 0.9% (w/v) NaCl containing 0.1% (w/v) L-ascorbic acid. The dose volume was 4 µL/rat

a) Surgery

Rats were anaesthesised with 5% (w/w) isoflurane (IsoFlo®, Abbott, UK), delivered in 100% (w/w) O_2 for 2 minutes in an anaesthetic chamber. Anaesthesia was confirmed by the absence of reflex to toe pinching and eye tapping. Following this, the head of the rat was shaved, and the rat was secured in a prone position with the ear bars placed symmetrically into a Kopf® stereotaxic frame (David Kopf Instruments, USA) and tooth-bar set at -3.3 mm (Paxinon and Watson, 2004). The isoflurane was delivered at 5% (w/w) through a nose cone to maintain anaesthesia. The temperature was maintained at 37 ºC during the entire procedure using a homoeothermic blanket with rectal probe. The secured rat was surgically prepared by disinfecting the scalp with diluted chlorhexidine gluconate [0.4% (w/v)] (Hibiscrub®, Mölnlycke Health Care Ltd, UK) and followed by *s.c.* injection with 1 mg/kg bupivacaine HCl (Marcaine®, AstraZeneca Ltd, UK) at the site of incision. Eye gel (Viscotears®, Alcon Laboratories Ltd, UK) was generously applied on the rat eyes to prevent eye dryness during the surgery. Subsequently, the isoflurane flow was reduced to 3% (w/w). The complete surgical set-up is illustrated in **Figure 2.4.1**.

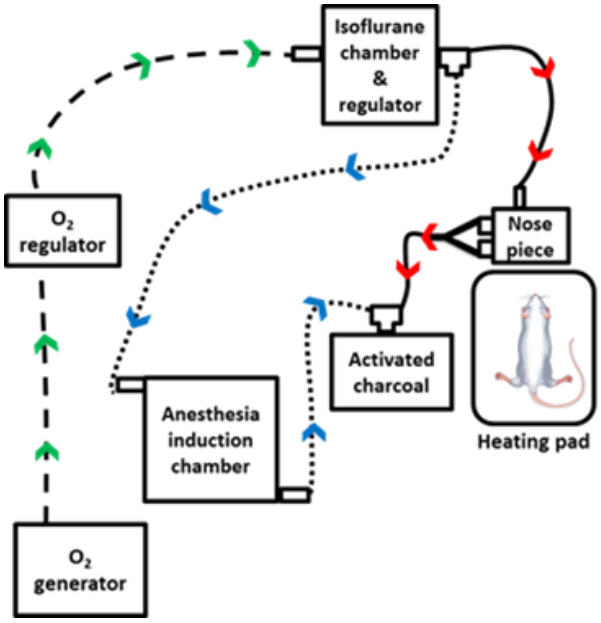

Figure 2.4.1: Surgical setup for stereotaxic brain lesion procedure.

Flowing O_2 (►) is mixed with isoflurane in the isoflurane chamber. Blue circuit (►) is activated for induction of anaesthesia by isoflurane in the anaesthesia induction chamber. Red circuit (►) is activated once the anaesthetised rat is placed on the heating pad for maintaining of anaesthesia. Flowing isoflurane was terminally adsorbed on the activated charcoal.

b) Lesion induction

An incision was made on the scalp with a sterile disposable scalpel (SP Services Ltd, UK) to expose the skull. The skull was cleaned of tissues remnant with the scalpel blade and cleaned from blood with sterile cotton buds, exposing bregma. During this time, the isoflurane dose was reduced to and maintain between 1-2% (w/w). Coordinate of the striatum on the left hemispheres were taken from the bregma according to the rat brain atlas of Paxinos and Watson (2004): anterior = +1.0 mm, lateral = +3.0 mm, and ventral = -5.5 mm) (**Figure 2.4.2**) using a Vernier scale on the stereotaxic frame. A burr hole (0.5 mm ID) was then made in the skull over the lesion site. The needle tip was slowly lowered to the lesion site, and the left striatum was injected with 6-OHDA (4 µL at 1 µL/min over 4 minutes) using a 10 µL 1701ASRN Hamilton® microsyringe fitted with a 26s-gauge Hamilton needle (Essex Scientific Laboratory Supplies Ltd, UK). The total amount of 6-OHDA injected was 4, 8 or 12 µg in a total volume of 4 µL. Sham rats were injected with vehicle [4 µL of 0.9% (w/v) NaCl containing 0.1% (w/v) L-ascorbic acid] using the same co-ordinates. The needle was left at the injection site for 4 minutes to ensure complete diffusion of 6-OHDA into surrounding tissues and prevent reflux along the needle tract and

was then slowly removed. The incision was closed with 16 mm Ethicon-coated vicryl absorbable sutures (Johnson's & Johnson's, UK) and 5% (w/w) prilocaine and lidocaine cream (EMLA™, AstraZeneca Ltd, UK) was applied on the wound area. Glucose [5% (w/v) in 0.9% (w/v) NaCl, 10 mL] was injected *i.p.* to avoid dehydration. Subsequently, the rat was injected *s.c.* with 0.01 mg/kg buprenorphine HCl (Alstoe Animal Health, UK). The rat was taken out from the stereotaxic frame to the pre-warmth cage for recovery before returning to the housing unit at BSU. Surgical equipment was sterilised with autoclave machine (Prestige Medical Ltd, UK) prior to and in-between procedures.

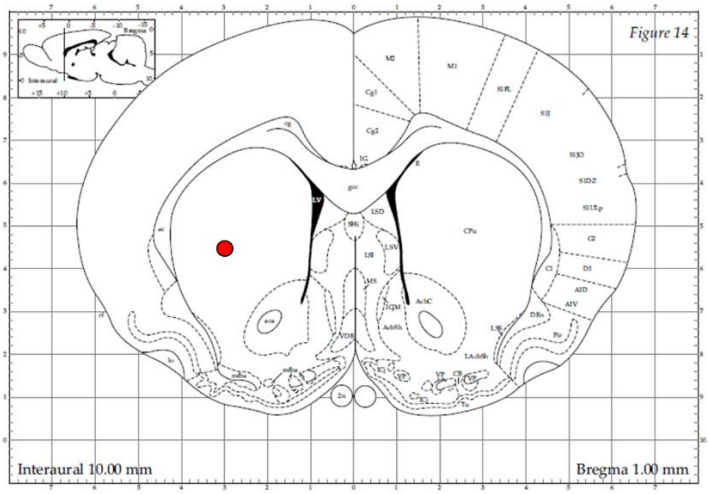

Anatomical location	From the bregma (mm)
Anterior-Posterior (AP)	+1.0
Medial-Lateral (ML)	+3.0
Dorsal-Ventral (DV)	-5.5

Figure 2.4.2: Site and co-ordinate of left striatum base on Paxinos and Watson (2004) for intrastriatal injection of 6-OHDA in rat. The red dot (●) depicts the site of injection in the striatum.

c) Post-operative care

Rats were given water-softened pellet and Recovery DietGel® (ClearH_2O®, UK) for 3 days after surgery. The rats were weighed daily until reaching their pre-operative weight. If their weight was reduced by 5% of their pre-surgery body weight, the rats were injected *i.p.* with 5% (w/v) glucose in 0.9% (w/v) NaCl. **Figure 2.4.3** showed the body weight for rats before and after the brain lesion procedures. The body weights were slightly decreased a day after the procedures but slowly regained the pre-surgical body weight 4 to 5 days after the surgery and were steadily increased afterwards which suggest a good recovery.

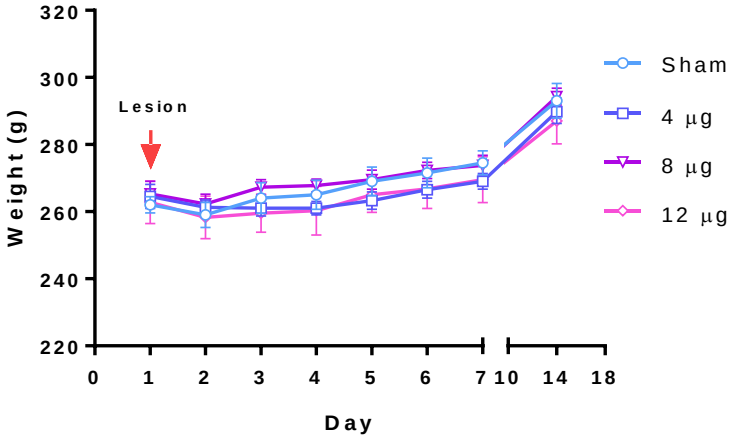

Figure 2.4.3: Recorded body weight on the day of lesion and after lesioned for up to 14 days. n=4 rats.

2.4.5 *D-amphetamine rotation test*

On the day 14th after the lesion, the rats were subjected to D-amphetamine rotation test using an automated rotometer system (RotoRat™, Med Associates, Inc., USA). This study was performed to evaluate the effect of partial-lesioned in the rat striatum as D-amphetamine induced imbalance in dopamine release from the presynaptic terminal between intact and lesioned sites. The imbalance of dopamine level between these two sites induce ipsilateral rotations towards the lesioned site (Torres and Dunnett, 2007). **Figure 2.4.4** illustrates the principles of this behaviour assessment.

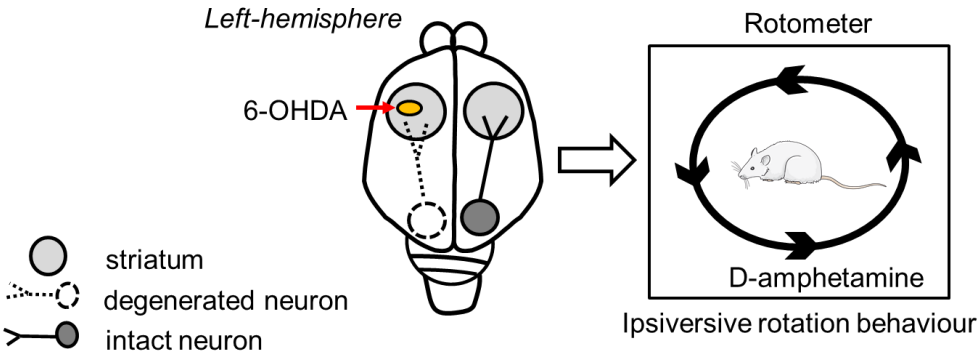

Figure 2.4.4: Illustration of the 6-OHDA lesioned in the left striatum and the expected ipsilateral rotation after injection with D-amphetamine.

To determine D-amphetamine induces rotations, rats were strapped with a tethered jacket attached to a sensor in the rotometer. The rats were allowed to acclimatise to the

rotometers for 30 minutes after which baseline activity was recorded using the RotoRat™ hardware and RotoRat™ software Version 2.0 for 30 minutes. Following this, the rats were injected *i.p*. with 2.5 mg/kg D-amphetamine sulphate (Tocris Bioscience, UK) prepared in 0.9% (w/v) NaCl and the number of rotations were recorded for 3 hours. The sensor was set to record the 45˚ rotation in one-minute period. The numbers of complete 360º rotations were collated into 10-minutes time bin for the total of 3 hours. Data was automatically recorded into two columns, which display counter-clockwise and clockwise rotations. To calculate the complete circle rotation (360˚ rotation), the data were divided by eight since 360÷45 = 8 followed by subtracting counter clockwise rotations from clockwise rotations to give the net ipsilateral rotations per 10 minutes per animal (**Figure 2.4.5**).

There was no significant different of D-amphetamine induced ipsilateral rotations between 6-OHDA treated group and vehicle treated group (**Figure 2.4.5e**). The lack of difference between groups was due to the high variation of rotational behaviour in 6-OHDA-treated group (**Figure 2.4.5b, c,** and **d**). Indeed, this observation is in accordance with previous reports that showed a lack of relationship between the number of net ipsilateral rotations and the size of lesion in the unilateral 6-OHDA partial lesion PD model (Hudson et al., 1993, Hefti et al., 1980).

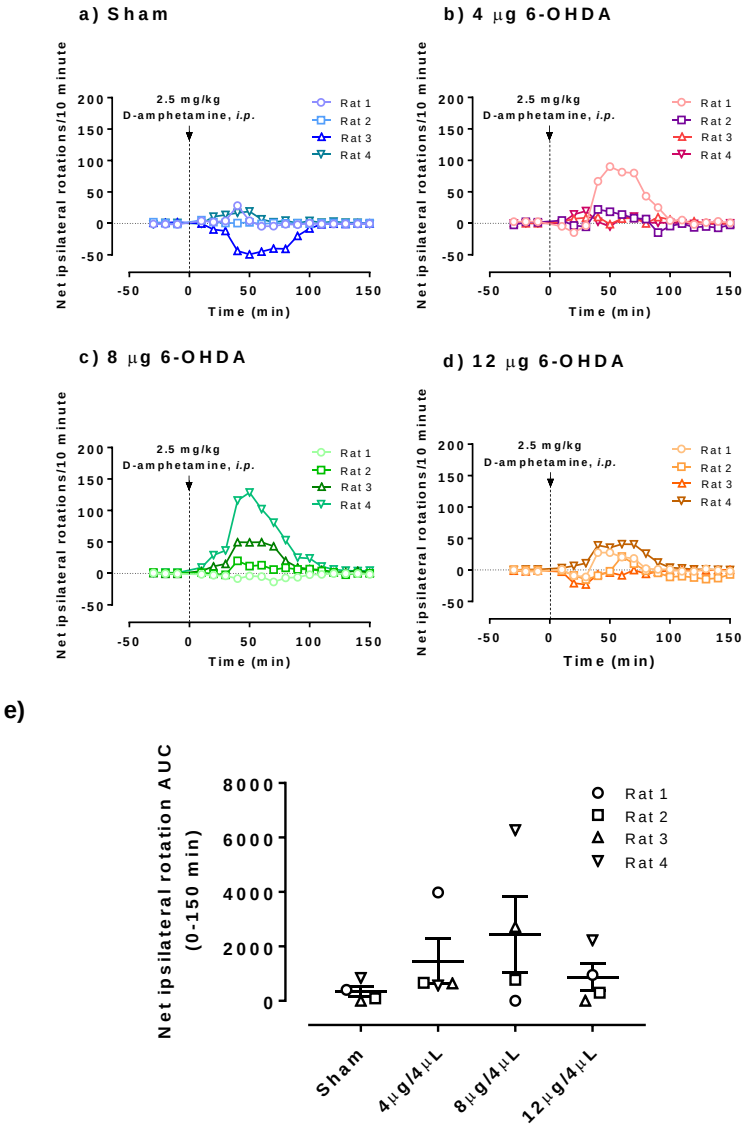

Figure 2.4.5: D-Amphetamine rotation test for 6-OHDA unilateral striatal lesioned rat.

Individual net ipsilateral rotation of rat injected with D-amphetamine for a) Vehicle b) 4 µg/µL 6-OHDA c) 8 µg/µL 6-OHDA and d) 12 µg/µL 6-OHDA. e) The mean AUC of net ipsilateral rotation for each treatment group. Data are mean+SEM (n=4 rats). 1-way ANOVA analysis showed no significant different.

2.4.6 *Brain fixation*

Rats were terminally anaesthetised with 600 mg/kg pentobarbital sodium (Merial Animal Health Ltd, UK) two-days after D-amphetamine test. The brain was perfused-fixed with 50 mL 4% (w/v) PFA in 0.1 M PBS, pH 7.4 by transcardial perfusion using a 19G needle attached to a 50 mL syringe. The brain was post-fixed with 4% (w/v) PFA for 3 days. The fixed brain was then cryoprotected with 30% (w/v) sucrose (Sigma-Aldrich, UK) containing

0.05% (w/v) sodium azide (NaN_3; Sigma-Aldrich, UK) in 0.1 M PBS (pH 7.4) until the tissue sank (~3-5 days).

2.4.7 *Brain sections*

Coronal sections (30 µm) of rat brains were cut using a freezing microtome (Leica SM 2000R; Leica Biosystem, UK). Substantia nigra pars compacta (SNpc) was sectioned at the level of the third nerve and striatum was sectioned approximately between -1.4 mm to 2.0 mm AP from the bregma (Paxinos G. & Franklin F., 2004). Striatum sections were categorised anatomically into caudal (AP: ~-1.4 mm from the bregma), medial (AP: ~1.0 mm from the bregma) and rostral (AP: ~2.0 mm from the bregma). Free floating sections were collected into 24-well plates (5 sections/well) filled with 0.1 M PBS and 0.05% (w/v) NaN_3 for immunohistochemical staining.

2.4.8 *Immunohistochemical staining*

a) Day 1

Coronal brain sections (2-4 sections) of SNPc and striatum were incubated with 0.3% (w/v) H_2O_2 in 0.1 M PBS, pH 7.4 (1 mL) for 30 minutes on a shaker to block the endogenous peroxidase at room temperature. The sections were washed with 0.05% (w/v) Triton-X100 in 0.1 M PBS, pH 7.4 (PBS-T) followed by incubation with 1% (w/v) BSA in PBS-T on a shaker for at least one hour. Subsequently, the sections were incubated for at least 12h on a shaker with 1 mL polyclonal rabbit anti-rat tyrosine hydroxylase (TH) primary antibody (Pel-Freeze Biologicals, USA) prepared in 1% (w/v) BSA in PBS-T [1:500 (v/v) and 1:200 (v/v) dilutions for SNPc and striatum respectively].

b) Day 2

The sections were washed with 1 mL PBS-T followed by incubation for one hour on a shaker with 0.5 mL biotinylated goat anti-mouse IgG secondary antibody (Vector Laboratories, UK) prepared in PBS-T at room temperature. The sections were washed with 1 mL PBS-T followed by incubation with 1 mL avidin-biotin complex (ABC) reagent (Vector Laboratories, UK) for 45 minutes on a shaker. Subsequently, the sections were washed with 0.1M PBS followed by incubation with 1 mL 0.05% (w/v) 3,3'-diaminobenzidine (DAB) prepared in 0.01% (w/v) H_2O_2 in 0.1 M PBS for ~3 minutes. The

sections were transferred into 1 mL PBS whereby the washing steps were repeated three times. Two to four sections were mounted onto coated adhesion slides (Polysine®, Thermo Scientific, UK) and were dried overnight.

c) Day 3

Dried sections were dehydrated with three series of increasing ethanol concentrations [70, 98 and 100% (v/v)] for 5 minutes each. Following this, the sections were immersed in Histoclear® clearing agent (Fisher Scientific, Leicestershire, UK) for 15 minutes. Immediately after taking out from the Histoclear® solution, the sections were covered with DePeX mounting medium (VWR International, UK). The sections were covered with a coverslip (22x50cm; VWR International, UK), and left to dry in fume cupboard overnight.

2.4.9 *Quantification of immunoreactive cells*

Positively stained TH cells in the SNPc were counted bilaterally from three to five sections per rat at 10X magnification under a light microscope (Zeiss Axioskop, Carl Zeiss, UK) in a blinded manner. The number of positively labelled cells was expressed as the mean of the counts obtained from the representative sections (n=3-5). Positively stained TH cells in the striatum on the other hand were determined by measuring the optical density (OD) using ImageJ software (Version 1.32; National Institute of Health, USA) due to the high density of TH staining in this region (Schneider et al., 2012). SNPc images (**Figure 2.4.6)** were taken using the Axio Vision software, powered by the Zeiss Axiocam camera. Striatum images were taken with DSLR camera (Nikon, Japan) in AV mode **(Figure 2.4.8, *top panel*).**

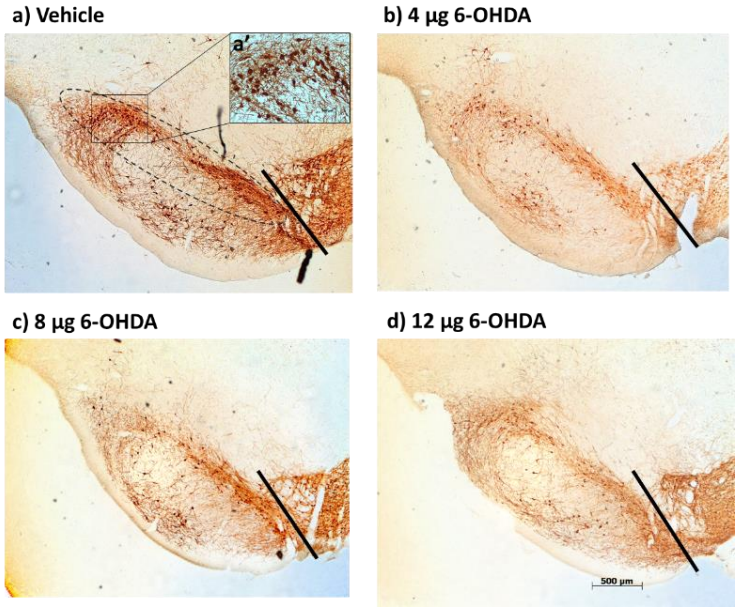

Figure 2.4.6: Representative photomicograph of brain coronal section at 2.5X magnification showing basal ganglia.

*The oval circle in **a**) indicates the SNPc region where TH⁺ cells were counted. Inset **a'**) shows the TH⁺ cells at 10X magnification. The black line on each photomicrograph marks the third cranial nerve that demarcate the dopaminergic neurons cell bodies in SNPc and VTA.*

The percentage of TH^+ cells in SNPc relative to the contralateral site after striatal injection with 4 µg/µL, 8 µg/µL and 12 µg/µL 6-OHDA were 51%, 58% and 65% respectively (**Figure 2.4.7**). Comparison of the ipsilateral sites in vehicle lesioned group with 6-OHDA lesioned groups revealed significant different in the percentage of TH^+ cells for 4 µg/µL and 8 µg/µL 6-OHDA, but not for 12 µg/µL which only showed a trend towards significant cell loss. It has been reported by Lee et al. (1996) that the TH^+ cells did not necessarily correlate with the 6-OHDA dose infused into the striatum.

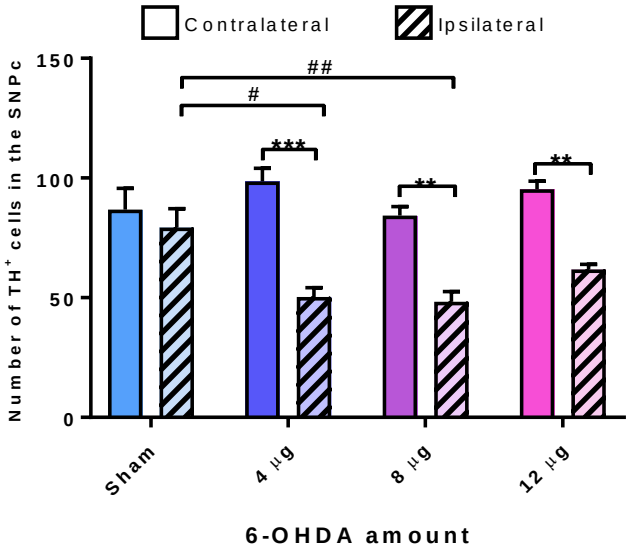

Figure 2.4.7: TH⁺ cell counts in the ipsilateral and contralateral SNPc.

*Data are expressed as mean+SEM (n=4 rats). Graph a) ** $p < 0.01$, *** $p < 0.001$ compared to the contralateral hemisphere. # $p < 0.05$, ## $p < 0.01$ compared to the ipsilateral hemisphere of vehicle group (two-way ANOVA followed by Holm-Šídák multiple comparison test).*

Analysis of the intensity of TH staining in the caudal, medial and rostral striatum revealed a substantial lesioned in the medial striatum (AP: 1.0 mm from the bregma) in agreement with the co-ordinate where 6-OHDA was injected (**Figure 2.4.8b, *top panel*)**; Paxinos G. & Franklin F., 2004). The percentage of optical density for TH staining in medial striatum relative to the contralateral site for 4 µg/µL, 8 µg/µL and 12 µg/µL 6-OHDA were 67%, 52% and 53% respectively (**Figure 2.4.8b*, bottom panel***). Based on these data, 8 µg/4 µL 6-OHDA was selected as the optimum dose to induce partial lesion in the striatum.

TOP

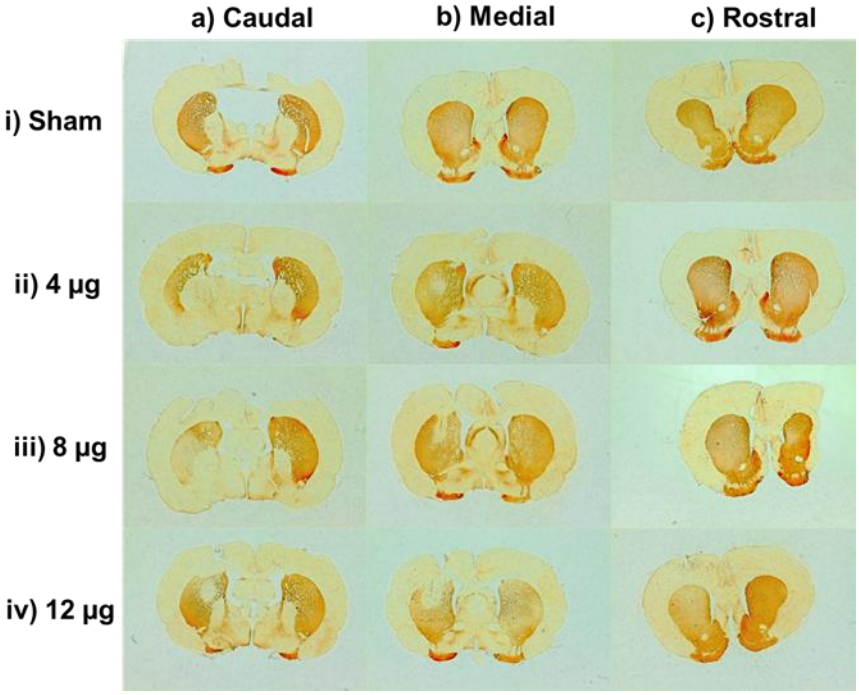

BOTTOM

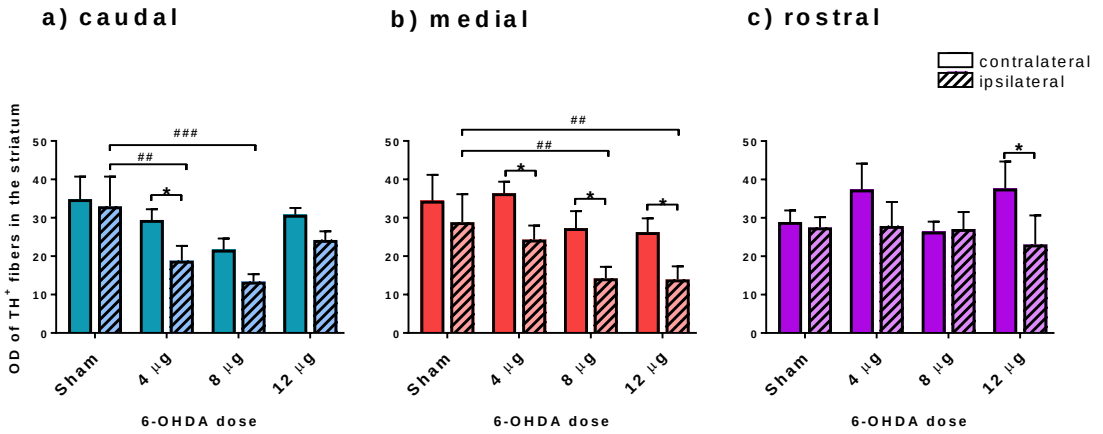

Figure 2.4.8: *Top panel:* Representative photomicrographs of TH⁺ striatum. *Bottom panel:* Optical density for TH immunostaining in a) caudal, b) medial and c) rostral striatum following intrastriatal administration of varying doses of 6-OHDA.

*Data are expressed as mean+SEM (n=4 rats). ** p < 0.01, *** p < 0.001 compared to the contralateral hemisphere. # p < 0.05, ## p < 0.01 compared to the ipsilateral hemisphere of vehicle group (two-way ANOVA followed by Holm-Šídák multiple comparison test).*

CHAPTER 3

EVALUATION OF NOVEL 3-HYDROXY-4-PYRIDINONE BIDENTATE IRON CHELATORS PENETRATION TO THE BRAIN

3 Evaluation of novel 3-hydroxy-4-pyridinone bidentate iron chelators penetration to the brain

3.1 *Introduction*

In pilot clinical trials investigating the effect of orally active hydoxypyridinone (HPO) iron chelators in PD patients, deferiprone (CP20) has been shown to improve the motor symptom and slow disease progression (Devos et al., 2014, Abbruzzese et al., 2011). However, CP20 showed poor efficacy following oral administration as 85% of the administered dose undergoes extensive metabolism to inactive glucuronide metabolites (Singh et al., 1992). For this reason, repeated administration of large doses of CP20 (30 mg/kg/day) is required to maintain effective plasma levels. However, large doses of CP20 are associated with agranulocytosis and cytopenia that are prevalent in older patients (Andres et al., 2002, Mohan et al., 2015, Rajagopal, 2005). Since over 1% of general population over the age 60 years old are affected with PD (de Lau and Breteler, 2006), long-term treatment with CP20 is not viable. To overcome this problem, a set of CP20 derivatives with chiral N-hydroxyalkyl substituent (CN compounds) were designed to limit glucuronidation and showed better efficacy than CP20 after oral administration in rats (**Figure 3.1.1**; Hider et al., 2011).

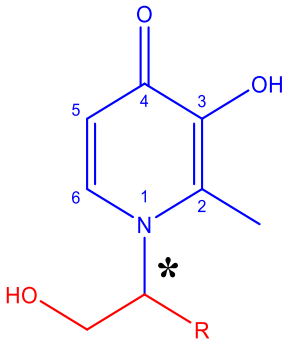

Figure 3.1.1: General chemical structure of CP20 chiral N-hydroxyalkyl derivatives (CN compounds). Structure in **blue** shows the main CP20 structure, while structure in **red** show additional functional group. Carbon atom marked with ***** is chiral centre and R represent alkyl functional group.

Interestingly, these CP20 derivatives exhibited better toxicity profiles than CP20 as assessed in mice (Hider et al., 2011a). The combination of the better efficacy and reduced

toxicity profiles of the CN compounds prompts further investigation as potential drugs for the treatment of PD.

In addition to the CN compounds, one derivative of CP20 (CP84) containing a N-phenyl substituent is also of interest. CP84 has iron affinity constant similar to CP20 and showed greater brain permeability than CP20 in *in vitro* study (Fuchs, 2015). CP84 inhibited aggregation of amyloid-β in presence of metals ion and showed superior antioxidant activity compare to α-tocopherol and butylated hydroxytoluene (BHT) (Schugar et al., 2007). However, CP84 has poor brain penetrability, and so was modified to target the BBB glucose transporter. Glucose transporters are abundantly express at BBB as described in detail in **Section 1.1.9.** As a proof of concept to specifically target glucose transporter at blood-brain barrier (BBB), glucose conjugated CP84 (FCF132) was sucessfully synthesised (Schugar et al., 2007, Roy et al., 2010) and investigated in these studies.

The ability of theses iron chelators to cross the BBB in order to reach the target site is vital for potential treatment of PD. Indeed, the positive outcome with CP20 in PD patients was partly due to its ability to enter the brain via passive membrane diffusion (Glickstein et al., 2005, Hider et al., 2011b). In fact, CP20 not only chelates excess iron in brain, but also the CP20-iron complex formed in the brain is also able to permeate out and redistribute iron to the circulated transferrin in the plasma (Evans et al., 2012, Abbruzzese et al., 2011, Ayton et al., 2016, Cabantchik et al., 2013). As the BBB is a complex lipid barrier with multitude of transport mechanisms as described in **Section 1.1.9**, single alteration in the CP20 chemical structure could alter brain permeability. The addition of chiral hydroxyalkyl or phenyl groups on CP20 molecule increase lipophilicity and might consequently improve simple membrane diffusion of novel HPOs as explained in **Section 1.1.9**. Likewise, presence of glucose on HPO molecule might enhance brain permeability via interaction with specific transporters at BBB. Therefore, it is crucial to determine the brain permeability for this new set of compounds.

In this study, a set of CP20 derivatives with chiral N-hydroxylalkyl substituent were evaluated for brain permeability by using *in situ* brain perfusion technique. In addition to these chiral N-hydroxyalkyl derivatives, two other HPOs were also evaluated for brain permeability with one of them specifically target the glucose transporters at BBB.

3.1.1 *Hypothesis*

It was hypothesised that modification to the structure of CP20 can improve the efficiency of BBB transport because of increase in lipophilicity or addition of glucose moiety.

3.1.2 *Aims*

To test this hypothesis, *in situ* brain perfusion studies were performed with the following aims:

a) To evaluate the brain permeability of novel HPO bidentate iron chelators in comparison with CP20.

b) To evaluate the effect of chirality of CN compounds to the brain uptake.

c) To evaluate the contribution of transporters to the HPO brain uptake.

d) To evaluate the relationship between brain uptake and HPO.

3.2 *Materials and methods*

In situ brain perfusion studies were performed to evaluate the brain permeability of CP84, FCF132, CN116, CN118, CN126, CN128, CN226 and CN228 (**Table 3.2.1**). Brain uptake and rate of brain uptake for all the HPOs were determined and compared with CP20. Selected HPOs were evaluated for interaction with transporters at BBB by using selective transport inhibitors. Finally, least-square regression analysis was performed between HPO brain uptake and selected HPO physicochemical properties namely lipophilicity (cLogP), molecular weight (MW) and total polar surface area (TPSA). Detailed methodology is described below.

3.2.1 *Animals*

Male Wistar rats weighing between 250-300 g (Harlan UK Ltd) and were housed between 2-4 rats per cage at BSU, King's College London as described in **Section 2.1.2**.

3.2.2 *HPO*

Nine HPOs including CP20 (**Table 3.2.1**) were evaluated for brain permeability using the validated *in situ* brain perfusion technique as described in **Chapter 2**. CP20 was purchased from Sigma (UK). All other compounds were donated by Professor Robert C. Hider to perform this study. The synthesis route and potential application of the novel iron chelators was patented under the patent number EP 2692724 A1 (Hider et al., 2011a).

3.2.3 *Brain uptake studies*

HPOs listed in **Table 3.2.1** were evaluated for their brain permeability. In order to determine the brain uptake of novel HPOs, *in situ* brain perfusions were performed with 500 µM HPO as described in **Section 2.2.15**. Briefly, a polyethylene (PE) cannula was inserted into carotid arteries of anesthetised and heparinised rat one at a time. Jugular veins were cut to allow outflow drainage of NRS perfusion fluid from the perfused brain. After flushing of cerebral blood with perfusion fluid, perfusion with HPO was started for 20 minutes as optimum perfusion time as described in detail in **Section 2.1.14**. At the end of 20 minutes, the cannulas were removed from the rat carotid arteries and the perfusate was collected from the end of the cannula for HPO quantification in the perfusate by HPLC. Following this, the rat was decapitated, the brain was taken out and process as described in **Section 2.1.7** for quantification of HPO in the brain by HPLC.

Table 3.2.1: List of HPOs, their chemical structures and selected physicochemical properties [lipophilicity (cLogP), molecular weight (MW) and total polar surface area (TPSA)].

HPO and chemical structures					
CP20	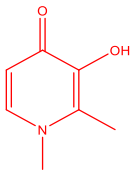	*cLogP* **-0.903** *MW* **139.1** *TPSA* **40.5**			
CP84	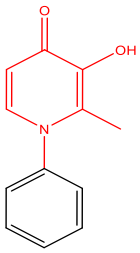	*cLogP* **0.269** *MW* **201.2** *TPSA* **40.5**	**FCF132**	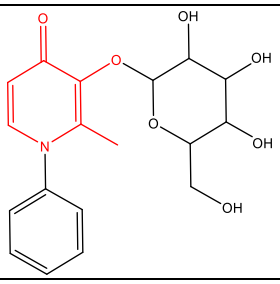	*cLogP* **-1.506** *MW* **363.4** *TPSA* **119.7**
CN116	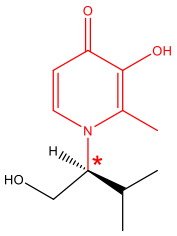	*cLogP* **-0.496** *MW* **211.3** *TPSA* **60.8**	**CN118**	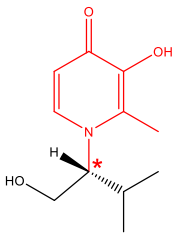	*cLogP* **-0.496** *MW* **211.3** *TPSA* **60.8**
CN126	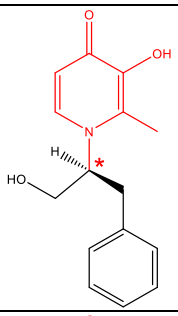	*cLogP* **0.558** *MW* **273.3** *TPSA* **60.8**	**CN128**	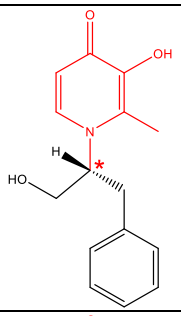	*cLogP* **0.558** *MW* **273.3** *TPSA* **60.8**
CN226	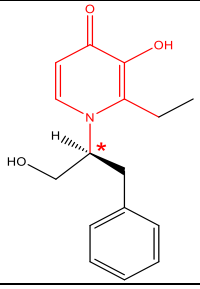	*cLogP* **1.130** *MW* **287.4** *TPSA* **60.8**	**CN228**	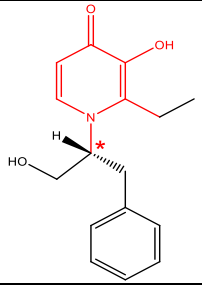	*cLogP* **1.130** *MW* **287.4** *TPSA* **60.8**

Chemical structure was drawn using ChemDraw Software (Version 15.1; Perkin-Elmer, USA). CP20 chemical structure was coloured red. Paired of CN compound was enantiomer at chiral carbon (*) with 6-suffixed indicate S-orientation while 8-suffixed indicate R-orientation.

3.2.4 *Brain uptake-inhibition studies*

Brain uptake-inhibition study was performed on selected HPO using either substrate inhibition or specific transporters inhibitor to evaluate the contribution of any transport mechanism to the brain uptake. CP20, CP84, FCF132, CN118, CN128 and CN226 were employed on this study.

a) Concentration-competition study

CP84 (5, 50 or 250 µM) was perfused into the rat brain for 20 minutes to determine whether uptake was saturable. At the end of 20 minutes, the PE cannulas were removed from the rat carotid arteries and the perfusate was collected from the end of the cannula for HPO quantification in the perfusate by HPLC**.** Following this, the rat was decapitated, the brain was taken out and process as described in **Section 2.1.7** for quantification of HPO in the brain by HPLC.

b) Transporter inhibition study

i) **CP84: competition with BCH (large neutral amino acid, LAT-1) analogue**

CP84 (50 or 500 µM) was co-perfused with 2-amino-2-norbornanecarboxylic acid (BCH; Sigma, UK), a known inhibitor for LAT-1 carrier for 20 minutes. The reported concentration of BCH (10 mM) that sufficiently inhibits LAT-1 was used in this study (Ennis et al., 1998). At the end of 20 minutes, the PE cannulas were removed from the rat carotid arteries and the perfusate was collected from the end of the cannula for HPO quantification in the perfusate by HPLC**.** Following this, the rat was decapitated, the brain was taken out and process as described in **Section 2.1.7** for quantification of HPO in the brain by HPLC.

ii) **FCF132 (glycosylated HPO): Low-glucose study**

Experiments with lower concentration of glucose (1 mM) in the perfusate were performed to reduce substrate competition between glucose and FCF132 for GLUT-1. To support normal brain physiology and metabolism during perfusion with lower glucose, 1 mM pyruvate was supplemented in the NRS (Cater et al., 2001). At the end of 20 minutes, the PE cannulas were removed from the rat carotid arteries and the perfusate was collected from the end of the cannula for HPO quantification in the perfusate by HPLC**.** Following

this, the rat was decapitated, the brain was taken out and process as described in **Section 2.1.7** for quantification of HPO in the brain by HPLC.

iii) **Brain efflux-pump inhibition study for CP20, CN118, CN128 and CN226**

Selected HPO namely CP20, CN118, CN128 and CN226 (500 µM) were co-perfused with a P-glycoprotein (Pgp) efflux-pump inhibitor, cyclosprorin A (CsA) for 20 minutes. Concentration of CsA used was 5 µM to cause substantive inhibition of Pgp efflux-pump as reported in literatures (Avdeef and Sun, 2011). At the end of 20 minutes, the PE cannulas were removed from the rat carotid arteries and the perfusate was collected from the end of the cannula for HPO quantification in the perfusate by HPLC**.** Following this, the rat was decapitated, the brain was taken out and process as described in **Section 2.1.7** for quantification of HPO in the brain by HPLC.

3.2.5 *Brain uptake calculation*

Brain uptake was calculated as described in **Section 2.1.11**. Brain uptake of total HPO in whole brain ($R_{Br,u}$) and capillary depleted brain ($R_{Cd,u}$) were compared to evaluate the HPO trapping in BCEC. Additionally, brain uptake of unbound HPO in brain ($R_{Cd,uu}$) was used to describe the pharmacologically active HPO in brain. $R_{Cd,uu}$ was transformed to rate of brain uptake ($K_{in,Cd,uu}$) by dividing with total perfusion time as described in **Section 2.1.11**.

For concentration-competition study with CP84, total flux ($J_{in,total}$) was calculated as follows:

$$J_{in,total}(nmol/min/g) = K_{in,Cd,uu} * C \qquad \textbf{Equation 3.2.1}$$

Where $K_{in,Cd,uu}$ is the rate of brain uptake for HPO perfused at a defined concentration, *C*. $J_{in,total}$ was fitted into Michaelis-Menten kinetics which consist of saturable (facilitated diffusion) and unsaturable (membrane diffusion) components of brain uptake (Pardridge, 1983; **Equation 3.2.2**):

$$J_{in,total} = \frac{V_{max} * C}{K_m + C} + (K_d * C) \qquad \textbf{Equation 3.2.2}$$

Where V_{max} is the maximal velocity of brain uptake for saturable component, K_m is the concentration of HPO at half-V_{max} and K_d is the membrane diffusion constant of unsaturable component. The K_d was determined by calculating the slope of flux against

concentration for values after saturation using least-square linear regression analysis. Saturation points are the points which the values did not significantly different from each other. The K_d was multiplied with *C* to obtain the brain uptake of unsaturable component, i.e. membrane diffusion, D_m (**Equation 3.2.3**).

$$D_m = K_d * C \qquad \textbf{Equation 3.2.3}$$

$J_{in,net}$ was obtained by subtracting D_m from $J_{in,total}$ (**Equation 3.2.4**).

$$J_{in,net} = J_{in,total} - D_m \qquad \textbf{Equation 3.2.4}$$

Nonlinear regression analysis (Michaelis-Menten) were performed for $J_{in,net}$ to obtain V_{max} and K_m for facilitated diffusion transport (**Equation 3.2.5**).

$$J_{in,net} = \frac{V_{max} * C}{K_m + C} \qquad \textbf{Equation 3.2.5}$$

3.2.6 *Relationship between brain uptake and HPOs physicochemical properties*

Brain uptake was plotted against HPO physicochemical properties [lipophilicity (cLogP), molecular weight (MW) and total polar surface area (TPSA)] derived from ChemDraw Software (Version 15.1). Least-square linear regression analysis was performed to investigate the relationship between brain uptake and the physicochemical properties.

3.2.7 *Statistical and data analysis*

Data from all experiments are presented as mean + or ± standard error of the mean (SEM). Due to the broad range of experimental design and methods, specific details of statistical analyses performed on individual data sets will be presented in the context of the data. Statistical significance was taken as follows: Not significant $p > 0.05$, * $p < 0.05$, ** $p < 0.01$, *** $p < 0.001$. All statistical analyses were performed using GraphPad Prism 7 (GraphPad Software, Inc, USA).

3.3 *Results*

3.3.1 *Brain uptake of novel HPOs*

In order to compare the brain permeability of novel HPOs with CP20, *in situ* brain perfusion with the novel HPOs (500 µM) was performed for 20 minutes in rats. Brain uptake of total HPO in whole brain ($R_{Br,u}$) and in capillary depleted brain ($R_{Cd,u}$) was calculated by finding a ratio between the total concentration of HPO in brain and unbound HPO in perfusate as described in **Section 2.1.11**. All the HPO evaluated penetrated the brain to some extent except FCF132 **(Figure 3.3.1)**. $R_{Br,u}$ showed the sum of brain uptake of total HPO in brain capillary endothelial cells (BCEC) and brain parenchyma. On the other hand, $R_{Cd,u}$ showed brain uptake of total HPO only in brain parenchyma. There were no significant differences between $R_{Br,u}$ and $R_{Cd,u}$; F (16, 87) = 5.218, for all of the HPOs perfused which indicate no trapping in BCEC. For this reason, only uptake into capillary depleted brain will be considered from this point.

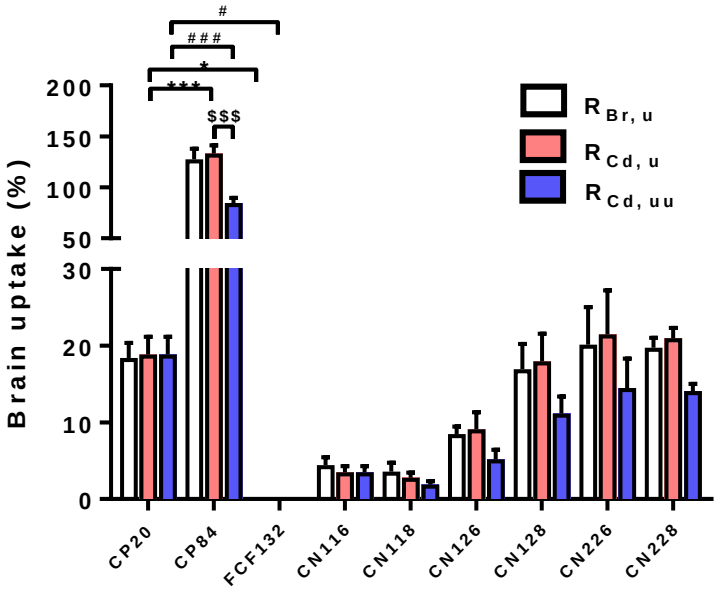

Figure 3.3.1: Brain uptake of HPO iron chelators for total HPO in whole brain ($R_{Br,u}$), total HPO in capillary depleted brain ($R_{Cd,u}$) and unbound HPO ($R_{Cd,uu}$) in capillary depleted brain over 20 minutes *in situ* brain perfusion.

Data are expressed as mean+SEM (n=3-10 rats). $p < 0.05$, *** $p < 0.001$ HPOs $R_{Cd,u}$ compared to CP20 $R_{Cd,u}$. # $p < 0.05$, ### $p < 0.001$ HPOs $R_{Cd,uu}$ compared to CP20 $R_{Cd,uu}$. $$$ $p < 0.001$ compared between $R_{Cd,u}$ and $R_{Cd,uu}$. No significant different, $p > 0.05$ compared **i)** between R_{Bru} and R_{Cdu} for matched HPO **ii)** between $R_{Cd,uu}$ for enantiomer pair; CN116 vs CN118, CN126 vs CN128, CN226 vs CN228 (2-way ANOVA followed by Holm-Šídák multiple comparison test).*

Brain uptake of total HPO in capillary depleted brain ($R_{Cd,u}$) includes the bound and unbound HPO in the brain parenchyma, therefore, it describes brain uptake beyond BBB and the affinity of HPO towards brain tissue (**Figure 3.3.1**). $R_{Cd,u}$ for CP84 was considerably greater than CP20 (7.1-fold). FCF132 however was undetectable in brain after perfusion despite having glucose moiety attached to the parent molecule. CN116, CN118, CN126, CN128, CN226 and CN228 brain uptake showed no significant different compared to CP20. In addition, enantiomer pair of CN compounds (CN116 vs CN118; CN126 vs CN128; CN226 vs CN228) were also not different from each other, without any trend towards significant.

Brain uptake for unbound HPO in brain ($R_{Cd,uu}$) described the uptake of pharmacologically relevant HPOs in brain tissue since only unbound HPO can chelate iron (**Figure 3.3.1**). The $R_{Cd,uu}$ to $R_{Cd,u}$ ratio for matched HPOs reflect the unbound portion of HPOs in the brain. The $R_{Cd,uu}$ to $R_{Cd,u}$ ratio for CP20 and CN116 were 1.0, and therefore were 100% unbound in the brain. The $R_{Cd,uu}$ to $R_{Cd,u}$ ratio for CP84, CN118, CN128, CN226 and CN228 were between 0.62 to 0.69 which translate into 62% to 69% unbound HPOs in the brain. The $R_{Cd,uu}$ to $R_{Cd,u}$ ratio for CN126 was the lowest among all HPOs, which was 0.56 (56% unbound in brain). Statistically, the unbound CP20 in the brain ($R_{Cd,uu}$) was not significantly different from the total CP20 in the brain ($R_{Cd,u}$). Likewise, all other HPOs were also showed no significant difference except for CP84 where the $R_{Cd,uu}$ was 1.6-fold lower than the $R_{Cd,u}$. Comparison of $R_{Cd,uu}$ for HPOs with CP20 revealed that only $R_{Cd,uu}$ for CP84 was higher than CP20 by 4.5-fold, while $R_{Cd,uu}$ for other HPOs were not significantly different than CP20, although $R_{Cd,uu}$ for CN116, CN118 and CN126 tended to be reduced suggesting a trend towards lower brain uptake than CP20. Additionally, $R_{Cd,uu}$ and $R_{Cd,u}$ for CN compounds enantiomer pair was not different from each other.

The rate of brain uptake for unbound HPO in brain ($K_{in,Cd,uu}$) was calculated as described in **Section 2.1.11**. The $K_{in,Cd,uu}$ ranked from the fastest to the slowest was: CP84>CN226>CN228>CP20>CN128>CN126>CN116>CN118<FCF132 (**Table 3.3.1**). The $K_{in,Cd,uu}$ for CP84 was 4.5-fold faster than CP20. The $K_{in,Cd,uu}$ for CN128, CN226 and CN228 were not different than CP20. On the other hand, the $K_{in,Cd,uu}$ for CN126, CN116 and CN118 were 3.6-, 5.2- and 9.4-folds slower than CP20. Additionally, $K_{in,Cd,uu}$ for CN compounds enantiomer pair was not different from each other.

Table 3.3.1: Rate of brain uptake for unbound HPO in brain ($K_{in,Cd,uu}$) over 20 minutes *in situ* brain perfusion.

HPOs	$K_{in,Cd,uu}$ (µL/min/g)		n
CP20	9.4±1.1		10
CP84	42.3±2.6	***	5
CN116	1.8±0.4	*	3
CN118	1.0±0.2	**	3
CN126	2.6±0.6	*	3
CN128	5.6±1.1		3
CN226	7.2±1.9		3
CN228	7.1±0.4		3

*Data are expressed as mean±SEM (n=3-10 rats). * p < 0.05, ** p < 0.01, *** p < 0.001 compared to CP20. No significant different, p > 0.05 when enantiomer pair was compared; CN116 vs CN118, CN126 vs CN128, CN226 vs CN228 (1-way ANOVA followed by by Holm-Šídák multiple comparison test).*

3.3.2 *HPO brain uptake relationship with lipophilicity (cLogP)*

Lipophilicity plays an important role in brain uptake for molecules that are not a substrate for any transporters via passive membrane diffusion and can be used to investigate the mechanism of HPOs transport across BBB. Predicted lipophilicity (cLogP) was employed in this study as a measured of HPOs lipophilicity. CP84 and CN compounds were between 3 to 108-folds more lipophilic than CP20. On the other hand, FCF132 was 4-fold less lipophilic than CP20 (**Figure 3.3.2**).

In order to see a relationship between HPO brain uptake and cLogP, least-square linear regression analysis was performed on the plot of HPO $R_{Cd,uu}$ against cLogP (**Figure 3.3.2**). Overall the HPOs $R_{Cd,uu}$ tended to have a positive linear relationship with cLogP although this was not significant. However, when comparing the CN compounds alone, there was a significant linear relationship with cLogP.

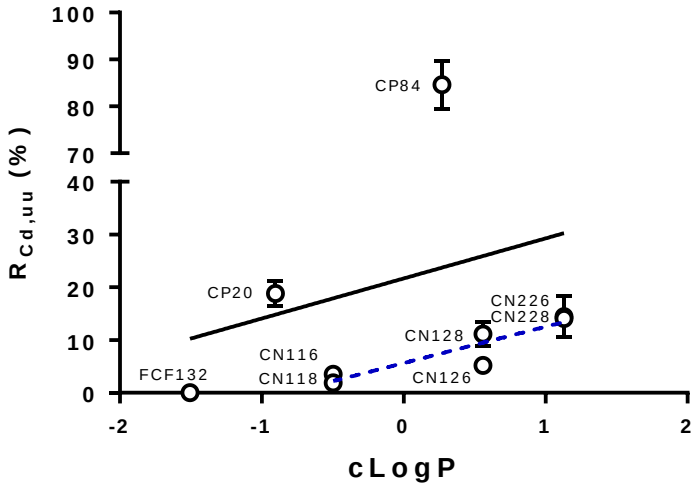

	a) Black line (all HPOs)	b) Blue line (CN compounds only)
r^2	0.0625	0.6444
df	36	16
p	0.1391	<0.0001 *

Figure 3.3.2: Regression analysis of $R_{Cd,uu}$ plotted against HPO lipophilicity (cLogP).

Black circle *(○) represents $R_{Cd,uu}$ for HPO.* ***Black line*** *(—) represents best-fit line for least-square regression analysis on compounds represented by* ***black circle*** *(○).* ***Blue dotted line*** *(…) represents best-fit line for least-square linear regression analysis performed on CN compounds. HPOs cLogP were obtained using a ChemDraw Software version 15.1. Data are expressed as mean±SEM (n=3-5 rats). Significant difference (*) for least-square linear regression analysis was set at p <0.05. Co-efficient of variation (r^2), degree of freedom (df: n-2) and p values for all lines were calculated using GraphPad Prism 7 software.*

3.3.3 *Brain uptake-inhibition studies*

To evaluate the contribution of transporters to the brain uptake of HPOs, selected HPOs were perfused with inhibitors of the proposed transporters. In addition, FCF132, an HPO that has a glucose moiety conjugated to the pyridinone ring (**Table 3.2.1**), was also evaluated for uptake in a lower non-physiological concentration of glucose in order to determine if glucose in the perfusion fluid was inhibiting or competing for the glucose transporter (GLUT1).

a) Evaluation of the carrier-mediated uptake of CP84 into brain

CP84 showed a very high uptake into the brain compared to CP20 suggesting that it might be carrier-mediated. To ascertain whether CP84 was carrier-mediated by a specific transporter into the brain, a range of concentrations of CP84 (5-500 µM). $R_{Cd,uu}$ for group perfused with 5 µM CP84 was 2.1-fold higher compared to brain uptake for group perfused with 500 µM CP84 (**Figure 3.3.3**). There was no different in $R_{Cd,uu}$ for the groups perfused with 50 and 250 µM CP84 compared to group perfused with 500 µM CP84 which indicate saturation of transporter. There was a concentration related decrease in $R_{Cd,uu}$, such that with increasing concentration $R_{Cd,uu}$ values reduced up to 250 µM. there was no further reduction when CP84 concentration was increased to 500 µM suggesting saturation of the transporter.

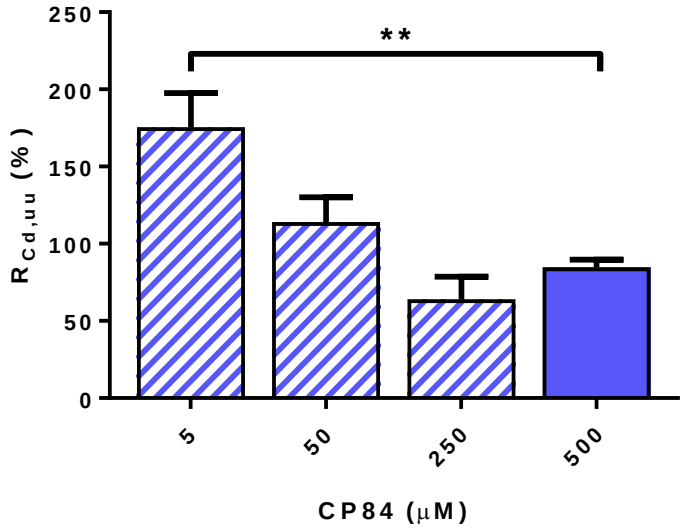

Figure 3.3.3: Self-inhibition study for CP84 at various concentrations

*Data are expressed as mean+SEM (n=3-5 rats). The 500 µM CP84 data was taken from **Figure 3.3.1**. ** p < 0.01 compared to group perfused with 500 µM CP84 (1-way ANOVA followed by Dunnett's test).*

There was a concentration-related decrease in rate of uptake with increasing concentration of CP84. The rate of uptake ($K_{in,Cd,uu}$) for 50 and 250 µM CP84 showed no different with CP84 $K_{in,Cd,uu}$ perfused with 500 µM CP84 (**Table 3.3.2**). In contrast, CP84 $K_{in,Cd,uu}$ perfused with 5 µM CP84 was 2.1-fold faster than CP84 $K_{in,Cd,uu}$ perfused with 500 µM CP84.

Table 3.3.2: Rate of brain uptake for total CP84 in brain ($K_{in,Cd,uu}$) over 20 minutes *in situ* brain perfusion with various concentration of CP84.

CP84 (µM)	$K_{in,Cd,uu}$ (µL/min/g)	n
5	87.8±11.0 **	3
50	57.0±8.1	4
250	32.0±7.3	3
500	42.3±2.6	5

*Data are expressed as mean±SEM (n=3-5 rats). ** p < 0.01 compared to group perfused with 500 µM CP84 (1-way ANOVA followed by Dunnett's test).*

$R_{Cd,uu}$ was converted to total flux that described the velocity of CP84 uptake at different concentration as showed in **Figure 3.3.4**. The membrane diffusion constant, K_d for CP84 flux determined by the slope of unsaturable component (**Figure 3.3.4, blue line**) was 29.6±0.8 µL/min/g. CP84 flux at 50 µM concentration showed initial saturation of the uptake process. Non-linear regression analysis following a Michaelis-Menten kinetics was performed on the saturable component to obtain the maximum velocity (V_{max}) and half-maximal concentration (K_m) of CP84 transport (**Figure 3.3.4, red line**). V_{max} and K_m for CP84 transport was 13.1±3.5 nmol/min/g and 135.7±2.8 µM respectively.

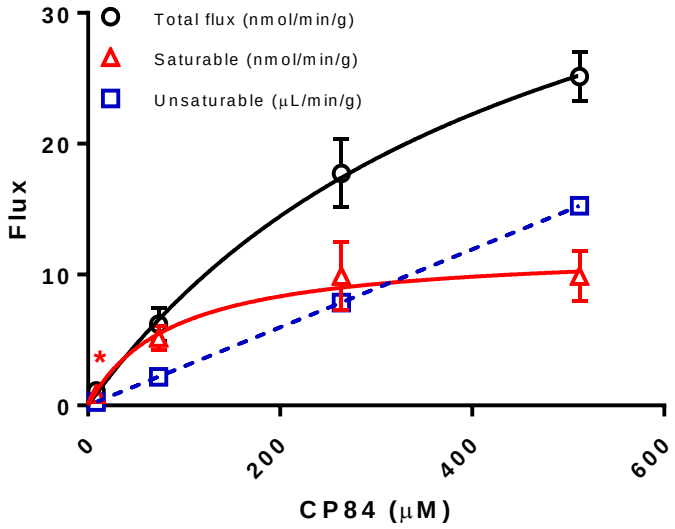

Figure 3.3.4: CP84 flux derived from bar graph in Figure 3.3.4.

*Least-square linear regression analysis was performed on the unsaturable component (□) of CP84 flux to obtain membrane diffusion constant, K_d. For unsaturable component (□), the SEM were very small compared to the scale and was not visible in the graph. Nonlinear regression analysis following a Michaelis-Menten model was fitted for saturable component (Δ) of CP84 flux to obtain V_{max} and K_m. Data are expressed as mean±SEM (n=3-5 rats). * p < 0.05, compared to group perfused with 500 µM CP84 of the saturable component (1-way ANOVA followed by Dunnett's test).*

CP84 was postulated to be a substrate for large amino acid transporter (LAT1) based on the N-phenyl group in the chemical structure. Therefore, a specific inhibitor of LAT1, 2-amino-2-norbornanecarboxylic (BCH), was co-perfused with 50 or 500 µM CP84 for 20 minutes. The reported concentration for BCH (10 mM) that sufficiently inhibit LAT1 was used in this study (Ennis et al., 1998). BCH caused reduction in CP84 brain uptake for rats perfused with 50 or 500 µM CP84 which confirmed contribution of LAT1 in CP84 brain uptake (**Figure 3.3.5**).

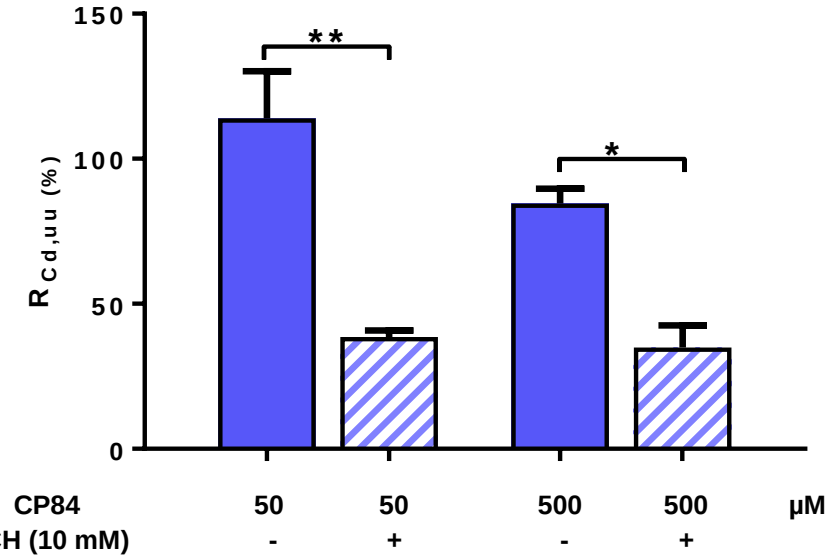

Figure 3.3.5: Inhibition study of CP84 with 10 mM BCH.

*The data for 50 µM and 500 µM CP84 without 10 mM BCH were taken from **Figure 3.3.4**. Data are expressed as mean+SEM (n=3-5 rats). ** p < 0.01, compared to 50 µM CP84 perfused without 10 mM BCH; * p< 0.05, compared to 500 µM CP84 perfused without 10 mM BCH (2-way ANOVA followed by Holm-Šídák multiple comparison test).*

$K_{in,Cd,uu}$ for 500 µM CP84 perfused with 10 mM BCH was 1.9-fold slower than perfusion without 10 mM BCH. On the other hand, $K_{in,Cd,uu}$ for 50 µM CP84 perfused with 10 mM BCH was 3.0-folds slower than perfusion without 10 mM BCH (**Table 3.3.3**).

Table 3.3.3: Rate ($K_{in,Cd,uu}$) of CP84 brain uptake co-perfused with 10 mM BCH over 20 minutes *in situ* brain perfusion.

CP84	$K_{in,Cd,uu}$ (µL/min/g)	
	No BCH	10 mM BCH
50 µM	57.0±8.1	19.3±1.1 **
500 µM	42.3±2.6	17.4±3.8 *

*Data are expressed as mean+SEM (n=3-5 rats). * p< 0.05 compared to 500 µM CP84 perfused without 10 mM BCH, ** p < 0.01 compared to 50 µM CP84 perfused without 10 mM BCH; (2-way ANOVA followed by Holm-Šídák test multiple comparison test).*

b) Evaluation of FCF132 uptake into brain in low glucose

In the previous section (**Section 3.3.1**), it was revealed that FCF132 failed to get into the brain. It was postulated that the physiological concentration of glucose (10 mM) might competitively inhibited the GLUT-1 transporter. Therefore, a lower concentration of glucose was used in the perfusion fluid (1 mM). Perfusion fluid was supplemented with 1 mM pyruvate to compensate the lower glucose to support normal brain metabolism (Broer et al., 1998). It was determined from this experiment that none of the FCF132 was detected even though when lower concentration of glucose was used (**Figure 3.3.6**).

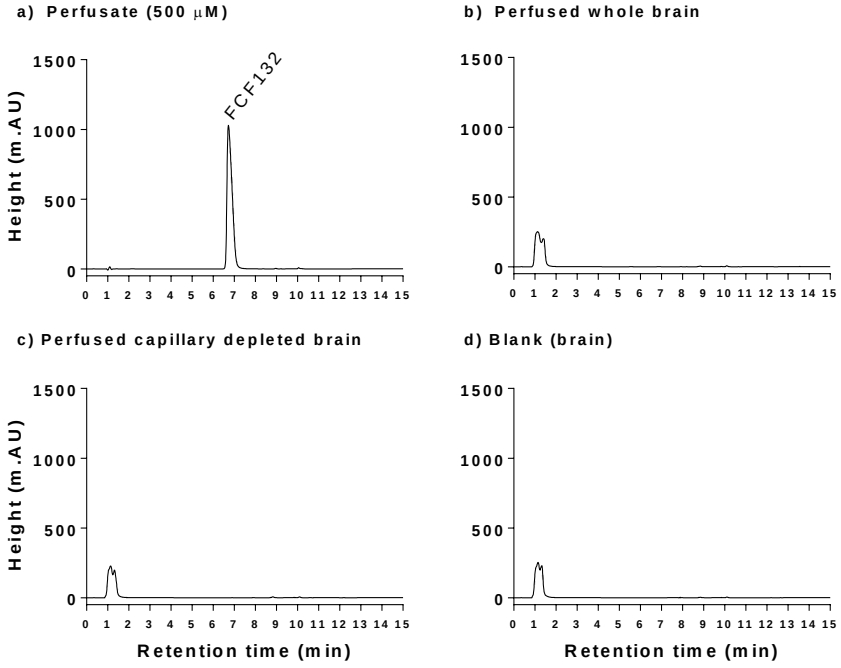

Figure 3.3.6: Chromatograms of FCF132 in lower glucose condition *a)* FCF132 perfusate *b)* FCF132 perfused whole brain *c)* FCF132 perfused capillary depleted brain *d)* blank (whole brain). FCF132 retention time was ~6.7 minute.

c) Evaluation of the affinity of CP20, CN118, CN128 and CN226 for the Pgp efflux pump

In order to determine the role of the Pgp efflux pump in brain uptake, CP20, CN118, CN128 and CN226 were co-perfused with 5 µM CsA, a Pgp efflux-pump inhibitor. $R_{Cd,uu}$ for CP20, CN118 and CN128 co-perfused with CsA were not different from $R_{Cd,uu}$ for CP20, CN118 and CN128 perfused without CsA (**Figure 3.3.7**). By contrast $R_{Cd,uu}$ for CN226 co-perfused with CsA were increased by 2.1-fold compared to $R_{Cd,uu}$ for CN226 perfused without CsA. This observation confirmed that CN226 is a substrate–for PgP efflux pump. $R_{Cd,uu}$ for CN226 co-perfused with CsA was 2.1- and 2.6-folds higher than $R_{Cd,u}$ for CP20 perfused without and with CsA respectively. Conversely, $R_{Cd,uu}$ for CN118 perfused without CsA were 7.5-fold lower than $R_{Cd,uu}$ for CP20 perfused without CsA.

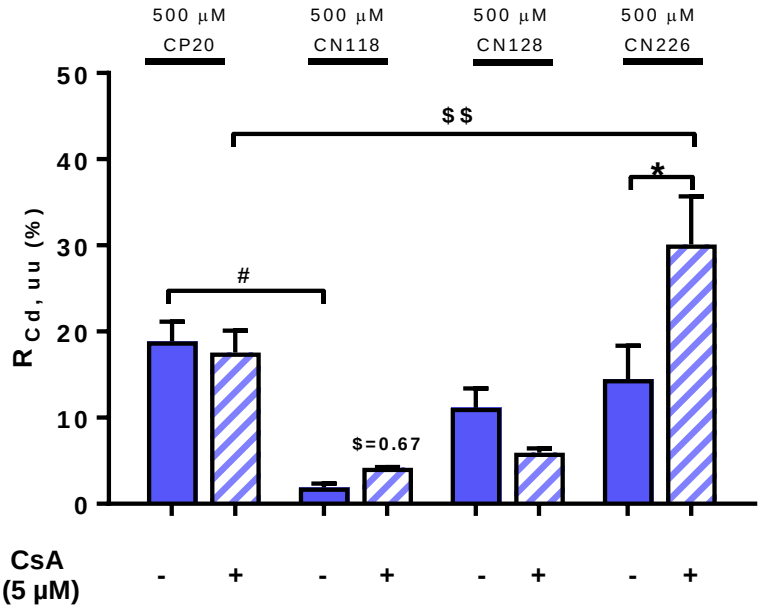

Figure 3.3.7: Effect of Pgp inhibitor on the brain uptake of selected HPOs.

*The data for 500 µM CP20, CN118, CN128 and CN226 without 5 µM CsA were taken from **Figure 3.3.2.** Data are expressed as mean+SEM (n=3-5 rats). * p< 0.05 compared to group perfused without 5 µM CsA. # p < 0.05 compared to CP20 perfused without 5 µM CsA. $$ p < 0.01 compared to CP20 perfused with 5 µM CsA (two-way ANOVA followed by Holm-Šídák multiple comparison test).*

$K_{in,Cd,uu}$ for CP20, CN118 and CN128 co-perfused with CsA were not different from $K_{in,Cd,uu}$ for CP20, CN118 and CN128 perfused without CsA (**Table 3.3.4**). In contrast, $K_{in,Cd,uu}$ for CN226 co-perfused with CsA were faster by 2.0-fold compared to $K_{in,Cd,uu}$ for CN226 perfused without CsA. This observation confirmed that CN226 were substrates for Pgp

efflux pump transporters. $K_{in,Cd,uu}$ for CN226 co-perfused with CsA was 1.6-fold faster than $K_{in,Cd,uu}$ for CP20 with CsA. Conversely, $K_{in,Cd,uu}$ for CN118 without CsA were 9.9-fold slower than $K_{in,Cd,uu}$ for CP20 without CsA.

Table 3.3.4: Rate ($K_{in,Cd,uu}$) of selected HPOs brain uptake co-perfused with 5 µM CsA over 20 minutes *in situ* brain perfusion.

HPO (500 µM)	$K_{in,Cd,uu}$ (µL/min/g)	
	No CsA	5 µM CsA
CP20	9.4±1.1	8.8±1.3
CN118	1.0±0.2 #	2.1±0.04
CN128	5.6±1.1	3.0±0.2
CN226	7.2±1.9	15.1±2.8 ***, $$**

*Data are expressed as mean±SEM (n=3-5 rats). * p < 0.05 compared to group perfused without 5 µM CsA. # p < 0.05-compared to CP20 perfused without 5 µM CsA. $$ p <0.01 compared to CP20 perfused with 5 µM CsA (2-way ANOVA followed by Holm-Šídák multiple comparison test).*

3.3.4 *Relationship of brain uptake with physicochemical properties before and after inhibition studies.*

Brain uptake ($R_{Cd,uu}$) of HPOs before and after inhibition studies were plotted against their physicochemical properties namely lipophilicity (cLogP), molecular weight (MW) and total polar surface area (TPSA) followed by analysis with least-square linear regression analysis (**Figure 3.3.8**).

Initially, there was no significant relationship between $R_{Cd,uu}$ for HPOs and cLogP. However, after transport inhibition study with selected HPOs, a positive relationship emerged between $R_{Cd,uu}$ and cLogP that was statistically significant (**Table 3.3.8a**).

MW for novel iron chelators are between 1.4- to 2.6-folds higher than CP20. There was no significant relationship between $R_{Cd,uu}$ and MW. Transport inhibition with selected HPOs did not improve the relationship (**Table 3.3.8b**).

TPSA for CP84 is the same as CP20. TPSA for all CN compounds was 1.5-folds higher than CP20. FCF132 shows the highest TPSA which is 3.0-fold higher than CP20. There was a negative relationship between $R_{Cd,uu}$ and TPSA both before and after inhibition studies (**Table 3.3.8c**).

a) Lipophilicity

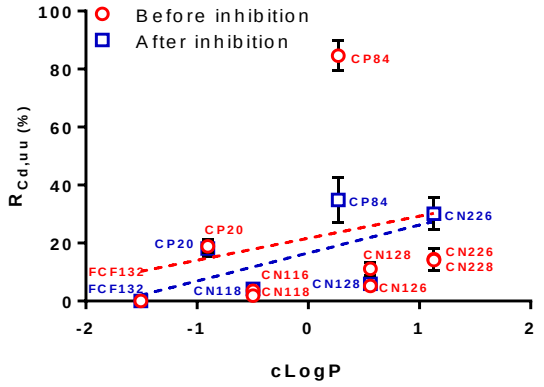

	Red line (control brain uptake)	Blue line (after inhibition of uptake or efflux)
r^2	0.0903	0.4834
p	0.0668	0.0003 *

b) Molecular weight

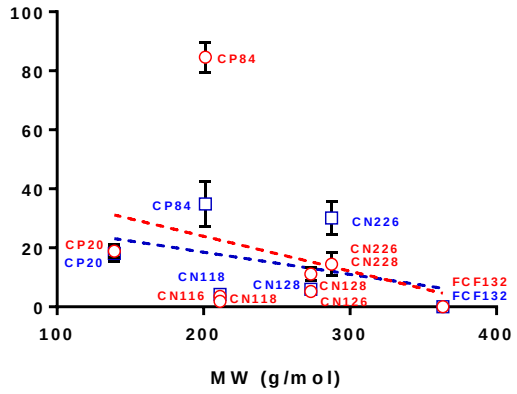

	Red line (control brain uptake)	Blue line (after inhibition of uptake or efflux)
r^2	0.0663	0.0805
p	0.1187	0.2006

c) Total polar surface area

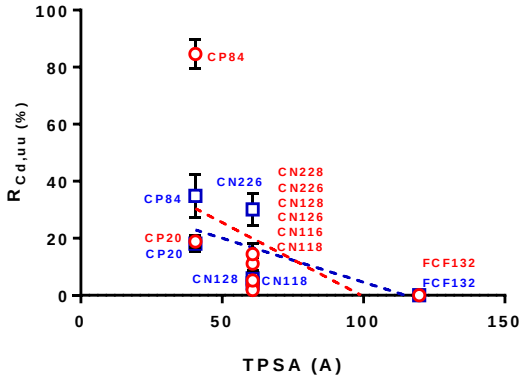

	Red line (control brain uptake)	Blue line (after inhibition of uptake or efflux)
r^2	0.1956	0.3218
p	0.0054 *	0.0059 *

Figure 3.3.8: Regression analysis of brain uptake of total HPO in brain ($R_{Cd,u}$) plotted against HPO physicochemical properties.

*Graphs show selected HPO $R_{Cd,uu}$ plotted against a) lipophilicity (cLogP) b) molecular weight (MW), c) total polar surface area (TPSA). Red circle (○) represents $R_{Cd,uu}$ **before** perfusion with transport inhibitors. Blue square (□) represents $R_{Cd,uu}$ **after** perfusion with transport inhibitors. Red dotted line (…) represents best-fit line for regression analysed on compounds represented by red circle (○). Blue dotted line (…) represents best-fit line for least square-linear regression analysis performed on compounds represented by blue square (□). Data are expressed as mean±SEM (n=3-5 rats). HPO physicochemical properties were obtained using ChemDraw Software version 15.1. Significant difference (*) for linear regression analysis was set at $p < 0.05$. Co-efficient of variation (r^2), degree of freedom (Df; n-2) and p values were calculated using linear-regression analysis.*

3.4 *Discussion*

In situ brain perfusion was performed in rats in this study to evaluate the brain permeability of novel HPO iron chelators compared to CP20. It was hypothesised that the structure modification of CP20 could enhanced brain uptake. The current study revealed that, of the seven novel HPOs that permeated the brain, only CP84 showed marked increment increase in the rate of brain uptake compared to CP20. Indeed, FCF132, which contains the glucose moiety, was, by contrast unable to cross the BBB.

3.4.1 *Summary of the findings*

CP20 successfully crossed the BBB by simple membrane diffusion which agrees with previous finding (Habgood et al., 1999, Hider et al., 2011b, Glickstein et al., 2005). Only CP84 has a faster rate of brain uptake than CP20 while the three HPOs (CN128, CN226 and CN228) have equal rate of brain uptake with CP20. On the other hand, the rate of brain uptake for the other three HPOs (CN116, CN118 and CN126) were slower than CP20. A glycosylated HPO, FCF132 did not permeate the brain at all. There was no different in the rate of brain uptake for the HPO chiral pair (CN116 vs CN118; CN126 vs CN128; CN226 vs CN228). Transport inhibition studies showed that CP84 is a substrate for L-type amino acid transporter-1 (LAT1), while CN226 is a substrate for Pgp efflux pump. Total polar surface area (TPSA) exhibit the best relationship with the rate of brain uptake followed by lipophilicity (cLogP). In contrast, molecular weight seems not to play an important role for this set of compounds. Summary of overall finding was compiled in **Table 3.4.1**.

Table 3.4.1: Summary of the findings

	Rate of brain uptake			Physicochemical properties			Unbound
	No inhibitor	**With influx inhibitor**	**With efflux inhibitor**	**Lipophilicity (cLogP)**	**Molecular weight (MW)**	**TPSA**	**Brain**
CP20	**+ +**	**na**	**nc**	**+ +**	**+**	**+**	**+ + + +**
CP84	+ + +	+ + + +	na	**+ + + +**	**+ +**	**+**	**+ + +**
FCF132	nd	nd	na	**+**	**+ + + +**	**+ + +**	na
CN116	+	na	na	**+ +**	**+ +**	**+ +**	**+ + + +**
CN118	+	na	nc	**+ +**	**+ +**	**+ +**	**+ + +**
CN126	+	na	na	**+ + +**	**+ + +**	**+ +**	**+ +**
CN128	+ +	na	nc	**+ + +**	**+ + +**	**+ +**	**+ + +**
CN226	+ +	na	+ + +	**+ + + +**	**+ + +**	**+ +**	**+ + +**
CN228	+ +	na	na	**+ + + +**	**+ + +**	**+ +**	**+ + +**

*CP20 is highlighted in **green**. nc=no change, na=not applicable, nd= not detected.*

Legend: + = low; ++ = mild; +++ = moderate; ++++ = high

HPOs that leak into perivascular space (PVS) around brain arterioles and venules, which exhibits minimal barrier properties, do not penetrate the brain due to the presence of astrocytic end feet that surround the PVS (Sofroniew, 2015). These astrocytic end feet form a barrier similar to BBB termed the glial limitans which prevents the entry of HPOs into brain parenchyma. Additionally, specialised brain structure collectively known as circumventricular organs (CVOs), which include choroid plexus, are also supplied with 'leaky capillaries' (Gross, 1992, Ganong, 2000). However, specialised epithelial wall that line these structures are sealed with tight junctions likened to BBB, preventing HPOs entry into brain parenchyma (Gross, 1992, Langlet et al., 2013). Methodologically, these routes of HPOs penetration has been considered in this study by subtracting the total brain uptake with the non-permeant BBB marker, ^{14}C-sucrose (**Section 2.1.14a**). In addition, highly perfused choroid plexus that are easily accessible anatomically were removed during brain dissection before the brain homogenisation process to minimise experimental error (**Section 2.1.7**).

3.4.2 *Brain uptake of CP20*

There was no difference in brain uptake of CP20 in brain between whole brain and capillary depleted brain. The distinction between uptake into whole brain and capillary depleted brain is important to avoid false positive interpretation of HPO uptake (Paris-Robidas et al., 2016). This is because, whole brain uptake comprised the HPO contained in brain capillary endothelial cells (BCEC) and brain parenchyma, whereas capillary depleted brain uptake showed HPO only in brain parenchyma (Triguero et al., 1990). This data showed

that CP20 did not accumulate in BCEC and successfully traverse beyond BBB into the brain parenchyma and is in agreement with previous findings of Roy et al. (2010).

After 20 minutes *in situ* brain perfusion, CP20 was detected in capillary depleted brains with total and unbound brain uptake of 21%. This study is not the first to report CP20 brain uptake in rats using *in situ* brain perfusion method. An *in situ* brain perfusion with CP20 performed in Wistar rat for 1 minute showed approximately 1% of CP20 perfused get into the brain (Habgood et al., 1999). Regardless of the lower CP20 uptake due to shorter perfusion, the rate of uptake per unit time of unbound CP20 in brain was not significantly different from the current study (12.9±1.2 vs 9.4±1.1 µL/min/g) which confirmed the validity of this technique across different laboratories. The rate of uptake for CP20 in this study is comparable to other CNS-targeted drugs such as the serotonin receptor (5HT1) agonist, rizatriptan (Summerfield et al., 2007) and the anticancer drug, vincristine (Greig et al., 1990). A recent report on CP20 brain uptake using 20 minutes *in situ* brain perfusion in Dunkin-Hartley guinea pigs (Roy et al., 2010) showed 2-fold lower rate of CP20 brain uptake than previously reported in rats (Habgood et al., 1999). This was probably because of the interspecies difference as variation in brain uptake of the same drug between Wistar rats and Dunkin-Hartley guinea pigs can be as high as 7-folds (Tóth et al., 2014). Indeed, variations in gene sequences and level of protein expression across species including human may affect the activities of metabolic enzymes and transporters at BBB (Syvanen et al., 2009). For example, higher concentration of Pgp inhibitor were needed in Guinea pigs than in rats to achieve a similar increase in brain concentration of a Pgp substrate (Cutler et al., 2006). However, this does not explain the discrepancy of brain uptake observed for CP20 between rats and Guinea pig as the current study showed that CP20 was not a substrate for Pgp. This may suggest the differential contribution of other efflux pumps families or alternatively enhanced brain metabolism in one but not in the other species (Syvanen et al., 2009). There is no systematic study or evidence on which rodent species better represents brain uptake in humans, and therefore it is not possible to conclude which species should be used to determine brain uptake. However, rats pose a number of advantages over other rodent species due to their wide use to model CNS associated diseases such as Parkinson's disease, ischaemic stroke and traumatic brain injury which means comparison and translation between studies are possible (Duty and Jenner, 2011, Fluri et al., 2015, Xiong et al., 2013). Nevertheless, it has previously been reported than brain uptake of CP20 in rats was primarily governed by simple membrane

diffusion as reported by Habgood et. al. (1999), Glickstein et. al. (2005) and Hider et. al. (2011) which corresponds to the linearity of brain uptake for CP20 for up to 60 minutes perfusion showed in the current study (**Figure 2.1.21**).

3.4.3 *Brain uptake of novel HPOs*

As for CP20, there was no difference in brain uptake of novel HPOs between whole brain and capillary depleted brain apart from FCF132, these data confirmed the successful penetration of HPO into the brain parenchyma. FCF132 was not detected in either whole brain or capillary depleted brain suggesting poor penetration of the BBB. In this section, brain uptake of novel HPO iron chelators will be discussed.

a) CP84

Following 20 minutes *in situ* brain perfusion, CP84, a N-phenyl derivative of CP20 perfused at 500 µM showed remarkably higher brain uptake than CP20. The rate of brain uptake for unbound CP84 in brain was 87.8±11.0 µL/min/g compared to CP20 (9.4±1.1 µL/min/g). To put this into a perspective, rate of brain uptake for CP84 is comparable to other CNS active drug such as butanediol (Abbott, 2004), prazosin (Cisternino et al., 2004), pramipexole (Okura et al., 2007), theophylline (Liu et al., 2004) and tolbutamide (Murakami et al., 2000). In addition, the rate of brain uptake for CP84 was also comparable to the essential amino acids, L-lysine and L-glutamine (Smith, 2000).

The high rate of brain uptake for CP84 could not be explained by its lipophilicity, therefore, it can be concluded that CP84 may entered the brain via a carrier-mediated process in addition to the passive membrane diffusion. To confirm that CP84 brain uptake was by a carrier mediated transport, *in situ* brain perfusion with CP84 were performed for 20 minutes over a wide concentration range to see if at high concentration of CP84, the transporter was saturated. It was revealed that the rate of brain uptake for CP84 showed concentration-related decrease suggesting that CP84 brain uptake was carrier-mediated (Greenwood et al., 1982, Chapy et al., 2016). Interaction with a specific transporter is not a sole indicator for a high brain uptake at the BBB. Diazepam and sertraline are a perfect example of CNS active compound that has extremely high rate of brain uptake just by a simple membrane diffusion and not carrier mediated (Dubey et al., 1989, Badhan et al., 2014), therefore, it is possible that CP84 is also able to get into the brain via simple

diffusion in addition to the carrier-mediated process. To look on more detail on the transport kinetics of CP84, the rate of brain uptake was transformed into flux which showed the velocity of the transport process at the different CP84 concentrations. It was discovered that after a non-linear regression analysis using Michaelis-Menten model, the V_{max} and K_m for CP84 were 13.1±3.5 nmol/min/g and 135.7±2.8 µM respectively**.** The second mechanism was non-saturable uptake through membranes diffusion with K_d of 29.6±0.8 µL/min/g. These results confirmed that CP84 crossed the BBB by carrier-mediated transport process in addition to passive membrane diffusion.

The chemical structure of CP84 is different from CP20 by a single additional phenyl moiety linked to the main 3-hydroxy-4-pyridinone ring (**Table 3.2.1**). This phenyl functional group can potentially interact with L-type amino acid transporter-1 (LAT1) that are abundantly expressed at the BBB (Boado et al., 1999, Boado et al., 2004). Indeed, several new compounds and pro-drugs bearing a phenyl group in the chemical structure have been successfully transported into the brain by targeting LAT1 (Peura et al., 2013, Peura et al., 2011). Additionally, an established pro-drug in clinic that is used as the main line of treatment for Parkinson's disease patients, L-dopa, utilises LAT1 at the BBB (Kageyama et al., 2000). As the evidence showed that CP84 brain uptake was partly carrier-mediated and its chemical structure contained N-phenyl group, it was proposed that CP84 is transported into the brain by means of the N-phenyl group interaction with LAT1 at the BBB. This appeared to be the case as brain uptake of CP84 was inhibited by BCH, the specific LAT1 inhibitor. Interestingly after BCH inhibition, the CP84 rate of brain uptake was about 20 µL/min/g which close to the K_d for CP84 which suggest the mechanism of CP84 brain uptake was mainly via membrane diffusion during LAT1 inhibition with BCH.

In summary, the strategy of adding phenyl group to the N1 of hydroxypyridinine ring increased the brain uptake of CP84 compared to CP20 by interaction with LAT1, however, CP84 was also crossed the BBB via membrane diffusion to a limited extent.

b) FCF132

The glucose transporter under subfamily 1 (GLUT1) is highly expressed at the BBB to transport glucose into the brain (Zheng et al., 2010, Ojelabi and Carruthers, 2015, Qutub and Hunt, 2005, Dwyer and Pardridge, 1993). Due to the high expression of GLUT1 at the BBB, targeting GLUT1 to enhance brain uptake could be one of the best strategies to circumvent the BBB. In this study, CP84 was conjugated with a glucose moiety to the 2-OH pyridinone ring to form FCF132 and evaluated for brain uptake with *in situ* brain perfusion. It was expected that brain uptake would be at least comparable to CP84 and higher than CP20. However, conjugation of glucose moiety to the parent molecules was showed to be counterproductive as FCF132 was not detected in the brain after 20-minute perfusion. The chromatogram of rat brain perfused with FCF132 also failed to show the presence of CP84, a metabolite of FCF132 which its presence might suggest FCF132 permeability into brain followed by metabolism to CP84. Lacking chromatogram peaks for FCF132 and CP84 in the perfused brain homogenate conclude that FCF132 was not transported at all. Indeed, it was reported previously that iodinated FCF132 also showed inability to cross the BBB (Roy et al., 2010). In that study, it was suggested that the addition of I^{125} for radioactivity detection might cause steric hindrance for FCF132 interaction to GLUT1. However, that was not the case, since the current study also showed undetectable FCF132 in the brain after perfusion. Similar negative outcome has been reported for other glucosylated HPO iron chelators. Glycosylated CP20 was undetectable in brain in contrast to the parent molecules which showed about 5% brain uptake (Roy et al., 2010). Nevertheless, there are reports of successful penetration of drug conjugated with glucose at BBB (Bonina et al., 2000, Bonina et al., 2003, Chen et al., 2009). In those studies, different glycol-conjugates such as 7-chlorokynurenic acid (Bonina et al., 2000), dopamine (Bonina et al., 2003) and ibuprofen (Chen et al., 2009) have been synthesized as candidates for the treatment of CNS diseases and showed increment in BBB permeability.

From these studies, it was unclear why FCF132 was unable to penetrate the BBB. It may be that, due to low affinity for GLUT1, FCF132 uptake was blocked by high levels of glucose in the NRS perfusion fluid. However, following *in situ* brain perfusion with FCF132 with lower concentration of glucose (1 mM) there was still no evidence of brain uptake. Due to the mix of report on success and failure of brain penetration by glycol-conjugates, a close examination of the mechanism of glucose binding to GLUT1 is warranted. This is

because, interaction for correct positioning and orientation of glucose molecules must occur for succesful transport (Deng et al., 2014). When the chemical structure of FCF132 was examined, the OH group on C3 of the pyridinone ring form a glycosidic bond with the OH group on C1 of the glucose ring.

According to a study by Mueckler and Makepeace (2009), the OH group on C1 of the glucose ring is vital for binding into the GLUT1 binding site via hydrogen bonds. Indeed, evidence based on competitive inhibition studies on erythrocyte GLUT1 showed that OH groups on C1 and C3 are paramount for glucose binding as they serve as hydrogen bond acceptor (**Figure 3.4.1**; Barnett et al., 1975, Carruthers et al., 2009). OH group on C4 is also capable to form hydrogen bond with GLUT1 and this was supported by the observation that galactose, which is an epimer of glucose at C4, has 10 times lower binding affinity than glucose for GLUT1. The most recent model of GLUT1 binding with glucose produced by Mucklear (2013) showed that OH group on C1, C3, C4 and C6 form hydrogen bonds with the active site, and this supported the earlier theory (Mueckler and Makepeace, 2009). Only the OH on C2 is free to form hydrogen bond within the GLUT1 active site. Additionally, it has been shown that bulky substitution of OH at C1 prevent binding to GLUT1 on the active site, while similar-size substitution at C6 did not (Carruthers et al., 2009).

a)

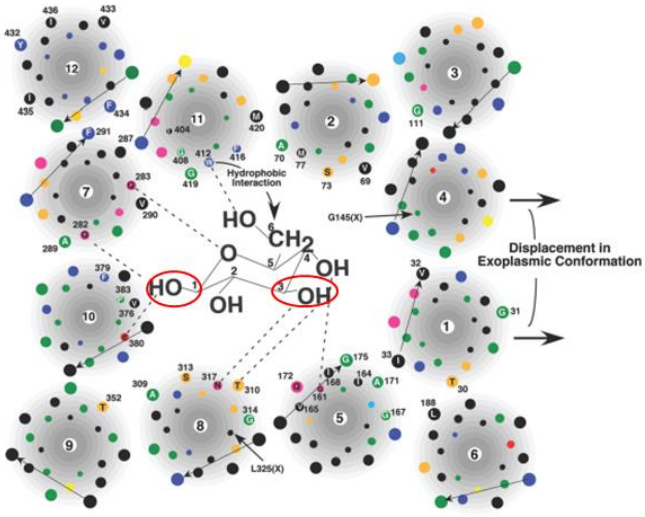

b)

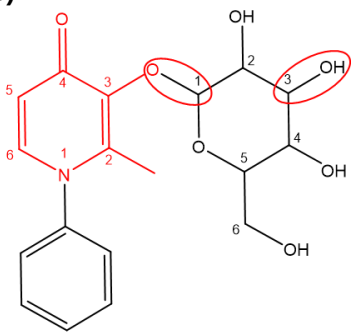

Figure 3.4.1: ***a)*** **Interaction of –OH group on glucose molecule to the GLUT-1 active site. Taken from Mueckler and Makepeace (2009)** ***b)*** **FCF132 chemical structure. The circled OH-functional groups are vital for glucose recognition site at GLUT-1 activite site.**

Furthermore, previous reported success of brain penetration of glycosyl conjugate was when the glucose forms a glycosidic bond with OH on C2 or C6 of glucose ring (Chen et al., 2009). This might explain the undetectable level of glycosylated CP20 and FCF132 as both HPOs form glyosidic bond with OH on C1 of glucose ring. Therefore, it seems that, although the OH on C2 and C6 on glucose ring form a hydrogen bond within the GLUT1 active site, this binding can be compromised for successful glucose transport. Having said this, the selection of which OH on glucose ring to form the glycosidic bond is highly important for successful brain penetration of glycosylated HPO. Base on this observation, it can be concluded that, to design a new compound conjugated with glucose, OH on C2 or C6 of glucose ring would be favourable for successful brain uptake. In summary, the strategy of adding glucose moiety by forming a glycosidic bond between the 1-OH of glucose and the 3-OH of hydroxypyridinine ring was counterproductive as it halts the brain uptake of FCF132 (glycosylated form of CP84). It is already known that free OH-1 of the glycosyl group is most crucial for the identification of D-glucose by GLUT1 (Thérèse et al., 1996; Mehdi et al., 1999).

c) CN compounds (CN116, CN118, CN126, CN128, CN226 & CN228)

The CN compounds can be clustered into three groups namely CN 11, CN 12 and CN 22 based on increasing lipophilicity. Each group contains two iron chelators with chiral alkyl substituent containing -OH functional group at N1 which are enantiomer pair: [CN 11: CN116 (*S*-) and CN118 (*R*-); CN 12: CN126 (*S*-) and CN128 (*R*-); CN 22: CN226 (*S*-) and CN228 (*R*-)]. In this study, brain permeability of the CN compounds was evaluated and compared to CP20. Additionally, the enantiomer pairs in each group were also compared to evaluate if there is any effect of optical stereoisomerism in the brain uptake. The results showed that there was no significant different of rate of brain uptake for CN128, CN226 and CN228 and CP20 compared to CP20. Conversely, CN116 and CN118 showed slower rate of brain uptake than CP20. Comparison between enantiomer pairs showed no significant different in brain uptake suggesting that optical stereoisomerism in these set of molecules did not contribute to variation in brain uptake. Indeed, in general compounds that crossed the BBB via passive membrane diffusion, optical stereoisomerism seems not to be an important factor compare to compound that is carrier-mediated (Chang et al., 2015, Fong, 2015).

The lack of relationship between brain uptake and lipophilicity has been reported elsewhere (Liu et al., 2011, Summerfield et al., 2007). It has been demonstrated in the earlier studies that prediction of brain permeability of HPOs based on lipophilicity was not sufficient (Habgood et al., 1999). In that study, a set of CP20 derivatives with N-alkyl or N-hydroxyalkyl substituents with lipophilicity higher than CP20 were evaluated for brain permeability. However, two of the CP20 derivatives with N-hydroxyalkyl substituent that have lipophilicity 1.2 and 3.0-folds higher than CP20 were not detected in the brain. It was revealed in the study that only N-alkyl substituent of CP20 with cLogP 2.9- to 466-folds higher contributed to the positive relationship between brain uptake and lipophilicity. It was then suggested that the additional -OH caused the formation of extra hydrogen bond with surrounding water which requires more energy for breaking the bond. This mechanism contributes to additional barrier for brain penetration (Rafi et al., 2012). Indeed, the total polar surface area (TPSA) that account for the combined surface area between interaction of electronegative atom such as oxygen and nitrogen with hydrogen was 1.5-fold higher than CP20 for all of the CN compounds. Similarly, CN compounds are also a group of CP20 derivatives with N-hydroxyalkyl substituents which may explain the lack of relationship between brain uptake and lipophilicity. Moreover, Frieden et al. (2009) have argued against the traditional notion among the pharmaceutical scientist and clinicians that lipophilicity was the main driving force of BBB permeation. Their findings showed that the intermolecular hydrogen bond was the main driving force for the 41 CNS drugs tested for brain permeability and not the lipophilicity. Their findings were further substantiated by a larger set of 246 drugs which showed that intermolecular hydrogen bonding was certainly the primary driving force for brain permeability (Chen et al., 2011).

Nevertheless, although extra hydroxyl group presented additional barrier for brain permeation, simultaneous increase in lipophilicity which is between 2.6- to 108-folds higher than CP20 may compensate for this as they were not significantly different than CP20 rather than not getting into the brain at all. Additionally, the lack of observable brain uptake for the N-hydroxyalkyl substituent of CP20 in the previous study might partly be because of the short perfusion time (1 minute) which did not allow sufficient duration of slowly permeable compounds through passive membrane diffusion. Furthermore, the study employed UV as the detection method for HPOs levels in brain after separation by HPLC which was less sensitive for such a short perfusion time compared to detection via liquid scintillation spectroscopy or mass-spectrometry (MS) (Habgood et al., 1999).

Besides the energy barrier conferred by the extra OH-group on the brain uptake of CN compounds, the interaction of the CN compounds with efflux pump such as Pgp abundantly expressed at BBB was also possible (Loscher and Potschka, 2005, Bartels, 2011). Pgp efflux pump are abundantly expressed in rat BBB and is known to favour small lipophilic molecules as its substrate and lowering BBB permeation which offsetting their much higher partition into the BBB membrane (Mikitsh and Chacko, 2014, (Friden et al., 2009, Fridén, 2014). The data revealed that out of the four HPO tested, only CN226 was showed to be a substrate for Pgp efflux pump where cyclosporin A caused approximately 50% increase in brain uptake. This lead to increase in CN226 brain uptake by 2-folds compared to CP20. In order to decrease glucuronidation in the liver, CP20 chemical structure was altered to form CN compounds with the simultaneous increase in total polar surface area and lipophilicity which showed that increase in total polar surface area predominantly affect the rate of brain uptake for CN118 and CN126 (Hider et al., 2011a). However, in the case of CN226, the similarity in the rate of brain uptake compare to CP20 was probably because of the combination of these two factors; the higher intermolecular hydrogen bond formation with the surrounding H_2O that limit brain permeation and the increase in lipophilicity which made CN226 more permeable to cell membrane but was then favoured by efflux pumps.

One interesting point to bring up is that, CN 12 and CN 22 group of compounds contained a phenyl functional group without enhancement of brain uptake seen on CP84. This might suggest that orientation of the phenyl functional group in these compounds not favour interaction with a specific carrier-mediated transporter such as LAT1 (Killian and Chikhale, 2001). Rather surprisingly, there was indeed an interaction with LAT1, but without a subsequent internalisation into the brain (Killian et al., 2007). In summary, brain uptake of CN compounds was not different to CP20, except for CN226 which showed 2-fold higher brain uptake in the presence of Pgp efflux pump inhibitor, cyclosprorine A.

3.4.4 *Brain distribution of novel HPO iron chelators*

CP20 showed negligible non-specific binding to brain tissue which suggest that theoretically, all CP20 in the brain can chelate iron. This assumption is in line with the free-drug hypothesis, which stated that only drugs in the unbound form are pharmacologically relevant (Liu and Chen, 2015). Other novel HPOs except CN116 however, showed a certain degree of binding to brain tissue. Lipophilicity higher than CP20 for these novel

HPOs could be one of the determining factors to this observation as brain tissue contains approximately 11% of lipid by weight (Jeffrey and Summerfield, 2007). Indeed, evaluation of thirty-three CNS active drugs showed less unbound fraction in the brain compared to plasma which only contain around 0.7% lipid (Maurer et al., 2004). Interestingly, CN118 showed a different profile of binding in the brain tissues compare to its enantiomer CN116 with the former been 60% unbound while the latter been 100% unbound to brain tissues, although this was not eventually translated into differences between rates of brain uptake for CN116 and CN118. For some novel HPOs that showed a certain degree of affinity towards brain tissues, this in turn may be a factor that contributes to the lower iron chelation activity than CP20. In contrast, affinity of HPOs towards brain tissues could be therapeutically advantageous for prolong action of iron chelation as the brain tissues act as a reservoir that continuously released bound HPOs (Loryan and Hammarlund-Udenaes, 2014).

To summarise, CP20 was superior in term of rate of brain uptake compared to other novel HPOs as it was not bound to brain tissues. However, for the novel iron chelators, affinity towards brain tissue may benefit in term of longer exposure in brain tissues.

3.4.5 *Advantages and shortcomings of this study*

The *in-situ* brain perfusion technique attempted to overcome the limitation of *in vivo* systemic injection for determination of brain permeability which are pharmacokinetically difficult to interpret due to wide peripheral distribution and metabolism (Boje, 2001, Smith and Allen, 2003b). Cannulation of carotid arteries in *in situ* brain perfusion allow direct delivery of artificial blood containing HPOs to the brain, thus avoiding peripheral distribution and metabolism (Murakami et al., 2000, Smith and Allen, 2003a). HPOs that get into the brain after perfusion at an optimum time can be determined by quantification method such as HPLC. By this technique, lower concentration of HPOs can be used and HPOs brain uptake can be confidently measured relative to the systemic injection. Furthermore, this technique offers a flexibility to manipulate the artificial blood for the identification and characterisation of transporters by inhibitors as described in **this chapter.**

This technique is however technically challenging which requires substantial amount of training for isolation and cannulation of the carotid arteries. Secondly, the perfusion is

performed in anaesthetised rats and therefore does not truly represent brain uptake in awake animals. Thirdly, the artificial blood does not contain erythrocytes which have pH buffering capacity and helps in contributing to the viscosity of the actual blood (Boje, 2001, Jensen, 2004, Windberger et al., 2003). Some of these issues have been addressed in this study by continuous infusion of oxygen in the artificial blood, adding HEPES to maintain the pH at physiological level and adding physiological concentration of BSA to increase the solution viscosity. Data for optimisation as shown in **Chapter 2** suggest that the perfused brain is viable, and the BBB is intact for up to 60 minutes. The capillary depletion technique to determine HPOs trapped in the brain capillary endothelial cells is prone to artefacts due to redistribution of trapped HPOs during centrifugation process (Bickel, 1998). However, this is very unlikely base on the molecular weight of HPOs that are small (<500 Da).

The UV detection method for HPOs identification in perfused brain after separation by HPLC in the current study is the least sensitive method for biological measurement. The best option is by employing MS or MS/MS detection method for analysis. This technique offer sensitivity down to nanomole and picomole concentration in biological samples (Avdeef and Sun, 2011, Tabanor et al., 2016). Because of this, lower concentration of HPOs in artificial blood can be infused to more represent achievable HPOs concentration in human plasma. However, this requires sophisticated LCMS machine which is not available in all laboratory. Nevertheless, the current technique employed in this thesis to determine brain permeability is sufficient for brain uptake comparison between novel HPOs and CP20, and for determination of contribution of transporter-mediated uptake.

3.4.6 *Conclusion*

The present study aimed to evaluate the rate of brain uptake of novel HPOs iron chelators and compare with CP20. From the results obtained, only CP84 showed faster rate of brain uptake than CP20 while six others novel HPOs showed no difference or slower rate of brain uptake. The glycosylated HPO FCF132 unexpectedly did not get into the brain at all suggesting lack of FCF132 affinity towards glucose transporter. Also, the brain uptake for S- and R- enantiomer pairs of CN compounds did not show any different indicating stereoisomerism had no effect for these set of compounds. In addition, CP84 was shown to be a substrate for LAT-1 transporter explaining its increased rate of brain uptake compared to CP20, while CN226 was a substrate for Pgp efflux-pump suggesting that it

was expelled from the brain after crossing the BBB. There was a positive linear relationship between brain uptake and lipophilicity only when transporters/pumps were inhibited, while negative linear relationship between brain uptake and polarity was observed both before and after inhibition, signifying that polarity is the best descriptors of brain uptake for this set of compounds. Therefore, in this study, the hypothesis that modification to the structure of CP20 can improve the efficiency of BBB transport was partly accepted as only CP84 showed increase in the rate of brain uptake compared to CP20 while other novel HPOs rate of brain uptake were unchanged or lower than CP20.

As a potential neuroprotection agent, brain permeability is only one of the prerequisites. To select the best candidate as a neuroprotection agent, an evaluation of the neuroprotective ability of novel HPOs is warranted. Therefore, in the following chapter, the evaluation of neuroprotection of these novel HPOs with neuroblastoma cell lines, SH-SY5Y will be covered in detail.

CHAPTER 4

NEUROPROTECTION STUDY OF HPOS WITH NEUROBLASTOMA CELL LINES (SH-SY5Y)

4 Neuroprotection study of novel HPOS with neuroblastoma cell line (SH-SY5Y)

4.1 *Introduction*

In the preceding chapter, novel HPO iron chelators were evaluated for their brain permeability with *in situ* brain perfusion. As presented in **Chapter 3**, seven from eight of the novel HPO iron chelators tested crossed the BBB and get into the brain. Ability to cross the BBB is a prerequisite for Parkinsonian drugs to elicit their pharmacological effects in the brain (Smith et al., 2012, Bezard et al., 2013). Iron content in substantia nigra generally increases by 10-fold at 40 years of age compared to infants without any problem (Reeve et al., 2014). However, dysfunction of tightly regulated brain iron homeostasis occurs in PD which cause excessive accumulation of free iron (Double et al., 2000). A rise in the level of labile iron pool (LIP; **Section 1.1.4**) subsequently generates free-radicals through Fenton reaction and induce oxidative stress (Kruszewski, 2003). Oxidative stress has been implicated in the pathogenesis of PD as described in detail in **Section 1.1.4**. Transgenic mice that overexpressed ferritin were less prone to various PD toxins inducers through sufficient sequestration of LIP (Kaur et al., 2009). This further suggest the use of iron chelators as a potential treatment for PD (Perez et al., 2008, Mounsey and Teismann, 2012). Indeed, synthetic and natural iron chelators have been shown to slow down disease progression in *in vitro* and *in vivo* PD models by attenuating dopaminergic neurons death (Mounsey and Teismann, 2012, Hatcher et al., 2009).

Among the clinically available iron chelators (**Section 1.1.6**), deferiprone (CP20) is the most promising for PD treatment as it is orally active, can penetrate the brain, the CP20-iron complex is neutral and can distribute iron to extracellular transferrin (Devos et. al., 2014). Studies in *in vitro* and *in vivo* models of PD showed that CP20 conferred neuroprotection better than other clinically available iron chelators (Dexter et al., 2011; Molina-Holgado et. al., 2008; Devos et. al., 2014). In human, CP20 exhibited better motor performance as early as 6 months after treatment compared to control (Devos et. al., 2014). Although CP20 is extensively metabolised in the liver, the 3,4-hydroxypyridinone scaffold of CP20 is easily functionalised for improvement of physicochemical and biological properties, while retaining their affinity to iron and other important characteristics for potential PD treatment (Santos et al., 2012).

To confirm that the brain permeable novel HPOs could also confer neuroprotection, SH-SY5Y cell line was used to model the dying neurons in this study. SH-SY5Y cell line is a catecholaminergic which expresses DAT that closely resembles the affected dopaminergic neurons in the substantia nigra *pars compacta* (SNPc) in PD brain (Kovalevich and Langford, 2013b, Filograna et al., 2015). H_2O_2, 6-OHDA and MG132 were employed in this study to induce cell death. Selection of these toxins in this study is relevant due to the reported accumulation of iron in *in vitro* and *in vivo* models of PD that associate with the toxicity of the toxins (Wang et al., 2004, Panopoulos et al., 2005). Apart from that, ferric ion (Fe^{3+}) in the form of co-ordination complex with NTA (FeNTA) was used as a direct source of iron and to evaluate the ease of novel HPOs to chelate iron. Therefore, based on the results from the experiment described in the preceding chapter, seven of the novel brain penetrant HPOs were chosen along with CP20 for *in vitro* neuroprotection study with SH-SY5Y cell lines.

4.1.1 *Hypothesis*

It was hypothesised that novel HPOs iron chelators would confer protection against H_2O_2, 6-OHDA, MG132 and FeNTA (1:3) induced toxicity in SH-SY5Y cells.

4.1.2 *Aims*

To test the hypothesis, SH-SY5Y cells were pre-treated with HPOs before exposing to toxins with the following aims.

a) Confirm the lack of cell death induced by HPOs iron chelators.

b) Confirm the induction of cell death when exposed to IC_{50} concentrations of H_2O_2, 6-OHDA, MG132 and FeNTA (1:3).

c) Compare the effect of novel HPO iron chelators on toxin-induced cell death.

d) Compare the neuroprotection of novel HPO iron chelators with CP20.

e) Compare the neuroprotection between enantiomers pair of novel HPO iron chelators.

4.2 *Materials and methods*

4.2.1 *SH-SY5Y cells culture*

Human neuroblastoma cells line (SH-SY5Y) at passage 18 was obtained from the European Collection of Cell Cultures (ECCC). The cells were grown in T175 cm2 (T175) (ThermoFisher, UK) containing 20 mL Dulbecco's Modified Eagle medium (DMEM) supplemented with 10% (v/v) fetal bovine serum (FBS) and 0.01% (v/v) penicillin-streptomycin-neomycin (PSN) antibiotic mixture (complete-DMEM) as described in **Section 2.2.3**. Briefly, at 80% confluence, the cells were washed with DPBS, trypsinised with 0.05% trypsin-EDTA in phosphate buffer and centrifuged at 200 g for 5 minutes. The cell pellet was re-suspended with 1 mL complete-DMEM at a density $1x10^5$ cells/mL. One hundred microliters of working cell suspension were pipetted into 96-well plates and incubated in CO_2 incubator at 37 ºC for at least 12 h.

4.2.2 *Preparation of 3-hydroxy-4-pyridinones (HPOs) solution*

Main stock solution for HPOs were dissolved in sterile distilled water, except for CP84 which was dissolved in 10% (v/v) DMSO. HPOs with concentration between 50 to 1250 µM were prepared in serum-free DMEM and were used to incubate with the SH-SY5Y cells. The final DMSO concentration when exposed to cells was below 1% (v/v).

4.2.3 *Preparation of neurotoxins solution*

Five different neurotoxins namely H_2O_2, 6-OHDA, MG132 and FeNTA (1:3) were employed in this study to induce cell death. The preparation of the toxins was outlined below:

a) H_2O_2

Working stock solution (2.2 mM) for IC_{50} concentration of H_2O_2 (220 µM) was prepared fresh in serum-free DMEM on the day of the experiment from the 200 mM H_2O_2 main stock solution in serum-free DMEM. Left-over of working stock solution was frozen at -20 ºC and was used within one month after preparation.

b) 6-OHDA

Working stock solution (400 µM) for IC_{50} concentration of 6-OHDA (40 µM) was prepared fresh in serum-free DMEM on the day of the experiment from the 40 mM 6-OHDA main stock solution in serum-free DMEM containing 0.06% (w/v) ascorbic acid. Left-over of working stock solution was frozen at -20 ºC and was used within one month after preparation.

c) MG132

Working stock solution (3500 pM) for IC_{50} concentration of MG132 (350 pM) was prepared fresh in serum-free DMEM on the day of the experiment from the 10 mM MG132 main stock solution in 100% DMSO. Left-over of working stock solution was not re-used as MG132 lost it activity after freezing-thawing cycles.

d) FeNTA (1:3)

Working stock solution (4600 µM) for IC_{50} concentration of FeNTA (1:3) (460 µM) was prepared fresh in serum-free DMEM on the day of the experiment from the 125 mM FeNTA (1:3) main stock solution in serum-free DMEM. Left-over of working stock solution was frozen at -20 ºC and was used within one month after preparation.

4.2.4 *In vitro neuroprotection studies*

After an overnight incubation in CO_2 incubator, the cells were treated with 50, 100, 500 and/or 1250 µM of HPOs in serum-free DMEM and were incubated for 20 h in the CO_2 incubator. Control cells were incubated with vehicle in serum-free DMEM. After 20 h incubation with HPOs, neurotoxins at 10-fold of the IC_{50} concentration were pipetted into

the well (11 µL) and incubated for 20 h. When 20 h incubation time had passed, the viable cells were estimated with MTT assay (**Figure 4.2.1**).

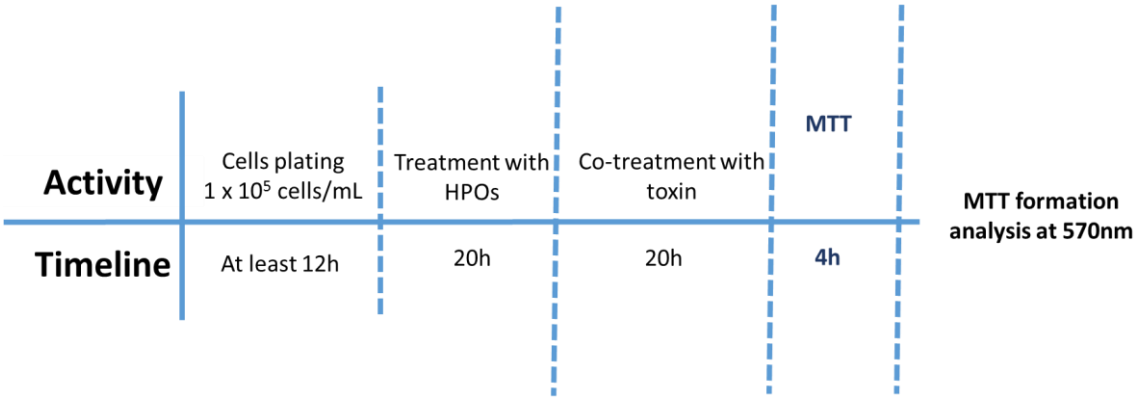

Figure 4.2.1: Experimental timeline for *in vitro* neuroprotection study with SH-SY5Y.

4.2.5 *Determination of cell viability with MTT assay*

Cell viability after SH-SY5Y co-treated with HPOs and toxin was estimated with MTT assay. After 20 h co-treatment with neurotoxins, the medium was replaced with serum-free DMEM containing 0.5 mg/mL MTT and incubated for 4 h at 37 ºC in the CO_2 incubator. At the end of the incubation, the medium was removed by quick inversion into the sink and lightly tapped on paper towel to remove excess liquid. The formed MTT formazan crystal was solubilised with 100 µL 100% DMSO and absorbance at 570 nm was taken with a microplate reader. The percentage of viable cells was calculated by finding a ratio between treated cells and control cells with serum-free DMEM as described in **Section 2.2.8.**

4.2.6 *Comparison between pFe^{3+} for HPOs and cell viability after treatment with toxins*

The iron (Fe^{3+}) affinity constant (pFe^{3+}) values for HPOs were determined spectrophotometrically by automated potentiated titration (Kong et al., 2006) and was provided by Dr Xiao Kong from Institute of Pharmaceutical Science (IPS), King's College London. The pFe^{3+} value is a negative logarithm of free Fe^{3+} concentration at physiological pH (pH 7.4) when the total Fe^{3+} concentration, $[Fe^{3+}]_{total}$ is 1 µM and the total HPO concentration, $[HPO]_{total}$ is 10 µM. The higher the pFe^{3+} value indicates a higher affinity towards Fe^{3+} ion. The pFe^{3+} values for HPOs were outlined in **Table 4.2.1**.

Table 4.2.1: pFe^{3+} values for HPOs as determined by potentiometric technique

HPO	pFe^{3+}
CP20	20.20
CP84	20.00
CN116	20.40
CN118	20.40
CN126	20.18
CN128	20.18
CN226	19.80
CN228	19.80

pFe^{3+} at pH 7.4 when $[Fe^{3+}]_{total}$ is 1 µM and $[HPO]_{total}$ is 10 µM

4.2.7 *Data analysis*

Experiments were performed in at least triplicate on three separate occasion with data expressed as mean+SEM (n=3). Two-way ANOVA followed by Holm-Šídák multiple comparison test was performed to compare between cells treated with toxin and cells co-treated with HPOs and toxin. The same way of analysis was performed to compare between cells co-treated with CP20 and toxin with the rest of cells co-treated with HPOs other than CP20, and toxin. Comparisons between enantiomer pairs was also observed to look for any statistical difference.

4.3 *Results*

To evaluate the neuroprotective effect of the novel HPOs, the SH-SY5Y cells were pre-treated with 50, 100 500 or 1250 µM HPOs for 20 h before being exposed to neurotoxins for a further 20 h. The cell viability of the SH-SY5Y after treatments was assessed by MTT assay.

4.3.1 *Effect of HPOs on viability of SH-SY5Y cells exposed to H_2O_2*

In order to evaluate the neuroprotective ability of novel HPOs, SH-SY5Y cell were treated with various concentrations of HPOs (50 to 500 µM) with or without the IC_{50} concentration of H_2O_2 (220 µM). Control cells were treated with serum-free DMEM only or H_2O_2 in serum-free DMEM. At the end of the treatment, the cell viability was measured by MTT assay as described in **Section 2.2.8**.

Treatment of SH-SY5Y cells with 50, 100 and 500 µM HPOs only did not affect cells viability when compared to untreated control. By contrast, SH-SY5Y cells exposed to 220 µM H_2O_2 for 20 h showed approximately between 47% to 52% cell viability compared to -H_2O_2 (**Figure 4.3.1**). In general, treatment of SH-SY5Y cells with HPOs 20 h prior to co-treatment with H_2O_2 for a further 20 h protected against H_2O_2-induced loss of cell viability, but to different degrees.

CP20 protected against H_2O_2-induced cell loss, with a significant 27% reduction at 100 µM compared to H_2O_2 alone (**Figure 4.3.1a**). By contrast, CP84 co-treated with H_2O_2 did not protect against H_2O_2-induced cell loss at any concentration (**Figure 4.3.1b**).

Both CN116 and CN118 protected against H_2O_2 toxicity which was significant at 50 and 100 µM (CN116) and 50 µM (CN118) respectively.

Similarly, CN126 and CN128 appeared to protect against H_2O_2-induced cell death. CN126 produced a non-concentration-related improvement in cell viability by approximately 30% compared to H_2O_2 alone (+H_2O_2), however the protection following CN128 was not significant.

Both CN226 and CN228 produced a significant, non-concentration-related protection of around 40% compared to $+H_2O_2$.

There was no difference in cell viability when the equimolar concentrations of enantiomer pairs, (CN116 vs CN118, CN126 vs CN128 and CN226 vs CN228), co-incubated with H_2O_2 were compared. Likewise, comparison of equimolar concentrations between novel HPOs and CP20 reveals no significant different.

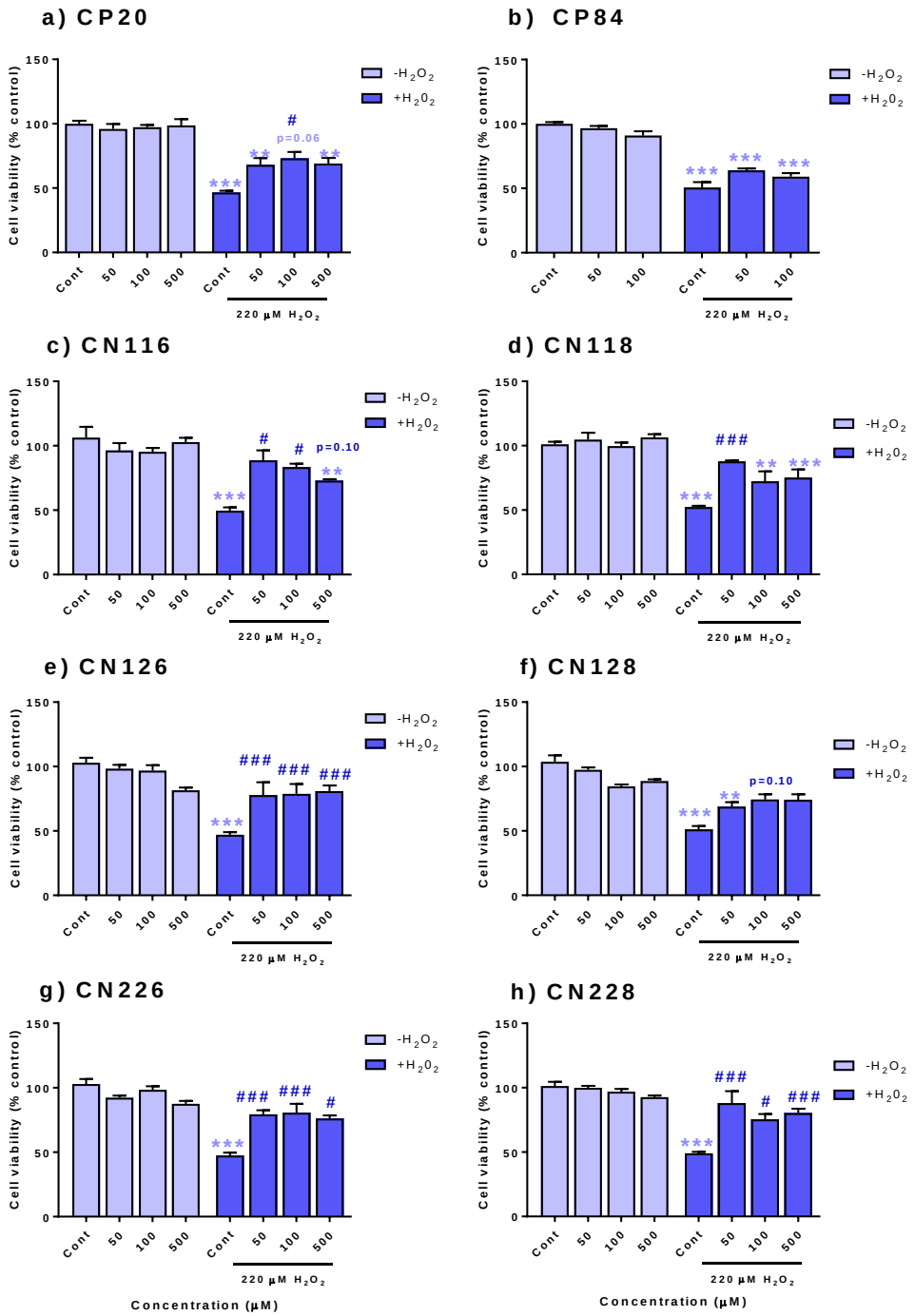

Figure 4.3.1: Effect of H_2O_2 on cell viability assessed by MTT assay after pre-incubation with novel HPO iron chelators.

*SH-SY5Y cells were pre-incubated for 20h with HPOs followed by 20h co-incubation with 220 µM H_2O_2. Data are expressed as mean+SEM (n=3). ** p < 0.05, *** p < 0.001 compared between HPOs treatments without H_2O_2 (-H_2O_2) and HPOs treatments with H_2O_2 (+H_2O_2). # p < 0.05, ### p < 0.001 compared between HPOs treatments with H_2O_2 (+H_2O_2) and control with H_2O_2 (+H_2O_2). No significant different, p > 0.05 compared* ***i)*** *between HPOs treatments without H_2O_2 (-H_2O_2) and control without H_2O_2 (-H_2O_2)* ***ii)*** *between CP20 treatments with H_2O_2 (+H_2O_2) and novel HPOs with H_2O_2 (+H_2O_2)* ***iii)*** *between HPO enantiomer pairs (CN116 vs CN118, CN126 vs CN128 and CN226 vs CN228) treatments with H_2O_2 (2-way ANOVA followed by Holm-Šídák multiple comparison test).*

4.3.2 *Effect of HPOs on viability of SH-SY5Y cells exposed to 6-OHDA*

SH-SY5Y cell were treated with various concentrations of HPOs (50 to 500 µM) with or without the IC_{50} concentration of 6-OHDA (40 µM) prepared in 0.006% (w/v) ascorbic acid. Control cells were treated with serum-free DMEM containing 0.006% (w/v) ascorbic acid only or 6-OHDA in serum-free DMEM containing 0.006% (w/v) ascorbic acid. At the end of the treatment, the cell viability was measured by MTT assay as described in **Section 2.2.8**.

As expected, treatment of SH-SY5Y cells with 50, 100 and 500 µM HPOs alone did not affect cells viability when compared to control and exposure to 40 µM 6-OHDA for 20 h showed between 48 to 57% cell viability which were significantly reduced compared to control (**Figure 4.3.2**). Generally, treatment of SH-SY5Y cells with HPOs 20 h prior to co-treatment with 6-OHDA showed significant protection against 6-OHDA-induced cell loss.

CP20 showed a protection against 6-OHDA toxicity in a concentration-dependant manner (22% and 51% improvement) at 100 µM and 500 µM respectively (**Figure 4.3.2a**). Similarly, CP84 protected against 6-OHDA induced cell death by approximately 30% in a non-concentration-dependant manner at 50 and 100 µM (**Figure 4.3.2b**).

CN116, CN118, CN126, CN128, CN226 or CN228 exhibited a non-concentration related prevention of cell death in between 27 to 41% at all concentrations compared to 6-OHDA alone (+6-OHDA) **(Figure 4.3.2c, d & e)**.

There was no difference in cell viability when the equimolar concentrations of enantiomer pairs (CN116 vs CN118, CN126 vs CN128 and CN226 vs CN228), co-treated with 6-OHDA were compared. However, comparison of equimolar concentrations between novel HPOs and CP20 co-incubated with 6-OHDA showed that CN118 (50 µM), CN226 (100 and 500 µM) and CN228 (100 and 500 µM) improved cell viability.

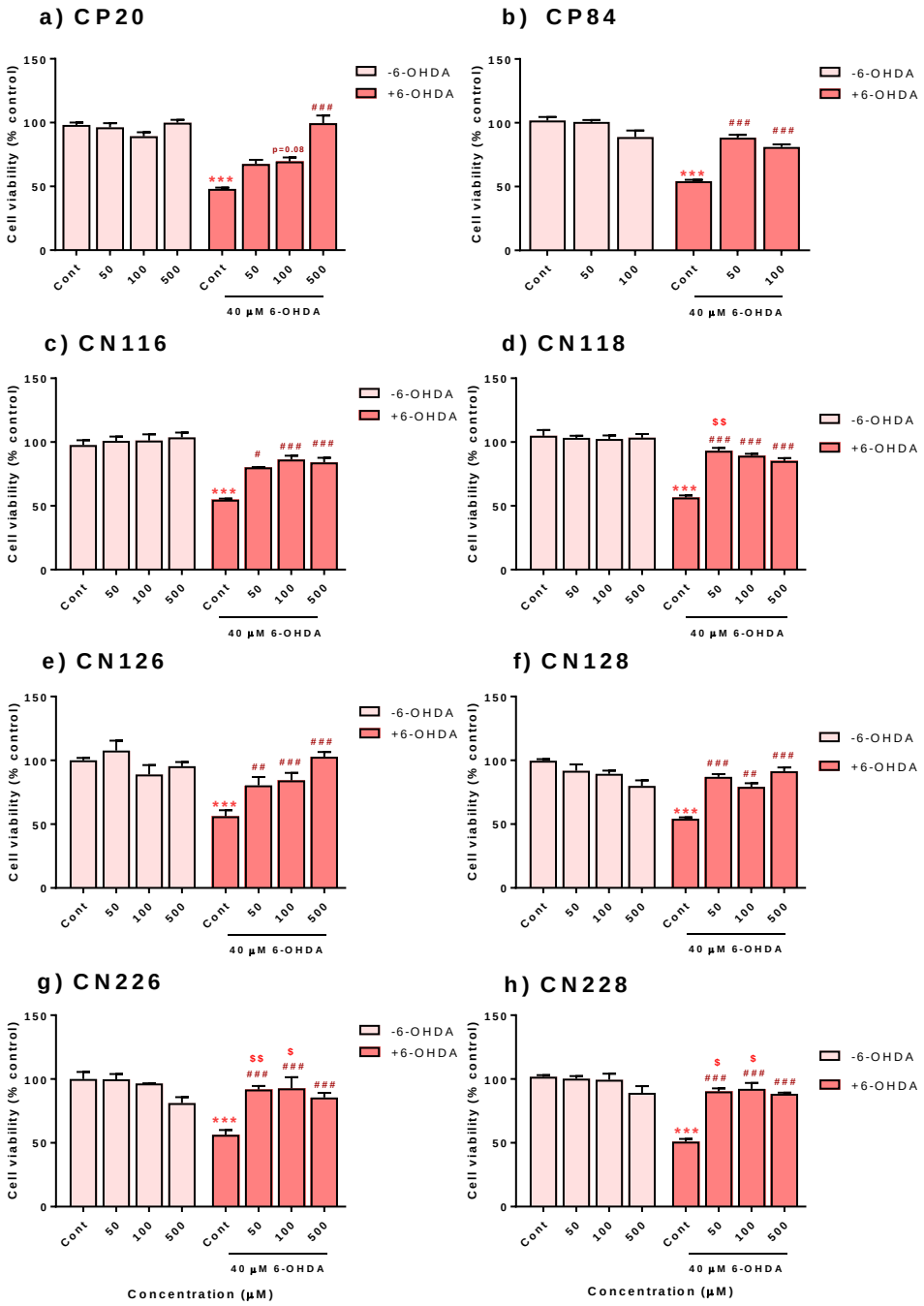

Figure 4.3.2: Effect of 6-OHDA on cell viability assessed by MTT assay after pre-incubation with novel HPO iron chelators.

*SH-SY5Y cells were pre-incubated for 20h with HPOs followed by 20h co-incubation with 40 µM 6-OHDA. Data are expressed as mean+SEM (n=3). *** p < 0.001 compared between HPOs treatments without 6-OHDA (-6-OHDA) and HPOs treatments with 6-OHDA (+6-OHDA). # p < 0.05, ## p < 0.01, ### p < 0.001 compared between HPOs treatments with 6-OHDA (+6-OHDA) and control with 6-OHDA (+6-OHDA). $ p < 0.05, $$ p < 0.01 compared between CP20 treatments with 6-OHDA (+6-OHDA) and novel HPOs with 6-OHDA (+6-OHDA). No significant different, p > 0.05 compared* ***i)*** *between HPOs treatments without 6-OHDA (-6-OHDA) and control without 6-OHDA (-6-OHDA)* ***ii)*** *between HPO enantiomer pairs (CN116 vs CN118, CN126 vs CN128 and CN226 vs CN228) treatments with H_2O_2 (2-way ANOVA followed by Holm-Šídák multiple comparison test).*

4.3.3 *Effect of HPOs on viability of SH-SY5Y cells exposed to MG132*

SH-SY5Y cells were treated with various concentrations of HPOs (50 to 500 µM) with or without the IC_{50} concentration of MG132 (350 pM) prepared in 0.001% (v/v) DMSO. Control cells were treated with serum-free DMEM containing 0.001% (v/v) DMSO only or MG132 in serum-free DMEM containing 0.001% (v/v) DMSO. At the end of the treatment, the cell viability was measured by MTT assay as described in **Section 2.2.8**.

Treatment of SH-SY5Y cells with 50, 100 and 500 µM HPOs only did not affect cells viability when compared to untreated control. Conversely, SH-SY5Y cells exposed to 350 pM MG132 for 20 h showed approximately between 51 to 56% cell viability which were significantly lower compared to untreated control (**Figure 4.3.3**). Comparison of equimolar concentrations between HPOs without MG132 and HPOs with MG132 revealed significant reduction in cell viability except for CN128 at 50 µM concentration where there was no significant different (**Figure 4.3.3**). Overall, treatment of SH-SY5Y cells with HPOs for 20 h prior had no effect on MG132-induced cell death.

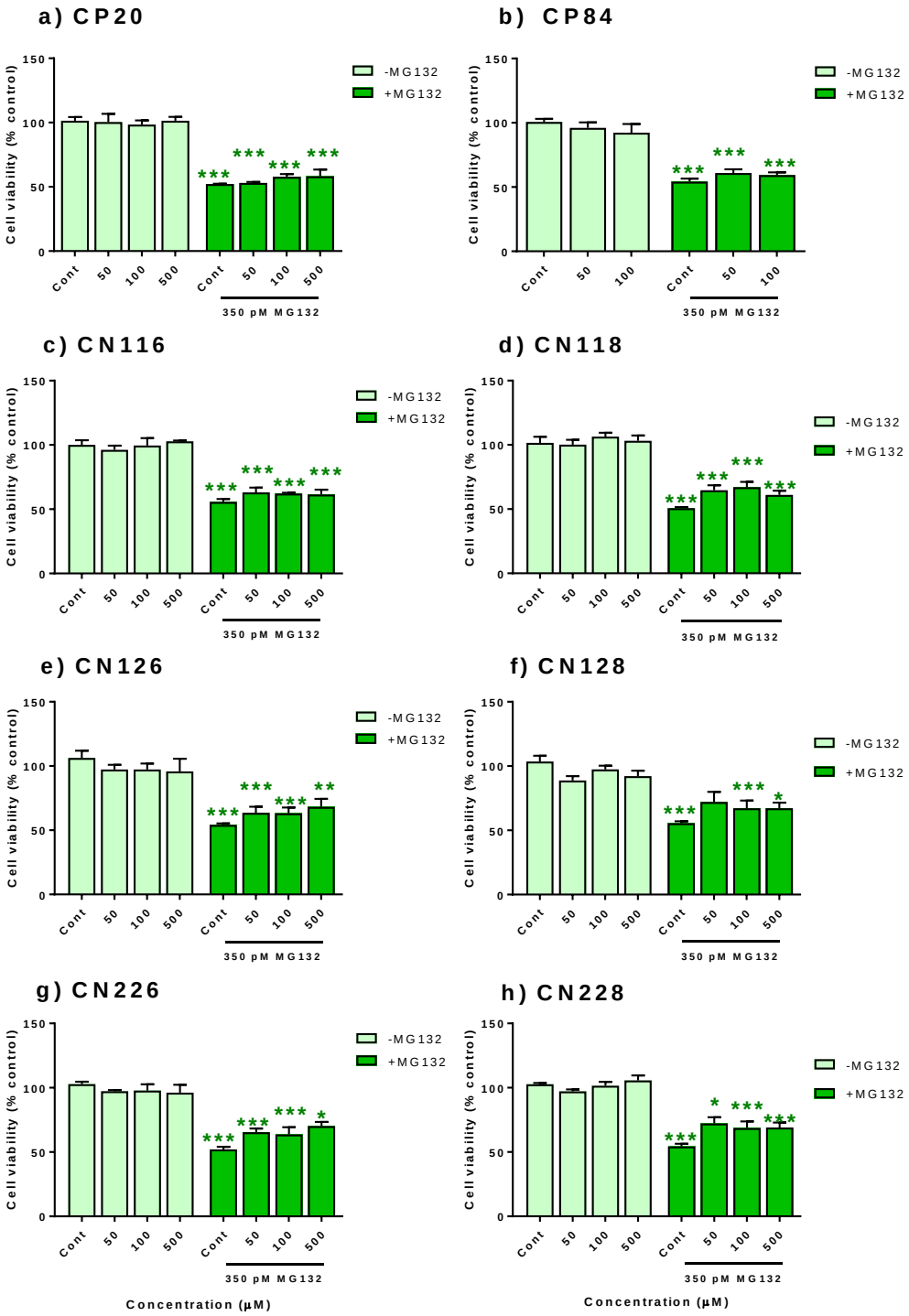

Figure 4.3.3: Effect of MG132 on cell viability assessed by MTT assay after pre-incubation with novel HPO iron chelators.

*SH-SY5Y cells were pre-treated for 20h with HPOs followed by 20h co-treatment with 350 pM MG132. Data are expressed as mean+SEM (n=3). *** p < 0.001 compared between HPOs treatments without MG132 (-MG132) and HPOs treatments with MG132 (+MG132). No significant different, p > 0.05 compared **i)** between HPOs treatments without MG132 (-MG132) and control without MG132 (-MG132) **ii)** between HPO enantiomer pairs (CN116 vs CN118, CN126 vs CN128 and CN226 vs CN228) treatments with H_2O_2 (2-way ANOVA followed by Holm-Šídák multiple comparison test).*

4.3.4 *Effect of HPOs on viability of SH-SY5Y cells exposed to FeNTA*

SH-SY5Y cell were treated with various concentrations of HPOs (50 to 1250 µM) with or without the IC_{50} concentration of FeNTA (460 µM) alone. Control cells were treated with serum-free DMEM or FeNTA (1:3) in serum-free DMEM. At the end of the treatment, the cell viability was measured by MTT assay as described in **Section 2.2.8**.

None of the HPOs altered the viability of SH-SY5Y cells at any concentrations except for CN126 which showed reduced cell viability at the highest concentrations (500 and 1250 µM) compared to untreated control. As expected, SH-SY5Y cells exposed to FeNTA (450 µM) for 20 h produced between 43 and 48% loss in cell viability which were significantly lower compared to untreated controls (**Figure 4.3.4**).

CP20 (1250 µM) reduced FeNTA-induced cell death by 23% (**Figure 4.3.4a**), however, CP84 (50 and 100 µM) failed to show any protection (**Figure 4.3.4b**).

Although CN116 failed to show any protection against FeNTA-induced cell death **(Figure 4.3.4c)**, its stereoisomer CN118 (500 and 1250 µM) protected against FeNTA-induced cell death by 19 and 14% respectively **(Figure 4.3.4d)**.

By contrast, both CN126 and its stereoisomer CN128 protected the SH-SY5Y cell from FeNTA-induced toxicity (CN126: 26 and 29% protection; CN128: 33% and 23% protection) at 500 and 1250 µM **(Figure 4.3.4e & f)**.

Both CN226 and CN228 reduced FeNTA-induced cell death at 100, 500 and 1250 concentrations**,** with almost complete protection at the highest concentration **(Figure 4.3.4g & h)**.

Comparison of equimolar concentrations of enantiomer pairs, (CN116 vs CN118, CN126 vs CN128 and CN226 vs CN228), on FeNTA-induced cell death showed no significant different. By contrast, comparison of equimolar concentrations between novel HPOs and CP20 reveals enhanced protection by 29%, 37% and 36% for CN128, CN226 and CN228 respectively, at 500 µM **(Figure 4.3.4**).

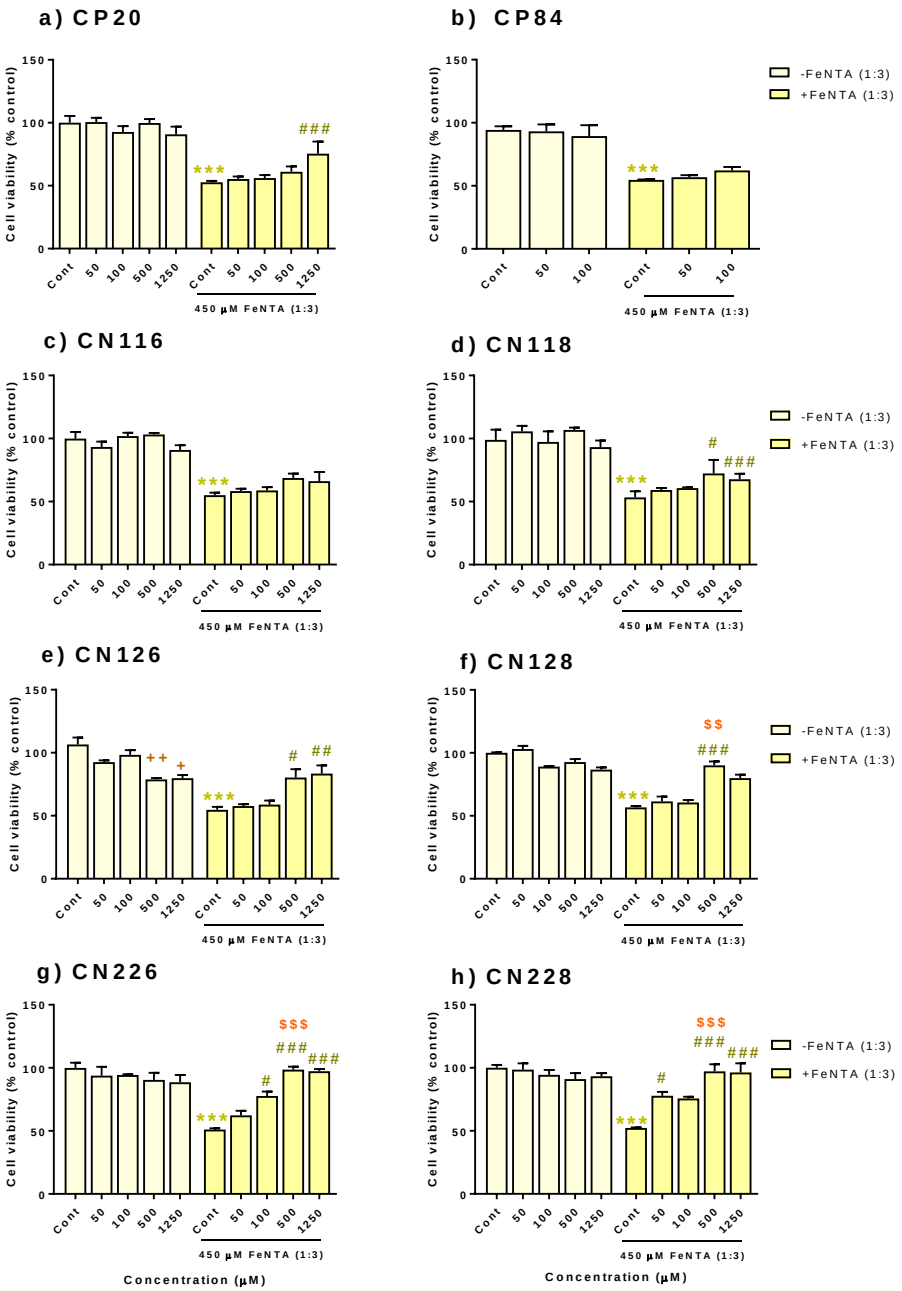

Figure 4.3.4: Effect of FeNTA (1:3) on cell viability assessed by MTT assay after pre-incubation with novel HPO iron chelators.

*SH-SY5Y cells were pre-treated for 20h with HPOs followed by 20h co-treatment with 460 µM FeNTA (1:3). Data are expressed as mean+SEM (n=3). + p < 0.05, ++ p < 0.01 compared between HPOs treatments with FeNTA (1:3) [+FeNTA (1:3)] and control without FeNTA (1:3) [-FeNTA (1:3)]. *** p < 0.001 compared between HPOs treatments without FeNTA (1:3) [-FeNTA (1:3)] and HPOs treatments with FeNTA (1:3) [+FeNTA (1:3)]. # p < 0.05, ## p < 0.01, ### p < 0.001 compared between HPOs treatments with FeNTA (1:3) [+FeNTA (1:3)] and control with FeNTA (1:3) [+FeNTA (1:3)]. $ p < 0.05, $$ p < 0.01, $$$ p < 0.001 compared between CP20 treatments with FeNTA (1:3) [+FeNTA (1:3)] and novel HPOs with FeNTA (1:3) [+FeNTA (1:3)]. No significant different, p > 0.05 compared **i)** between HPOs treatments without FeNTA (1:3) [-FeNTA (1:3)] and control without FeNTA (1:3) [-FeNTA (1:3)] **ii)** between HPO enantiomer pairs (CN116 vs CN118, CN126 vs CN128 and CN226 vs CN228) treatments with FeNTA (1:3) (2-way ANOVA followed by Holm-Šídák multiple comparison test).*

4.4 *Discussion*

In this study, *in vitro* neuroprotection study was performed in SH-SY5Y neuroblastoma cell lines exposed to the neurotoxins H_2O_2, 6-OHDA, MG132 and FeNTA, to evaluate the neuroprotective ability of novel HPO iron chelators. CP20 has been shown to be neuroprotective in *in vitro* and *in vivo* studies (Dexter et al., 2011, Molina-Holgado et al., 2008). Therefore, it was hypothesised that modification to the structure of CP20 would retained the neuroprotective ability of CP20. The current study revealed that, all seven novel HPOs showed some degree of neuroprotection against toxins insults on SH-SY5Y cells except for cells exposed to MG132 which although appear to show a mild neuroprotection however was not significant.

4.4.1 *Summary of the findings*

In general, all HPOs did not confer toxicity to SH-SY5Y on their own. Conversely, SH-SY5Y exposed to the toxins H_2O_2, 6-OHDA, MG132 and FeNTA induced cell death as expected. The novel HPOs produced the greatest protection against toxin-induced cell death when 6-OHDA was used as a toxin, although they also protected SH-SY5Y cells from H_2O_2 and FeNTA. In these conditions, the neuroprotection was increasingly pronounced as the lipophilicity of the HPOs increased. Among all the toxins employed, MG132 toxicity was the least protected by HPOs. CN118, CN226 and CN228 showed more protection at 50 and/or 100 µM in 6-OHDA-induced cell death than equimolar concentration of CP20. CN128, CN226 and CN228 showed a better protection from FeNTA-induced cell death than CP20 at 500 µM. Comparison between HPOs enantiomer pair did not show any difference in neuroprotection ability. Summary of overall finding was compiled in **Table 4.4.1**.

Table 4.4.1: Summary of the findings for *in vitro* neuprotection study with SH-SY5Y cells

Toxin	H_2O_2			6-OHDA			MG132			FeNTA (1:3)			
HPOs µM	50	100	500	50	100	500	50	100	500	50	100	500	1250
CP20	**nc**	**++**	**nc**	**nc**	**++**	**++++**	**nc**	**nc**	**nc**	**nc**	**nc**	**nc**	**++**
CP84	nc	nc	nd	+++	+++	nd	nc	nc	nd	nc	nc	nd	nd
CN116	+++	+++	++	+++	+++	+++	nc	nc	nc	nc	nc	nc	nc
CN118	+++	nc	nc	++++ $	+++	+++	nc	nc	nc	nc	nc	++	+
CN126	++	++	+++	+++	+++	++++	nc	nc	nc	nc	nc	+++	+++
CN128	nc	++	nc	+++	++	++++	nc	nc	nc	nc	nc	++++ $	+++
CN226	++	+++	++	++++ $	++++ $	+++	nc	nc	nc	+	++	++++ $	++++
CN228	+++	++	+++	++++ $	++++ $	+++	nc	nc	nc	++	++	++++ $	++++

CP20 is highlighted in green. nc=no change, nd=not determined. + = low; ++ = mild; +++ = moderate; ++++ = high, neuroprotection compared to control with toxin only. $ = Better neuroprotection compared to equimolar concentration of CP20 with toxins

4.4.2 *Neuroprotection of HPOs against H_2O_2 toxicity in SH-SY5Y*

H_2O_2 was employed to model the SH-SY5Y cells death and to evaluate the effect of novel HPOs iron chelator due to its relationship with iron in producing $OH^{\bullet-}$ radical through the Fenton reaction. $OH^{\bullet-}$ radical is a highly reactive radical that caused disintegration of biological membranes through lipid peroxidation, caused protein misfolding and point mutations in DNA sequences (Guo et al., 2013). Therefore, the aim of this study was to determine whether co-treatment of HPOs with H_2O_2 would protect against SH-SY5Y cell death by minimising the toxic effect of $OH^{\bullet-}$ radical formed through iron chelation. These data support the idea as CP20 and the novel HPOs reduced H_2O_2-induced cell death between 48 to 79%.

This is the first time that the protective effect of CP20 on H_2O_2-induced toxicity in SH-SY5Y cells has been reported, therefore, direct comparison with the existing study is not possible. Nevertheless, CP20 has been shown to protect primary cortical neuronal cultures from H_2O_2- induced cell death as measured by reduced LDH release (Molina-Holgado et al., 2008). Moreover, CP20 has been shown to reduce the production of $OH^{\bullet-}$ radical through Fenton reaction by spectroscopy analysis which suggest that this is probably one of the main mechanism of CP20 protection against H_2O_2 toxicity (Devanur et al., 2008b, Timoshnikov et al., 2015). As expected due to their structural similarities with CP20, with the exception of CP84, the novel HPOs also showed significant protection against H_2O_2 toxicity in SH-SY5Y cells, and this was comparable to CP20. CN116, CN118, CN126, CN226 and CN228 co-treated with H_2O_2 significantly protected from H_2O_2 toxicity at 50 µM while CP20 only did so only at 100 µM which might suggest higher chelation potency for novel HPOs. The neuroprotection might be partly due to the pFe^{3+} as determined by potentiometric titration which were similar to that of CP20. Interestingly, the enantiomer pair of HPOs did not show any differences in neuroprotection suggesting little or no contribution of stereochemistry to the activity of HPOs. As for CP84, although there appeared to be a small protection against cell death, this was not significant.

Although the existing studies of CP20 on H_2O_2-induced toxicity *in vitro* are scanty, neuroprotection studies with DFO and H_2O_2 can be compared with the current results. Although DFO is structurally different to the HPOs used in this study as it is in which it is a larger hexadentante molecule, DFO and HPOs are both Fe(III) iron chelator. Therefore, the reported mechanisms of neuroprotection of DFO is expected to be similar to HPOs

through their primary pharmacological action. Previous study showed that SH-SY5Y cells pre-treated with DFO for 2 hours completely abolished H_2O_2-induced autophagy (Castino et al., 2011). Besides DFO, a novel fluorinated derivative of CP20, Apo6856 (**Figure 4.4.1**) also protected SH-SY5Y against H_2O_2 toxicity in a concentration dependent manner (Premyslova et al., 2016, Tam et al., 2014). Treatment with Apo6856 also caused a concentration- and time-dependent up-regulation of Nrf2 activity in SH-SY5Y cells and modulated the expression of genes in a pattern consistent with downregulation of inflammation and ROS production and increased cellular antioxidant defence capacity.

a) CP20 **a) Apo6856**

Figure 4.4.1: Chemical structure of a) CP20 and b) Apo6856, a fluorinated derivative of CP20. Functional group highlighted in red denotes the structural different from CP20. Atoms highlighted in blue indicates the pharmacophore that is important for the bidentate co-ordination with iron.

It is likely that CP20 and the novel HPOs would also act via the same molecular mechanism due to the close structural and functional similarity to Apo6856 in manifesting the neuroprotection in H_2O_2-treated SH-SY5Y cells. However, this is not conclusive and remain speculative until the molecular mechanism of CP20 and novel HPOs in H_2O_2-treated SH-SY5Y are studied in detail.

In summary, all novel HPOs except CP84 showed comparable neuroprotection to CP20 against H_2O_2-induced cell death. Most of the novel HPOs started to show significant neuroprotection at 50 µM in contrast to 100 µM for CP20 suggesting better efficacy than CP20. It is suggested that the mechanism of neuroprotection of the novel HPOs against H_2O_2 toxicity was mainly through the chelation of excess intracellular iron which is associated with H_2O_2 toxicity.

4.4.3 *Neuroprotection of HPOs against 6-OHDA toxicity in SH-SY5Y*

6-OHDA was employed to induce SH-SY5Y cell death and to evaluate the ability of novel HPOs to protect SH-SY5Y from 6-OHDA-induced cell death. As a metabolite of dopamine, 6-OHDA was used as a toxin to induce SH-SY5Y cell death through the generation of ROS through interaction with O_2 (**Section 2.2.1b**). Furthermore, the oxidation product of 6-OHDA, *p*-quinone, is a highly reactive electrophile that formed an adduct with nucleophilic groups of intracellular proteins (Soto-Otero et al., 2000, Napolitano et al., 1995). Most importantly, 6-OHDA induced the accumulation of iron into the cells by enhancement of iron cell-uptake mechanisms which accelerate the process of cell death by producing more ROS via Fenton reaction. Therefore, SH-SY5Y cells treated with iron chelators are expected to slow down or inhibit cell death and reduce cell death.

The data revealed that CP20 protected against 6-OHDA-induced cell death in a concentration dependent manner with significant protection at 100 and 500 µM concentration. Furthermore, cell viability for SH-SY5Y cells was also reverted to the control level at 500 µM concentration in agreement with a recent report (Workman et al., 2015). Interestingly, novel HPO iron chelators showed significant protection against 6-OHDA induced cell death at all of the concentration tested with CN118, CN226 and CN228 inhibiting toxin-induced cell death to the control level at lower HPOs concentrations. These HPOs also showed significant reduction in cell death in comparison to equimolar concentrations of CP20. This observation supports the hypothesis made by Workman et al. (2015) that increasing the lipophilicity of HPO chelators enhances neuroprotection of SH-SY5Y cell death induced by 6-OHDA. It was suggested that increased in lipophilicity made the HPO more accessible to intracellular iron by crossing the biological membranes which include the mitochondrial membranes. Since the pFe^{3+} for the novel HPO iron chelators (pFe^{3+}=19.80-20.40) was similar to the pFe^{3+} for CP20 (pFe^{3+}=20.20), it is likely that this contributed less to the different in extent of iron chelation compare to lipophilicity.

It has been demonstrated by Kobayashi et al. (2008) that 6-OHDA and iron mixture generates higher level of H_2O_2 and *p*-quinone than 6-OHDA alone. It was suggested that a semiquinone radical is formed through a reduction of Fe^{3+} as an intermediate before the semiquinone is oxidised to *p*-quinone by O_2 with ROS produced along the course of the reaction (**Figure 4.4.2**).

Figure 4.4.2: Production of ROS during 6-OHDA metabolism to *p*-quinone (Izumi et. al., 2005).

Indeed, ROS generated during *p*-quinone formation has been reported to be the primary contributor of 6-OHDA toxicity and reducing *p*-quinone level was found to be neuroprotective (Izumi et. al., 2005, Storch et al., 2000). Additionally, this observation was further supported by several neuroprotection studies *in vitro* using different type of iron chelators that managed to prevent the 6-OHDA induced cell death (Zheng et al., 2006, Cacciatore et al., 2013). In the situation where semiquinone formation is halted by efficient iron chelation, 6-OHDA would be the predominant species. 6-OHDA has been reported to inhibit Complex I and Complex IV of mitochondrial respiratory chain, but further experiment showed that these electron transport chain inhibitions did not lead to interruption in ATP production. This might explain the complete prevention of 6-OHDA-induced cell death in some of the treatment group with HPOs.

To summarise, novel HPOs showed a pronounced neuroprotection against 6-OHDA-induced cell death with some of them are a better neuroprotectant at equimolar concentrations (CN118, CN226 and CN228) of CP20. It is proposed that the mechanism of neuroprotection of the novel HPOs against 6-OHDA-induced cell death was through the inhibition of *p*-quinone metabolite formation from 6-OHDA that requires iron.

4.4.4 *Neuroprotection of HPOs against MG132*

MG132 was chosen to induce SH-SY5Y cell death due to its proteasomes inhibition property that emulate the toxicity of mutant or aggregated α-synuclein found in dopaminergic neuron of patients with familial PD. α-Synuclein is targeted for degradation by the UPS pathway, however, mutant or aggregated α-synuclein can interact with the proteasomes active sites and inhibits its activity (McNaught et al., 2002, Snyder et al., 2003). Inhibition of UPS also lead to accumulation of iron by decreasing the iron binding proteins (IRPs) degradation. IRP bind to iron response element (IRE) on mRNA of proteins

that involve with iron uptake, regulation and metabolism (Xie et al., 2010b, Wang et al., 2007, Guo et al., 1995). Simultaneous accumulation of intracellular proteins and iron-induced free-radicals could aggravate the oxidative stress through free-radical generation (Kalivendi et al., 2004). Therefore, the aim of this study was to determine whether by chelating iron in MG132-treated SH-SY5Y cells, the cell death could be prevented. Neither CP20 nor the novel HPOs protected against MG132-induced toxicity. This is consistent with the previous report that, the antioxidant N-acetylcysteine failed to protect against MG132-induced cell death (Cheng et al., 2016, Zafar et al., 2007). UPS inhibition results in the build-up of damaged and unwanted intracellular proteins. These data confirm that chelation of iron alone is not sufficient to prevent MG132-induced cell death. Remarkably, repression of p53 level by genetic silencing or inhibiting p53 activity prevented cell death resulted from proteasomes inhibition (Lopes et al., 1997, Nair et al., 2006, Dietrich et al., 2003). This may suggest that, apart from iron-induced free radicals, other distinct factors might predominantly contribute to cell death after proteasomes inhibition. It may be argued that proteasome dysfunction is not a primary phenomenon in PD as seen using proteasomes inhibitors such as MG132, lactasystin or PSI, but rather a secondary phenomenon as a result of damaged caused by oxidative stress. Oxidative stress induces misfolding and aggregation of proteins such as α-synuclein that in turn inhibit proteasomes function. Therefore, the treatment approach might strictly depend on the nature of the cause of the UPS inhibition.

To sum up, CP20 and the novel HPOs showed no neuroprotection against MG132-induced cell death. It is proposed that the main pathogenesis of MG132 toxicity was not sufficiently prevented by treatment with HPOs iron chelator alone, which presumably because MG132 toxicity predominantly involved other pathways that do not involve iron.

4.4.5 *Neuroprotection of HPOs against FeNTA*

In this study, the FeNTA (1:3) complex (shortened to FeNTA) was used to induce iron toxicity in SH-SY5Y cells. In addition, FeNTA can be used to evaluate the efficiency of iron transfer to HPOs in which case FeNTA act as non-transferrin bound iron (NTBI) to HPOs. High concentration of NTBI characterised the intracellular physiology of cells with iron overload. This is the first reported study of CP20 neuroprotection on FeNTA-induced cell death using SH-SY5Y cells. CP20 exhibited a concentration-dependant neuroprotection against FeNTA toxicity with significant protection at 1250 µM. This agrees with a previous

study where, CP20 prevented FeNTA toxicity in a concentration dependant manner in primary cortical neurons albeit at relatively lower concentrations (30 and 100 µM) (Molina-Holgado et al., 2008). The discrepancies in the concentrations of CP20 that conferred neuroprotection was due to the different types of cells employed between these studies. Primary cortical neurones are more sensitive to FeNTA toxicity (IC_{50} = 10 µM) than SH-SY5Y cells which require higher concentrations to incur cell death (IC_{50} = 460 µM). This is likely to be due to the buffering provided by the iron storage protein, ferritin, which is overexpressed in cancer cell lines (Guan et al., 2017, Selig et al., 1993). Nevertheless, both studies showed the same efficiency (about 3-folds of the IC50 concentrations for FeNTA) of CP20 to significantly chelate iron from NTA. Remarkably, novel HPOs CN116, CN118, CN226 and CN228 prevented cell death at or below the IC_{50} concentration of FeNTA which suggest that iron transfer and re-distributes from NTA to these HPOs. This redistribution more readily occurs at lower concentrations compared to CP20 which only significantly protected cells from FeNTA toxicity at the concentration of two-folds of FeNTA IC_{50} (1250 µM). On the other hand, CN116 and CP84 did not protect SH-SY5Y cells at all from FeNTA insult.

Additionally, CN128, CN226 and CN228 were superior than CP20 neuroprotection at equimolar concentration (500 µM). It is even more interesting to emphasise that the degree of neuroprotection of novel HPOs used in this study are more related to the lipophilicity than the pFe^{3+}. Similar observations were also found when other toxins were used to induced cell death as has been explained in the previous sections. It has been suggested that FeNTA complex can permeate through biological membranes (Bunescu et al., 2008) and bidentate chelators such as CP20 could competitively chelate iron in a concentration-dependant manner from an existing iron complex (Devanur et al., 2008a). The suggested mechanism of iron transfer from FeNTA to HPOs is presented in **Figure 4.4.3**. Base on the current results, it can be proposed that FeNTA induced iron toxicity intracellularly and HPOs with higher lipophilicity could gain sufficient concentration in the cytoplasm to prevent iron-induced cell death. The results suggest the suitability of novel HPOs to treat localised brain iron accumulation as seen in PD brain. This is crucial as traditional iron chelator, DFO, although could efficiently chelate iron, has very low membrane permeability and has limited ability to cross biologicals membranes (Guan et al., 2017).

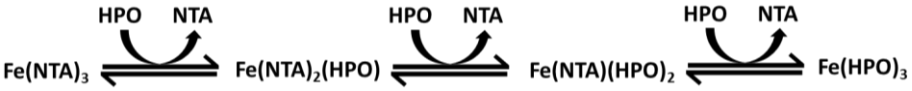

Figure 4.4.3: Suggested mechanism of Fe(III) transfer-equilibration between NTA and HPOs.

In summary, all the novel HPOs protected against FeNTA-induced cell death with some of them showing better neuroprotection (CN128, CN226 and CN228) than CP20 at equimolar concentrations. It is proposed that the neuroprotection of HPOs against FeNTA-induced cell death was improved as the lipophilicity increased.

4.4.6 *Advantages and shortcomings of this study*

Cell-based assay is widely employed for evaluating and screening potential neuroprotective agent due to their physiology and mechanisms closely related to the cells in living animals but with added flexibility (Burroughs et al., 2012, Zhang et al., 2014). Additionally, experiment on cell lines for testing neuroprotection agents are less expensive than testing in living animals. Homogeneous neuroblastoma cell lines such as SH-SY5Y is one of the important tools widely employed during the early stage for screening potential new drug in PD research. Importantly, SH-SY5Y cell line is a catecholaminergic neuroblastoma cell line from human origin. This cell line expresses both DAT and TH which resembles the affected dopaminergic neurons in the substantia nigra *pars compacta* (SNPc) in PD brain (Kovalevich and Langford, 2013b, Filograna et al., 2015). Being immortalised, the cells are easy to grow, rapidly reaches confluence in culture, stable for multiple passages and can be stored frozen in contrast to primary cell cultures. Because of these reasons, SH-SY5Y cells is suitable for initial screening for large set of potential neuroprotection agents for PD (Xicoy et al., 2017, Xie et al., 2010a). Moreover, large array of neurotoxins with different mechanisms of toxicity could be used to induce cell death by adding into the cell culture medium. As discussed in this chapter, novel HPOs prevented SH-SY5Y cell death when exposed to H_2O_2, 6-OHDA and iron, but not with MG132. This observation could be used to justify the primary mode of action of HPOs when oxidative-stress is predominant in inducing cell death.

However, *in vitro* cell lines are expected to behave differently than the cells *in vivo* due to their isolation from living system, that may affect the results in the current study. Additionally, cell lines such as SH-SY5Y are cancerous and therefore the cell cycle

regulations are atypical from mature neuron which has limited ability to divide. Indeed, the rapid cell proliferation of SH-SY5Y is due to the chronic activation of MAPK-ERK signalling pathway by mutated Ras and leads to alteration of genes transcription that are important for cell-cycles. Thus, SH-SY5Y may utilize different mechanisms of cell death than in mature primary neurons because of the MAPK-ERK overactivation (Abramova et al., 2002). Moreover, cancerous cells such as SH-SY5Y are known to express multitudes of cell-survival mechanism that render the cells resistance to chemotherapeutic agent. For example, toxin such as iron (FeNTA) employed in the current study showed higher IC_{50} value (50-fold) in comparison to primary neuronal culture that significantly more sensitive to these toxins (Molina-Holgado et al., 2008). Indeed, tumour cell lines such as SH-SY5Y and HepG2 are relatively insensitive to iron chelation by iron chelators due to increase ferritin level in these cells (Selig et al., 1993, Selig et al., 1998, Guan et al., 2017). In this situation, higher concentration of iron chelators is needed to completely deplete cellular iron and causing cell death.

Continuously dividing cells like SH-SY5Y makes it difficult to determine whether the observed neuroprotection is solely because of prevention of cell death and not induction of cell proliferation (Datki et al., 2003). Because of this reason, serum which provide important biological factors for cell growth was omitted during the neuroprotection phase of this study. Serum removal helps to synchronise the development stage of the dividing SH-SY5Y cell line by enabling cells to enter the nondividing state (G0) characterised by low metabolic activity (Langan and Chou, 2011). Lower IC_{50} value for toxin is achievable when serum is removed as absence of serum in cell culture media retards cell growth. However, omission of serum introduces other disadvantages. Serum deprivation has been shown to cause progressive decline in SH-SY5Y cell viability with almost 50% cell reduction after 4 days without serum due to increase in pro-apoptotic and autophagic proteins (Kim et al., 2008, Bar-Am et al., 2005, Xu et al., 2013). This to some extent may have affected the degree of the measured cell viability in toxin-induced cell death but this has been considered in the current experiment design by running a simultaneous negative-control.

Although SH-SY5Y cell lines shares some important characteristics of dopaminergic neurons that enable their usage to screen neuroprotection agents, array-based comparative genomic hybridization studies have identified significant chromosomal

aberration which contributes to different genetics information compared to dopaminergic neurones in brain (Do et al., 2007, Skibinski and Finkbeiner, 2011). This may explain lower expression of TH and DAT in SH-SY5Y cells, which may mean that the mechanism of toxicity and neuroprotection are different than primary dopaminergic neurons (Presgraves et al., 2004). For example, 6-OHDA could confer its toxicity both extracellularly and intracellularly as discussed in **Chapter 2.** Mechanism of intracellular toxicity of 6-OHDA is dependent on the expression of DAT, thus may create variations in the cellular response to exogenous stimuli between SH-SY5Y and primary neurones. In addition, SH-SY5Y cell that have undergone multiple passages could lose their neuronal and dopaminergic characteristic as they accumulate genetic and epigenetic alterations. Accumulated genetic and epigenetic alterations after multiple passage make it hard to get reproducible and reliable results. This could be prevented by using cells at low passage number as in the current study.

Since SH-SY5Y cells grown *in vitro* is an open system as opposed to neurons in the brain that are separated from systemic circulation by BBB, question may arise on the validity of observed neuroprotection *in vivo*. This is because, potential neuroprotection agent that shows promising results *in vitro* might not work *in vivo* due to poor brain permeability. This issue has been addressed in **Chapter 3** and **5**, whereby HPOs were assessed for brain permeability by *in situ* brain perfusion and after *i.p.* injections. Besides the brain permeability issue, the concentration of compounds that showed neuroprotection may not necessarily achieved in the brain eventhough they could cross the BBB (Weber, 2015).

Despite all the disadvantages and limitations discussed above, cell lines such as SH-SY5Y has served an important role for studying the mechanism of toxins in causing cell death in PD and also to explore neuroprotection strategies to prevent or delay cell death (Falkenburger and Schulz, 2006). It should be acknowledged that the effect of potential neuroprotection agents may not be fully represent to pharmacologic effects *in vivo*. For this reason, subsequent studies in animal model of PD is vital to confirm the results from *in vitro* cell cultures study.

4.4.7 *Summary*

The differences of HPOs ability to exhibit neuroprotection in these *in vitro* models appears to be related to the pathogenesis that leads to cell loss. In this circumstance, it can be speculated that cell death pathogenesis that predominantly involved iron accumulation could be prevented by chelating excess iron with HPOs. Having said this, SH-SY5Y cell death caused by exposure to 6-OHDA could be prevented nearly 100% when treated with HPOs. Paradoxically, FeNTA-induced cell death was not prevented as efficiently as in 6-OHDA-induced cell death. This could be explained based on the competition between NTA and HPOs to chelate iron. Iron chelation with HPOs also significantly prevented H_2O_2-induced cell death possibly through the chelation of excess iron which subsequently reduced $OH^{\bullet-}$ radical synthesis from the Fenton reaction. Toxicity of MG132 was not reduced by iron-chelation suggesting that the mechanism of toxicity does not involved ROS generated by iron alone. However, it needs to be emphasised that the data from the current study only come from a single method of detecting cell death. The MTT assay relies on measuring mitochondrial enzyme activity (Wang et al., 1996). It has been reported that some compounds can modulate the enzyme activity or directly interact with MTT which confound the final results (Hsu et al., 2003, Devika and Stanely Mainzen Prince, 2008). Other cell viability methods such as measurement of ATP level or trypan blue exclusion assay could be used for confirmation of the results. Additionally, molecular study to reveal the downstream mechanism towards neuroprotection of these novel HPOs is also of great interest.

4.4.8 *Conclusion*

The present study aimed to evaluate the neuroprotection of novel HPOs and compare with CP20. Treatment of SH-SY5Y cell with HPOs alone did not induce cell death, while treatment with toxins only at the IC_{50} concentration induced cell death. Novel HPOs managed to prevent cell death associated with exposure to neurotoxins to various degree suggesting an involvement of iron in the promotion of cell death, except for MG132. CN118, CN226 and CN228 showed better neuroprotection than the equimolar concentration of CP20 in 6-OHDA-induced cell death. Similarly, CN126, CN226 and CN228 were superior than equimolar concentration of CP20 towards protection against FeNTA-induced cell death. Chirality in novel HPOs chemical structure did not cause different in neuroprotection capability. In conclusion, the hypothesis that novel HPOs are

neuroprotective in *in vitro* model of PD are accepted. Due to the neuroprotection shown *in vitro*, it is not known whether these compounds will show neuroprotection *in vivo*. For this reason, selected HPOs were chosen for a further neuroprotection study utilising an *in vivo* rat model of PD.

CHAPTER 5

NEUROPROTECTION STUDY OF NOVEL HPOs WITH 6-OHDA LESIONED RAT MODEL OF PARKINSON'S DISEASE

5 Neuroprotection study of novel HPOs with 6-OHDA lesioned rat model of Parkinson's disease

5.1 *Introduction*

At the start of these studies it was hypothesised that the novel HPOs based on the structure of CP20 could cross the BBB and show neuroprotection in Parkinson's disease (PD). In **Chapter 3** of this thesis the first part of this hypothesis was tested. Studies were described that showed that, of all the HPOs studies, only CP84 had a superior rate of brain uptake compared to CP20, and that although the rate of brain uptake for CN128, CN226 and CN228 were not different than CP20, those of CN116, CN118 and CN126 were lower. In **Chapter 4,** the second part of this hypothesis was tested. The neuroprotection ability of all brain permeable novel HPOs was investigated *in vitro* using toxin-treated SH-SY5Y neuroblastoma cells. In this study, novel HPOs showed a tendency for positive correlation between their neuroprotective potency and lipophilicity, especially against 6-OHDA and FeNTA induced cell death.

In the studies described in this chapter the overall hypothesis was tested by comparing the ability of selected HPOs to protect against cell death *in vivo*. This assesses both the properties of CNS penetration and neuroprotection. From the previous results CP84, CN128 and CN226, along with CP20 were selected to take forward into these studies. Studies on the effect of CP20 in *in vivo* model of PD have been reported in the literature (Dexter et al., 2011, Devos et al., 2014). CP20 was found to be neuroprotective in 6-OHDA treated rats and MPTP treated mice. In addition, recently, clinical trials to assess the effect of CP20 in PD patients (FAIRPARK) showed reduction in iron level in the nigrostriatal system and improved motor score after 6- to 12-months treatment (Devos et al., 2014a, Martin-Bastida et al., 2017). CP20 was therefore included in these studies as a positive control.

Although CP84 showed limited neuroprotection compared to other novel HPOs, its high brain permeability relative to other HPOs, and significant protection against 6-OHDA toxicity warranted its inclusion in this *in vivo* study. Both CN128 and CN226 showed similar

or better CNS penetration and neuroprotection than CP20. Of the enantiomeric pair, CN126 and CN128, both showed similar neuroprotection in the *in vitro* models, but the latter showed a 2-fold greater brain uptake which was not significantly different to CP20. For this reason, CN128 was taken forward to the *in vivo* neuroprotection study. By contrast, the enantiomeric pair, CN226 and CN228, showed equal brain permeability and *in vitro* neuroprotection suggest that chirality did not play a role in brain permeability or neuroprotection against the selected toxins. However, only CN226 was selected due to its preferable physical property that remain dry at room temperature in contrast to CN228 that is hygroscopic.

The choice of compounds taken forward was based not only on their brain penetrability and neuroprotective effect *in vitro*, but also on their pharmacokinetic profile and evidence of *in vivo* iron chelating activity. Previously, oral treatment with CN128 and CN226 in iron-overloaded rat revealed ability of these HPOs to excrete iron (Hider et al., 2011a, Lu, 2016). In addition, CN128 has been shown to be the most efficient iron-chelating agent among the novel iron chelators when assessed in iron-overloaded rat due to improved bioavailability than CP20 (Hider et al., 2011a, Lu, 2016, Paiboonsukwong et al., 2016). CN128 also exhibited better toxicity profile than CP20 in preventing reduction of leukocytes counts in rats and monkeys (Paiboonsukwong et al., 2016).

Based on the current and previous findings along with toxicity profiles assessed in rats and monkeys (Paiboonsukwong et al., 2016), it is speculated that CP84, CN128 and/or CN226 would be neuroprotective and could perform better in human than CP20. However, before this can be tested in human, data from animal studies is needed to progress to the clinical phase. Therefore, to assess the neuroprotective ability of CP84, CN128 and CN226, neuroprotection study was performed along with CP20 as a positive control in partial unilateral 6-OHDA-lesioned rats.

5.1.1 *Hypothesis*

It was hypothesised that CP84, CN128 and CN226 are neuroprotective against 6-OHDA-induced degeneration of dopaminergic neurons in the rat nigrostriatal pathway *in vivo.*

5.1.2 *Aims*

To test the hypothesis, rats were treated with equimolar doses of HPOs before, during and after a partial 6-OHDA lesion. Using 6-OHDA- or sham-lesioned rats, these studies had the following aims:

a) Confirm that CP20, CP84, CN128 and CN226 is absorbed into systemic circulation after *i.p.* injection.

b) Assess the effect of selected HPOs on body weight.

c) Evaluate the effect of selected HPOs on D-amphetamine-induced rotational behaviour.

d) Investigate the effect of selected HPOs on striatal level of dopamine and serotonin and their metabolites.

e) Determine the effect of selected HPOs on dopaminergic cell death in the SNPc.

5.2 *Materials and methods*

5.2.1 *Experimental animals*

Male Wistar rats weighing between 250-300 g (Harlan UK Ltd) and were housed between 2-4 rats per cage at BSU, King's College London as described in **Section 2.2.2**.

5.2.2 *Pharmacokinetics evaluation of selected novel 3-hydroxy-4-pyridinone iron chelators in rats*

Rats (n=3-4 per treatment group) were injected *i.p*. in a volume of 5 mL/kg with 200 µmol/kg (CP84) or 500 µmol/kg (CP20, CP84, CN128 and CN226). All HPOs were prepared in 0.9% (w/v) NaCl, except for CP84 that contained a final concentration of 0.1% (v/v) DMSO in 0.9% (w/v) NaCl.

a) Samples collection

Blood sample were collected into heparinised tube at 5, 10, 20, 60, 120, 240, and 360 min after *i.p.* injection from the rat lateral vein using 23G wing infusion needle (Terumo®; MediSupplies, UK). Rat tail was immersed into warm (40 ˚C) tap water 2 minutes prior to blood sampling to visualise the lateral vein and to assist blood flow during sample collection. Plasma samples were obtained from the collected blood via centrifugation at 5400 g for 10 min and were stored in -70 ˚C until use. Rats were terminally anaesthetised with 600 mg/kg pentobarbital sodium (Merial Animal Health Ltd, UK) at the terminal time point (360 min) and the brain was taken out. The brain was homogenised in PhyBS [1:1 (w/v)] and stored in -70 ˚C until use.

b) Samples preparation and analysis

Plasma and brain samples obtained from HPOs treated rats were prepared and analysed using a validated method as described in **Section 2.3**. In short, internal standard, IS (200 µM; 10-fold concentration) was added into plasma and brain homogenate collected from the treated rats. Following this, the samples were extracted with TFA as described in **Section 2.3.5**. Briefly, clear supernatant was collected after centrifugation at 20800 g for 45 minutes and 30 µL was injected into HPLC system along with standard calibration curve. The HPLC method for analysis of HPOs in the plasma and brain samples was

performed as described in detail in **Section 2.1.9b**. The HPLC response signal was taken as the ratio of HPO and IS peak height and converted into concentration (µM) using linear equation obtained from the standard calibration curve. The HPOs concentrations in plasma and brain from treated rats were corrected for protein binding as described in detail in **Section 2.1.10.**

c) Data analysis

The pharmacokinetic parameters were calculated by non-compartmental analysis (plasma data after extravascular input) using Microsoft Excel Solver add-in, PK-Solver 2.0 (Zhang et al., 2010). One-way ANOVA followed by Dunnett's test was performed to compare between the PK parameters.

5.2.3 *6-OHDA model of PD for neuroprotection study*

Male Wistar rats (n=6 per group; 250-300 g) were pre-treated with CP20 or CN128 three days prior to 6-OHDA lesion and for four days after the lesion following a dosage regime reported by Dexter et al. (2011). CP20 and CN128 (70 µmol/kg) or vehicle (5 mL/kg; 0.9% (w/v) NaCl) were injected *i.p* twice daily with 12 h gap between treatments (doses at 9 a.m. and 9 p.m). On the day of the surgery only the first *i.p.* injection was performed 30 minutes prior to induction of the lesion. The dose of 6-OHDA-HCl (Sigma-Aldrich, UK) was calculated as a free base and dissolved in 0.9% saline containing 0.1% (w/v) L-ascorbic acid on ice on the day of surgery. Aliquots (1000 µL) were protected from light exposure and stored on ice until the surgical procedure. The intra-striatal lesion was induced by injection of 6-OHDA (8 µg/4 µL) as described in **Section 2.4.4**. Similarly, control animals received sham injection (4 µL of 0.9% saline containing 0.1% (w/v) L-ascorbic acid. The weights of all the rats were recorded daily before and after surgery. At the end of the treatment period, the rats entered a 'wash-out' period for seven days. Behavioural assessment as described below (**Section 5.2.4**) was performed on day 12th of the experimental timeline as illustrated in **Figure 5.2.1.**

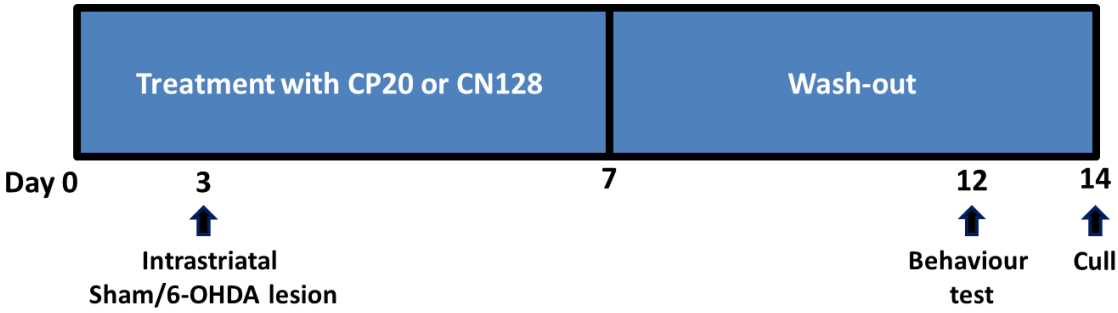

Figure 5.2.1: Overview of experimental timeline.

Rats were treated twice daily with CP20 or CN128 (70 µmol/kg, i.p.) or vehicle for 7 days. Intrastriatal 6-OHDA (8 µg/4 µL) or sham-lesions (vehicle) were performed 30 minutes after drug administration on the third day of HPOs treatment. Following a 7 days wash-out period, the rats were culled.

5.2.4 *D-amphetamine rotation test*

On the day 9th after lesioned, D-amphetamine rotation test using a rotometer (RotoRat^{TM}, Med Associates, Inc., USA) was performed on the rats as described in **Section 2.4.5**. In brief, the rats were injected *i.p* with 2.5 mg/kg D-amphetamine sulphate (Tocris Bioscience, UK) prepared in 0.9% (w/v) saline. The rotations were recorded for a total of 3 h after D-amphetamine injection by a sensor attached to a tethered jacket that was strapped on the rats. Prior to injection with D-amphetamine, the rotational baseline was recorded for 30 minutes following acclimatisation to the rotometers. Data was collected using the RotoRat^{TM} hardware and RotoRat^{TM} software Version 2.0 followed by analysis to determine net ipsilateral rotations as described in **Section 2.4.5.**

5.2.5 *Determination of dopamine and serotonin level by HPLC-ECD*

a) Striatum dissection

The brain was removed from the skull and cleaned of meninges and striatum dissected. The brain was cut laterally with single-edge blade (VWR International Ltd, UK) at the level of optic tracts (**Figure 5.2.2a**).

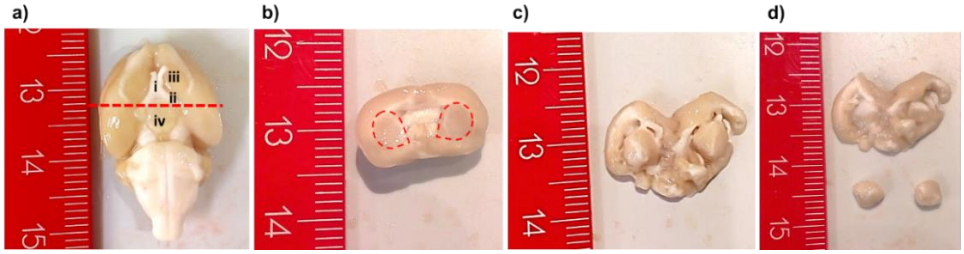

Figure 5.2.2: Steps of striatum dissection on the isolated perfused brain.

***a**) Rat brain at ventral position i = optic chiasma, ii = optic tracts, iii = middle olfactory tracts and iv = mammillary bodies (Ibe et al., 2014). Dotted straight line indicates the position of horizontal brain cutting into halve **b**) the coronal slice of the upper part of the halve brain. Dotted circled shows the location of striatum in the left and right hemispheres of brain **c**) Striatal tissues were separated from the rest of brain tissues **d**) Isolated striatal tissues with white matter mostly removed and stored in -70 ºC for HPLC analysis.*

The upper-half part of the brain was positioned into coronal section. White matter was pulled away with a pair of forceps and striatum as shown in **Figure 5.2.2b** was dissected out and put into a pre-weighed microcentrifuge tube stored on dry ice. Similar steps were repeated for contralateral side of striatum. The isolated striata were stored in -70 ºC until analysis with HPLC.

b) Sample preparation

Striatum was weighed and diluted 1:9 (v/v) with 0.4 M perchloric acid containing 0.01% (w/v) sodium metabisulfite ($Na_2S_2O_5$) and 1 mM EDTA (PCA). DHBA at a final concentration of 1 µM was added into the mixture and function as an internal standard. The mixture was homogenised with a sonic homogeniser for 30 to 60 seconds (Sonics & Materials Inc, USA). The homogenate was centrifuge for 10 minutes at 20800 *g* at 4 ˚C. Finally, the supernatant was collected and store at -70 ˚C.

c) Standard

Main stock (1 mM) for dopamine and serotonin with their metabolites (DOPAC, HVA, 5-HT & 5-HIAA) were prepared in PCA. A range of working stock solutions (10-640 µM) of dopamine and serotonin with their metabolites was prepared in PCA. The injected standards were prepared by 1:9 (v/v) dilution in PCA. 2,3-Dihydroxybenzoic acid (DHBA) was used as an internal standard. Similarly, 1 mM of DHBA main stock was prepared in PCA, diluted 1:99 (v/v) to 10 µM in 0.4 M PCA as working stock solution. Working stock solution of DHBA was added into individual standard at 1:9 (v/v) dilution (final = 1 µM). Additionally, a standard that consist of dopamine and metabolites at a selected single concentration was also prepared in PCA. All chemicals were obtained from Sigma-Aldrich, UK unless stated otherwise.

d) Mobile phase

Mobile phase was 0.1 M sodium dihydrogen orthophosphate (NaH_2PO_4) containing of 1 mM EDTA, 0.01% (w/v) octane sulfonic acid (OSA) in 12% (v/v) methanol, pH adjusted to 3.2 with phosphoric acid. Mobile phase was filtered with polyamide membrane filters (0.45 µm pore size; Sartorius Stedim UK Limited, UK).

e) HPLC conditions

The quantification was performed on an Ultimate 3000 Standard LC Systems equipped with quaternary pump delivery system (LPG-3400SD), autosampler (WPS-3000(T)SL Analytical) and INTRO electrochemical detector (Antec Scientific, USA). A column set in the system was a Spherisorb ODS (2) 3 µm particle size HPLC column (SpheriClone 0.46 cm x 10 cm; Phenomenex, UK) was equilibrated at 30 ºC. Sample elution was performed under isocratic mode at a flow rate of 1.0 mL/min. A potential of 0.72V was maintained across the electrode, filter was set at 5 seconds, sensitivity range was set at 20 nA/V and injection volume was 10 µL. Concentrations of catecholamines are calculated by using peak height ratio (versus DHBA).

f) a) Representative dopamine and serotonin with metabolites at 1 µM

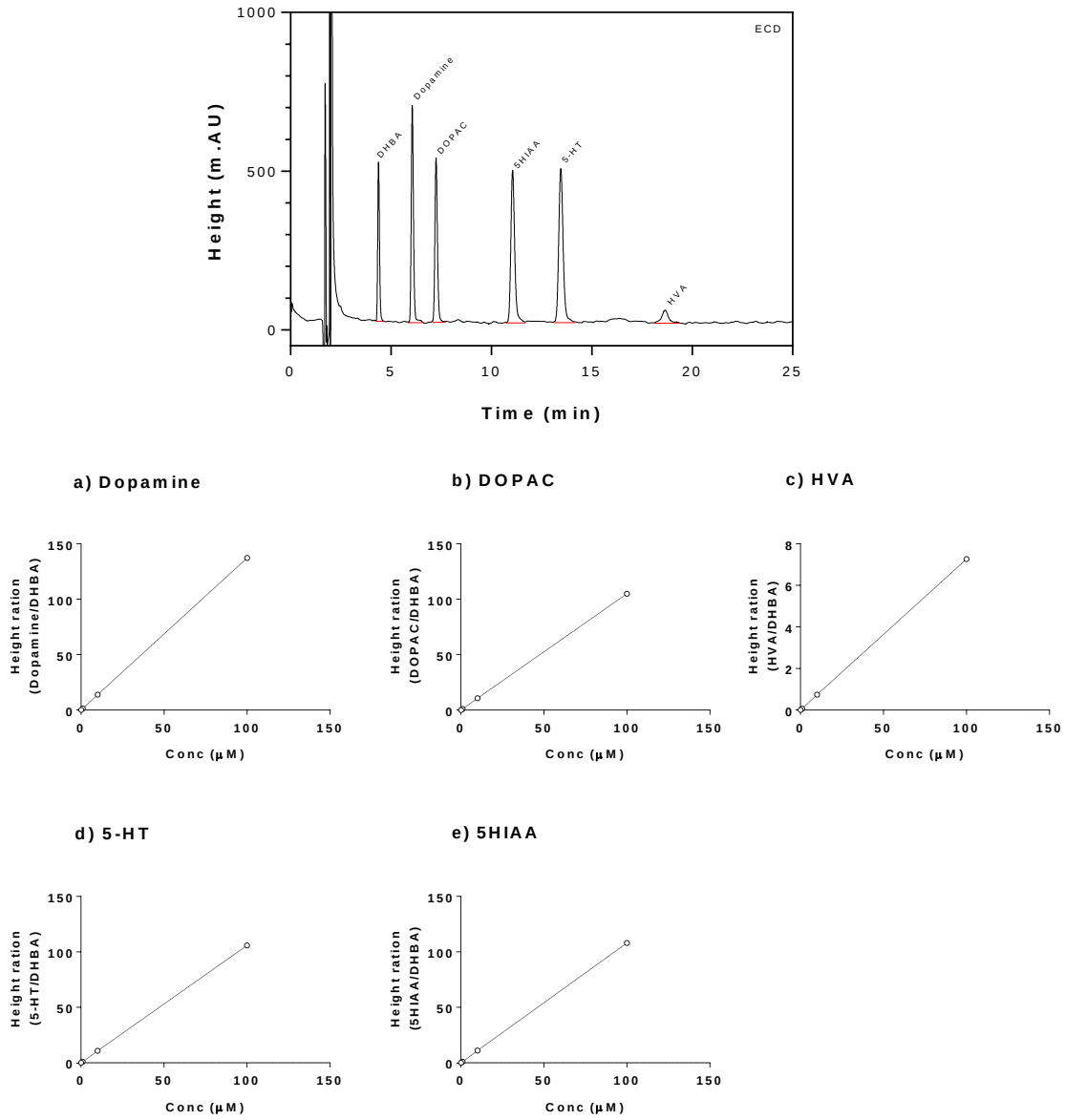

Figure 5.2.3: Representative chromatogram and standard curves for dopamine and serotonin with their metabolites.

The catecholamines of interest are DHBA (RT = ~4.4 min), dopamine (RT = ~6.1 min), DOPAC (RT = ~7.3 min), HVA (RT = ~18.7 min), 5-HT (RT = 13.4 min) and 5HIAA (RT = ~11.1 min) Calibration curves was constructed from 0.1, 1, 10 and 100 µM concentrations.

5.2.6 *Brain fixation and sectioning*

Following dissection of the anterior part of the brain for removal of the striatum, the posterior part of the brain was post-fixed with 4% (w/v) PFA for 6 days. The fixed brain was then cryoprotected with 30% (w/v) sucrose containing 0.05% (w/v) sodium azide (NaN_3) in 0.1 M PBS (pH 7.4) until the tissue sank (~3-5 days). The processed brains were cut coronally into 30 µm sections at the level of 3rd cranial nerve using a freezing microtome and collected into 24-well plates containing 0.1 M PBS, pH 7.4 with 0.05% (w/v) NaN_3 as described in **Sections 2.4.6** & **2.4.7**.

5.2.7 *Immunohistochemistry*

Coronal brain sections were assessed for TH immunoreactivity in the SNPc by immunoperoxidase staining, as described in detail in **Section 2.4.8**. In short, the coronal sections (30 µm) were incubated in 24-well plates with primary antibody against TH (1:500) overnight at room temperature. On the subsequent day, the sections were incubated with biotinylated secondary antibody (1:200) for 1 hour and further 45 minutes incubation with the ABC kit at room temperature. The antibody complex was visualised by exposing the sections to 1 mL 0.05% (w/v) DAB prepared in 0.01% (w/v) H_2O_2 in 0.1 M PBS for ~3 minutes. The sections were then mounted onto coated adhesion microscope slides, dehydrated, cover slipped and examined as described in **Section 2.4.9**.

5.2.8 *Data and statistical analysis*

Data are expressed as individual, mean+SEM or mean±SEM of experimental groups (n=6 rats per group). Dopamine turnover was calculated by finding the ratio between the concentration of dopamine metabolites (DOPAC & HVA) over concentration of dopamine:

$$Dopamine\ turnover = \frac{[DOPAC]+[HVA]}{[dopamine]} \qquad \textbf{Equation 5.2.1}$$

Serotonin turnover was calculated by finding the ratio between the concentration of serotonin metabolite (5-HIAA) over concentration of serotonin (5-HT)

$$Serotonin\ turnover = \frac{[5-HIAA]}{[5-HT]} \qquad \textbf{Equation 5.2.2}$$

GraphPad Prism 7 software was used for statistical analysis. Difference between control and treatment groups was analysed with one-way or two-way ANOVA followed by Holm-Šídák multiple comparison test where appropriate. $p<0.05$ was considered significant.

5.3 *Results*

5.3.1 *Pharmacokinetics study for HPO dose justification*

In **Chapter 3** it was shown that some of the novel HPOs can enter the brain, however, brain levels are determined not only by this ability, but also be the pharmacokinetics (PK) of a compound following parenteral administration. For this reason, prior to commencing the *in vivo* neuroprotection study, a PK study was performed to validate the dose selected and confirmation of brain penetration in a whole *in vivo* setup. Male Wistar rats were injected *i.p.* with 500 µmol/L CP20, CP84, CN128 and CN226 followed by plasma sampling for up to 360 minutes to determine the PK profiles. CP20, CN128 and CN226 did not show any sign of acute toxicity after *i.p.* injections, except for rat injected with CP84 that exhibited seizure within 5 minutes after injection. The dose for CP84 was reduced to 200 µmol/kg with similar observation. Therefore, PK study for CP84 was discontinued, and CP84 was not used for further study. Apart from CP84 toxicity, rats injected with CP20 exhibited increase in salivation that subsides 60 minutes after injection. This sign was not observed for rats treated with CN128 and CN226. The validated bioanalytical method was successfully applied to quantify the concentration of selected HPOs in plasma and brain homogenate after *i.p.* injection of 500 µmol/kg HPOs dose (**Figure 5.3.1**).

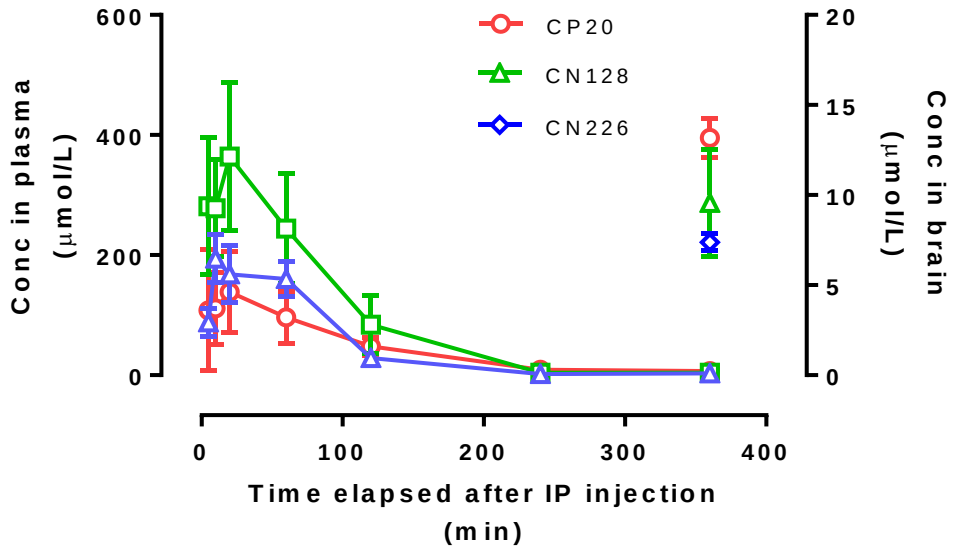

Figure 5.3.1: Concentration in plasma/brain against plasma sampling time after *i.p.* injection with 500 µmol/kg HPOs.

The PK parameters for plasma obtained after analysis with PK Solver (Zhang et al., 2010) are summarised in **Table 5.3.1**. CP20 was rapidly absorbed and reached maximum concentration in plasma (T_{max}) in 27 minutes. Likewise, CN128 and CN226 also reached T_{max} within 30 minutes after *i.p.* injection. The rapid absorption phase was followed by exponential declined in plasma which correspond to the short half-lives ($t_{1/2}$) of 61, 40 and 47 minutes after T_{max} for CP20, CN128 and CN226 respectively. CP20, CN128 and CN226 were also characterised by high volume of distributions (V_d) between 1.5 to 2.8 L/kg with rate of clearances (C_L) between 0.02 to 0.03 L/kg/min. The concentrations of CP20, CN128 and CN226 in plasma at the terminal time points (360 min) were between 2.9 to 7.0 µM. Furthermore, HPOs appeared to accumulate in the brain at the terminal time point with concentrations approximately 2-fold of that found in plasma. Overall, there was no significant different when CN128 and CN226 pharmacokinetic parameters were compared with CP20. Nevertheless, CN128 showed a trend towards higher C_{max} than CP20 (p=0.19). Since the PK profile following *i.p.* injection for CN128 and CN226 were not different than CP20 in addition to equal brain permeability and neuroprotection *in vitro*, only CN128 was selected for *in vivo* neuroprotection study.

Table 5.3.1: Pharmacokinetic profile for CP20, CN128 and CN226 after 500 µmol/kg single *i.p.* injection.

Parameter	CP20	CN128	CN226
MW	139.1	273.3	287.4
Injected dose (µmol/kg)	500	500	500
Injected dose (mg/kg)	70	160	160
T_{max} (min)	26.7±10.1	15.0±5.0	30.0±15.3
$t_{1/2}$ (min)	60.7±11.0	40.2±14.3	46.8±3.0
C_{max} (µmol/L)	149.8±69.7	369.4±123.2	193.8±36.2
AUC_{0-t} (mmol/L/min)	16.1±3.4	32.8±12.9	18.6±4.0
$AUC_{0-\infty}$(mmol/L/min)	19.8±4.8	33.2±12.7	18.8±4.1
V_d (L/kg)	2.8±1.3	1.5±1.0	2.0±0.5
Cl (L/kg/min)	0.03±0.01	0.02±0.01	0.03±0.01
$C_{last\ (plasma)}$ (µmol/L)	7.0±1.3	4.3±1.5	2.9±0.8
$C_{last\ (brain)}$ (µmol/L)	13.2±1.1	9.6±3.0	7.4±0.5

Pharmacokinetics parameters were derived from analysis using Excel solver add-in (PK Solver) provided by Zhang et al. (2010). Data are expressed as mean+SEM (n=3-4 rats). Statistical analysis (one-way ANOVA) showed no significant different.

5.3.2 *Effects of partial striatal 6-OHDA lesion and HPOs treatment on rat body weight*

The rat body weights steadily increased when the HPO/vehicle dosage regime started on day 1 (**Figure 5.3.2**). The body weight dropped by 3% a day after the brain lesion procedures but slowly attained the pre-surgical body weight about 4 days after the surgery. By day 9th after the surgery, all rats had exceeded their pre-surgical body weight. Rats treated with either 70 µmol/kg CP20 or CN128 twice daily for 7 days did not show any abnormal symptoms during the dosing regimen.

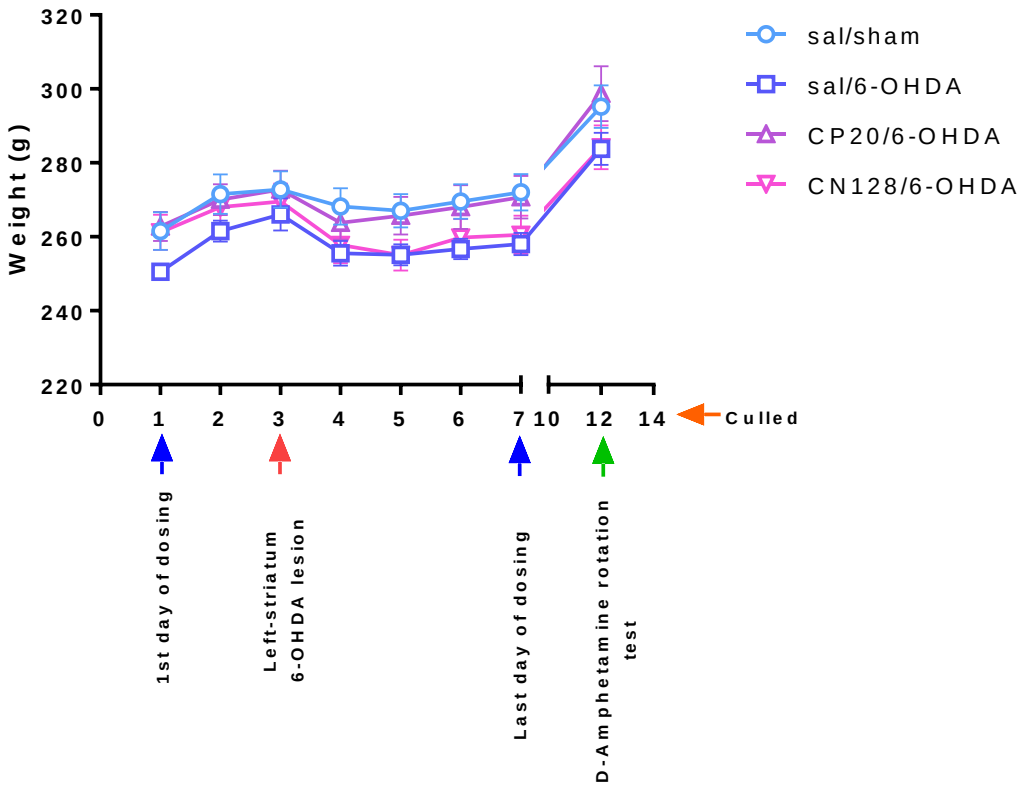

Figure 5.3.2: Weight of rats over the course of *in vivo* neuroprotection study.

Data are mean±SEM (n=6 rats).

5.3.3 *Effects of toxins and HPOs treatment on D-amphetamine-induced ipsilateral rotations*

There was no significant different on D-amphetamine induced ipsilateral rotations between saline/6-OHDA group and saline/sham, CP20/6-OHDA and CN128/6-OHDA groups (**Figure 5.3.3**) similar to the finding observed during the selection of 6-OHDA dose (**Section 2.4.5)**.

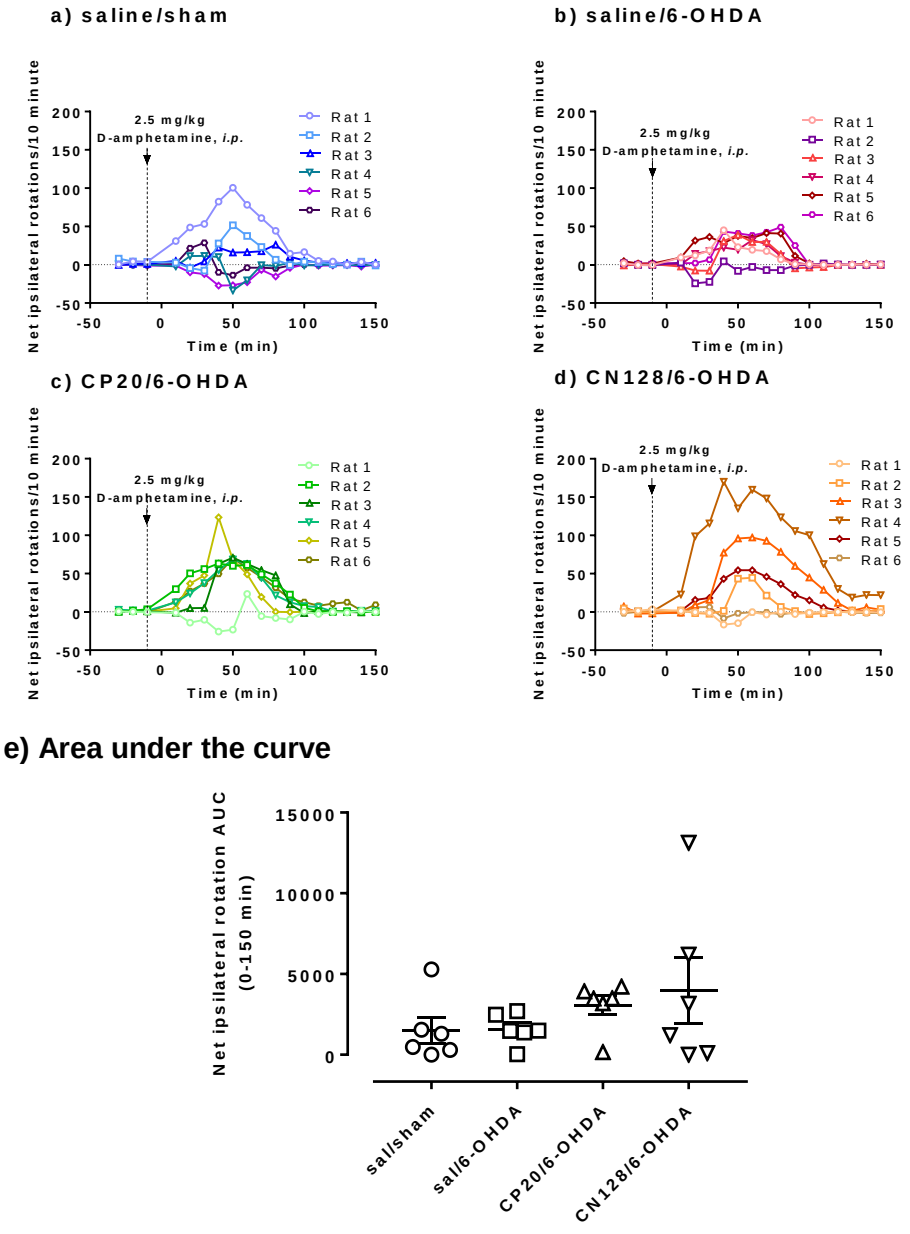

Figure 5.3.3: D-Amphetamine rotation test for 6-OHDA unilateral striatal lesioned rat. *Graphs a), b), c) and d) show data for net ipsilateral rotation shows individual data. Data are individual rat or mean±SEM (n=6 rats). Statistical analysis with one-way ANOVA showed no significant different.*

5.3.4 *Effects of toxins and HPOs treatment on catecholaminergic neurotransmitters in striatum*

Striatum from non-lesioned (contralateral) and 6-OHDA-lesioned (ipsilateral) sides were dissected and processed for the measurement of dopamine or serotonin and metabolites levels by HPLC-ECD. Treatment with either CP20 or CN128 had no effect on the dopamine level in the contralateral side when compared to the saline-treatment groups (**Figure 5.3.4**).

There was no different on the level of dopamine in the sham-lesioned striatum compared to the non-lesioned striatum in the saline-treatment group (negative control) (**Figure 5.3.4a**). By contrast, intra-striatal injection of 6-OHDA caused depletion of dopamine in the ipsilateral side by 64% compared to the contralateral side in the saline-treatment group (positive control). Treatment with CP20 and CN128 protected against 6-OHDA induced dopamine depletion by only causing 38% and 31% dopamine depletion respectively in the 6-OHDA ipsilateral side compared to the contralateral side of striatum, with no difference in the dopamine levels in the contralateral side of SNPc for rats treated with CN128 or CP20.

Neither 6-OHDA lesioned nor HPOs treated group showed significant different on the level of DOPAC and HVA in the striatum when compared to the saline-treatment + sham-lesioned group (**Figure 5.3.4b** & **c**).

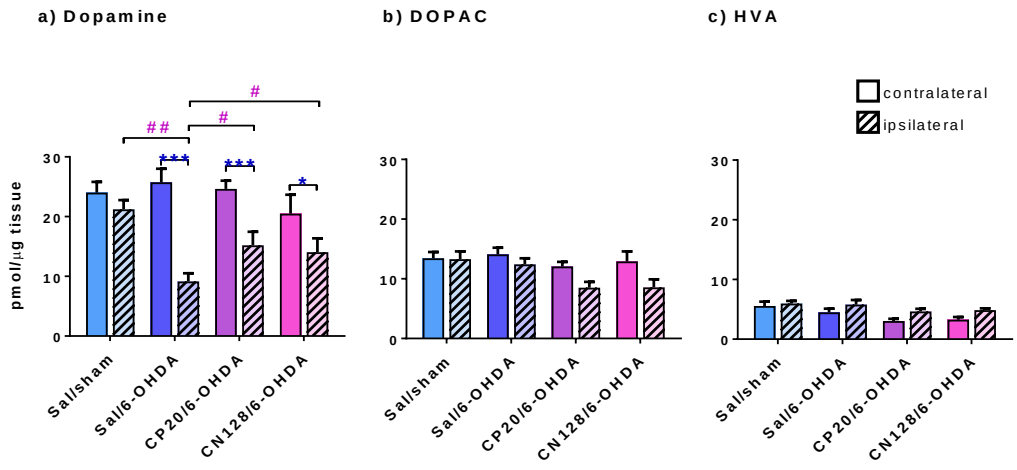

Figure 5.3.4: Dopamine and metabolites measurement in striatum. *Level of dopamine, DOPAC and HVA in the striatum as determined by HPLC-ECD. Data are mean+SEM (n=6 rats). * p<0.05, *** p<0.001 compared to ipsilateral side; # p<0.05, ## p<0.01compared to Sal/6-OHDA ipsilateral side (two-way ANOVA followed by Holm-Šídák multiple comparison test).*

Dopamine turnover was calculated by the formula described in **Equation 5.2.1**. Treatment of CP20 and CN128 did not have any effect on the dopamine turnover in the non-lesioned side (**Table 5.3.2**). Intra-striatal injection of 6-OHDA lead to significant 2.6-fold increase in dopamine turnover. Treatment with both CP20 and CN128 prevented the 6-OHDA-induced increment in dopamine turnover in the ipsilateral side such that turnover values were not different to saline/sham treated controls or values on the contralateral non-lesioned side.

Table 5.3.2: Dopamine turnover in rat striatal tissue.

	Dopamine turnover [DOPAC]+[HVA]/[dopamine]	
Treatment	**contralateral**	**ipsilateral**
Sal/sham	0.82±0.05	0.90±0.08 ##
Sal/6-OHDA	0.79±0.07	2.04±0.38 **
CP20/6-OHDA	0.69±0.03	0.84±0.13 ##
CN128/6-OHDA	0.97±0.18	0.97±0.22 ##

*Data are mean or mean±SEM (n=6 rats). ** p<0.01 compared to contralateral side of the corresponding group; ## p<0.01 compared to Sal/6-OHDA ipsilateral side (two-way ANOVA followed by Holm-Šídák multiple comparison test).*

Treatment with either CP20 or CN128 had no effect on the serotonin level the on the contralateral side when compared to the saline-treatment groups. There was no different on the level of serotonin in the sham-lesioned striatum compared to the non-lesioned striatum in the sham-lesioned group (negative control) (**Figure 5.3.5a**). In contrast, intra-striatal injection of 6-OHDA caused depletion on the level of serotonin in the ipsilateral side by 33% compared to the contralateral side in the 6-OHDA-lesioned group (positive control). By contrast there was no difference in the levels of serotonin between the ipsilateral and contralateral sides in either the CP20 and CN128 treatment group. However, there was a small but significant increase in the level of serotonin on the contralateral sides of the 6-OHDA-lesioned group and CN128 treated animals.

Neither 6-OHDA lesioned nor HPOs treated group showed significant different on the level of 5HIAA in the striatum when compared to the saline-treatment + sham-lesioned group (**Figure 5.3.5b**).

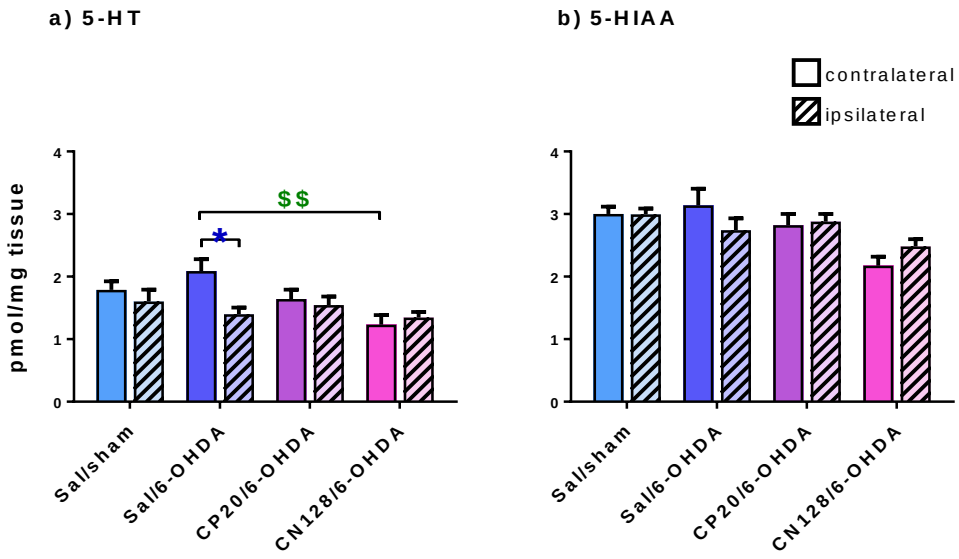

Figure 5.3.5: 5-HT and metabolite measurement in striatum.

*Level of 5-HT and 5-HIAA in the striatum as determined by HPLC-ECD. Data are mean+SEM (n=6 rats). * p<0.05 compared to ipsilateral side; $$ p<0.01 compared between contralateral sides (two-way ANOVA followed by Holm-Šídák multiple comparison test).*

Serotonin turnover was calculated by the formula described in **Equation 5.2.2**. Treatment of CP20 and CN128 did not have any effect on the serotonin turnover in the non-lesioned side (**Table 5.3.5**). Intra-striatal injection of 6-OHDA not significantly changed serotonin turnover although there was a trend towards increase serotonin turnover (p=0.06). Treatment with CP20 and CN128 prevented 6-OHDA induced increased in serotonin turnover in the lesioned side compared to the non-lesioned side.

Table 5.3.3: Serotonin turnover in rat striatal tissue.

Treatment	Serotonin turnover [5-HIAA]/[5-HT]	
	contralateral	ipsilateral
Sal/sham	1.76±0.07	1.77±0.18
Sal/6-OHDA	1.51±0.18	2.18±0.11
CP20/6-OHDA	1.81±0.0.03	1.91±0.12
CN128/6-OHDA	1.92±0.26	1.86±0.08

Data are mean or mean±SEM (n=6 rats). Statistical analysis with two-way ANOVA showed no significant different.

5.3.5 *Effects of toxins and HPOs treatment on TH-positive cells in SNPc*

Brain coronal sections at the level of SNPc were stained for TH by immunoperoxidase method to quantify the number of TH^+ cells. The TH^+ cells in the non-lesioned (contralateral) and 6-OHDA lesioned (ipsilateral) sides of SNPc were counted manually for analysis in a blinded manner.

Treatment with either CP20 or CN128 alone had no effect on the number of TH^+ cells on the contralateral side when compared to the saline-treatment groups (**Figure 5.3.6**). There was no different on the number of TH^+ cells in the SNPc of sham-lesioned compared to the contralateral side in the saline-treatment group (negative control) (**Figure 5.3.7**). By contrast, intra-striatal injection of 6-OHDA (8 µg) reduced the number of TH^+ cells in SNPc by 46% compared to the contralateral side in the saline-treatment group (positive control). Treatment with CP20 and CN128 significantly protected against 6-OHDA-induced TH^+ cell loss in the SNPc of ipsilateral side with only 20% and 14% loss of cells respectively compared to the contralateral side which was not a statistically significant difference.

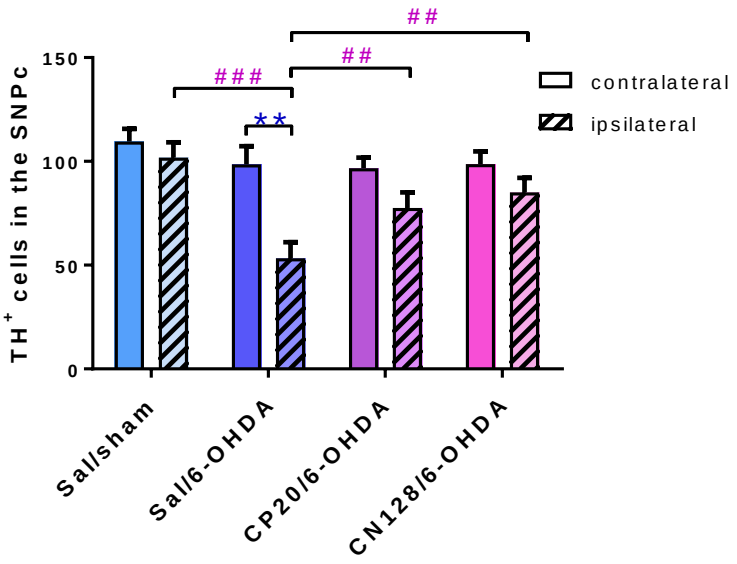

Figure 5.3.6: TH^+ staining cells in the SNPc.

*Data are mean or mean+SEM (n=6 rats). ** p<0.01 compared to ipsilateral side; ## p<0.01, ### p<0.001 compared to Sal/6-OHDA ipsilateral side (2-way ANOVA followed by Holm-Šídák multiple comparison test). Data are mean+SEM (n=6 rats). ** p<0.01 compared to ipsilateral side; ## p<0.01, ### p<0.001 compared to Sal/6-OHDA ipsilateral side (2-way ANOVA followed by Holm-Šídák multiple comparison test).*

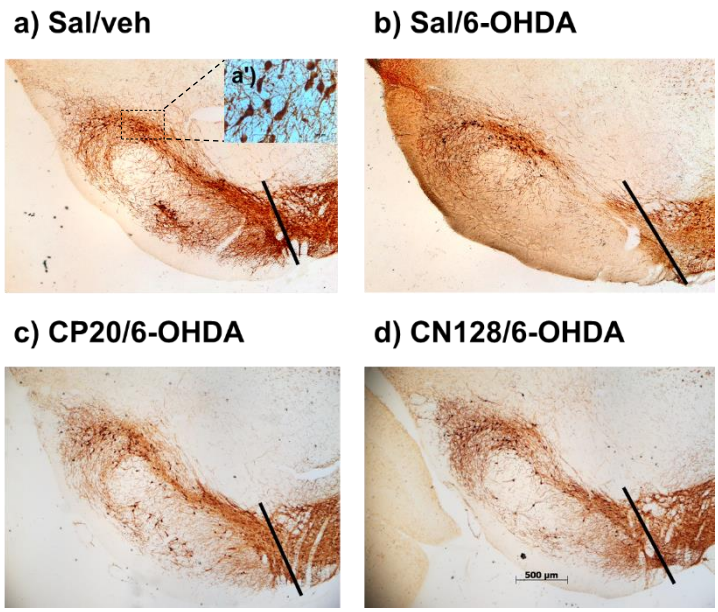

Figure 5.3.7: Representative photomicograph of brain coronal section showing TH^+ cells in SNPc region.

The black line marks the third cranial nerve that demarcate the dopaminergic neurons cell bodies in SNPc and VTA. TH^+ cells in ipsilateral SN in (a) vehicle-lesioned and saline treated rats; (b) 6-OHDA-lesioned (8 µg/4 µl) and saline treated rats (c) 6-OHDA-lesioned (8 µg/4 µl) and CP20-treated (70 µmol/kg/twice-daily/7 days, i.p) rats, (d) 6-OHDA-lesioned (8 µg/4 µl) and CN128-treated (70 µmol/kg/twice-daily/7 days, i.p) rats. Inset a') a typical TH^+ cell. Scale bar = 500 µm and inset scale bar = 50 µm are representative of all images.

5.4 *Discussion*

In this study, it was hypothesised that CP84, CN128 and CN226 would confer a neuroprotection against the 6-OHDA-induced dopaminergic neuron degeneration in basal ganglia. However, after preliminary assessment of pharmacokinetic (PK) profile of these HPOs, only CN128 was chosen for *in vivo* neuroprotection study. The effect of intraperitoneal injection of CP20 and CN128 on 6-OHDA induced degeneration of dopaminergic neuron in SNPc was investigated *in vivo*. The D-amphetamine induced ipsilateral rotation were first assessed one week after termination of CP20 and CN128 treatment in rats, 12 days following the 6-OHDA or sham lesion. Secondly, striatal tissues from rat brains were dissected and processed two-days after rotational test to measure dopamine and serotonin together with their metabolites by HPLC-ECD. Finally, brain coronal sections at the level of SNPc and striatum for 6-OHDA lesioned rats treated with CP20 and CN128 were assessed by TH immunohistochemistry to establish whether they exert a protective effect by preventing dopaminergic cell loss in the SNPc.

5.4.1 *Pharmacokinetic study*

CP20 has previously been assessed of its PK profile after systemic injection and was shown to penetrate the brain (Fredenburg et al., 1996b). Indeed, *in situ* brain perfusion of CP20 in rats as explained in **Chapter 3** support these previous reports of CP20 brain penetration in *in vivo* set up. Additionally, it has been revealed from the *in situ* brain perfusion experiment that CN128 and CN226 brain permeability were not different than CP20. Nevertheless, investigation of PK is important to gain a better understanding on the distribution and clearance for novel HPOs after a systemic injection, and to confirm brain penetration in *in vivo* rat model. Therefore, the aim of the study was to characterise the PK profile of the novel HPOs in plasma after *i.p.* injection and compared to CP20. Additionally, the level of HPOs in brain were measured at the terminal sampling time (360 min).

The reported CP20 dose employed that succesfully showed neuroprotection in rats was 70 µmol/kg (single *i.p.*dose) which was below the sensitivity limit of the current analytical method (Dexter et al., 2011). Nevertheless, since the aim of the current study is for the confirmation of plasma exposure and brain permeability of novel HPOs after *i.p.* injection in rats, a higher dose was preferred. The dose selected for this PK study (500 µmol/kg)

was based on a previous PK study on HPOs performed by Fredenburg et al. (1993 & 1996). However, rats injected with 500 µmol/kg CP84 exhibited convulsion within 5 minutes after injection which suggest a CNS-related toxicity (Schlag et al., 2000, Kontoghiorghes, 1991). This observation corresponded to the rapid brain permeability of CP84 in *in situ* brain perfusion experiment (**Chapter 3**). Additionally, convulsion after single dose administration of 4000 µmol/kg CP20 by intravenous route has been described, but this only occur within 2 to 8 h after treatment (European Medicines Agency, 2005, Hider et al., 1990). The dose of CP84 was reduced to 200 µmol/kg with similar outcome, and therefore CP84 was dropped for further studies despite it showing promising result in term of brain permeability in *in situ* brain perfusion experiment, although only showed mild neuroprotection in *in vitro* study (**Chapter 4**). One noticeable observation in all rats after injection with CP20 was increased in salivation that diminished within 60 minutes in line with the $t_{1/2}$ for CP20. This observation was not seen in other rats treated with CN128 or CN226. Indeed, hypersalivation has been reported to be a unique symptom for rat treated only with CP20 and not for other derivatives of CP20 (Hider et al., 1990, European Medicines Agency, 2005). The cause of this observation is unclear, however increase in salivation is often associated with cholinergic toxicity (Takakura et al., 2003). Unfortunately, there are no studies that specifically focus on the interaction between CP20 and cholinergic transmission has been reported partly because the hypersalivation was only observed in rats but not in human suggesting interspecies different in CP20 toxicity (Porter, 1996, Olivieri et al., 1998). CP20 has been shown to significantly deplete leukocytes counts in control and iron overloaded mice (Porter et al., 1991). Indeed, CP20 appeared to induce neutropenia and agranulocytosis in 7% of Thalassemia patients within 6 months of treatment, which ceased after discontinuation of the therapy (Devos et al., 2014, Martin-Bastida et al., 2017). Remarkably, sub-chronic toxicity study of CN128 in rat and cynomolgus monkey revealed no reduction in leukocytes count and pathological changes in sternal bone marrow which was observed in CP20-treated animals, suggesting better toxicity profile for CN128 than CP20 (Paiboonsukwong et al., 2016).

The selected dose was sensitive enough for the detection of CP20, CN128 and CN226 in the plasma and brain up to 360 minutes post-injection by the established HPLC-UV method. Blood sampling time was limited to 360 minutes based on the previous report of rapid elimination of CP20 in plasma and almost undetectable in the plasma after 12 h of intravenous injection (Fredenburg et al., 1993). This also allows sufficient HPOs levels

remained in the brain for sensitive measurement by HPLC-UV. CP20, CN128 and CN226 reach maximal concentration in plasma (T_{max}) in less than 30 minutes after *i.p.* injection. Half-life ($t_{1/2}$) for CP20 in this study was 61 min which is within the range of previously reported $t_{1/2}$ (72±30 minutes) after a single bolus injection in rats (Fredenburg et al., 1996). Likewise, CN128 and CN226 also rapidly cleared from the plasma with $t_{1/2}$ less than 60 minutes. The short $t_{1/2}$ for CP20, CN128 and CN226 agreed with their high volume of distribution (V_d) which is approximately 2.0 L/kg. This suggest that the HPOs were disributed extravascularly since the V_d exceeded the total plasma volume in rat (31.6 mL/kg) which is related to their lipophilicity (Bijsterbosch et al., 1981). Similar pattern of pharmacokinetic profile were observed in human when CP20 was ingested orally where the T_{max} was less than 60 minutes and the $t_{1/2}$ was between 1.5 to 2 h after the oral consumption (Hoffbrand, 2005). In addition to the high V_d, the HPOs were also rapidly cleared from the plasma with rate of clearance (C_L) was aprroximately 0.03 L/kg/min which agreed with reported CP20 C_L in rats and humans (Quanquan et al., 2010, Fredenburg et al., 1993, Thuma et al., 1998). Most importantly, novel HPOs level were successfully measured in the brain at 360 minutes post-injection, and the level was not different than CP20. This confirms brain penetration of CP20, CN128 and CN226 observed in *in situ* brain perfusion experiment as discussed in **Chapter 3**.

The most recent study performed by intragastric administration of 1000 µmol/kg CP20 showed a shorter half-life (21 min) (Quanquan et. al., 2010). This observation was expected by the means of the CP20 administration which made it succeptible to the first-pass metabolism in the liver. Indeed, CP20 has been reported to undergo extensive metabolism in the liver to glucuronide conjugate (85% of the administered dose) and rapidly excreted in the urine of man (Hoffbrand et al., 1998, Hoffbrand et al., 2003). The PK profiles in this study is of importance since CN128 was previously reported to have a better efficacy in mobilising iron from the liver in iron-loaded rats after an oral administration due CN128 slower rate of conversion to glucuronide metabolite (2-folds slower) than CP20, and therefore would be expected to show higher C_{max} than CP20 (Lu, 2016, Hider et al., 2011a, Paiboonsukwong et al., 2016). This could be further reflected by higher CN128 oral bioavailability in rats (82%) than CP20 (56%) (Paiboonsukwong et al., 2016, Singh et al., 1992). This contradiction in HPOs level could be explained by the route of administration of HPOs in this study that was by *i.p.* injection. In this circumstance, CP20 and CN128 are readily reaching the systemic circulation after absorption through

the peritoneal tissues lining and rapidly distributed peripherally as showed by its high V_d which is 1.5 L/kg. In contrast, oral administration of CN128 would reaches the liver in the first instance where most of the metabolism occur, before entering the sytemic circulation (Badria et al., 2015). Nevertheless, in this study, CN128 showed a trend towards higher C_{max} than CP20 (p=0.19) which might support the report of slower glucuronides formation in the liver (Lu, 2016, Hider et al., 2011a, Singh et al., 1992).

This study provide a direct evidence of the presence of HPOs in plasma and brain after 500 µmol/kg *i.p.* injection in rats. However, the dose employed in this study is not suitable for the sub-chronic experimental design for *in vivo* neuroprotection study. Furthermore, administration of high dose of HPO in non-systemic iron overlead rats sub-chronically often lead to toxicity due to depletion of systemic iron (Sauerbeck et al., 2013, Mounsey and Teismann, 2012). Neuroprotection study for CP20 performed by Dexter et al. (2011) used a lower dose of CP20 (70 µmol/kg) in *in vivo* PD model of rat in contrast to 600 µmol/kg CP20 for iron-mobilisation study in iron-overload rat model (Crowe and Morgan, 1994). In his study, a unilateral 6-OHDA rat model of PD were treated with CP20 at 70 µmol/kg twice daily for 5 days. The treatment regime started a day before lesion and the study managed to show significant neuroprotection as assessed by TH^+ cell counting in SNPc and dopamine level in sriatum (Dexter et al., 2011). Based on this reported study, the same dose regiment was emplyoed for assesment of novel HPO neuroprotection *in vivo*.

5.4.2 *Effect of unilateral partial 6-OHDA-lesioned on D-amphetamine induced rotation*

The current study showed that the D-amphetamine rotation test failed to cause significant different in rotational activity on the unilateral partial 6-OHDA-lesioned rats compared to sham-lesioned rats. This finding replicated the data presented in **Section 2.5.5** whereby intra-striatal injection with 4 µg, 8 µg or 12 µg 6-OHDA were not significantly differed in rotational behaviour compared to sham-lesioned rats. Similarly, treatment with CP20 or CN128 also did not cause different in the rotation induced by D-amphetamine when compared to control.

Amphetamine-induced rotations have previously been shown to correlate with the size of 6-OHDA-lesion (Carmen et al., 1991, Przedborski et al., 1995, Kirik et al., 1998), however,

there is a threshold for induction of behavioural impairment. Amphetamine-induced rotation start to show in rats with 40-50% reduction in total striatal DA content, and 30-50% loss of TH cell bodies (Hefti et al., 1980; Lee et al., 1996; Przedborski et al., 1995). In the present study, there was approximately 60% loss of striatal DA content and 50% loss of the number of nigral dopamine cell bodies, so one might expect to see some rotational activity. However, the number of TH^+ cells was only counted in one level of the SNPc, and the degree of cell loss may be less in more rostral and caudal areas, allowing compensation for the lesion. In addition, the degree of cell loss may be on the cusp of allowing rotations to be observed, with ipsilateral postsynaptic receptor changes balancing the contralateral DA release induced by amphetamine (Carmen et. al., 1991). Indeed, in agreement with the present study, the lack of significant rotational activity in partial-lesioned compared to sham-lesioned rats has been previously reported (Robinson et al., 1994). On the other hand, the site of the striatum where the profound lesion occurred may also contributed to the absence of asymmetrical rotational behaviour in this study. Olds et al. (2006) demonstrated that cell loss at the lateral portion of striatum lead to profound asymmetrical rotation in contrast to cell loss at the central and/or medial portion of striatum which showed very low asymmetrical rotations in rats after D-amphetamine injection. In the present study, striatum immuno-stained for TH showed profound dopaminergic fibre loss in the central portion of the striatum which correspond to the site where the syringe was lowered during 6-OHDA infusion (**Figure 2.4.8, *top panel*** in **Section 2.4.9**). Therefore, it seems inappropriate to use the amphetamine rotation test as an indication of lesion size and hence protection induced by the HPOs in the current study. Other spontaneous behavioural test that evaluate locomotor activities such as cylinder and rotarod tests could be explored to give insight on the effect of 6-OHDA lesion and treatment with HPOs (Carvalho et al., 2013, Decressac et al., 2012), however, these too require lesions of >50% (Kirik et al., 1998). Overall, it can be concluded that the size and site of 6-OHDA lesioned in the striatum are important for D-amphetamine rotation behavioural read-out to be consistently observed.

As there was clearly loss of dopamine cell bodies and striatal dopamine levels in the 6-OHDA-lesioned rats, it is apparent that no conclusion about the protective nature for CP128 or CP20 can be made from these data. It may be that the behavioural studies were performed before the full extent of the lesion had developed, or that the compensatory mechanisms such as increased dopamine turnover in the striatum had developed that

were sufficient to overcome the partial 64% lesion induced in these studies (Marinova-Mutafchieva et al., 2009).

5.4.3 *Effect of CP20 and CN128 on 6-OHDA-induced alterations of dopamine and serotonin levels in striatum*

Despite the fact that the D-amphetamine-induced rotation study failed to show a difference in 6-OHDA lesioned compared to sham-lesioned rats, 6-OHDA (8 µg) injected into the ipsilateral striatum caused depletion of dopamine level by 64% of control which suggest degeneration and loss of axonal projection of dopaminergic neurons in the striatum that originates from SNPc (Haber et al., 2000, Wall et al., 2013, Reynolds and Wickens, 2000). The observed depletion level of dopamine in ipsilateral striatum was consistent with previous studies targeting partial lesion and correspond to the early phase of PD (Zigmond et al., 1989, Walker et al., 2013, Branchi et al., 2010). Similarly, serotonin level in the ipsilateral striatum was also depleted although milder (33%) than dopamine depletion which was expected due to direct injection of 6-OHDA into the striatum would also killed the serotonergic terminals by oxidative stress (Smith and Cass, 2007). However, close inspection on the level of serotonin showed no significant different when ipsilateral sides were compared. This is further supported by lack of different in serotonin turnover between ipsilateral and contralateral sides in 6-OHDA-lesioned group. Therefore, the effect of CP20 and CN128 on the level of serotonin in the striatum were inconclusive and may require additional experimental data for confirmation. Nevertheless, higher turnover rate of dopamine in the ipsilateral striatum compared to sham-lesioned suggesting increased in activity of the remaining dopaminergic terminals to synthesis dopamine in order to compensate for dopamine loss after 6-OHDA lesioned (Meiser et al., 2013, Robinson et al., 1994).

Treatment with CP20 and CN128 had no effect on the basal level of dopamine and serotonin suggesting that the rate limiting enzyme in dopamine (tyrosine hydroxylase, TH) and serotonin (tryptophan hydroxylase, TPH) were not affected. This is important since iron is an important co-factor for those enzymes and inhibition of these enzymes would exacerbate rather than improve the symptoms of PD (Zhou et al., 2005, Daubner et al., 2011). Indeed, previous report showed that measurement of dopamine and serotonin with their metabolites 2 h after 70 µmol/kg *i.p.* injection of CP20 in rats revealed no changed except for HVA and 5-HIAA that reduced approximately by 40 and 20% respectively, which

returned to control level within 6 h after injection (Waldmeier et al., 1993). As hypothesized, intraperitoneal injection of CP20 and CN128 protected against 6-OHDA-induced depletion of dopamine by approximately 30% compared to dopamine content in saline/6-OHDA-lesioned rats which agreed with a finding reported by Dexter et al. (2011). In addition, CP20 and CN128 fully protected against the reduction in serotonin level induced by 6-OHDA probably because a smaller density of striatal serotonergic compared to dopaminergic terminals (Zhou et al., 2005). Although CP20 and CN128 did not fully prevent dopamine level depletion to the level as in sham-lesioned rats, the dopamine turnover was not significantly different than the sham-lesioned rat which might suggest that functionally the dopamine neurons were normal. Thus, the lesion threshold for an increase in activity of the remaining neurons was not reached due to the smaller level of dopamine loss which, therefore, did not interfere with the normal function of the nigro-striatal pathway (Dexter et al., 2011, Robinson et al., 1994). Intraperitoneal injection of other novel iron chelator, VK28 also showed protection against 6-OHDA-induce dopamine reduction in striatum, although it did not maintain the dopamine turnover at the control level (Shachar et al., 2004).

5.4.4 *Effect of CP20 and CN128 on 6-OHDA-induced dopaminergic cell loss in SNPc*

Depletion of dopamine after 6-OHDA intra-striatal injection was accompanied by a moderate 46% reduction in TH^+ cell in the SNPc compared to control as would be expected for targeting partial lesion (Penttinen et al., 2016, Rodrigues et al., 2003). Although 6-OHDA doses less than 8 µg can also create a partial lesion, this is less recommended as the variation in lesion size was higher with smaller amount of 6-OHDA (Duty and Jenner, 2011). On the other hand, intra-striatal injection of 6-OHDA exceeding 10 µg has been reported to non-specifically causing tissue damaged and striatal cell loss around the lesion site (Bjorklund et al., 1997, Przedborski et al., 1995). The lower percentage of TH^+ cell loss in SNPc agrees with the higher percentage of dopamine depletion in the striatum as reported by Debeir et al. (2005) and Penttinen et al. (2016). This is because, intra-striatal injection of 6-OHDA causes immediate degeneration of dopaminergic terminals in proximity to injection site by extracellular production of ROS (Ferger et al., 2001, Debeir et al., 2005). Some 6-OHDA was taken up by the surviving axon terminal through DAT and followed by slower retrograde loss of dopaminergic cell bodies through a combination of oxidative stress and inhibition of mitochondrial respiratory chain within a week after

lesion (Lu et al., 2014, Rodriguez-Pallares et al., 2007). Furthermore, the observed TH^+ cell loss was prominent in the dorsal tier of the SNPc which correspond to the nigro-striatal dopaminergic projection which supports the retrograde degeneration mechanism of 6-OHDA through interaction with DAT transporter (Storch et al., 2004). This observation confirmed that the axons of neuronal cell bodies in SNPc are terminated in the striatum (Reynolds and Wickens, 2000). The delayed loss of dopaminergic cell bodies mimics the dying back theory of PD pathogenesis and allow a therapeutic intervention well suited for a neuroprotection study with CP20 and CN128 (Tagliaferro and Burke, 2016, Dauer and Przedborski, 2003). Additionally, 6-OHDA-lesioned rats exhibited increased in iron level in striatum and SNPc which is relevant to investigate the neuroprotective effect using iron chelator (Wang et al., 2004, Virel et al., 2014b). To support this further, HPOs showed better neuroprotection in 6-OHDA-induced SH-SY5Y cell death compared to other type of toxins which suggest part if not full, involvement of iron in causing cell death as discussed in detail in **Chapter 4**.

CP20 and CN128 have been shown to enter the brain as measured by *in situ* brain perfusion and systemic *i.p.* injection. In contrast to the observe milder effect of CP20 and CN128 in preventing reduction of dopamine level in the striatum, CP20 and CN128 fully protected against the loss of dopaminergic cell bodies in SNPc which agreed with previous study using CP20 (Dexter et al., 2011, Zhu et al., 2017a). It could be that higher concentration of 6-OHDA at the injection site and surrounding tissues prevented the action of CP20 and CN128 in reducing oxidative stress in the striatum. On the other hand, delayed retrograde axonal degeneration of dopaminergic neurons and distance from the injection site allow sufficient period for CP20 and CN128 to protect dopaminergic neurons in the SNPc. The ability of CP20 and CN128 to protect against 6-OHDA neurodegeneration was more likely by the iron chelation itself. Furthermore, oxidative stress after 6-OHDA or MPTP administration has been shown to increase iron level in basal ganglia (Virel et al., 2014a, Hall et al., 1992, He et al., 1996). However, the processes by which 6-OHDA causes iron accumulation in the basal ganglia is not conclusive and may involve multiple mechanisms such as release of iron from intracellular iron storage protein, ferritin (Jameson et al., 2004) and up regulation of the divalent metal transporter (DMT1) that translocate sequestered vesicular iron into cytoplasm as free-labile iron (Jia et al., 2015, Jiang et al., 2010). Additionally, intracerebral injection of 6-OHDA may disturbed the BBB integrity due to the invasive nature of the lesioned

procedure causing leakage of plasma iron that are normally transported into the brain by transferrin receptor (TfR) (Bien-Ly et al., 2014). This view is supported by Walker et al. (2013) who demonstrated brain oedema associated with deposition of iron along the needle path after intra-striatal injection of 6-OHDA in rats. Moreover, oxidative-stress causes by 6-OHDA could also make BBB more permeable to iron by microglial activation (Virel et al., 2014a, Zhu et al., 2017b). Free non-chelated irons are neurotoxic due to their contribution in exacerbating oxidative stress (Friedman, 2011). Indeed, free irons have been shown to cause brain inflammation by activation of NFkB, IL6 and TNF-α which can be prevented by iron-chelating drugs such as DFO, (−)-epigallocatechin-3-gallate (EGCG) and R-apomorphine (Li et al., 2016, Levites et al., 2001, Youdim et al., 2000, Grunblatt et al., 2001). To further support the involvement of iron in neurodegenerative mechanism, mice on restricted-iron diet were more resistance towards MPP^+ toxicity and did not exhibit impaired in motor behaviour after MPTP treatment (Levenson et al., 2004).

In theory, therefore, HPOs such as CP20 and CN128 could conferred neuroprotection by two mechanisms. First is by direct chelation of labile-iron pool thus minimised one of the reactants needed for Fenton reaction (Devanur et al., 2008b). Secondly is by mobilising intracellular chelated iron to systemic circulation. This is because, a completely chelated iron by bidentante iron chelators such as CP20 and CN128 has a net zero charge and therefore are membrane permeable (Hider et al., 1990, Paiboonsukwong et al., 2016). Furthermore, chelated-iron in systemic circulation are readily transferred to circulating apo-transferrin due to relatively lower pFe^{3+} of CP20 and CN128 compared to transferrin (Hider et al., 1990, Devanur et al., 2008a). Indeed, the most recent report evaluating CP20 neuroprotection revealed almost 60% reduction of ferric iron deposits in the SNPc of 6-OHDA-lesioned rats (Levenson et al., 2004).

5.4.5 *Advantages and shortcomings of this study*

Testing neuroprotection agents in living animals may provide a better approximation of the pharmacological and physiological processes occur in humans than testing in *in vitro* cell lines. Over the years, several *in vivo* models of PD have been developed in laboratories to cater for the increasing needs for evaluation and discovery of the first functional and effective neuroprotection agent in clinic (Tieu, 2011, Duty and Jenner, 2011). Although none of the *in vivo* PD models reflects all the pathologies and symptoms of PD in man, these models play an important role for pre-clinical evaluation of potential treatment for

PD. Indeed, *in vivo* models of PD have successfully offered insights into the understanding of the cell death processes, aetiology, pathology as well as molecular mechanisms of neurodegeneration (Blesa et al., 2012). The decision of which *in vivo* PD models to choose is normally based on the type of investigation required. Here, the 6-OHDA rat model was chosen since 6-OHDA has been shown to promote abnormal iron accumulation in the basal ganglia which exacerbate oxidative stress by iron participation in Fenton reaction (Zhu et al., 2017, Virel et al., 2014, Wang et al., 2015). Indeed, elevated iron levels in the basal ganglia is one of the known pathological signs of PD brain (Mochizuki and Yasuda, 2012). Therefore, this model would be relevant to evaluate the effect of HPO iron chelators in preventing loss of dopaminergic neurons in the basal ganglia. Additionally, *in vitro* neuroprotection study in **Chapter 4** showed the neuroprotective effect of HPOs in reducing 6-OHDA-induced cell death. The pathological events associated with 6-OHDA *in vivo* PD model mirror some of PD pathology in human such as mitochondrial impairment, increase in ROS level, increase in inflammatory markers, reduce striatal dopamine level, reduce TH protein expression and reduce of antioxidant enzymes level (Duty and Jenner, 2011). These pathological markers are highly reproducible in different species and laboratories (Duty and Jenner, 2011). Most importantly, this model allows assessment of degenerated dopaminergic neurons by behavioural observation, quantification of neurotransmitter level and immunostaining of dopaminergic markers as described in this chapter.

Unilateral injection of 6-OHDA into the striatum was preferred in this study to create a partial lesioned associated with gradual loss of dopaminergic neurons over a period of weeks (~50% cell death) (Marinova-Mutafchieva et al., 2009, Moon et al., 2010). Less severe and progressive cell loss in this model represent a better approximate of the early stage and slow development of PD in humans. This provide a window of opportunity where administration of HPOs would be effective to confer neuroprotection. Injection of 6-OHDA into other sites of the nigro-striatal tract such SNPc or MFB to create partial lesioned is much difficult to construct due to smaller target area and therefore is easily off-target (Duty and Jenner, 2011). Additionally, injection into these areas cause extensive loss of dopaminergic neurons. Indeed, SNPc and MFB targeted lesioned is most often used to create full lesioned (>70% cell death) which is more appropriate for symptomatic study of PD (Duty and Jenner, 2011).

Despite all the advantages described above, 6-OHDA PD model unfortunately does not offer the full spectrum of PD pathology as in man. Lewy body primarily consist of α-synuclein which serve as pathological hallmark in PD brain is absent (Bezard et al., 2013). Furthermore, neurodegeneration observed in 6-OHDA model is only restricted to the nigrostriatal tract and not in other part of the brain which are greatly affected in actual PD (Simola et al., 2007, Braak et al., 2003). Indeed, post-mortem studies on PD brain revealed that Lewy body accumulated in stages outside basal ganglia, and thus affected other part of the brain prior to the basal ganglia (Braak et al., 2003). In this sense, the neuroprotection seen in 6-OHDA PD model does not capture this stage of disease development and progression which might be important for early intervention or providing clue to the mechanism of neurodegeneration. Recent advances in PD model reveals that rats injected with proteasomes inhibitors exhibited neuronal loss in the locus coeruleus, dorsal motor nucleus of the vagus and nucleus basalis of Meynert which is associated with protein inclusion similar to Lewy body pathology (McNaught et al., 2004, Bentea et al., 2016). However, this model is not properly validated and is difficult to reproduce (Kordower et al., 2006, Cook and Petrucelli, 2009). Hence, it might take several more years before construction of this model is refined and validated to be advantageous for a better model of PD.

The 6-OHDA model is relatively more difficult to construct which requires stereotaxic surgical skills in contrast to MPTP which can be administered by systemic injections (Jackson-Lewis and Przedborski, 2007). This is because, 6-OHDA does not cross the BBB and therefore requires precise intracerebral injection. Implication from this invasive technique is that the BBB integrity may be compromised due to damage cause by the inserted needle. PD brain is associated with accumulation of iron in the basal ganglia and this is replicated in 6-OHDA model. It has been shown that misregulation of iron transport and BBB breakdown occur as results of oxidative stress and inflammation induced by 6-OHDA (Carvey et al., 2005). However, a study revealed higher level of iron accumulated around the needle tract of 6-OHDA injection site in the striatum due to physical damage in addition to iron misregulation (Virel et al., 2014). Because of this, HPOs iron chelators may not be as effective in preventing cell death in the striatum compared to other area distance unaffected by the physical BBB damage such as SNPC. This suggest that inaccurate results could be obtained in this type of model such as underestimation of neuroprotection. An alternative model that could be used in this study to overcome this limitation is by using

MPTP-mice model of PD. Like 6-OHDA, MPTP-treated mice also show abnormal iron accumulation in the basal ganglia due to iron misregulation (You et al., 2015, Mandel et al., 2004). Indeed, this model has been successfully employed to show the neuroprotective effect of CP20 (Devos et al., 2014).

The motor behaviour of unilateral partial-lesioned is less robust than unilateral full-lesioned of 6-OHDA model as described in **Chapter 2** and **Chapter 5**. Due to less reliable behaviour readout in unilateral partial 6-OHDA-lesioned, a slightly different approach could be taken in the current study. Bilateral partial 6-OHDA-lesioned offers additional brain samples for different purpose that might be advantageous in the current study (Roedter et al., 2001). For example, halves hemisphere could be dedicated for immunostaining and other halves could be used for biochemical analysis for both striatum and SNPc. This approach would generate and provide more comprehensive and valuable data from just a single treatment group. Furthermore, the bilateral degeneration of the nigro-striatal tract is more reflective of that seen in PD. On the negative side, this model would take more time to construct and additional sham-lesioned groups for the studied compounds.

Even though intrastriatal 6-OHDA-lesioned provides a reproducible model of nigrostriatal degeneration, there is still variability in the extent of the lesion depending on the striatal co-ordinate and amount injected (Duty and Jenner, 2011). Interestingly, even different size of needle employed (26 vs 30G) to create lesion following an exact protocol also lead to a significant variation in lesion size (Penttinen et al., 2016). Most recently, Penttinen et al. (2016) had evaluated and classified the neurodegeneration after 6-OHDA lesioned at various co-ordinate into progressive, stable and regressive based on behavioural observation for up to 14 weeks following striatal lesion. This study provides an excellent guidance for the selection of co-ordinate for striatum that best represent PD progression in human. In this sense, co-ordinate for striatum that lead to progressive neurodegeneration shown in this study is of interest.

In conclusion, none of the toxin induced neurodegeneration model able to recapitulate all features of PD in human. Proteasome-inhibition model appeared to have more complete features of PD, however this model is hard to reproduce and therefore its validity is questioned (Cook and Petrucelli, 2009). In the absence of a perfect PD model, the 6-

OHDA-lesioned rat model seem to be adequate for early *in vivo* assessment of HPOs iron chelator neuroprotection.

5.4.6 *Conclusion*

Based on the data obtained, CP20 and CN128 showed a comparable pharmacokinetics profile after a single *i.p.* injection. D-amphetamine rotation test failed to show any different to control group which include the 6-OHDA-lesioned rats. Nevertheless, CP20 and CN128 managed to prevent the dopamine level depletion in rat striatal tissues by approximately 30%. This was further supported by prevention of nigral cell death assessed in SNPc. Therefore, it can be concluded that CP20 and CN128 were neuroprotective against 6-OHDA-induced nigrostriatal degeneration as shown by unaltered dopamine and serotonin turnovers and prevention of dopaminergic cell loss in SNPc. The protection against dopamine depletion seen after treatment with iron chelators might suggest a potential disease modifying effect due to the iron chelation. Indeed, focal administration of deferasirox (DFX), a tridentate iron chelator and deferioxamine (DFO), a hexadentate iron chelator into a striatum of 6-OHDA lesioned rats abolished the production of hydroxyl radicals by Fenton reaction as measured by microdialysis (Dexter et al., 2011). Additionally, CP20 also has been shown to diminish $OH^{\bullet}$ radical production in the presence of iron and H_2O_2 *in vitro* (Devanur et al., 2008b). Therefore, the mechanism of neuroprotection was likely by the iron chelating property of CP20 and CN128.

CHAPTER 6

GENERAL DISCUSSION

6 General Discussion

6.1 *Thesis hypothesis and aims*

Accumulating lines of evidence have demonstrated the neuroprotective ability of iron chelators in PD (Kaur et al., 2003, Youdim et al., 2004, Zheng et al., 2005, Ben-Shachar et al., 1991, Xu et al., 2008, Avramovich-Tirosh et al., 2007, Dexter et al., 2011, Devos et al., 2014, Martin-Bastida et al., 2017, Wang et al., 2017, Gotsbacher et al., 2017). Specifically, CP20, an orally active HPO bidentate iron chelator, has undergone early stage clinical trials showing promising results (Devos et al., 2014, Martin-Bastida et al., 2017). However, the associated neutropenia and agranulocytosis of CP20 treatment reported in 15% of the recruited PD patients could limit it usage in a wider population (Devos et al., 2014). In order to address this problem, several HPO analogues (CN compounds) have been developed based on the chemical structure of CP20 in order to retain their iron binding ability (Hider et al., 2011). In addition, a glycosylated HPO together with the parent HPO were also developed to target the GLUT transporter at BBB (Roy et al., 2010). Acute studies in mice revealed that the toxicity for these novel HPOs (CN compounds) were lower than CP20 (Hider et al., 2011). As CP20 has been shown to cross the BBB and neuroprotective in animals and humans, it was hypothesised that the novel HPO iron chelators based on the CP20 structure and glycosylated HPO are able to cross the BBB and show neuroprotection in PD. Consequently, the aims of the studies described in this thesis were to investigate the brain permeability of novel HPOs in rats and their neuroprotection ability in *in vitro* and *in vivo* model of PD. Data obtained from the current studies revealed that the novel HPOs can cross the BBB as long as there is a balance between intermolecular hydrogen bond and lipophilicity as well as recognition by transport system at BBB. Modification of CP20 structure for brain permeable HPOs did not eliminate the neuroprotection capability as seen in *in vitro* and *in vivo* neuroprotection studies as the affinity towards iron (pFe^{3+}) is only slightly altered as well as maintaining permeation across biological membranes and barrier.

6.2 *Summary of the findings*

The present study examined the brain permeability of novel HPOs in rats. Additionally, the effect of the novel HPOs on toxin-induced cell death in SH-SY5Y cell line and rats were evaluated. The following results were obtained in the individual studies:

a) Rate of brain penetration for three novel HPOs (CN128, CN226 and CN228) were comparable to CP20 in rats. CP84 showed higher brain uptake while CN116, CN118 and CN126 showed lower brain uptake than CP20. In contrast, glycosylated HPO (FCF132) failed to get into the brain.

b) Novel HPOs showed different degrees of neuroprotection in toxins-induced SH-SY5Y cell death with the best neuroprotection observed in 6-OHDA-induced cell death while no protection was observed in MG132-induced cell death.

c) Chirality in the chemical structures of novel HPOs neither contributed to the differences in brain uptake in rats nor in *in vitro* neuroprotection study with SH-SY5Y cell lines.

d) Selected HPOs (CP20, CN128 and CN226) did not show any signs of acute toxicity in rats when injected *i.p.* at 500 µmol/kg dose, while CP84 was toxic at 200 and 500 µmol/kg doses.

e) CP20 and CN128 prevented the toxin-induced neuron cell loss in the nigrostriatal dopamine pathway in 6-OHDA-lesioned rats.

In conclusion, these studies showed that the novel HPOs developed based on the chemical structure of CP20 were able to cross the blood brain barrier in rats. However, attachment of glucose moiety to CP84 (FCF132) was counter-productive and prevented brain uptake. Additionally, novel HPOs conferred neuroprotection in H_2O_2, 6-OHDA and/or FeNTA-induced cell death but not in MG132-induced cell death *in vitro*. CN128 was further evaluated for neuroprotection in 6-OHDA PD model and replicated the neuroprotection observed in *in vitro* study. This confirms that iron plays a role in degenerative process of dopaminergic neurons and that targeting free labile-iron pool (LIP) in brain using the novel iron chelators might be neuroprotective against progressive dopaminergic cell loss in PD.

6.3 *Did the modifications of the chemical structure of CP20 permit BBB permeability and show neuroprotection?*

The primary motivation for alteration of CP20 chemical structure by adding extra functional group was to make the novel HPOs more resistance to metabolism in the liver especially from glucuronidation after oral ingestion, hence increase their bioavailability and lower oral dose could be possible (Hider et al., 2011, Hider et al., 1990, Singh et al., 1992, Singh et al., 1996). Additionally, the novel HPOs were designed to preserve the oxygen ligands on the molecule that are important to chelate iron and therefore the affinity towards iron determined by potentiometric measurements are within the same range as CP20 (Kong et al., 2006). The bioavailability, toxicity and efficacy of novel HPOs have been evaluated in rodents and primates in the previous studies (Paiboonsukwong et al., 2016, Hider et al., 2011, Lu, 2016). Novel HPOs that showed good oral bioavailability as assessed by iron excretion efficiency in iron overloaded rat were taken forward for evaluation of brain permeability in this study with the aim to develop as a neuroprotection agent in PD. This is because, changing the chemical structure also changed the physicochemical properties such as lipophilicity, molecular size and hydrogen bond formation with surrounding water which could affect BBB permeability and therefore the extend of iron chelation in the brain that is important for neuroprotection (Mikitsh and Chacko, 2014).

6.3.1 *Brain permeability of novel HPOs*

The current study showed that the physicochemical properties play a role in brain permeability of HPOs that crossed the BBB via membrane diffusion. The total polar surface area (TPSA) for HPOs which indicate the propensity to form hydrogen bonds appears to show a better relationship with brain uptake compare to lipophilicity (cLogP, **Chapter 3**). Hence, a general increase in lipophilicity of novel HPOs does not necessarily guarantee a proportional increase in rate of brain permeability when compare to CP20 as one might expect (Hider et al., 2011, Liu et al., 2011, Habgood et al., 2000, Habgood et al., 1999). This observation is supported by recent finding that showed brain permeability for CNS drugs used in clinics are primarily dictate by their intermolecular hydrogen bond rather than lipophilicity (Frieden et al., 2009, Chen et al., 2011). Nevertheless, it seems that as the lipophilicity increases, it does helps to counter the effect of increase hydrogen bonding between novel HPOs and surrounding water so that the rate of brain permeability

was not different than CP20. This is obvious among the CN compounds which have higher but constant TPSA than CP20 in addition to increasing lipophilicity.

In addition, functional group that is recognised by endogenous transport systems may improve or deter brain uptake as seen for CP84 and FCF132 respectively. It was revealed that CP84 not only crossed the BBB via membrane diffusion but is also a substrate for large amino acid transporter (LAT) which enhance the rate of brain uptake. Several CNS drugs used LAT to cross the BBB which include L-DOPA (antiparkinsonian), melphalan (anticancer) and gabapentin (anticonvulsant). Indeed, the LAT appear more versatile in accommodating pseudo-nutrients and drug conjugates when compare to GLUT (Pavan et al., 2008, Yang et al., 2001). Although targeting LAT as means to deliver HPOs to the brain in PD sounds promising, it would pose another challenge. This is due to the fact that L-DOPA, the primary drug for the treatment of PD is also a substrate for LAT (del Amo et al., 2008, Geier et al., 2013). It is not a good idea to co-administer drugs that target the same transporters to treat PD as drugs that target LAT1 would require dose adjustment due to competition between drugs for the transport binding site (Bitner et al., 2015, Jost and Bruck, 2002). Dose increment of L-DOPA, for example, could lead to unpredictable levels of the drug in plasma and brain and thus increase the risk of severe adverse effects such as peripheral cardiovascular and gastrointestinal symptoms, and central motor and non-motor side effects (eg dyskinesias, insomnia, hallucinations and psychosis) (Foster and Hoffer, 2004, Barbeau, 1976). In contrast to CP84, FCF132, a glucose conjugated form of CP84 was specifically designed to target GLUT but failed to cross the BBB. FCF132 lost membrane diffusion capacity due to decrease in lipophilicity and increase molecular weight after conjugation with glucose. Additionally, the conjugated glucose did not in any way facilitated brain uptake of FCF132. It is apparent from this and other studies targeting the glucose transporter (GLUT) at BBB that is not the best option due to several reasons. Firstly, glucose recognition site in GLUT1 at BBB is very restrictive and therefore only allow conjugation of HPOs at C2 and C6 for substrate recognition (Mueckler and Thorens, 2013, Mueckler and Makepeace, 2009, Carruthers et al., 2009). Several attempts using various synthetic method to conjugate HPO at C6 of glucose molecule have failed to yield HPO 6-glycoconjugate (Fuchs, 2015). Secondly, glucose is exclusively served as the energy source at BBB and brain under normal physiologically condition which explain the high affinity of GLUT1 at BBB (K_m= 1 mM) (Gorovits and Charron, 2003). Under normal physiological concentration of glucose, GLUT1 is always saturated with

glucose which compete with glucose conjugated HPOs which translate into higher concentration of HPO glycol-conjugate in plasma are required for successful brain crossing (Giknis and Clifford, 2008, Subramanian et al., 2013).

6.3.2 *In vitro neuroprotection of brain permeable HPOs*

As various iron chelators including CP20 have been shown to be neuroprotective in *in vitro* and *in vivo* model of PD (Dexter et al., 2011, Forni et al., 2008, Zorzi et al., 2011, Youdim et al., 1999, Shachar et al., 2004, Gal et al., 2005, Zheng et al., 2005, Zhu et al., 2007, Yassin et al., 2000, Kaur et al., 2003, Reznichenko et al., 2010, Leaver et al., 2009, Xu et al., 2008, Xu et al., 2011), these brain penetrant novel HPOs were evaluated for their neuroprotective potential. It was clear from the *in vitro* neuroprotection study with SH-SY5Y cell lines that brain permeable HPOs are neuroprotective towards all the toxins employed except for MG132 which indirectly suggest the involvement of iron in cell death (**Chapter 4**). As explained in **Chapter 1,** iron participates in the Fenton reaction producing highly reactive hydroxyl radical ($OH^{\bullet}$). However, it can be speculated that extensive accumulation of intracellular proteins with multiple signalling routes causes cell death which cannot be prevented by iron chelators alone. This is supported by accumulation of pro-apoptotic signalling protein p53 in dopaminergic cells exposed to MG132 due to decrease degradation by proteasomes system (Lopes et al., 1997, Nair et al., 2006, Dietrich et al., 2003). Genetics silencing of p53 or inhibition of p53 activity however protected against MG132-induced cell death (Lopes et al., 1997, Nair et al., 2006). Besides, it can generally be observed in the current study that the efficacy of novel HPOs positively correlate with lipophilicity and less with iron affinity constant (pFe^{3+}) which might suggest better ability to penetrate SH-SY5Y cell membrane for chelating more iron (Workman et al., 2015).

6.3.3 *Pharmacokinetics of brain permeable HPOs*

Selected novel HPOs (CP84, CN128 and CN226) were administered intraperitoneally (*i.p.*) in rats to confirm the brain distribution seen in *in situ* brain perfusion experiment and to see the pharmacokinetics profile of novel HPOs. Although, novel HPOs were intended for oral consumption, oral administration of crude drugs would require large doses to attain therapeutic concentration in plasma especially for drugs such as CP20 that have very high first-pass effect in the liver (Singh et al., 1992, Bellanti et al., 2014). The requirement for

oral large doses for compound that still unknown to show neuroprotection in animal model of PD is not feasible in term of time and resources for chemical synthesis. Nevertheless, the aim of the current study is to confirm the neuroprotection ability in animal model of PD and not the oral bioavailability which justify the method of HPOs administration by intraperitoneal route. In this study CP84 was neurotoxic through the unknown mechanism(s) in rats as shown by sudden aggressive behaviour and seizure after intraperitoneal injection. However, this was not the case for other novel HPOs. It might be that the massive uptake of CP84 as showed in *in situ* brain perfusion study caused rapid depletion of free iron in the brain and interfere with the activity of essential enzymes. Aldehyde oxidase, an enzyme responsible for serotonin degradation requires iron (Mackler et al., 1979, Mackler et al., 1978) and depletion of iron would increase serotonin level in the brain which has been shown to be associated with seizure (Bidabadi and Mashouf, 2009, Idro et al., 2010, Baf et al., 1994). Interestingly, despite structural alteration, total brain concentration for novel HPOs in rats were not different than CP20. This observation could be due to the high volume of distribution (V_d) which is common for lipophilic HPOs (Bijsterbosch et al., 1981, Quanquan et al., 2010, Fredenburg et al., 1993, Thuma et al., 1998). Furthermore, CN226 was shown to be a substrate for Pgp efflux pump at BBB which might limit brain distribution despite being more lipophilic than CP20 (**Chapter 3**).

6.3.4 *In vivo neuroprotection of brain permeable HPO*

Although three novel HPOs were initially selected, only CN128 was further tested for neuroprotection in 6-OHDA rat model of PD. CP84 was discarded due to toxicity while CN226 PK profile was not different to CP20 in addition to be a substrate for Pgp efflux pump (**Chapters 3 & 5**). In this study, CN128 along with CP20 were shown to be neuroprotective by preventing the depletion of dopamine level in striatum and nigral cell loss in SNPc in 6-OHDA rat model of PD. This finding corroborates the study performed by Dexter et. al. (2010) in which three clinically available iron chelators (deferoxamine, deferasirox and CP20) exhibited neuroprotection in 6-OHDA rat with CP20 being the most potent. The most recent finding also showed remarkable neuroprotection of CP20 in MPTP-mice model (Devos et al., 2014). Indeed, Phase I and II randomised double blinded placebos controlled clinical trial for 6 months to assessed CP20 neuroprotection in early stage PD patients (mean age 65 years old) showed promising results which suggest the applicability of PD models as a tool for selecting promising neuroprotective agents (Martin-

Bastida et al., 2017, Devos et al., 2014a). One major limitation of the current study is that no measurement of labile iron pool (LIP; **Chapter 1**) were performed in *in vitro* and *in vivo* neuroprotection studies, thus the mechanism by which the HPOs elicited their neuroprotective effect is not conclusive (Jiang et al., 2010).

One problem associated with CP20 therapy is the extensive glucuronidation in the liver which in turn require large oral dose to attain therapeutic concentration in plasma (Singh et al., 1992, Bellanti et al., 2014). CP20 is also associated with blood toxicity with agranulocytosis is the prominent one (Elalfy et al., 2012, Tricta et al., 2016). In the aforementioned clinical trials, although the dose given to the PD patients were 3-fold lower than Thalassemia patients, 15% of the recruited PD subjects were dis-continued from the treatment due to agranulocytosis and neutropenia. Furthermore, the incident of agranulocytosis and neutropenia increases with age (Andres et al., 2002, Mohan et al., 2015, Rajagopal, 2005). Therefore, while CP20 could delayed progression of PD, the associated toxicities would limit its used in PD patients which the majority age of onset is over 60 years old (Mourot-Cottet et al., 2016). Interestingly, equimolar dose of CN128 when administered to iron-loaded rodents and primates showed 3-fold better iron excretion suggesting improved oral bioavailability (Hider et al., 2011a, Lu, 2016, Paiboonsukwong et al., 2016). Analysis of glucuronide metabolite for CN128 in rat urine revealed 21-fold less glucuronide compare to CP20 (Paiboonsukwong et al., 2016, Singh et al., 1992). Remarkably, CN128 also exhibited better toxicity profile than CP20 in preventing reduction of leukocytes counts in rats and monkeys (Paiboonsukwong et al., 2016). Higher oral bioavailability and lower rate of glucuronidation in the liver than CP20 in experimental animals provide additional advantage for the development of CN128 as an efficient and less toxic orally active iron chelator for neuroprotection in PD (Paiboonsukwong et al., 2016). However, the data reported in this thesis could not support the improved bioavailability of CN128 compare to CP20 due the route of administration was intraperitoneal and not oral. Nevertheless, current study confirmed equivalent brain permeability and neuroprotective ability of CN128 to CP20 despite structural modification.

6.3.5 *Conclusion*

Taking all things together, structural modification of CP20 still allow brain uptake of novel HPOs except for glucose conjugated HPOs which was not optimally designed for substrate recognition at GLUT. It appears that additional polar group in novel HPOs limit brain

permeability but increasing lipophilicity help to overcome the problem. Novel HPOs showed neuroprotection in in vitro PD models with some showing better protection than CP20. Of these, CP128 was chosen for assessment of in vivo neuroprotection in a rat model of PD. Interestingly the neuroprotection shown by CP128 was similar to that of CP20 despite higher lipophilicity and reported improve bioavailability possibly due to high volume of distribution and route of HPOs administration (*i.p.*) employed in the current study. However, with the lower potential for neutropenia, these studies suggest that this compound may be a candidate for future clinical trials for disease modification on man.

6.4 *PD models to evaluate neuroprotection*

Searching for effective neuroprotection agents in human has proceeded up to this time with little success. MAO-B specific inhibitor selegiline, for example, was previously thought to be the first successful neuroprotective agent in clinic. However, studies in human reveal that the effect of MAO-B inhibitor was primarily symptomatic rather than neuroprotective (LeWitt, 1994, Stocchi and Olanow, 2003, Athauda and Foltynie, 2015). Many factors have been suggested to contribute to this failure such as animal models that do not reflect widespread pathology of PD and poor experimental design in preclinical and clinical research. Consequently, there is a dire need for better animal models that cover overall pathology and symptoms in human PD as well as providing prediction of effective neuroprotective agents for successful translation in clinical trial (Duty and Jenner, 2011). Currently available animal models only impart part of the overall pathology of PD with each model hold certain degree of relevance to answer the research question (Bezard et al., 2013). Most importantly, Lewy body inclusion which serve as the pathological hallmark in autopsied PD brain is absent in all animal models. The finding that Lewy body mainly compose of aggregated α-synuclein leads to creation of transgenic mice that expressed mutant α-synuclein or overexpress wild-type α-synuclein with the propensity to aggregate (Fernagut and Chesselet, 2004, Kurz et al., 2012). Unfortunately, these mice showed mix results in term of relationship between α-synuclein and neuronal death which makes them unreliable and not robust as a model for neuroprotection study.

6.4.1 *Validity of the PD models to study neuroprotective ability of HPOs*

It was suggested that dopaminergic neurons are susceptible to oxidative stress due to metabolism of dopamine by monoamine oxidase (MAO) that produces hydrogen peroxide

(Nicolaus, 2005, Zucca et al., 2017, Gerlach et al., 2003). This condition exacerbates when the capacity of iron storage protein become limited due to accumulation of iron in aging brain. Iron has a central role in generating the highly destructive hydroxyl radical ($OH^{\bullet-}$) which damage biomolecules and initiate neurodegeneration processes as seen in PD (Berg et al., 2001, Medeiros et al., 2016). Furthermore, dopamine could also react with iron to produce dopamine-o-quinones that is also redox active and able to promote α-synuclein aggregation (Bisaglia et al., 2010, Lee et al., 2011). Although the level of iron in the SH-SY5Y cells and rat brain after exposure to toxins was not determined in this study, previous reports revealed that exposure to H2O2, 6-OHDA, MG132 or MPTP increase iron level inside the cells in in vitro and/or in vivo models of PD by modulating expression of protein that regulates iron such as transferrin, transferrin receptor, divalent metal transporter 1 (DMT1), ferroportin and/or ferritin (Dev et al., 2015, Andriopoulos et al., 2007, Wang et al., 2009, Kobayashi et al., 2008, Howitt et al., 2009, Li et al., 2012). In regard to 6-OHDA rat model of PD that was employed in this study, this model is relevant to study the neuroprotective effect of iron chelator such as HPOs since multiple studies have shown iron accumulation in striatum and SNPc in this model which suggest dysregulation of iron (He et al., 1996, Kondoh et al., 2005, Virel et al., 2014). Furthermore, autopsy and radiological studies have reported accumulation of iron in the basal ganglia of PD patients which confirmed the translational characteristic of this model into human (Dexter et al. 1994; Berg 2006; Wypijewska et al. 2010). It has been shown that dysregulation of iron transport and BBB breakdown occur as results of oxidative stress and inflammation induced by 6-OHDA (Carvey et al., 2005). Although 6-OHDA rat model exhibited iron accumulation, but the effect of iron accumulation is only secondary to the 6-OHDA administration. Since, CP20 and/or CN128 treatments in 6-OHDA model and human suggested neuroprotection, a more relevant and applicable PD model for testing HPOs iron chelator would be iron rat model of PD (Devos et al., 2014, Dexter et al., 2011). This iron rat model of PD can be used to evaluate the direct effect of iron chelation as well as dose-response relationship (Junxia et al., 2003).

6.4.2 *Suggestion for improvements in neuroprotection studies*

Bezard et al., (2013) criticised the widely used experimental design for neuroprotection study in animal model of PD. Most often, the putative neuroprotective agent is administered before or during brain lesion. According to the authors, the experimental design fails to represent the actual situation whereby the agent is likely to be administered

in PD patients only when about 50% of neurons had already loss. Proposal for ideal experimental design in pre-clinical research was further suggested. This includes the use of progressive animal model of PD instead of acute model, administration of putative neuroprotective agents after creation of lesion and finally the use of non-human primates to verify the neuroprotection of promising neuroprotection agents (Bezard et al., 2013). The second proposal is only possible when progressive animal models are made available to test neuroprotective agents. For example, 6-OHDA administered intrastriatally as discussed in this thesis cause rapid cell death and treatment with HPOs after creation of lesion would evaluate neurorestorative potential rather than neuroprotection. This justify the approach taken in the current study whereby HPOs were administered *i.p.* two days and within 1h before 6-OHDA lesion so that HPOs reaching the striatum can protect from acute cell death. In addition to these, a better tools and biological markers for early definitive diagnosis of PD in clinic is as equally important as better animal models. PD diagnosis is usually made when the disease has reached a stage where more than 70% of dopaminergic neurons in SNPc had diminished (Lohle and Reichmann, 2010, Schapira, 2009). This stage of PD may be considered too late to observe an effective neuroprotection if there is any. This could be one of the reasons that until now, none of the promising neuroprotective agent tested pre-clinically succeeded in clinical trials, in addition to not having better animal models.

6.5 *Future outlook*

It can be seen from this study that by modifying HPOs chemical structure could lead to no change, enhance or diminish brain uptake independent on the physicochemical properties of the compound, recognition by efflux pump as well as being a substrate for carrier-mediated transporters. Chemical modification of drug requires knowledge in synthetic chemistry and the synthetic route is tailored base on the chemical structures. Chemical modification also needs to take into account the size of the molecule so that the molecular weight not exceeding 400D for good BBB membrane permeability (Hitchcock and Pennington, 2006, Lipinski et al., 2001). Additionally, steric hindrance introduce by the ancillary functional group may prevent substrate recognition when carrier-mediated transporter is targeted (Li et al., 2015). To rationalise the molecular design of novel HPOs to target the BBB, computational modelling should be incorporated during drug development process. This computational approach predicts how molecular changes

affect the free-energy of solvation in which case low free-energy indicates better BBB crossing (Goncalves and Stassen, 2003, Jia et al., 2002). Similarly, computational method can be used to evaluate the likelihood of ligand-transporter interaction for successful drug uptake into the brain (Matsson and Bergström, 2015, Schlessinger et al., 2013).

In respect to method of drug delivery to the brain, brain permeable nanoparticle vesicles such as liposomes, polymersomes and exosomes are recently received much attention (Saraiva et al., 2016). This method avoids the chemical modification of HPOs that has been pharmacologically optimised since the HPOs are incorporated into the brain permeable nanoparticles. Additionally, the nanoparticle can be designed to increase brain uptake by attaching with ligand or antibody for receptor-mediated endocytosis (**Chapter 1**). One ligand of interest which is relevant for iron chelation is transferrin. This transferrin coated nanoparticles with incorporated HPOs could be recognised by transferrin receptors (TfR) that abundantly expressed at BBB (Liu et al., 2006, Ayton et al., 2016). Additionally, the trancytosed transferrin could also chelate and help with iron distribution in addition to incorporated HPOs. One major drawback of this approach is that nanoparticles are not orally stable and hence limits their application if oral route is the method of choice for convenience and compliance among aging PD patients (Pridgen et al., 2015).

It is unclear whether iron chelation only is sufficient to prevent neurodegeneration in PD. It would be likely sufficient if the neurodegeneration is primarily cause by abnormal iron accumulation and not a secondary phenomenon. Since the current clinical diagnosis cannot determine which factors is the main contributors in neurodegeneration of PD, wide spectrum neuroprotection agents with limited side effects is coveted. It would be interesting if drugs could target more than one mechanism apart from iron chelation for disease improvement in PD. Premyslova et al. (2016) has recently reported that a brain-penetrant fluorinated derivative of CP20 modulated multiple genes expression that led to downregulation of inflammation and ROS production and increased cellular antioxidant defence capacity in SH-SY5Y cells. Other researchers have taken an approach by combining an iron chelator with MAO-B inhibitor pharmacophores in a single molecule with promising results (Bar-Am et al., 2015, Gal et al., 2006, Youdim et al., 2005). One potential molecule exenatide, a synthetic glucagon-like-peptide-1 (GLP-1) was shown to affect a wide range of pathological processes in PD which has led some to speculate that this class of agent has the greatest potential to be a successful neuroprotection agent in

human (Athauda and Foltynie, 2015, Bertilsson et al., 2008, Aviles-Olmos et al., 2013). However, although this may sound promising, compound that act on multiple target may exert multiple side effects when introduce into the systemic circulation. Therefore, another area of research that focus on targeted drug delivery to the brain especially to the site where neuroprotection is needed (basal ganglia) is likewise important.

6.5.1 *Suggested further studies*

With respect to the current study, CN128 merits further investigation in order to confirm it neuroprotective effect. The suggested further studies are:

a) Evaluate the neuroprotection of CN128 after oral administration and compare with CP20.

Administration of CN128 in the current study to 6-OHDA rat model of PD was performed through intraperitoneal (i.p.) injection. This route of administration require much less dose than oral route with the aim to confirm the neuroprotection capability of CN128 in comparison with CP20. Data from the current study showed that CN128 was neuroprotective as CP20 after i.p. injection. However, CN128 was designed to resist glucuronidation in the liver better than CP20 after oral consumption (Hider et al., 2011). Supporting data from previous studies showed that CN128 has profound bioavailability than CP20 after oral administration in rodents and primates (Hider et al., 2011, Paiboonsukwong et al., 2016). This would suggest that CN128 which has been confirmed to exhibit neuroprotective capability in this study may show better neuroprotection when administered orally at equimolar dose of CP20 in animal models of PD.

b) Evaluate different doses of CN128 to see if the neuroprotection is dose dependent and to evaluate the limit of toxicity in PD models.

Current study only tests a single dose of CN128 which and therefore the dose-response relationship could not be elucidated. Dose of CN128 at 70 µmol/kg (i.p.) in the current study protected against 6-OHDA induced cell death by 32%. However, it is not known whether this was the maximum neuroprotection possible and whether the neuroprotection was dose-dependent. Additionally, the suggested future study will provide toxicity profiles at different doses by evaluating effect of CN128 on total body iron content and the extend

of inhibition on iron containing biomolecules in comparison to CP20. Supporting data revealed that CN128 is less toxic at equimolar dose in rodents and primates despite much CN128 reaches the blood stream after oral administration, however, the cause of reduce toxicity remains unknown (Paiboonsukwong et al., 2016, Hider et al., 2011).

c) Evaluate the neuroprotection of CN128 in PD models induced by different toxins.

Different toxins have unique mechanisms to induce Parkinson's disease that are associated with iron toxicity. This provide proof, justification and confirmation of the use of iron chelators as neuroprotection agent.

i) **MPTP**

MPTP crosses the BBB and is metabolise by monoamine oxidase B (MAOB) in astrocytes to MPP^+ (Sai et al., 2013). MPP^+ mechanism of toxicity is primarily through inhibition of Complex I of mitochondrial transport chain in dopaminergic neurons which lead to increase concentration of reactive oxygen species (ROS; Marella et al., 2009, Choi et al., 2011). cDNA microarray study in mice model of MPTP also revealed upregulation of cytotoxic cytokines which include IL-1β, IL-6, IL-7 and IL-10 (Mandel et al., 2000, Youdim et al., 2002). These pro-inflammatory mediators have recently been shown to cause iron accumulation in neurons (explain further below in (ii); You et al., 2017). Combination of increase ROS and iron accumulation induce oxidative stress in this model.

ii) **Lipopolysaccharide (LPS)**

LPS induces neuroinflammation and activates microglia to release the pro-inflammatory mediator IL-6 (You et al., 2017, Urrutia et al., 2013). Released IL-6 in turn causes an increase in expression of iron-regulator protein (hepcidin) that inhibit iron transporter (ferroportin) on neuron membranes. This cause accumulation of iron in neuron that involve in oxidative stress and eventually cell death.

Clearly both these models could be used to evaluate the in vivo neuroprotective effect of iron chelators. To increase the predictability of preclinical in vivo assessment, the effect of the iron chelator should be evaluated in a number of models using toxins that induce cell death by different mechanisms of action.

d) Evaluate the effect of CN128 treatment on other neurovascular units such as astrocytes and microglia.

The study reported in this thesis only look at the effect of CN128 on dopaminergic neurons. However, surrounding cells such as astrocytes and microglia are also involved in the pathogenesis of dopaminergic cell death in animal models of PD (Sai et al., 2013, You et al., 2017). Comprehensive understanding on the overall effect of CN128 on these important neurons associated cells will provide in-depth mechanisms on CN128 neuroprotection.

e) Evaluate the effect of CN128 on the brain level of iron and on the expression of iron regulatory proteins.

Previous studies suggested that iron is accumulated in PD brain especially in basal ganglia and contributes to oxidative stress (Hartmann, 2004, Wang et al., 2016). The accumulated iron is likely to be caused by metabolism of dopaminergic neurons and dysregulation of iron transport and storage (Zucca et al., 2017). Indeed, 6-OHDA, LPS and MPTP animal model of PD exhibit accumulation of iron in the basal ganglia which is translated to what occurrs in man (Dev et al., 2015, Andriopoulos et al., 2007, Wang et al., 2009, Kobayashi et al., 2008, Howitt et al., 2009, Li et al., 2012). Current study did not evaluate the effect of CN128 on the level of iron and expression of iron regulatory proteins in the basal ganglia to support the mechanism of neuroprotection observed in PD model, and so this should be addressed in a future study.

f) Assess the inhibitory property of CN128 onto iron containing enzymes especially in the basal ganglia such as tyrosine hydroxylase (TH) and catechol-O-methyl transferase (COMT).

Many of the enzymes in basal ganglia require iron as a co-factor for reaction. In particular, TH is responsible for the hydroxylation of tyrosine to L-DOPA, the precursor for dopamine in dopaminergic neurons (Rausch et al., 1988). Iron is also a co-factor for COMT, the enzyme responsible for dopamine degradation in synaptic cleft (Waldmeier et al., 1993, Bastos et al., 2014). It is important to determine the extent of the inhibition of these enzymes by the iron chelator to give insight into the potential inhibitory effect on dopamine

formation or dopamine metabolism as this could distinguish between neuroprotection and symptomatic improvement in PD models.

6.6 *Final conclusion*

As hypothesised, data from the current study revealed that novel HPO iron chelators based on the CP20 structure can crossed the BBB, except for glucose conjugated HPO which suggest limitation of targeting GLUT at BBB. The brain permeable HPOs also exhibited neuroprotection in SH-SY5Y cell lines and this was confirmed *in vivo* using CN128 as the best representative of the novel HPOs. It is too early to confirm that HPOs iron chelator such as CP20 and CN128 are neuroprotective in human until clinical trials with PD subjects that may take years are completed (Ravina et al., 2003, van der Brug et al., 2015). It is important to highlight again that PD is a multifactorial disease, and until today the exact cause that initiate neurodegeneration in PD brain is unknown (Sheikh et al., 2013, Schlossmacher et al., 2017). Nevertheless, abnormal iron accumulation has been repeatedly observed in the post-mortem brain of PD patients which suggest that iron accumulation could be one of the culprits either primary or secondary to the neurodegeneration and treatment with iron chelators are therefore potentially neuroprotective (Hartmann, 2004, Wang et al., 2016).

REFERENCES

ABBOTT, N. J. 2004. Prediction of blood-brain barrier permeation in drug discovery from in vivo, in vitro and in silico models. *Drug Discov Today Technol,* 1**,** 407-16.

ABBOTT, N. J. 2005. Dynamics of CNS barriers: evolution, differentiation, and modulation. *Cell Mol Neurobiol,* 25**,** 5-23.

ABBOTT, N. J., PANTABENDIGE, A. A. K., DOLMAN, D. E. M., YUSOF, S. R. & BEGLEY, D. J. 2010. Structure and function of the blood-brain barrier. *Neurobiology of Disease,* 37**,** 13-25.

ABBRUZZESE, G., COSSU, G., BALOCCO, M., MARCHESE, R., MURGIA, D., MELIS, M., GALANELLO, R., BARELLA, S., MATTA, G., RUFFINENGO, U., BONUCCELLI, U. & FORNI, G. L. 2011. A pilot trial of deferiprone for neurodegeneration with brain iron accumulation. *Haematologica,* 96**,** 1708-11.

ABRAMOVA, N. A., CASSARINO, D. S., KHAN, S. M., PAINTER, T. W. & BENNETT, J. P. 2002. Inhibition by R(+) or S(–) pramipexole of caspase activation and cell death induced by methylpyridinium ion or beta amyloid peptide in SH-SY5Y neuroblastoma. *Journal of Neuroscience Research,* 67**,** 494-500.

ALEXANDER, G. E. 2004. Biology of Parkinson's disease: pathogenesis and pathophysiology of a multisystem neurodegenerative disorder. *Dialogues in Clinical Neuroscience,* 6**,** 259-280.

ALGREN, D. A. 2010. Review of Oral Iron Chelators (Deferiprone and Deferasirox) for the Treatment of Iron Overload in Pediatric Patients.

AL-REFAIE, F. N., SHEPPARD, L. N., NORTEY, P., WONKE, B. & HOFFBRAND, A. V. 1995. Pharmacokinetics of the oral iron chelator deferiprone (L1) in patients with iron overload. *British Journal of Haematology,* 89**,** 403-408.

ALSHAMMARI, T. M., AL-HASSAN, A. A., HADDA, T. B. & ALJOFAN, M. 2015. Comparison of different serum sample extraction methods and their suitability for mass spectrometry analysis. *Saudi Pharm J,* 23**,** 689-97.

AMIN, M. L. 2013. P-glycoprotein Inhibition for Optimal Drug Delivery. *Drug Target Insights,* 7**,** 27-34.

ANDERSON, B. D. 1996. Prodrugs for improved CNS delivery. *Advanced Drug Delivery Reviews,* 19**,** 171-202.

ANDRES, E., KURTZ, J. E., MARTIN-HUNYADI, C., KALTENBACH, G., ALT, M., WEBER, J. C., SIBILIA, J., SCHLIENGER, J. L., DUFOUR, P. & MALOISEL, F. 2002. Nonchemotherapy drug-induced agranulocytosis in elderly patients: the effects of granulocyte colony-stimulating factor. *Am J Med,* 112**,** 460-4.

ANDRES-MATEOS, E., PERIER, C., ZHANG, L., BLANCHARD-FILLION, B., GRECO, T. M., THOMAS, B., KO, H. S., SASAKI, M., ISCHIROPOULOS, H., PRZEDBORSKI, S., DAWSON, T. M. & DAWSON, V. L. 2007. DJ-1 gene deletion reveals that DJ-1 is an atypical peroxiredoxin-like peroxidase. *Proc Natl Acad Sci U S A,* 104**,** 14807-12.

ANDREW, R., WATSON, D. G., BEST, S. A., MIDGLEY, J. M., WENLONG, H. & PETTY, R. K. H. 1993. The determination of hydroxydopamines and other trace amines in the urine of Parkinsonian patients and normal controls. *Neurochemical Research,* 18**,** 1175-1177.

ANDRIOPOULOS, B., HEGEDUSCH, S., MANGIN, J., RIEDEL, H. D., HEBLING, U., WANG, J., PANTOPOULOS, K. & MUELLER, S. 2007. Sustained hydrogen peroxide induces iron uptake by transferrin receptor-1 independent of the iron regulatory protein/iron-responsive element network. J Biol Chem, 282, 20301-8.

ANGLADE, P., VYAS, S., JAVOY-AGID, F., HERRERO, M. T., MICHEL, P. P., MARQUEZ, J., MOUATT-PRIGENT, A., RUBERG, M., HIRSCH, E. C. & AGID, Y. 1997. Apoptosis and autophagy in nigral neurons of patients with Parkinson's disease. *Histol Histopathol,* 12**,** 25-31.

ANTONY, P. M., DIEDERICH, N. J., KRUGER, R. & BALLING, R. 2013. The hallmarks of Parkinson's disease. *Febs j,* 280**,** 5981-93.

APOPHARMA INC. 2011. *Ferriprox (R) [package insert]* [Online]. Weston, FL: ApoPharma Inc. Available: http://www.accessdata.fda.gov/drugsatfda_docs/label/2011/021825lbl.pdf 2017].

ARIMOTO, T. & BING, G. 2003. Up-regulation of inducible nitric oxide synthase in the substantia nigra by lipopolysaccharide causes microglial activation and neurodegeneration. *Neurobiol Dis,* 12**,** 35-45.

ARMBRUSTER, D. A. & PRY, T. 2008. Limit of blank, limit of detection and limit of quantitation. *Clin Biochem Rev,* 29 Suppl 1**,** S49-52.

ATHAUDA, D. & FOLTYNIE, T. 2015. The ongoing pursuit of neuroprotective therapies in Parkinson disease. *Nat Rev Neurol,* 11**,** 25-40.

AVDEEF, A. & SUN, N. 2011. A new in situ brain perfusion flow correction method for lipophilic drugs based on the pH-dependent Crone-Renkin equation. *Pharm Res,* 28**,** 517-30.

AVDEEF, A. 2001. Physicochemical profiling (solubility, permeability and charge state). *Curr Top Med Chem,* 1**,** 277-351.

AVDEEF, A. 2011. How well can in vitro brain microcapillary endothelial cell models predict rodent in vivo blood-brain barrier permeability? *European Journal of Pharmaceutical Sciences,* 43**,** 109-124.

AVILES-OLMOS, I., DICKSON, J., KEFALOPOULOU, Z., DJAMSHIDIAN, A., ELL, P., SODERLUND, T., WHITTON, P., WYSE, R., ISAACS, T., LEES, A., LIMOUSIN, P. & FOLTYNIE, T. 2013. Exenatide and the treatment of patients with Parkinson's disease. *The Journal of Clinical Investigation,* 123**,** 2730-2736.

AYTON, S., LEI, P., MCLEAN, C., BUSH, A. I. & FINKELSTEIN, D. I. 2016. Transferrin protects against Parkinsonian neurotoxicity and is deficient in Parkinson's substantia nigra. *Signal Transduction And Targeted Therapy,* 1**,** 16015.

BACHER, A. 2005. Effects of body temperature on blood gases. *Intensive Care Med,* 31**,** 24-7.

BADHAN, R. K., CHENEL, M. & PENNY, J. I. 2014. Development of a physiologically-based pharmacokinetic model of the rat central nervous system. *Pharmaceutics,* 6**,** 97-136.

BADRIA, F. A., IBRAHIM, A. S., BADRIA, A. F. & ELMARAKBY, A. A. 2015. Curcumin Attenuates Iron Accumulation and Oxidative Stress in the Liver and Spleen of Chronic Iron-Overloaded Rats. *PLOS ONE,* 10**,** e0134156.

BAF, M. H., SUBHASH, M. N., LAKSHMANA, K. M. & RAO, B. S. 1994. Alterations in monoamine levels in discrete regions of rat brain after chronic administration of carbamazepine. Neurochem Res, 19, 1139-43.

BANKS, W. A. 2009. Characteristics of compounds that cross the blood-brain barrier. *BMC Neurology,* 9(Suppl 1)**,** 1-5.

BANKS, W. A. 2016. From blood-brain barrier to blood-brain interface: new opportunities for CNS drug delivery. *Nat Rev Drug Discov,* 15**,** 275-292.

BAR-AM, O., AMIT, T., KUPERSHMIDT, L., ALUF, Y., MECHLOVICH, D., KABHA, H., DANOVITCH, L., ZURAWSKI, V. R., YOUDIM, M. B. & WEINREB, O. 2015. Neuroprotective and neurorestorative activities of a novel iron chelator-brain selective monoamine oxidase-A/monoamine oxidase-B inhibitor in animal models of Parkinson's disease and aging. *Neurobiol Aging,* 36**,** 1529-42.

BAR-AM, O., WEINREB, O., AMIT, T. & YOUDIM, M. B. 2005. Regulation of Bcl-2 family proteins, neurotrophic factors, and APP processing in the neurorescue activity of propargylamine. *Faseb j,* 19**,** 1899-901.

BARBEAU, A. 1976. Neurological and psychiatric side-effects of L-DOPA. Pharmacology & Therapeutics. Part C: Clinical Pharmacology and Therapeutics, 1, 475-494.

BARNEOUD, P., DESCOMBRIS, E., AUBIN, N. & ABROUS, D. N. 2000. Evaluation of simple and complex sensorimotor behaviours in rats with a partial lesion of the dopaminergic nigrostriatal system. *Eur J Neurosci,* 12**,** 322-36.

BARNETT, J. E., HOLMAN, G. D., CHALKLEY, R. A. & MUNDAY, K. A. 1975. Evidence for two asymmetric conformational states in the human erythrocyte sugar-transport system. *Biochem J,* 145**,** 417-29.

BARTELS, A. L. 2011. Blood-brain barrier P-glycoprotein function in neurodegenerative disease. *Curr Pharm Des,* 17**,** 2771-7.

BASAVARAJ, S. & BETAGERI, G. V. 2014. Can formulation and drug delivery reduce attrition during drug discovery and development—review of feasibility, benefits and challenges. *Acta Pharmaceutica Sinica B,* 4**,** 3-17.

BASTOS, P., ARAUJO, J. R., AZEVEDO, I., MARTINS, M. J. & RIBEIRO, L. 2014. Effect of a natural mineral-rich water on catechol-O-methyltransferase function. Magnes Res, 27, 131-41.

BAUER, H. C., KRIZBAI, I. A., BAUER, H. & TRAWEGER, A. 2014. "You Shall Not Pass"-tight junctions of the blood brain barrier. *Front Neurosci,* 8**,** 392.

BEAL, M. F. 2003. Mitochondria, oxidative damage, and inflammation in Parkinson's disease. *Ann N Y Acad Sci,* 991**,** 120-31.

BEGLEY, D. J. 2004. Delivery of therapeutic agents to the central nervous system: the problems and the possibilities. *Pharmacol Ther,* 104**,** 29-45.

BÉLANGER, M., ALLAMAN, I. & MAGISTRETTI, PIERRE J. 2011. Brain Energy Metabolism: Focus on Astrocyte-Neuron Metabolic Cooperation. *Cell Metabolism,* 14**,** 724-738.

BELLANTI, F., DANHOF, M. & DELLA PASQUA, O. 2014. Population pharmacokinetics of deferiprone in healthy subjects. *British Journal of Clinical Pharmacology,* 78**,** 1397-1406.

BENOIT-BIANCAMANO, M. O., CONNELLY, J., VILLENEUVE, L., CARON, P. & GUILLEMETTE, C. 2009. Deferiprone glucuronidation by human tissues and recombinant UDP glucuronosyltransferase 1A6: an in vitro investigation of genetic and splice variants. *Drug Metab Dispos,* 37**,** 322-9.

BENTEA, E., VERBRUGGEN, L. & MASSIE, A. 2016. The Proteasome Inhibition Model of Parkinson's Disease. *Journal of Parkinson's Disease,* 7**,** 31-63.

BERNHARDT, P. V. 2007. Coordination chemistry and biology of chelators for the treatment of iron overload disorders. *Dalton Transactions***,** 3214-3220.

BERTILSSON, G., PATRONE, C., ZACHRISSON, O., ANDERSSON, A., DANNAEUS, K., HEIDRICH, J., KORTESMAA, J., MERCER, A., NIELSEN, E., RONNHOLM, H. & WIKSTROM, L. 2008. Peptide hormone exendin-4 stimulates subventricular zone neurogenesis in the adult rodent brain and induces recovery in an animal model of Parkinson's disease. *J Neurosci Res,* 86**,** 326-38.

BETARBET, R., SHERER, T. B., MACKENZIE, G., GARCIA-OSUNA, M., PANOV, A. V. & GREENAMYRE, J. T. 2000. Chronic systemic pesticide exposure reproduces features of Parkinson's disease. *Nat Neurosci,* 3**,** 1301-6.

BEZARD, E., YUE, Z., KIRIK, D. & SPILLANTINI, M. G. 2013. Animal Models of Parkinson's Disease: limits and relevance to neuroprotection studies. *Movement disorders : official journal of the Movement Disorder Society,* 28**,** 61-70.

BICKEL, U. 1998. Intravenous Injection/Pharmacokinetics. *In:* PARDRIDGE, W. M. (ed.) *Introduction to the Blood Brain Barrier, .* Cambridge: University Press, Cambridge.

BICKEL, U. 2005. How to measure drug transport across the blood-brain barrier. *NeuroRx,* 2**,** 15-26.

BIDABADI, E. & MASHOUF, M. 2009. Association between iron deficiency anemia and first febrile convulsion: A case–control study. Seizure, 18, 347-351.

BIEN-LY, N., YU, Y. J., BUMBACA, D., ELSTROTT, J., BOSWELL, C. A., ZHANG, Y., LUK, W., LU, Y., DENNIS, M. S., WEIMER, R. M., CHUNG, I. & WATTS, R. J. 2014. Transferrin receptor (TfR) trafficking determines brain uptake of TfR antibody affinity variants. *The Journal of Experimental Medicine,* 211**,** 233-244.

BIJSTERBOSCH, M. K., DUURSMA, A. M., BOUMA, J. M. W. & GRUBER, M. 1981. The plasma volume of the Wistar rat in relation to the body weight. *Experientia,* 37**,** 381-382.

BJORKLUND, A., ROSENBLAD, C., WINKLER, C. & KIRIK, D. 1997. Studies on neuroprotective and regenerative effects of GDNF in a partial lesion model of Parkinson's disease. *Neurobiol Dis,* 4**,** 186-200.

BLESA, J., PHANI, S., JACKSON-LEWIS, V. & PRZEDBORSKI, S. 2012. Classic and new animal models of Parkinson's disease. *J Biomed Biotechnol,* 2012**,** 845618.

BLUM, D., WU, Y., NISSOU, M. F., ARNAUD, S., ALIM LOUIS, B. & VERNA, J. M. 1997. p53 and Bax activation in 6-hydroxydopamine-induced apoptosis in PC12 cells. *Brain Res,* 751**,** 139-42.

BOADO, R. J., LI, J. Y. & PARDRIDGE, W. M. 2004. Developmental regulation of the rabbit blood-brain barrier LAT1 large neutral amino acid transporter mRNA and protein. *Pediatr Res,* 55**,** 557-60.

BOADO, R. J., LI, J. Y., NAGAYA, M., ZHANG, C. & PARDRIDGE, W. M. 1999. Selective expression of the large neutral amino acid transporter at the blood-brain barrier. *Proc Natl Acad Sci U S A,* 96**,** 12079-84.

BOHNERT, T. & GAN, L. S. 2013. Plasma protein binding: from discovery to development. *J Pharm Sci,* 102**,** 2953-94.

BOJE, K. M. 2001. In vivo measurement of blood-brain barrier permeability. *Curr Protoc Neurosci,* Chapter 7**,** Unit 7.19.

BONINA, F., ARENARE, L., IPPOLITO, R., BOATTO, G., BATTAGLIA, G., BRUNO, V. & DE CAPRARIIS, P. 2000. Synthesis, pharmacokinetics and anticonvulsant activity of 7-chlorokynurenic acid prodrugs. *International Journal of Pharmaceutics,* 202**,** 79-88.

BONINA, F., PUGLIA, C., RIMOLI, M. G., MELISI, D., BOATTO, G., NIEDDU, M., CALIGNANO, A., RANA, G. L. & CAPRARIIS, P. D. 2003. Glycosyl Derivatives of Dopamine and L-dopa as Anti-Parkinson Prodrugs: Synthesis, Pharmacological Activity and In Vitro Stability Studies. *Journal of Drug Targeting,* 11**,** 25-36.

BOON, J. Y., DUSONCHET, J., TRENGROVE, C. & WOLOZIN, B. 2014. Interaction of LRRK2 with kinase and GTPase signaling cascades. *Frontiers in Molecular Neuroscience,* 7**,** 64.

BOVÉ, J., PROU, D., PERIER, C. & PRZEDBORSKI, S. 2005. Toxin-Induced Models of Parkinson's Disease. *NeuroRx,* 2**,** 484-494.

BOYD, D., VECOLI, C., BELCHER, D. M., JAIN, S. K. & DRYSDALE, J. W. 1985. Structural and functional relationships of human ferritin H and L chains deduced from cDNA clones. *J Biol Chem,* 260**,** 11755-61.

BRAAK, H., DEL TREDICI, K., RUB, U., DE VOS, R. A., JANSEN STEUR, E. N. & BRAAK, E. 2003. Staging of brain pathology related to sporadic Parkinson's disease. *Neurobiol Aging,* 24**,** 197-211.

BRANCHI, I., D'ANDREA, I., ARMIDA, M., CARNEVALE, D., AJMONE-CAT, M. A., PEZZOLA, A., POTENZA, R. L., MORGESE, M. G., CASSANO, T., MINGHETTI, L., POPOLI, P. & ALLEVA, E. 2010. Striatal 6-OHDA lesion in mice: Investigating early neurochemical changes underlying Parkinson's disease. *Behav Brain Res,* 208**,** 137-43.

BROER, S., SCHNEIDER, H. P., BROER, A., RAHMAN, B., HAMPRECHT, B. & DEITMER, J. W. 1998. Characterization of the monocarboxylate transporter 1 expressed in Xenopus laevis oocytes by changes in cytosolic pH. *Biochem J,* 333 (Pt 1)**,** 167-74.

BUKHATWA, S., IRAVANI, M. M., ZENG, B. Y., COOPER, J. D., ROSE, S. & JENNER, P. 2009. An immunohistochemical and stereological analysis of PSI-induced nigral neuronal degeneration in the rat. *J Neurochem,* 109**,** 52-9.

BUNDGAARD, M. & ABBOTT, N. J. 2008. All vertebrates started out with a glial blood-brain barrier 4-500 million years ago. *Glia,* 56**,** 699-708.

BUNESCU, A., BESSE-HOGGAN, P., SANCELME, M., MAILHOT, G. & DELORT, A. M. 2008. Fate of the nitrilotriacetic acid-Fe(III) complex during photodegradation and biodegradation by Rhodococcus rhodochrous. *Appl Environ Microbiol,* 74**,** 6320-6.

BURROUGHS, S. L., DUNCAN, R. S., RAYUDU, P., KANDULA, P., PAYNE, A. J., CLARK, J. L., KOULEN, P. & KAJA, S. 2012. Plate reader-based assays for measuring cell viability, neuroprotection and calcium in primary neuronal cultures. *Journal of neuroscience methods,* 203**,** 141-145.

CABANTCHIK, Z. I. 2014. Labile iron in cells and body fluids: physiology, pathology, and pharmacology. *Frontiers in Pharmacology,* 5**,** 45.

CACCIATORE, I., FORNASARI, E., BALDASSARRE, L., CORNACCHIA, C., FULLE, S., DI FILIPPO, E., PIETRANGELO, T. & PINNEN, F. 2013. A Potent (R)-alpha-bis-lipoyl Derivative Containing 8-Hydroxyquinoline Scaffold: Synthesis and Biological Evaluation of Its Neuroprotective Capabilities in SH-SY5Y Human Neuroblastoma Cells. *Pharmaceuticals,* 6**,** 54.

CALABRESI, P., PICCONI, B., PARNETTI, L. & DI FILIPPO, M. 2006. A convergent model for cognitive dysfunctions in Parkinson's disease: the critical dopamine-acetylcholine synaptic balance. *Lancet Neurol,* 5**,** 974-83.

CAMPBELL, S. D., REGINA, K. J. & KHARASCH, E. D. 2014. Significance of lipid composition in a blood-brain barrier-mimetic PAMPA assay. *J Biomol Screen,* 19**,** 437-44.

CAPPELLINI, M. D., COHEN, A., ELEFTHERIOU, A., PIGA, A., PORTER, J. & TAHER, A. 2008. *Guidelines for the Clinical Management of Thalassaemia.* 2nd Revised ed. Nicosia (CY).

CAPPELLINI, M. D., PORTER, J., EL-BESHLAWY, A., LI, C.-K., SEYMOUR, J. F., ELALFY, M., GATTERMANN, N., GIRAUDIER, S., LEE, J.-W., CHAN, L. L., LIN, K.-H., ROSE, C., TAHER, A., THEIN, S. L., VIPRAKASIT, V., HABR, D., DOMOKOS, G., ROUBERT, B. & KATTAMIS, A. 2010. Tailoring iron chelation by iron intake and serum ferritin: the prospective EPIC study of deferasirox in 1744 patients with transfusion-dependent anemias. *Haematologica,* 95**,** 557.

CARDOSO, S. M., MOREIRA, P. I., AGOSTINHO, P., PEREIRA, C. & OLIVEIRA, C. R. 2005. Neurodegenerative pathways in Parkinson's disease: therapeutic strategies. *Curr Drug Targets CNS Neurol Disord,* 4**,** 405-19.

CAROSIO, R., ZUCCARI, G., ORIENTI, I., MANGRAVITI, S. & MONTALDO, P. G. 2007. Sodium Ascorbate induces apoptosis in neuroblastoma cell lines by interfering with iron uptake. *Molecular Cancer,* 6**,** 55.

CARRUTHERS, A., DEZUTTER, J., GANGULY, A. & DEVASKAR, S. U. 2009. Will the original glucose transporter isoform please stand up! *American Journal of Physiology-Endocrinology and Metabolism,* 297**,** E836-E848.

CARVEY, P. M., ZHAO, C. H., HENDEY, B., LUM, H., TRACHTENBERG, J., DESAI, B. S., SNYDER, J., ZHU, Y. G. & LING, Z. D. 2005. 6-Hydroxydopamine-induced alterations in blood–brain barrier permeability. *European Journal of Neuroscience,* 22**,** 1158-1168.

CASTANEDA, E., WHISHAW, I. & ROBINSON, T. 1990. Changes in striatal dopamine neurotransmission assessed with microdialysis following recovery from a bilateral 6-OHDA lesion: variation as a function of lesion size. *The Journal of Neuroscience,* 10**,** 1847-1854.

CASTANO, A., HERRERA, A. J., CANO, J. & MACHADO, A. 1998. Lipopolysaccharide intranigral injection induces inflammatory reaction and damage in nigrostriatal dopaminergic system. *J Neurochem,* 70**,** 1584-92.

CASTINO, R., FIORENTINO, I., CAGNIN, M., GIOVIA, A. & ISIDORO, C. 2011. Chelation of lysosomal iron protects dopaminergic SH-SY5Y neuroblastoma cells from hydrogen peroxide toxicity by precluding autophagy and Akt dephosphorylation. *Toxicol Sci,* 123**,** 523-41.

CATER, H. L., BENHAM, C. D. & SUNDSTROM, L. E. 2001. Neuroprotective role of monocarboxylate transport during glucose deprivation in slice cultures of rat hippocampus. *J Physiol,* 531**,** 459-66.

CECI, A., MANGIARINI, L., FELISI, M., BARTOLONI, F., CIANCIO, A., CAPRA, M., D'ASCOLA, D., CIANCIULLI, P. & FILOSA, A. 2011. The management of iron chelation therapy: preliminary data from a national registry of thalassaemic patients. *Anemia,* 2011**,** 435683.

CHAI, C. & LIM, K.-L. 2013. Genetic Insights into Sporadic Parkinson's Disease Pathogenesis. *Current Genomics,* 14**,** 486-501.

CHANG, K. L., PEE, H. N., YANG, S. & HO, P. C. 2015. Influence of drug transporters and stereoselectivity on the brain penetration of pioglitazone as a potential medicine against Alzheimer's disease. *Sci Rep,* 5**,** 9000.

CHAPY, H., SAUBAMEA, B., TOURNIER, N., BOURASSET, F., BEHAR-COHEN, F., DECLEVES, X., SCHERRMANN, J. M. & CISTERNINO, S. 2016. Blood-brain and retinal barriers show dissimilar ABC transporter impacts and concealed effect of P-glycoprotein on a novel verapamil influx carrier. *British Journal of Pharmacology,* 173**,** 497-510.

CHAPY, H., SMIRNOVA, M., ANDRÉ, P., SCHLATTER, J., CHIADMI, F., COURAUD, P.-O., SCHERRMANN, J.-M., DECLÈVES, X. & CISTERNINO, S. 2015. Carrier-Mediated Cocaine Transport at the Blood-Brain Barrier as a Putative Mechanism in Addiction Liability. *International Journal of Neuropsychopharmacology,* 18**,** pyu001.

CHASTON, T. B. & RICHARDSON, D. R. 2003. Iron chelators for the treatment of iron overload disease: relationship between structure, redox activity, and toxicity. *Am J Hematol,* 73**,** 200-10.

CHEN, H., WINIWARTER, S., FRIDEN, M., ANTONSSON, M. & ENGKVIST, O. 2011. In silico prediction of unbound brain-to-plasma concentration ratio using machine learning algorithms. *J Mol Graph Model,* 29**,** 985-95.

CHEN, Q., GONG, T., LIU, J., WANG, X., FU, H. & ZHANG, Z. 2009. Synthesis in vitro and in vivo Characterization of Glycosyl Derivatives of Ibuprofen as Novel Prodrugs for Brain Drug Delivery. *journal of Drug Targeting,* 4**,** 318-328.

CHENG, H.-C., ULANE, C. M. & BURKE, R. E. 2010. Clinical Progression in Parkinson's Disease and the Neurobiology of Axons. *Annals of neurology,* 67**,** 715-725.

CHINACHOTI, P. & STEINBERG, M. P. 1988. Interaction of Sucrose with Gelatin, Egg-Albumin and Gluten in Freeze-Dried Mixtures as Shown by Water Sorption. *Journal of Food Science,* 53**,** 932-&.

CHINNERY, P. F. & HUDSON, G. 2013. Mitochondrial genetics. *British Medical Bulletin,* 106**,** 135-159.

CHINTA, S. J. & ANDERSEN, J. K. 2008. Redox imbalance in Parkinson's disease. *Biochim Biophys Acta,* 1780**,** 1362-7.

CHOI, B. S. & ZHENG, W. 2009. Copper transport to the brain by the blood-brain barrier and blood-CSF barrier. *Brain Res,* 1248**,** 14-21.

CHOI, W. S., PALMITER, R. D. & XIA, Z. 2011. Loss of mitochondrial complex I activity potentiates dopamine neuron death induced by microtubule dysfunction in a Parkinson's disease model. J Cell Biol, 192, 873-82.

CIANCIULLI, P. 2008. Treatment of iron overload in thalassemia. *Pediatr Endocrinol Rev,* 6 Suppl 1**,** 208-13.

CIECHANOVER, A. 1998. The ubiquitin-proteasome pathway: on protein death and cell life. *The EMBO Journal,* 17**,** 7151-7160.

CIPOLLA, M. J. 2009. The Cerebral Circulation. *Integrated Systems Physiology: From Molecule to Function.* San Rafael (CA): Morgan & Claypool Life Sciences.

CISTERNINO, S., CHAPY, H., ANDRÉ, P., SMIRNOVA, M., DEBRAY, M. & SCHERRMANN, J.-M. 2013. Coexistence of Passive and Proton Antiporter-Mediated Processes in Nicotine Transport at the Mouse Blood–Brain Barrier. *The AAPS Journal,* 15**,** 299-307.

CISTERNINO, S., MERCIER, C., BOURASSET, F., ROUX, F. & SCHERRMANN, J. M. 2004. Expression, up-regulation, and transport activity of the multidrug-resistance protein Abcg2 at the mouse blood-brain barrier. *Cancer Res,* 64**,** 3296-301.

CONWAY, K. A., ROCHET, J. C., BIEGANSKI, R. M. & LANSBURY, P. T., JR. 2001. Kinetic stabilization of the alpha-synuclein protofibril by a dopamine-alpha-synuclein adduct. *Science,* 294**,** 1346-9.

COOK, C. & PETRUCELLI, L. 2009. A critical evaluation of the ubiquitin–proteasome system in Parkinson's disease. *Biochimica et Biophysica Acta (BBA) - Molecular Basis of Disease,* 1792**,** 664-675.

CORDATO, D. J. & CHAN, D. K. 2004. Genetics and Parkinson's disease. *J Clin Neurosci,* 11**,** 119-23.

CORNFORD, E. M., YOUNG, D., PAXTON, J. W., FINLAY, G. J., WILSON, W. R. & PARDRIDGE, W. M. 1992. Melphalan penetration of the blood-brain barrier via the neutral amino acid transporter in tumor-bearing brain. *Cancer Res,* 52**,** 138-43.

COSI, C., COLPAERT, F., KOEK, W., DEGRYSE, A. & MARIEN, M. 1996. Poly(ADP-ribose) polymerase inhibitors protect against MPTP-induced depletions of striatal dopamine and cortical noradrenaline in C57B1/6 mice. *Brain Research,* 729**,** 264-269.

CROWE, A. & MORGAN, E. H. 1994. Effects of chelators on iron uptake and release by the brain in the rat. *Neurochem Res,* 19**,** 71-6.

CUI, Z.-W., XIE, Z.-X., WANG, B.-F., ZHONG, Z.-H., CHEN, X.-Y., SUN, Y.-H., SUN, Q.-F., YANG, G.-Y. & BIAN, L.-G. 2015. Carvacrol protects neuroblastoma SH-SY5Y cells against Fe(2+)-induced apoptosis by suppressing activation of MAPK/JNK-NF-κB signaling pathway. *Acta Pharmacologica Sinica,* 36**,** 1426-1436.

CURTIUS, H. C., WOLFENSBERGER, M., STEINMANN, B., REDWEIK, U. & SIEGFRIED, J. 1974. Mass fragmentography of dopamine and 6-hydroxydopamine. Application to the determination of dopamine in human brain biopsies from the caudate nucleus. *J Chromatogr,* 99**,** 529-40.

CUTLER, L., HOWES, C., DEEKS, N. J., BUCK, T. L. & JEFFREY, P. 2006. Development of a P-glycoprotein knockout model in rodents to define species differences in its functional effect at the blood-brain barrier. J Pharm Sci, 95, 1944-53.

CZLONKOWSKA, A., KURKOWSKA-JASTRZEBSKA, I., CZLONKOWSKI, A., PETER, D. & STEFANO, G. B. 2002. Immune processes in the pathogenesis of Parkinson's disease - a potential role for microglia and nitric oxide. *Med Sci Monit,* 8**,** Ra165-77.

DATKI, Z., JUHASZ, A., GALFI, M., SOOS, K., PAPP, R., ZADORI, D. & PENKE, B. 2003. Method for measuring neurotoxicity of aggregating polypeptides with the MTT assay on differentiated neuroblastoma cells. *Brain Res Bull,* 62**,** 223-9.

DAUBNER, S. C., LE, T. & WANG, S. 2011. Tyrosine Hydroxylase and Regulation of Dopamine Synthesis. *Archives of biochemistry and biophysics,* 508**,** 1-12.

DAUCHY, R. T., BLASK, D. E. & SAUER, L. A. 2000. Preparation of the inguinal fat pad for perfusion in situ in the rat: a surgical technique that preserves continuous blood flow. *Contemp Top Lab Anim Sci,* 39**,** 29-33.

DAUER, W. & PRZEDBORSKI, S. 2003. Parkinson's Disease: Mechanisms and Models. *Neuron,* 39**,** 889-909.

DAUGHERTY, A. M. & RAZ, N. 2015. Appraising the Role of Iron in Brain Aging and Cognition: Promises and Limitations of MRI Methods. *Neuropsychology review,* 25**,** 272-287.

DE LAU, L. M. L. & BRETELER, M. M. B. 2006. Epidemiology of Parkinson's disease. *The Lancet Neurology,* 5**,** 525-535.

DEBEIR, T., GINESTET, L., FRANCOIS, C., LAURENS, S., MARTEL, J. C., CHOPIN, P., MARIEN, M., COLPAERT, F. & RAISMAN-VOZARI, R. 2005. Effect of intrastriatal 6-OHDA lesion on dopaminergic innervation of the rat cortex and globus pallidus. *Exp Neurol,* 193**,** 444-54.

DEL AMO, E. M., URTTI, A. & YLIPERTTULA, M. 2008. Pharmacokinetic role of L-type amino acid transporters LAT1 and LAT2. Eur J Pharm Sci, 35, 161-74.

DELAVILLE, C., DEURWAERDÈRE, P. D. & BENAZZOUZ, A. 2011. Noradrenaline and Parkinson's Disease. *Frontiers in Systems Neuroscience,* 5**,** 31.

DELLEDONNE, A., KLOS, K. J., FUJISHIRO, H., AHMED, Z., PARISI, J. E., JOSEPHS, K. A., FRIGERIO, R., BURNETT, M., WSZOLEK, Z. K., UITTI, R. J., AHLSKOG, J. E. & DICKSON, D. W. 2008. Incidental Lewy body disease and preclinical Parkinson disease. *Arch Neurol,* 65**,** 1074-80.

DENG, D., XU, C., SUN, P. C., WU, J. P., YAN, C. Y., HU, M. X. & YAN, N. 2014. Crystal structure of the human glucose transporter GLUT1. *Nature,* 510**,** 121-+.

DEV, S., KUMARI, S., SINGH, N., KUMAR BAL, S., SETH, P. & MUKHOPADHYAY, C. K. 2015. Role of extracellular Hydrogen peroxide in regulation of iron homeostasis genes in neuronal cells: Implication in iron accumulation. *Free Radic Biol Med,* 86**,** 78-89.

DEVANUR, L. D., EVANS, R. W., EVANS, P. J. & HIDER, R. C. 2008a. Chelator-facilitated removal of iron from transferrin: relevance to combined chelation therapy. *Biochem J,* 409**,** 439-47.

DEVANUR, L. D., NEUBERT, H. & HIDER, R. C. 2008b. The fenton activity of iron(III) in the presence of deferiprone. *J Pharm Sci,* 97**,** 1454-67.

DEVOS, D., MOREAU, C., DEVEDJIAN, J. C., KLUZA, J., PETRAULT, M., LALOUX, C., JONNEAUX, A., RYCKEWAERT, G., GARCON, G., ROUAIX, N., DUHAMEL, A., JISSENDI, P., DUJARDIN, K., AUGER, F.,

RAVASI, L., HOPES, L., GROLEZ, G., FIRDAUS, W., SABLONNIERE, B., STRUBI-VUILLAUME, I., ZAHR, N., DESTEE, A., CORVOL, J. C., POLTL, D., LEIST, M., ROSE, C., DEFEBVRE, L., MARCHETTI, P., CABANTCHIK, Z. I. & BORDET, R. 2014. Targeting Chelatable Iron as a Therapeutic Modality in Parkinson's Disease. *Antioxidants & Redox Signaling,* 21**,** 195-210.

DEVRAJ, K., KLINGER, M. E., MYERS, R. L., MOKASHI, A., HAWKINS, R. A. & SIMPSON, I. A. 2011. GLUT-1 GLUCOSE TRANSPORTERS IN THE BLOOD-BRAIN BARRIER: DIFFERENTIAL PHOSPHORYLATION. *Journal of neuroscience research,* 89**,** 10.1002/jnr.22738.

DEXTER, D. T., SIAN, J., ROSE, S., HINDMARSH, J. G., MANN, V. M., COOPER, J. M., WELLS, F. R., DANIEL, S. E., LEES, A. J., SCHAPIRA, A. H. & ET AL. 1994. Indices of oxidative stress and mitochondrial function in individuals with incidental Lewy body disease. *Ann Neurol,* 35**,** 38-44.

DEXTER, D. T., STATTON, S. A., WHITMORE, C., FREINBICHLER, W., WEINBERGER, P., TIPTON, K. F., DELLA CORTE, L., WARD, R. J. & CRICHTON, R. R. 2011. Clinically available iron chelators induce neuroprotection in the 6-OHDA model of Parkinson's disease after peripheral administration. *Journal of Neural Transmission,* 118**,** 223-231.

DEXTER, D. T., WELLS, F. R., AGID, F., AGID, Y., LEES, A. J., JENNER, P. & MARSDEN, C. D. 1987. Increased nigral iron content in postmortem parkinsonian brain. *Lancet,* 2**,** 1219-20.

DEXTER, D. T., WELLS, F. R., AGID, F., AGID, Y., LEES, A. J., JENNER, P. & MARSDEN, C. D. 1987. Increased nigral iron content in postmortem parkinsonian brain. *Lancet,* 2**,** 1219-20.

DEXTER, D. T., WELLS, F. R., LEES, A. J., AGID, F., AGID, Y., JENNER, P. & MARSDEN, C. D. 1989. Increased nigral iron content and alterations in other metal ions occurring in brain in Parkinson's disease. *J Neurochem,* 52**,** 1830-6.

DI, L., ARTURSSON, P., AVDEEF, A., ECKER, G. F., FALLER, B., FISCHER, H., HOUSTON, J. B., KANSY, M., KERNS, E. H., KRAMER, S. D., LENNERNAS, H. & SUGANO, K. 2012. Evidence-based approach to assess passive diffusion and carrier-mediated drug transport. *Drug Discovery Today,* 17**,** 905-912.

DIAS, V., JUNN, E. & MOURADIAN, M. M. 2013. The role of oxidative stress in Parkinson's disease. *J Parkinsons Dis,* 3**,** 461-91.

DICK, F. D., DE PALMA, G., AHMADI, A., SCOTT, N. W., PRESCOTT, G. J., BENNETT, J., SEMPLE, S., DICK, S., COUNSELL, C., MOZZONI, P., HAITES, N., WETTINGER, S. B., MUTTI, A., OTELEA, M., SEATON, A., SÖDERKVIST, P. & FELICE, A. 2007. Environmental risk factors for Parkinson's disease and parkinsonism: the Geoparkinson study. *Occupational and Environmental Medicine,* 64**,** 666-672.

DIETRICH, P., RIDEOUT, H. J., WANG, Q. & STEFANIS, L. 2003. Lack of p53 delays apoptosis, but increases ubiquitinated inclusions, in proteasomal inhibitor-treated cultured cortical neurons. *Molecular and Cellular Neuroscience,* 24**,** 430-441.

DINUNZIO, J. C. & WILLIAMS, R. O., 3RD 2008. CNS disorders--current treatment options and the prospects for advanced therapies. *Drug Dev Ind Pharm,* 34**,** 1141-67.

DO, J. H., KIM, I. S., PARK, T. K. & CHOI, D. K. 2007. Genome-wide examination of chromosomal aberrations in neuroblastoma SH-SY5Y cells by array-based comparative genomic hybridization. *Mol Cells,* 24**,** 105-12.

DOBBS, R. J., CHARLETT, A., PURKISS, A. G., DOBBS, S. M., WELLER, C. & PETERSON, D. W. 1999. Association of circulating TNF-alpha and IL-6 with ageing and parkinsonism. *Acta Neurol Scand,* 100**,** 34-41.

DOUBLE, K. L., MAYWALD, M., SCHMITTEL, M., RIEDERER, P. & GERLACH, M. 1998. In vitro studies of ferritin iron release and neurotoxicity. *J Neurochem,* 70**,** 2492-9.

DUBEY, R. K., MCALLISTER, C. B., INOUE, M. & WILKINSON, G. R. 1989. Plasma binding and transport of diazepam across the blood-brain barrier. No evidence for in vivo enhanced dissociation. *J Clin Invest,* 84**,** 1155-9.

DUONG, T. Q., IADECOLA, C. & KIM, S. G. 2001. Effect of hyperoxia, hypercapnia, and hypoxia on cerebral interstitial oxygen tension and cerebral blood flow. *Magn Reson Med,* 45**,** 61-70.

DUTTA, G., ZHANG, P. & LIU, B. 2008. The lipopolysaccharide Parkinson's disease animal model: mechanistic studies and drug discovery. *Fundam Clin Pharmacol,* 22**,** 453-64.

DUTY, S. & JENNER, P. 2011. Animal models of Parkinson's disease: a source of novel treatments and clues to the cause of the disease. *Br J Pharmacol,* 164**,** 1357-91.

DWYER, K. J. & PARDRIDGE, W. M. 1993. Developmental Modulation of Blood-Brain-Barrier and Choroid-Plexus Glut1 Glucose Transporter Messenger-Ribonucleic-Acid and Immunoreactive Protein in Rabbits. *Endocrinology,* 132**,** 558-565.

EARLE, K. M. 1968. Studies on Parkinson's disease including x-ray fluorescent spectroscopy of formalin fixed brain tissue. *J Neuropathol Exp Neurol,* 27**,** 1-14.

EKSTRAND, M. I., TERZIOGLU, M., GALTER, D., ZHU, S., HOFSTETTER, C., LINDQVIST, E., THAMS, S., BERGSTRAND, A., HANSSON, F. S., TRIFUNOVIC, A., HOFFER, B., CULLHEIM, S., MOHAMMED, A. H., OLSON, L. & LARSSON, N.-G. 2007. Progressive parkinsonism in mice with respiratory-chain-deficient dopamine neurons. *Proceedings of the National Academy of Sciences of the United States of America,* 104**,** 1325-1330.

ELALFY, M. S., SHEBL, S. S., BADR, M. A., ELSAFY, U. R., SALAMA, M. A., AL-TONBARY, Y., RAHMAN, Y. A., QARI, M. H., AL DAMNHOURI, G. A., AL HAWSAWI, Z., WALI, Y. A., YESILIPEK, M. A., KILINC, Y., YAZMAN, D., KARAKAS, Z. & TRICTA, F. 2012. Frequency of Agranulocytosis and Mild Neutropenia During Deferiprone Therapy in Clinical Practice. *Blood,* 120**,** 996-996.

EL-KATTAN, A. & VARMA, M. 2012. Oral absorption, intestinal metabolism and human oral bioavailability. *In:* PAXTON, D. J. (ed.) *Topics on Drug Metabolism.* InTech.

ELMORE, S. 2007. Apoptosis: A Review of Programmed Cell Death. *Toxicologic pathology,* 35**,** 495-516.

ENE, L., DUICULESCU, D. & RUTA, S. M. 2011. How much do antiretroviral drugs penetrate into the central nervous system? *Journal of Medicine and Life,* 4**,** 432-439.

ENGELHARDT, B. & SOROKIN, L. 2009. The blood-brain and the blood-cerebrospinal fluid barriers: function and dysfunction. *Semin Immunopathol,* 31**,** 497-511.

ENNIS, S. R. & BETZ, A. L. 1986. Sucrose permeability of the blood-retinal and blood-brain barriers. Effects of diabetes, hypertonicity, and iodate. *Invest Ophthalmol Vis Sci,* 27**,** 1095-102.

ENNIS, S., KAWAI, N., REN, X., ABDELKARIM, G. & KEEP, R. 1998. Glutamine uptake at the blood-brain barrier is mediated by N-system transport. *J Neurochem,* 71**,** 2565-2573.

EUROPEAN MEDICINES AGENCY 2005. Procedural steps taken before authorisation: background information on the procedure *In:* AGENCY, E. M. (ed.).

FALKENBURGER, B. H. & SCHULZ, J. B. 2006. Limitations of cellular models in Parkinson's disease research. *J Neural Transm Suppl***,** 261-8.

FEBBRARO, F., GIORGI, M., CALDAROLA, S., LORENI, F. & ROMERO-RAMOS, M. 2012. alpha-Synuclein expression is modulated at the translational level by iron. *Neuroreport,* 23**,** 576-80.

FERGER, B., ROSE, S., JENNER, A., HALLIWELL, B. & JENNER, P. 2001. 6-hydroxydopamine increases hydroxyl free radical production and DNA damage in rat striatum. *Neuroreport,* 12**,** 1155-9.

FERRER, I. 2011. Neuropathology and Neurochemistry of Nonmotor Symptoms in Parkinson's Disease. *Parkinson's Disease,* 2011**,** 708404.

FILOGRANA, R., CIVIERO, L., FERRARI, V., CODOLO, G., GREGGIO, E., BUBACCO, L., BELTRAMINI, M. & BISAGLIA, M. 2015. Analysis of the Catecholaminergic Phenotype in Human SH-SY5Y and BE(2)-M17 Neuroblastoma Cell Lines upon Differentiation. *PLOS ONE,* 10**,** e0136769.

FISCHER, H., GOTTSCHLICH, R. & SEELIG, A. 1998. Blood-brain barrier permeation: molecular parameters governing passive diffusion. *J Membr Biol,* 165**,** 201-11.

FISHER, S. A., BRUNSKILL, S. J., DOREE, C., CHOWDHURY, O., GOODING, S. & ROBERTS, D. J. 2013. Oral deferiprone for iron chelation in people with thalassaemia. *Cochrane Database of Systematic Reviews*.

FONG, C. W. 2015. Permeability of the Blood–Brain Barrier: Molecular Mechanism of Transport of Drugs and Physiologically Important Compounds. *The Journal of Membrane Biology,* 248**,** 651-669.

FORNI, G. L., BALOCCO, M., CREMONESI, L., ABBRUZZESE, G., PARODI, R. C. & MARCHESE, R. 2008. Regression of symptoms after selective iron chelation therapy in a case of neurodegeneration with brain iron accumulation. *Movement Disorders,* 23**,** 904-907.

FOSTER, H. D. & HOFFER, A. 2004. The two faces of L-DOPA: benefits and adverse side effects in the treatment of Encephalitis lethargica, Parkinson's disease, multiple sclerosis and amyotrophic lateral sclerosis. Med Hypotheses, 62, 177-81.

FOX, E., BUNGAY, P. M., BACHER, J., MCCULLY, C. L., DEDRICK, R. L. & BALIS, F. M. 2002. Zidovudine concentration in brain extracellular fluid measured by microdialysis: steady-state and transient results in rhesus monkey. *J Pharmacol Exp Ther,* 301**,** 1003-11.

FRANK-CANNON, T. C., ALTO, L. T., MCALPINE, F. E. & TANSEY, M. G. 2009. Does neuroinflammation fan the flame in neurodegenerative diseases? *Mol Neurodegener,* 4**,** 47.

FREDENBURG, A., SETHI, R., ALLEN, D. & YOKEL, R. 1996a. The pharmacokinetics and blood-brain barrier permeation of the chelators 1,2 dimethly-, 1,2 diethyl-, and 1-[ethan-1'ol]-2-methyl-3-hydroxypyridin-4-one in the rat. *Toxicology,* 108**,** 191-199.

FRIDÉN, M. 2014. Prediction of Drug Exposure in the Brain from the Chemical Structure. *In:* HAMMARLUND-UDENAES, M., DE LANGE, E. C. M. & THORNE, R. G. (eds.) *Drug Delivery to the Brain: Physiological Concepts, Methodologies and Approaches.* New York, NY: Springer New York.

FRIDEN, M., GUPTA, A., ANTONSSON, M., BREDBERG, U. & HAMMARLUND-UDENAES, M. 2007. In vitro methods for estimating unbound drug concentrations in the brain interstitial and intracellular fluids. *Drug Metab Dispos,* 35**,** 1711-9.

FRIDEN, M., WINIWARTER, S., JERNDAL, G., BENGTSSON, O., WAN, H., BREDBERG, U., HAMMARLUND-UDENAES, M. & ANTONSSON, M. 2009. Structure-brain exposure relationships in rat and human using a novel data set of unbound drug concentrations in brain interstitial and cerebrospinal fluids. *J Med Chem,* 52**,** 6233-43.

FRIEDMAN, J. 2011. Why Is the Nervous System Vulnerable to Oxidative Stress? *In:* GADOTH, N. & GÖBEL, H. H. (eds.) *Oxidative Stress and Free Radical Damage in Neurology.* Totowa, NJ: Humana Press.

GABRIČEVIĆ, M. & CRUMBLISS, A. L. 2003. Kinetics and Mechanism of Iron(III)−Nitrilotriacetate Complex Reactions with Phosphate and Acetohydroxamic Acid. *Inorganic Chemistry,* 42**,** 4098-4101.

GAL, S., FRIDKIN, M., AMIT, T., ZHENG, H. & YOUDIM, M. B. 2006. M30, a novel multifunctional neuroprotective drug with potent iron chelating and brain selective monoamine oxidase-ab inhibitory activity for Parkinson's disease. *J Neural Transm Suppl***,** 447-56.

GAL, S., ZHENG, H., FRIDKIN, M. & YOUDIM, M. B. 2005. Novel multifunctional neuroprotective iron chelator-monoamine oxidase inhibitor drugs for neurodegenerative diseases. In vivo selective brain monoamine oxidase inhibition and prevention of MPTP-induced striatal dopamine depletion. *J Neurochem,* 95**,** 79-88.

GANDHI, S., MUQIT, M. M., STANYER, L., HEALY, D. G., ABOU-SLEIMAN, P. M., HARGREAVES, I., HEALES, S., GANGULY, M., PARSONS, L., LEES, A. J., LATCHMAN, D. S., HOLTON, J. L., WOOD, N. W. & REVESZ, T. 2006. PINK1 protein in normal human brain and Parkinson's disease. *Brain,* 129**,** 1720-31.

GASSER, T. 2009. Mendelian forms of Parkinson's disease. *Biochimica et Biophysica Acta (BBA) - Molecular Basis of Disease,* 1792**,** 587-596.

GATTO, N. M., COCKBURN, M., BRONSTEIN, J., MANTHRIPRAGADA, A. D. & RITZ, B. 2009. Well-Water Consumption and Parkinson's Disease in Rural California. *Environmental Health Perspectives,* 117**,** 1912-1918.

GAUTIER, C. A., KITADA, T. & SHEN, J. 2008. Loss of PINK1 causes mitochondrial functional defects and increased sensitivity to oxidative stress. *Proc Natl Acad Sci U S A,* 105**,** 11364-9.

GEIER, E. G., SCHLESSINGER, A., FAN, H., GABLE, J. E., IRWIN, J. J., SALI, A. & GIACOMINI, K. M. 2013. Structure-based ligand discovery for the Large-neutral Amino Acid Transporter 1, LAT-1. Proceedings of the National Academy of Sciences of the United States of America, 110, 5480-5485.

GENESTRA, M. 2007. Oxyl radicals, redox-sensitive signalling cascades and antioxidants. *Cell Signal,* 19**,** 1807-19.

GERLACH, M., DOUBLE, K. L., YOUDIM, M. B. & RIEDERER, P. 2006. Potential sources of increased iron in the substantia nigra of parkinsonian patients. *J Neural Transm Suppl***,** 133-42.

GIKNIS, M. L. A. & CLIFFORD, C. B. 2008. Clinical laboratory parameters for Crl:WI (Han). *In:* RIVER, C. (ed.).

GIORGIO, M., TRINEI, M., MIGLIACCIO, E. & PELICCI, P. G. 2007. Hydrogen peroxide: a metabolic by-product or a common mediator of ageing signals? *Nat Rev Mol Cell Biol,* 8**,** 722-8.

GLICKMAN, M. H. & CIECHANOVER, A. 2002. The ubiquitin-proteasome proteolytic pathway: destruction for the sake of construction. *Physiol Rev,* 82**,** 373-428.

GLICKSTEIN, H., EL, R. B., SHVARTSMAN, M. & CABANTCHIK, Z. I. 2005. Intracellular Labile Iron Pools as Direct Targets of Iron Chelators: A Fluorescence Study of Chelator Action in Living Cells. *Blood,* 106**,** 3242-3250.

GLINKA, Y. Y. & YOUDIM, M. B. 1995. Inhibition of mitochondrial complexes I and IV by 6-hydroxydopamine. *Eur J Pharmacol,* 292**,** 329-32.

GLINKA, Y., TIPTON, K. F. & YOUDIM, M. B. 1998. Mechanism of inhibition of mitochondrial respiratory complex I by 6-hydroxydopamine and its prevention by desferrioxamine. *Eur J Pharmacol,* 351**,** 121-9.

GOLBE, L. I., DI IORIO, G., LAZZARINI, A., VIEREGGE, P., GERSHANIK, O. S., BONAVITA, V. & DUVOISIN, R. C. 1999. The Contursi kindred, a large family with autosomal dominant Parkinson's disease: implications of clinical and molecular studies. *Adv Neurol,* 80**,** 165-70.

GOMES, P. & SOARES-DA-SILVA, P. 1999. L-DOPA transport properties in an immortalised cell line of rat capillary cerebral endothelial cells, RBE 4. *Brain Res,* 829**,** 143-50.

GONG, B. & LEZNIK, E. 2007. The role of ubiquitin C-terminal hydrolase L1 in neurodegenerative disorders. *Drug News Perspect,* 20**,** 365-70.

GORELL, J. M., JOHNSON, C. C., RYBICKI, B. A., PETERSON, E. L. & RICHARDSON, R. J. 1998. The risk of Parkinson's disease with exposure to pesticides, farming, well water, and rural living. *Neurology,* 50**,** 1346-50.

GOTSBACHER, M. P., TELFER, T. J., WITTING, P. K., DOUBLE, K. L., FINKELSTEIN, D. I. & CODD, R. 2017. Analogues of desferrioxamine B designed to attenuate iron-mediated neurodegeneration: synthesis, characterisation and activity in the MPTP-mouse model of Parkinson's disease. Metallomics, 9, 852-864.

GREENAMYRE, J. T., BETARBET, R. & SHERER, T. B. 2003. The rotenone model of Parkinson's disease: genes, environment and mitochondria. *Parkinsonism Relat Disord,* 9 Suppl 2**,** S59-64.

GREENWOOD, J., LOVE, E. R. & PRATT, O. E. 1982. Kinetics of thiamine transport across the blood-brain barrier in the rat. *J Physiol,* 327**,** 95-103.

GREIG, N. H., SONCRANT, T. T., SHETTY, H. U., MOMMA, S., SMITH, Q. R. & RAPOPORT, S. I. 1990. Brain uptake and anticancer activities of vincristine and vinblastine are restricted by their low cerebrovascular permeability and binding to plasma constituents in rat. *Cancer Chemother Pharmacol,* 26**,** 263-8.

GRIFFITHS, P. D., DOBSON, B. R., JONES, G. R. & CLARKE, D. T. 1999. Iron in the basal ganglia in Parkinson's disease - An in vitro study using extended X-ray absorption fine structure and cryo-electron microscopy. *Brain,* 122**,** 667-673.

GRUNBLATT, E., MANDEL, S., MAOR, G. & YOUDIM, M. B. 2001. Effects of R- and S-apomorphine on MPTP-induced nigro-striatal dopamine neuronal loss. *J Neurochem,* 77**,** 146-56.

GUAN, H., YANG, H., YANG, M., YANAGISAWA, D., BELLIER, J. P., MORI, M., TAKAHATA, S., NONAKA, T., ZHAO, S. & TOOYAMA, I. 2017. Mitochondrial ferritin protects SH-SY5Y cells against H2O2-induced oxidative stress and modulates alpha-synuclein expression. *Exp Neurol,* 291**,** 51-61.

GUO, B., PHILLIPS, J. D., YU, Y. & LEIBOLD, E. A. 1995. Iron regulates the intracellular degradation of iron regulatory protein 2 by the proteasome. *J Biol Chem,* 270**,** 21645-51.

GUO, C., SUN, L., CHEN, X. & ZHANG, D. 2013. Oxidative stress, mitochondrial damage and neurodegenerative diseases. *Neural Regeneration Research,* 8**,** 2003-2014.

GUO, N. & PENG, Z. 2013. MG132, a proteasome inhibitor, induces apoptosis in tumor cells. *Asia-Pacific Journal of Clinical Oncology,* 9**,** 6-11.

GUREVICH, K. G. 2013. Effect of blood protein concentrations on drug-dosing regimes: practical guidance. *Theor Biol Med Model,* 10**,** 20.

GUYENET, P. G., MULKEY, D. K., STORNETTA, R. L. & BAYLISS, D. A. 2005. Regulation of ventral surface chemoreceptors by the central respiratory pattern generator. *J Neurosci,* 25**,** 8938-47.

HABER, S. N., FUDGE, J. L. & MCFARLAND, N. R. 2000. Striatonigrostriatal Pathways in Primates Form an Ascending Spiral from the Shell to the Dorsolateral Striatum. *The Journal of Neuroscience,* 20**,** 2369-2382.

HABGOOD, M. D., BEGLEY, D. J. & ABBOTT, N. J. 2000. Determinants of Passive Drug Entry into the Central Nervous System. *Cellular and Molecular Neurobiology,* 20**,** 231-253.

HABGOOD, M. D., LIU, Z. D., DEHKORDI, L. S., KHODR, H. H., ABBOTT, J. & HIDER, R. C. 1999. Investigation into the correlation between the structure of hydroxypyridinones and blood-brain barrier permeability. *Biochem Pharmacol,* 57**,** 1305-10.

HALD, A. & LOTHARIUS, J. 2005. Oxidative stress and inflammation in Parkinson's disease: is there a causal link? *Exp Neurol,* 193**,** 279-90.

HALL, S., RUTLEDGE, J. N. & SCHALLERT, T. 1992. MRI, brain iron and experimental Parkinson's disease. *J Neurol Sci,* 113**,** 198-208.

HALLIWELL, B. & GUTTERIDGE, J. M. 1984. Oxygen toxicity, oxygen radicals, transition metals and disease. *Biochem J,* 219.

HAMMARLUND-UDENAES, M., FRIDEN, M., SYVANEN, S. & GUPTA, A. 2008. On the rate and extent of drug delivery to the brain. *Pharm Res,* 25**,** 1737-50.

HANAGASI, H. A. & EMRE, M. 2005. Treatment of behavioural symptoms and dementia in Parkinson's disease. *Fundam Clin Pharmacol,* 19**,** 133-46.

HARRIS, D. C. 1977. Different metal-binding properties of the two sites of human transferrin. *Biochemistry,* 16**,** 560-4.

HARTMANN, A. 2004. Postmortem studies in Parkinson's disease. *Dialogues in Clinical Neuroscience,* 6**,** 281-293.

HASEGAWA, T., MATSUZAKI, M., TAKEDA, A., KIKUCHI, A., FURUKAWA, K., SHIBAHARA, S. & ITOYAMA, Y. 2003. Increased dopamine and its metabolites in SH-SY5Y neuroblastoma cells that express tyrosinase. *J Neurochem,* 87**,** 470-5.

HAVERFIELD, E. V., WEATHERALL, D. J., GRABER, A. Y., RAMIREZ, J. & RATAIN, M. J. 2005. Pharmacogenomics of Deferiprone Metabolism. *Blood,* 106**,** 2703-2703.

HE, L. & LEMASTERS, J. J. 2002. Regulated and unregulated mitochondrial permeability transition pores: a new paradigm of pore structure and function? *FEBS Lett,* 512**,** 1-7.

HE, Y., LEE, T. & LEONG, S. K. 2000. 6-Hydroxydopamine induced apoptosis of dopaminergic cells in the rat substantia nigra. *Brain Res,* 858**,** 163-6.

HE, Y., THONG, P. S., LEE, T., LEONG, S. K., SHI, C. Y., WONG, P. T., YUAN, S. Y. & WATT, F. 1996. Increased iron in the substantia nigra of 6-OHDA induced parkinsonian rats: a nuclear microscopy study. *Brain Res,* 735**,** 149-53.

HEFTI, F., MELAMED, E., SAHAKIAN, B. J. & WURTMAN, R. J. 1980. Circling behavior in rats with partial, unilateral nigro-striatal lesions: effect of amphetamine, apomorphine, and DOPA. *Pharmacol Biochem Behav,* 12**,** 185-8.

HEMMINGSEN, C., STAUN, M. & OLGAARD, K. 1998. The effect of 1,25-vitamin D3 on calbindin-D and calcium-metabolic variables in the rat. *Pharmacol Toxicol,* 82**,** 118-21.

HENDRICKS, B. K., COHEN-GADOL, A. A. & MILLER, J. C. 2015. Novel delivery methods bypassing the blood-brain and blood-tumor barriers. *Neurosurg Focus,* 38**,** E10.

HENTER, J. I. & KARLEN, J. 2007. Fatal agranulocytosis after deferiprone therapy in a child with Diamond-Blackfan anemia. *Blood,* 109**,** 5157-9.

HERSHKO, C. 1978. Determinants of fecal and urinary iron excretion in desferrioxamine-treated rats. *Blood,* 51**,** 415-23.

HERSHKO, C., KONIJN, A. M., NICK, H. P., BREUER, W., CABANTCHIK, Z. I. & LINK, G. 2001. ICL670A: a new synthetic oral chelator: evaluation in hypertransfused rats with selective radioiron probes of hepatocellular and reticuloendothelial iron stores and in iron-loaded rat heart cells in culture. *Blood,* 97**,** 1115.

HIDER, R. C. & LIU, Z. D. 2003. Emerging understanding of the advantage of small molecules such as hydroxypyridinones in the treatment of iron overload. *Current Medicinal Chemistry,* 10**,** 1051-1064.

HIDER, R. C., LIU, Z. D. & PIYAMONGKOL, S. 2000. The design and properties of 3-hydroxypyridin-4-one iron chelators with high pFe3 values. *Transfusion Science,* 23**,** 201-209.

HIDER, R. C., ROY, S., MA, Y. M., AND, X. L. K. & PRESTON, J. 2011a. The potential application of iron chelators for the treatment of neurodegenerative diseases. *Metallomics,* 3**,** 239-249.

HIDER, R. C., SINGH, S., PORTER, J. B. & HUEHNS, E. R. 1990. The Development of Hydroxypyridin-4-ones as Orally Active Iron Chelators. *Annals of the New York Academy of Sciences,* 612**,** 327-338.

HIDER, R., LIU, Z., YU, Y. & LI, Z. 2011a. Chiral 3-hydroxypyrid-4-one derivative, and synthesis and use thereof. China patent application EP20110862562.

HIRSCH, E. C. & HUNOT, S. 2009. Neuroinflammation in Parkinson's disease: a target for neuroprotection? *Lancet Neurol,* 8**,** 382-97.

HIRSCH, L., JETTE, N., FROLKIS, A., STEEVES, T. & PRINGSHEIM, T. 2016. The Incidence of Parkinson's Disease: A Systematic Review and Meta-Analysis. *Neuroepidemiology,* 46**,** 292-300.

HITCHCOCK, S. A. & PENNINGTON, L. D. 2006. Structure−Brain Exposure Relationships. *Journal of Medicinal Chemistry,* 49**,** 7559-7583.

HOFFBRAND, A. V., COHEN, A. & HERSHKO, C. 2003. Role of deferiprone in chelation therapy for transfusional iron overload. *Blood,* 102**,** 17-24.

HOFFBRAND, V. 2005. Deferiprone therapy for transfusional iron overload. *Best Practice & Research Clinical Haematology,* 18**,** 299-317.

HOKARI, M., WU, H. Q., SCHWARCZ, R. & SMITH, Q. R. 1996. Facilitated brain uptake of 4-chlorokynurenine and conversion to 7-chlorokynurenic acid. *Neuroreport,* 8**,** 15-8.

HOLCMAN, D. & YUSTE, R. 2015. The new nanophysiology: regulation of ionic flow in neuronal subcompartments. *Nat Rev Neurosci,* 16**,** 685-692.

HOOSAIN, F. G., CHOONARA, Y. E., TOMAR, L. K., KUMAR, P., TYAGI, C., DU TOIT, L. C. & PILLAY, V. 2015. Bypassing P-Glycoprotein Drug Efflux Mechanisms: Possible Applications in Pharmacoresistant Schizophrenia Therapy. *BioMed Research International,* 2015**,** 21.

HOPES, L., DEVOS, D., DELMAIRE, C., JISSENDI, P., ALAIN, D. & LUC, D. 2012. Volume and increased iron content in the basal ganglia and substantia nigra: Two potential early biomarkers of Parkinson's disease? *Movement Disorders,* 27**,** S239-S239.

HOPES, L., GROLEZ, G., MOREAU, C., LOPES, R., RYCKEWAERT, G., CARRIERE, N., AUGER, F., LALOUX, C., PETRAULT, M., DEVEDJIAN, J. C., BORDET, R., DEFEBVRE, L., JISSENDI, P., DELMAIRE, C. & DEVOS, D. 2016. Magnetic Resonance Imaging Features of the Nigrostriatal System: Biomarkers of Parkinson's Disease Stages? *PLoS One,* 11**,** e0147947.

HOWITT, J., PUTZ, U., LACKOVIC, J., DOAN, A., DORSTYN, L., CHENG, H., YANG, B., CHAN-LING, T., SILKE, J., KUMAR, S. & TAN, S. S. 2009. Divalent metal transporter 1 (DMT1) regulation by Ndfip1 prevents metal toxicity in human neurons. Proc Natl Acad Sci U S A, 106, 15489-94.

HU, Q. & WANG, G. 2016. Mitochondrial dysfunction in Parkinson's disease. 5**,** 14.

HUANG, J. & MAY, J. M. 2006. Ascorbic acid protects SH-SY5Y neuroblastoma cells from apoptosis and death induced by β-amyloid. *Brain Research,* 1097**,** 52-58.

HUDSON, J. L., VAN HORNE, C. G., STROMBERG, I., BROCK, S., CLAYTON, J., MASSERANO, J., HOFFER, B. J. & GERHARDT, G. A. 1993. Correlation of apomorphine- and amphetamine-induced turning with nigrostriatal dopamine content in unilateral 6-hydroxydopamine lesioned rats. *Brain Res,* 626**,** 167-74.

IANCU, R., MOHAPEL, P., BRUNDIN, P. & PAUL, G. 2005. Behavioral characterization of a unilateral 6-OHDA-lesion model of Parkinson's disease in mice. *Behavioural Brain Research,* 162**,** 1-10.

IDRO, R., GWER, S., WILLIAMS, T. N., OTIENO, T., UYOGA, S., FEGAN, G., KAGER, P. A., MAITLAND, K., KIRKHAM, F., NEVILLE, B. G. R. & NEWTON, C. R. J. 2010. Iron Deficiency and Acute Seizures: Results from Children Living in Rural Kenya and a Meta-Analysis. PLoS ONE, 5, e14001.

IKEBE, S.-I., TANAKA, M., OHNO, K., SATO, W., HATTORI, K., KONDO, T., MIZUNO, Y. & OZAWA, T. 1990. Increase of deleted mitochondrial DNA in the striatum in Parkinson's disease and senescence. *Biochemical and Biophysical Research Communications,* 170**,** 1044-1048.

IQBAL, M., OKAZAKI, Y. & OKADA, S. 2003. In vitro curcumin modulates ferric nitrilotriacetate (Fe-NTA) and hydrogen peroxide (H2O2)-induced peroxidation of microsomal membrane lipids and DNA damage. *Teratog Carcinog Mutagen,* Suppl 1**,** 151-60.

IRAVANI, M. M., KASHEFI, K., MANDER, P., ROSE, S. & JENNER, P. 2002. Involvement of inducible nitric oxide synthase in inflammation-induced dopaminergic neurodegeneration. *Neuroscience,* 110**,** 49-58.

IRAVANI, M. M., LEUNG, C. C., SADEGHIAN, M., HADDON, C. O., ROSE, S. & JENNER, P. 2005. The acute and the long-term effects of nigral lipopolysaccharide administration on dopaminergic dysfunction and glial cell activation. *Eur J Neurosci,* 22**,** 317-30.

ISMAIL, N., ISMAIL, M., FATHY, S. F., MUSA, S. N., IMAM, M. U., FOO, J. B. & IQBAL, S. 2012. Neuroprotective effects of germinated brown rice against hydrogen peroxide induced cell death in human SH-SY5Y cells. *Int J Mol Sci,* 13**,** 9692-708.

IZUMI, Y., SAWADA, H., SAKKA, N., YAMAMOTO, N., KUME, T., KATSUKI, H., SHIMOHAMA, S. & AKAIKE, A. 2005. p-Quinone mediates 6-hydroxydopamine-induced dopaminergic neuronal death and ferrous iron accelerates the conversion of p-quinone into melanin extracellularly. *J Neurosci Res,* 79**,** 849-60.

JACKSON-LEWIS, V. & PRZEDBORSKI, S. 2007. Protocol for the MPTP mouse model of Parkinson's disease. *Nat. Protocols,* 2**,** 141-151.

JAMESON, G. N. L., JAMESON, R. F. & LINERT, W. 2004. New insights into iron release from ferritin: direct observation of the neurotoxin 6-hydroxydopamine entering ferritin and reaching redox equilibrium with the iron core. *Organic & Biomolecular Chemistry,* 2**,** 2346-2351.

JAMUAR, S. S. & LAI, A. H. M. 2012. Safety and efficacy of iron chelation therapy with deferiprone in patients with transfusion-dependent thalassemia. *Therapeutic Advances in Hematology,* 3**,** 299-307.

JANKOVIC, J. 2008. Parkinson's disease: clinical features and diagnosis. *J Neurol Neurosurg Psychiatry,* 79**,** 368-76.

JAY, T. M., DIENEL, G. A., CRUZ, N. F., MORI, K., NELSON, T. & SOKOLOFF, L. 1990. Metabolic stability of 3-O-methyl-D-glucose in brain and other tissues. *J Neurochem,* 55**,** 989-1000.

JEFFREY, P. & SUMMERFIELD, S. G. 2007. Challenges for blood-brain barrier (BBB) screening. *Xenobiotica,* 37**,** 1135-51.

JELLINGER, K. A. 2000. Cell death mechanisms in Parkinson's disease. *J Neural Transm (Vienna),* 107**,** 1-29.

JELLINGER, K., LINERT, L., KIENZL, E., HERLINGER, E. & YOUDIM, M. B. 1995. Chemical evidence for 6-hydroxydopamine to be an endogenous toxic factor in the pathogenesis of Parkinson's disease. *J Neural Transm Suppl,* 46**,** 297-314.

JENNER, P. & OLANOW, C. W. 1996. Oxidative stress and the pathogenesis of Parkinson's disease. *Neurology,* 47**,** S161-70.

JENSEN, F. B. 2004. Red blood cell pH, the Bohr effect, and other oxygenation-linked phenomena in blood O2 and CO2 transport. *Acta Physiol Scand,* 182**,** 215-27.

JEON, B. S., JACKSON-LEWIS, V. & BURKE, R. E. 1995. 6-Hydroxydopamine lesion of the rat substantia nigra: time course and morphology of cell death. *Neurodegeneration,* 4**,** 131-7.

JIA, W., XU, H., DU, X., JIANG, H. & XIE, J. 2015. Ndfip1 attenuated 6-OHDA-induced iron accumulation via regulating the degradation of DMT1. *Neurobiol Aging,* 36**,** 1183-93.

JIANG, H., SONG, N., XU, H., ZHANG, S., WANG, J. & XIE, J. 2010. Up-regulation of divalent metal transporter 1 in 6-hydroxydopamine intoxication is IRE/IRP dependent. *Cell Res,* 20**,** 345-356.

JONG, A. & HUANG, S. H. 2005. Blood-brain barrier drug discovery for central nervous system infections. *Curr Drug Targets Infect Disord,* 5**,** 65-72.

KADIAN, N., RAJU, K. S., RASHID, M., MALIK, M. Y., TANEJA, I. & WAHAJUDDIN, M. 2016. Comparative assessment of bioanalytical method validation guidelines for pharmaceutical industry. *J Pharm Biomed Anal,* 126**,** 83-97.

KAGEYAMA, T., NAKAMURA, M., MATSUO, A., YAMASAKI, Y., TAKAKURA, Y., HASHIDA, M., KANAI, Y., NAITO, M., TSURUO, T., MINATO, N. & SHIMOHAMA, S. 2000. The 4F2hc/LAT1 complex transports L-DOPA across the blood-brain barrier. *Brain Research,* 879**,** 115-121.

KAKHLON, O. & CABANTCHIK, Z. I. 2002. The labile iron pool: characterization, measurement, and participation in cellular processes(1). *Free Radic Biol Med,* 33**,** 1037-46.

KARASOVA, J. Z., POHANKA, M., MUSILEK, K., ZEMEK, F. & KUCA, K. 2010. Passive diffusion of acetylcholinesterase oxime reactivators through the blood–brain barrier: Influence of molecular structure. *Toxicology in Vitro,* 24**,** 1838-1844.

KAUR, D., YANTIRI, F., RAJAGOPALAN, S., KUMAR, J., MO, J. Q., BOONPLUEANG, R., VISWANATH, V., JACOBS, R., YANG, L., BEAL, M. F., DIMONTE, D., VOLITASKIS, I., ELLERBY, L., CHERNY, R. A., BUSH, A. I. & ANDERSEN, J. K. 2003. Genetic or pharmacological iron chelation prevents MPTP-induced neurotoxicity in vivo: a novel therapy for Parkinson's disease. *Neuron,* 37**,** 899-909.

KEANE, P. C., KURZAWA, M., BLAIN, P. G. & MORRIS, C. M. 2011. Mitochondrial Dysfunction in Parkinson's Disease. *Parkinson's Disease,* 2011.

KILARSKI, L. L., PEARSON, J. P., NEWSWAY, V., MAJOUNIE, E., KNIPE, M. D., MISBAHUDDIN, A., CHINNERY, P. F., BURN, D. J., CLARKE, C. E., MARION, M. H., LEWTHWAITE, A. J., NICHOLL, D. J., WOOD, N. W., MORRISON, K. E., WILLIAMS-GRAY, C. H., EVANS, J. R., SAWCER, S. J., BARKER, R. A.,

WICKREMARATCHI, M. M., BEN-SHLOMO, Y., WILLIAMS, N. M. & MORRIS, H. R. 2012. Systematic review and UK-based study of PARK2 (parkin), PINK1, PARK7 (DJ-1) and LRRK2 in early-onset Parkinson's disease. *Mov Disord,* 27**,** 1522-9.

KILLIAN, D. M. & CHIKHALE, P. J. 2001. A bioreversible prodrug approach designed to shift mechanism of brain uptake for amino-acid-containing anticancer agents. *J Neurochem,* 76**,** 966-74.

KILLIAN, D. M., HERMELING, S. & CHIKHALE, P. J. 2007. Targeting the cerebrovascular large neutral amino acid transporter (LAT1) isoform using a novel disulfide-based brain drug delivery system. *Drug Deliv,* 14**,** 25-31.

KIM, N. R., PARK, S. W., LEE, J. G. & KIM, Y. H. 2008. Protective effects of olanzapine and haloperidol on serum withdrawal-induced apoptosis in SH-SY5Y cells. *Prog Neuropsychopharmacol Biol Psychiatry,* 32**,** 633-42.

KIM, R. H., SMITH, P. D., ALEYASIN, H., HAYLEY, S., MOUNT, M. P., POWNALL, S., WAKEHAM, A., YOU-TEN, A. J., KALIA, S. K., HORNE, P., WESTAWAY, D., LOZANO, A. M., ANISMAN, H., PARK, D. S. & MAK, T. W. 2005. Hypersensitivity of DJ-1-deficient mice to 1-methyl-4-phenyl-1,2,3,6-tetrahydropyrindine (MPTP) and oxidative stress. *Proc Natl Acad Sci U S A,* 102**,** 5215-20.

KIM, W. S., KÅGEDAL, K. & HALLIDAY, G. M. 2014. Alpha-synuclein biology in Lewy body diseases. *Alzheimer's Research & Therapy,* 6**,** 73-73.

KIRIK, D., ROSENBLAD, C. & BJORKLUND, A. 1998. Characterization of behavioral and neurodegenerative changes following partial lesions of the nigrostriatal dopamine system induced by intrastriatal 6-hydroxydopamine in the rat. *Exp Neurol,* 152**,** 259-77.

KITADA, T., PISANI, A., PORTER, D. R., YAMAGUCHI, H., TSCHERTER, A., MARTELLA, G., BONSI, P., ZHANG, C., POTHOS, E. N. & SHEN, J. 2007. Impaired dopamine release and synaptic plasticity in the striatum of PINK1-deficient mice. *Proc Natl Acad Sci U S A,* 104**,** 11441-6.

KLEIN, C. & WESTENBERGER, A. 2012. Genetics of Parkinson's Disease. *Cold Spring Harbor Perspectives in Medicine,* 2**,** a008888.

KNOTT, C., STERN, G. & WILKIN, G. P. 2000. Inflammatory regulators in Parkinson's disease: iNOS, lipocortin-1, and cyclooxygenases-1 and -2. *Mol Cell Neurosci,* 16**,** 724-39.

KOBAYASHI, H., OIKAWA, S., UMEMURA, S., HIROSAWA, I. & KAWANISHI, S. 2008. Mechanism of metal-mediated DNA damage and apoptosis induced by 6-hydroxydopamine in neuroblastoma SH-SY5Y cells. *Free Radic Res,* 42**,** 651-60.

KONG, X., ZHOU, T., NEUBERT, H., LIU, Z. & HIDER, R. C. 2006. 3-Hydroxy-2-(5-hydroxypentyl)-4H-chromen-4-one: a bidentate or tridentate iron(III) ligand? *J Med Chem,* 49**,** 3028-31.

KONTOGHIORGHES, G. 1991. In vivo testing of oral iron chelators intended for clinical use. *Blood,* 78**,** 535-7.

KONTOGHIORGHES, G. J. 1995. Comparative efficacy and toxicity of desferrioxamine, deferiprone and other iron and aluminium chelating drugs. *Toxicology Letters,* 80**,** 1-18.

KONTOGHIORGHES, G. J., BARR, J., NORTEY, P. & SHEPPARD, L. 1993. Selection of a new generation of orally active alpha-ketohydroxypyridine iron chelators intended for use in the treatment of iron overload. *Am J Hematol,* 42**,** 340-9.

KORDOWER, J. H., KANAAN, N. M., CHU, Y., SURESH BABU, R., STANSELL, J., TERPSTRA, B. T., SORTWELL, C. E., STEECE-COLLIER, K. & COLLIER, T. J. 2006. Failure of proteasome inhibitor administration to provide a model of Parkinson's disease in rats and monkeys. *Annals of Neurology,* 60**,** 264-268.

KOSTRZEWA, R. M. & JACOBOWITZ, D. M. 1974. Pharmacological Actions of 6-Hydroxydopamine. *Pharmacological Reviews,* 26**,** 199.

KOVALEVICH, J. & LANGFORD, D. 2013a. Considerations for the use of SH-SY5Y neuroblastoma cells in neurobiology. *Methods Mol Biol,* 1078**,** 9-21.

KRESS, G. J. & MENNERICK, S. 2009. Action potential initiation and propagation: upstream influences on neurotransmission. *Neuroscience,* 158**,** 211-222.

KRUSZEWSKI, M. 2003. Labile iron pool: the main determinant of cellular response to oxidative stress. *Mutat Res,* 531**,** 81-92.

KUDIN, A. P., BIMPONG-BUTA, N. Y., VIELHABER, S., ELGER, C. E. & KUNZ, W. S. 2004. Characterization of superoxide-producing sites in isolated brain mitochondria. *J Biol Chem,* 279**,** 4127-35.

KWIATKOWSKI, A., RYCKEWAERT, G., JISSENDI TCHOFO, P., MOREAU, C., VUILLAUME, I., CHINNERY, P. F., DESTEE, A., DEFEBVRE, L. & DEVOS, D. 2012. Long-term improvement under deferiprone in a case of neurodegeneration with brain iron accumulation. *Parkinsonism Relat Disord,* 18**,** 110-2.

LANGAN, T. J. & CHOU, R. C. 2011. Synchronization of mammalian cell cultures by serum deprivation. *Methods Mol Biol,* 761**,** 75-83.

LEAVER, K. R., ALLBUTT, H. N., CREBER, N. J., KASSIOU, M. & HENDERSON, J. M. 2009. Oral pre-treatment with epigallocatechin gallate in 6-OHDA lesioned rats produces subtle symptomatic relief but not neuroprotection. *Brain Research Bulletin,* 80**,** 397-402.

LEE, C. S., SAUER, H. & BJORKLUND, A. 1996. Dopaminergic neuronal degeneration and motor impairments following axon terminal lesion by instrastriatal 6-hydroxydopamine in the rat. *Neuroscience,* 72**,** 641-53.

LEE, G., DALLAS, S., HONG, M. & BENDAYAN, R. 2001. Drug transporters in the central nervous system: brain barriers and brain parenchyma considerations. *Pharmacol Rev,* 53**,** 569-96.

LEHMENSIEK, V., TAN, E. M., LIEBAU, S., LENK, T., ZETTLMEISL, H., SCHWARZ, J. & STORCH, A. 2006. Dopamine transporter-mediated cytotoxicity of 6-hydroxydopamine in vitro depends on expression of mutant alpha-synucleins related to Parkinson's disease. *Neurochem Int,* 48**,** 329-40.

LEPPENS-LUISIER, G., URNER, F. & SAKKAS, D. 2001. Facilitated glucose transporters play a crucial role throughout mouse preimplantation embryo development. *Human Reproduction,* 16**,** 1229-1236.

LEVENSON, C. W., CUTLER, R. G., LADENHEIM, B., CADET, J. L., HARE, J. & MATTSON, M. P. 2004. Role of dietary iron restriction in a mouse model of Parkinson's disease. *Experimental Neurology,* 190**,** 506-514.

LEVI, S. & ROVIDA, E. 2015. Neuroferritinopathy: From ferritin structure modification to pathogenetic mechanism. *Neurobiology of Disease,* 81**,** 134-143.

LEVITES, Y., WEINREB, O., MAOR, G., YOUDIM, M. B. & MANDEL, S. 2001. Green tea polyphenol (-)-epigallocatechin-3-gallate prevents N-methyl-4-phenyl-1,2,3,6-tetrahydropyridine-induced dopaminergic neurodegeneration. *J Neurochem,* 78**,** 1073-82.

LI, J., LU, Z., KONG, X., MA, Y., ZHANG, X., BANSAL, S. S., ABBATE, V. & HIDER, R. C. 2015. Design and synthesis of novel pegylated iron chelators with decreased metabolic rate. *Future Med Chem,* 7**,** 2439-49.

LI, N., RAGHEB, K., LAWLER, G., STURGIS, J., RAJWA, B., MELENDEZ, J. A. & ROBINSON, J. P. 2003. Mitochondrial complex I inhibitor rotenone induces apoptosis through enhancing mitochondrial reactive oxygen species production. *J Biol Chem,* 278**,** 8516-25.

LI, X. P., XIE, W. J., ZHANG, Z., KANSARA, S., JANKOVIC, J. & LE, W. D. 2012. A mechanistic study of proteasome inhibition-induced iron misregulation in dopamine neuron degeneration. *Neurosignals,* 20**,** 223-36.

LI, Y., PAN, K., CHEN, L., NING, J.-L., LI, X., YANG, T., TERRANDO, N., GU, J. & TAO, G. 2016. Deferoxamine regulates neuroinflammation and iron homeostasis in a mouse model of postoperative cognitive dysfunction. *Journal of Neuroinflammation,* 13**,** 268.

LIDDELOW, S. A. 2011. Fluids and barriers of the CNS: a historical viewpoint. *Fluids and Barriers of the CNS,* 8**,** 2-2.

LIDDELOW, S. A. 2015. Development of the choroid plexus and blood-CSF barrier. *Front Neurosci,* 9**,** 32.

LIMENTA, L. M. G., JIRASOMPRASERT, T., TANKANITLERT, J., SVASTI, S., WILAIRAT, P., CHANTHARAKSRI, U., FUCHAROEN, S. & MORALES, N. P. 2008. UGT1A6 genotype-related pharmacokinetics of deferiprone (L1) in healthy volunteers. *British Journal of Clinical Pharmacology,* 65**,** 908-916.

LIN, M. K. & FARRER, M. J. 2014. Genetics and genomics of Parkinson's disease. *Genome Medicine,* 6**,** 48.

LIPINSKI, C. A., LOMBARDO, F., DOMINY, B. W. & FEENEY, P. J. 2001. Experimental and computational approaches to estimate solubility and permeability in drug discovery and development settings. *Adv Drug Deliv Rev,* 46**,** 3-26.

LIU, M. & BING, G. 2011. Lipopolysaccharide Animal Models for Parkinson's Disease. *Parkinson's Disease,* 2011**,** 327089.

LIU, X. & CHEN, C. 2015. Free Drug Hypothesis for CNS Drug Candidates. *Blood-Brain Barrier in Drug Discovery.* John Wiley & Sons, Inc.

LIU, X., TESTA, B. & FAHR, A. 2011. Lipophilicity and its relationship with passive drug permeation. *Pharm Res,* 28**,** 962-77.

LIU, X., TU, M., KELLY, R. S., CHEN, C. & SMITH, B. J. 2004. Development of a computational approach to predict blood-brain barrier permeability. *Drug Metab Dispos,* 32**,** 132-9.

LOCKMAN, P. R., KOZIARA, J., RODER, K. E., PAULSON, J., ABBRUSCATO, T. J., MUMPER, R. J. & ALLEN, D. D. 2003. In vivo and in vitro assessment of baseline blood-brain barrier parameters in the presence of novel nanoparticles. *Pharm Res,* 20**,** 705-13.

LOHLE, M. & REICHMANN, H. 2010. Clinical neuroprotection in Parkinson's disease - still waiting for the breakthrough. *J Neurol Sci,* 289**,** 104-14.

LONG-SMITH, C. M., SULLIVAN, A. M. & NOLAN, Y. M. 2009. The influence of microglia on the pathogenesis of Parkinson's disease. *Prog Neurobiol,* 89**,** 277-87.

LOPES, U. G., ERHARDT, P., YAO, R. & COOPER, G. M. 1997. p53-dependent induction of apoptosis by proteasome inhibitors. *J Biol Chem,* 272**,** 12893-6.

LORYAN, I. & HAMMARLUND-UDENAES, M. 2014. Drug Discovery Methods for Studying Brain Drug Delivery and Distribution. *In:* HAMMARLUND-UDENAES, M., DE LANGE, E. C. M. & THORNE, R. G. (eds.) *Drug Delivery to the Brain: Physiological Concepts, Methodologies and Approaches.* New York, NY: Springer New York.

LORYAN, I., MELANDER, E., SVENSSON, M., PAYAN, M., KONIG, F., JANSSON, B. & HAMMARLUND-UDENAES, M. 2016. In-depth neuropharmacokinetic analysis of antipsychotics based on a novel approach to estimate unbound target-site concentration in CNS regions: link to spatial receptor occupancy. *Mol Psychiatry,* 21**,** 1527-1536.

LÖSCHER, W. & POTSCHKA, H. 2005. Blood-Brain Barrier Active Efflux Transporters: ATP-Binding Cassette Gene Family. *NeuroRx,* 2**,** 86-98.

LOSCHER, W. & POTSCHKA, H. 2005. Role of drug efflux transporters in the brain for drug disposition and treatment of brain diseases. *Prog Neurobiol,* 76**,** 22-76.

LOTHARIUS, J. & BRUNDIN, P. 2002. Pathogenesis of parkinson's disease: dopamine, vesicles and [alpha]-synuclein. *Nat Rev Neurosci,* 3**,** 932-942.

LOTHARIUS, J., DUGAN, L. L. & O'MALLEY, K. L. 1999. Distinct mechanisms underlie neurotoxin-mediated cell death in cultured dopaminergic neurons. *J Neurosci,* 19**,** 1284-93.

LU, X., KIM-HAN, J. S., HARMON, S., SAKIYAMA-ELBERT, S. E. & O'MALLEY, K. L. 2014. The Parkinsonian mimetic, 6-OHDA, impairs axonal transport in dopaminergic axons. *Molecular Neurodegeneration,* 9**,** 17.

LU, X.-H., FLEMING, S. M., MEURERS, B., ACKERSON, L. C., MORTAZAVI, F., LO, V., HERNANDEZ, D., SULZER, D., JACKSON, G. R., MAIDMENT, N. T., CHESSELET, M.-F. & YANG, X. W. 2009. Bacterial Artificial Chromosome Transgenic Mice Expressing a Truncated Mutant Parkin Exhibit Age-Dependent Hypokinetic Motor Deficits, Dopaminergic Neuron Degeneration, and Accumulation of Proteinase K-Resistant α-Synuclein. *The Journal of Neuroscience,* 29**,** 1962-1976.

LU, Z. 2016. *Investigation of The Efficacy of Some Hydroxypyridinone Iron Chelators.* Doctor of Philosophy, King's College London.

LUISSINT, A.-C., ARTUS, C., GLACIAL, F., GANESHAMOORTHY, K. & COURAUD, P.-O. 2012. Tight junctions at the blood brain barrier: physiological architecture and disease-associated dysregulation. *Fluids and Barriers of the CNS,* 9**,** 23-23.

MACKLER, B., PERSON, R., MILLER, L. R. & FINCH, C. A. 1979. Iron deficiency in the rat: effects on phenylalanine metabolism. Pediatr Res, 13, 1010-1.

MACKLER, B., PERSON, R., MILLER, L. R., INAMDAR, A. R. & FINCH, C. A. 1978. Iron deficiency in the rat: biochemical studies of brain metabolism. Pediatr Res, 12, 217-20.

MAKIS, A., CHALIASOS, N., ALFANTAKI, S., KARAGOUNI, P. & SIAMOPOULOU, A. 2013. Chelation therapy with oral solution of deferiprone in transfusional iron-overloaded children with hemoglobinopathies. *Anemia,* 2013**,** 121762.

MANDEL, S., GRUNBLATT, E. & YOUDIM, M. 2000. cDNA microarray to study gene expression of dopaminergic neurodegeneration and neuroprotection in MPTP and 6-hydroxydopamine models: implications for idiopathic Parkinson's disease. J Neural Transm Suppl, 117-24.

MANDEL, S., MAOR, G. & YOUDIM, M. B. 2004. Iron and alpha-synuclein in the substantia nigra of MPTP-treated mice: effect of neuroprotective drugs R-apomorphine and green tea polyphenol (-)-epigallocatechin-3-gallate. *J Mol Neurosci,* 24**,** 401-16.

MARELLA, M., SEO, B. B., YAGI, T. & MATSUNO-YAGI, A. 2009. Parkinson's disease and mitochondrial complex I: a perspective on the Ndi1 therapy. Journal of bioenergetics and biomembranes, 41, 493-497.

MARIANI, E., POLIDORI, M. C., CHERUBINI, A. & MECOCCI, P. 2005. Oxidative stress in brain aging, neurodegenerative and vascular diseases: an overview. *J Chromatogr B Analyt Technol Biomed Life Sci,* 827.

MARILYN J. CIPOLLA 2009. *The Cerebral Circulation,* San Rafael (CA), Morgan & Claypool Life Sciences.

MARINHO, H. S., REAL, C., CYRNE, L., SOARES, H. & ANTUNES, F. 2014. Hydrogen peroxide sensing, signaling and regulation of transcription factors. *Redox Biology,* 2**,** 535-562.

MARINOVA-MUTAFCHIEVA, L., SADEGHIAN, M., BROOM, L., DAVIS, J. B., MEDHURST, A. D. & DEXTER, D. T. 2009. Relationship between microglial activation and dopaminergic neuronal loss in the substantia nigra: a time course study in a 6-hydroxydopamine model of Parkinson's disease. *J Neurochem,* 110**,** 966-75.

MARTI, M. J., SAURA, J., BURKE, R. E., JACKSON-LEWIS, V., JIMENEZ, A., BONASTRE, M. & TOLOSA, E. 2002. Striatal 6-hydroxydopamine induces apoptosis of nigral neurons in the adult rat. *Brain Res,* 958**,** 185-91.

MARTIN-BASTIDA, A., WARD, R. J., NEWBOULD, R., PICCINI, P., SHARP, D., KABBA, C., PATEL, M. C., SPINO, M., CONNELLY, J., TRICTA, F., CRICHTON, R. R. & DEXTER, D. T. 2017. Brain iron chelation by deferiprone in a phase 2 randomised double-blinded placebo controlled clinical trial in Parkinson's disease. 7**,** 1398.

MAURER, T. S., DEBARTOLO, D. B., TESS, D. A. & SCOTT, D. O. 2004. RELATIONSHIP BETWEEN EXPOSURE AND NONSPECIFIC BINDING OF THIRTY-THREE CENTRAL NERVOUS SYSTEM DRUGS IN MICE. *Drug Metabolism and Disposition,* 33**,** 175.

MAYER, F., MAYER, N., CHINN, L., PINSONNEAULT, R. L., KROETZ, D. & BAINTON, R. J. 2009. Evolutionary conservation of vertebrate blood-brain barrier chemoprotective mechanisms in Drosophila. *The Journal of neuroscience : the official journal of the Society for Neuroscience,* 29**,** 3538-3550.

MCNAUGHT, K. S. & JENNER, P. 2000. Dysfunction of rat forebrain astrocytes in culture alters cytokine and neurotrophic factor release. *Neurosci Lett,* 285**,** 61-5.

MCNAUGHT, K. S., BELIZAIRE, R., ISACSON, O., JENNER, P. & OLANOW, C. W. 2003. Altered proteasomal function in sporadic Parkinson's disease. *Exp Neurol,* 179**,** 38-46.

MCNAUGHT, K. S., MYTILINEOU, C., JNOBAPTISTE, R., YABUT, J., SHASHIDHARAN, P., JENNERT, P. & OLANOW, C. W. 2002. Impairment of the ubiquitin-proteasome system causes dopaminergic cell death and inclusion body formation in ventral mesencephalic cultures. *J Neurochem,* 81**,** 301-6.

MCNAUGHT, K. S., PERL, D. P., BROWNELL, A. L. & OLANOW, C. W. 2004. Systemic exposure to proteasome inhibitors causes a progressive model of Parkinson's disease. *Ann Neurol,* 56**,** 149-62.

MCNAUGHT, K. S., SHASHIDHARAN, P., PERL, D. P., JENNER, P. & OLANOW, C. W. 2002b. Aggresome-related biogenesis of Lewy bodies. *Eur J Neurosci,* 16**,** 2136-48.

MEISER, J., WEINDL, D. & HILLER, K. 2013. Complexity of dopamine metabolism. *Cell Communication and Signaling : CCS,* 11**,** 34-34.

MENSCH, J., OYARZABAL, J., MACKIE, C. & AUGUSTIJNS, P. 2009. In Vivo, In Vitro and In Silico Methods for Small Molecule Transfer Across the BBB. *Journal of Pharmaceutical Sciences,* 98**,** 4429-4468.

MEREISH, K. A., ROSENBERG, H. & COBBY, J. 1982. Glucosylated albumin and its influence on salicylate binding. *J Pharm Sci,* 71**,** 235-8.

MERGENTHALER, P., LINDAUER, U., DIENEL, G. A. & MEISEL, A. 2013. Sugar for the brain: the role of glucose in physiological and pathological brain function. *Trends in neurosciences,* 36**,** 587-597.

MIKITSH, J. L. & CHACKO, A.-M. 2014. Pathways for Small Molecule Delivery to the Central Nervous System Across the Blood-Brain Barrier. *Perspectives in Medicinal Chemistry,* 6**,** 11-24.

MILLS, E., DONG, X.-P., WANG, F. & XU, H. 2010. Mechanisms of Brain Iron Transport: Insight into Neurodegeneration and CNS Disorders. *Future medicinal chemistry,* 2**,** 51-51.

MISRA, A., GANESH, S., SHAHIWALA, A. & SHAH, S. P. 2003. Drug delivery to the central nervous system: a review. *J Pharm Pharm Sci,* 6**,** 252-73.

MIYAZAKI, I., ASANUMA, M., HOZUMI, H., MIYOSHI, K. & SOGAWA, N. 2007. Protective effects of metallothionein against dopamine quinone-induced dopaminergic neurotoxicity. *FEBS Letters,* 581**,** 5003-5008.

MIZUNO, Y., OHTA, S., TANAKA, M., TAKAMIYA, S., SUZUKI, K., SATO, T., OYA, H., OZAWA, T. & KAGAWA, Y. 1989. Deficiencies in complex I subunits of the respiratory chain in Parkinson's disease. *Biochem Biophys Res Commun,* 163**,** 1450-5.

MOCHIZUKI, H. & YASUDA, T. 2012. Iron accumulation in Parkinson's disease. *J Neural Transm (Vienna),* 119**,** 1511-4.

MOHAN, A., JOSEPH, S., SIDHARTHAN, N. & MURALI, D. 2015. Carbimazole-induced agranulocytosis. *Journal of Pharmacology & Pharmacotherapeutics,* 6**,** 228-230.

MOLENDA, J. J., JONES, M. M., JOHNSTON, D. S., WALKER, E. M., JR. & CANNON, D. J. 1994. Mobilization of iron by chiral and achiral anionic 3-hydroxypyrid-4-ones. *J Med Chem,* 37**,** 4363-70.

MOLINA-HOLGADO, F., GAETA, A., FRANCIS, P. T., WILLIAMS, R. J. & HIDER, R. C. 2008. Neuroprotective actions of deferiprone in cultured cortical neurones and SHSY-5Y cells. *Journal of Neurochemistry,* 105**,** 2466-2476.

MOLINO, Y., JABES, F., LACASSAGNE, E., GAUDIN, N. & KHRESTCHATISKY, M. 2014. Setting-up an In Vitro Model of Rat Blood-brain Barrier (BBB): A Focus on BBB Impermeability and Receptor-mediated Transport. *Jove-Journal of Visualized Experiments*.

MOON, S. H., KIM, S. E., SON, J. Y., JUNG, I. S., KIM, S. J., KIM, J. S., MOON, B. S., LEE, J. J., LEE, B. C. & KIM, Y. K. 2010. Time course of striatal dopamine transporter loss in striatal 6-hydroxydopamine rat model of Parkinson's disease: A study with [123I]beta-CIT and small animal SPECT. *Journal of Nuclear Medicine,* 51**,** 1758.

MOOS, T. & MORGAN, E. H. 2001. Restricted transport of anti-transferrin receptor antibody (OX26) through the blood-brain barrier in the rat. *Journal of Neurochemistry,* 79**,** 119-129.

MORGAN, D. M. L. 1998. Tetrazolium (MTT) Assay for Cellular Viability and Activity. *In:* MORGAN, D. M. L. (ed.) *Polyamine Protocols.* Totowa, NJ: Humana Press.

MOTAIS, R., FIEVET, B., GARCIA-ROMEU, F. & THOMAS, S. 1989. Na+-H+ exchange and pH regulation in red blood cells: role of uncatalyzed H2CO3 dehydration. *Am J Physiol,* 256**,** C728-35.

MOUNSEY, R. B. & TEISMANN, P. 2012. Chelators in the treatment of iron accumulation in Parkinson's disease. *Int J Cell Biol,* 2012**,** 983245.

MOUROT-COTTET, R., MALOISEL, F., SÉVERAC, F., KELLER, O., VOGEL, T., TEBACHER, M., WEBER, J.-C., KALTENBACH, G., GOTTENBERG, J.-E., GOICHOT, B., SIBILIA, J., KORGANOW, A.-S., HERBRECHT, R. & ANDRÈS, E. 2016. Idiosyncratic Drug-Induced Severe Neutropenia and Agranulocytosis in Elderly Patients (≥75 years): A Monocentric Cohort Study of 61 Cases. *Drugs - Real World Outcomes,* 3**,** 393-399.

MUECKLER, M. & MAKEPEACE, C. (2009) Model of the exofacial substrate-binding site and helical folding of the human glut1 glucose transporter based on scanning mutagenesis. *Biochemistry,* 48**,** 5934-5942.

MUECKLER, M. & THORENS, B. 2013. The SLC2 (GLUT) family of membrane transporters. *Mol Aspects Med,* 34**,** 121-38.

MUNOZ, Y., CARRASCO, C. M., CAMPOS, J. D., AGUIRRE, P. & NUNEZ, M. T. 2016. Parkinson's Disease: The Mitochondria-Iron Link. *Parkinsons Dis,* 2016**,** 7049108.

MURAKAMI, H., TAKANAGA, H., MATSUO, H., OHTANI, H. & SAWADA, Y. 2000. Comparison of blood-brain barrier permeability in mice and rats using in situ brain perfusion technique. *Am J Physiol Heart Circ Physiol,* 279**,** H1022-8.

NAGATSU, T., MOGI, M., ICHINOSE, H. & TOGARI, A. 2000. Cytokines in Parkinson's disease. *J Neural Transm Suppl***,** 143-51.

NAIR, V. D., MCNAUGHT, K. S., GONZALEZ-MAESO, J., SEALFON, S. C. & OLANOW, C. W. 2006. p53 mediates nontranscriptional cell death in dopaminergic cells in response to proteasome inhibition. *J Biol Chem,* 281**,** 39550-60.

NAKASO, K., YOSHIMOTO, Y., YANO, H., TAKESHIMA, T. & NAKASHIMA, K. 2004. p53-mediated mitochondrial dysfunction by proteasome inhibition in dopaminergic SH-SY5Y cells. *Neurosci Lett,* 354**,** 213-6.

NAPOLITANO, A., CRESCENZI, O., PEZZELLA, A. & PROTA, G. 1995. Generation of the neurotoxin 6-hydroxydopamine by peroxidase/H2O2 oxidation of dopamine. *J Med Chem,* 38**,** 917-22.

NAVNTOFT, C. A. & DREYER, J. K. 2016. How compensation breaks down in Parkinson's disease: Insights from modeling of denervated striatum. *Movement Disorders,* 31**,** 280-289.

NGUYEN, L. A., HE, H. & PHAM-HUY, C. 2006. Chiral drugs: an overview. *Int J Biomed Sci,* 2**,** 85-100.

NI, Z., BIKADI, Z., ROSENBERG, M. F. & MAO, Q. 2010. Structure and Function of the Human Breast Cancer Resistance Protein (BCRP/ABCG2). *Current drug metabolism,* 11**,** 603-617.

NIKOLETOPOULOU, V., MARKAKI, M., PALIKARAS, K. & TAVERNARAKIS, N. 2013. Crosstalk between apoptosis, necrosis and autophagy. *Biochimica et Biophysica Acta (BBA) - Molecular Cell Research,* 1833**,** 3448-3459.

NOVAKOVIC, J., TESORO, A., THIESSEN, J. J. & SPINO, M. 2004. Metabolic and pharmacokinetic evaluation of a novel 3-hydroxypyridinone iron chelator, CP502, in the rat. *Eur J Drug Metab Pharmacokinet,* 29**,** 221-4.

OFFEN, D., ZIV, I., PANET, H., WASSERMAN, L., STEIN, R., MELAMED, E. & BARZILAI, A. 1997. Dopamine-induced apoptosis is inhibited in PC12 cells expressing Bcl-2. *Cell Mol Neurobiol,* 17**,** 289-304.

OJELABI, O. & CARRUTHERS, A. 2015. Acute Stimulation of GLUT1 Cell Surface Localization in Blood-Brain Barrier Endothelial Cells. *Faseb Journal,* 29.

OKURA, T., ITO, R., ISHIGURO, N., TAMAI, I. & DEGUCHI, Y. 2007. Blood-brain barrier transport of pramipexole, a dopamine D2 agonist. *Life Sci,* 80**,** 1564-71.

OLANOW, C. W. & PRUSINER, S. B. 2009b. Is Parkinson's disease a prion disorder? *Proc Natl Acad Sci U S A,* 106.

OLANOW, C. W., PERL, D. P., DEMARTINO, G. N. & MCNAUGHT, K. S. 2004. Lewy-body formation is an aggresome-related process: a hypothesis. *Lancet Neurol,* 3**,** 496-503.

OLANOW, C. W., STERN, M. B. & SETHI, K. 2009a. The scientific and clinical basis for the treatment of Parkinson disease (2009). *Neurology,* 72**,** S1-136.

OLDS, M. E., JACQUES, D. B. & KOPYOV, O. 2006. Relation between rotation in the 6-OHDA lesioned rat and dopamine loss in striatal and substantia nigra subregions. *Synapse,* 59**,** 532-44.

OLIVIERI, N. F., BRITTENHAM, G. M., MCLAREN, C. E., TEMPLETON, D. M., CAMERON, R. G., MCCLELLAND, R. A., BURT, A. D. & FLEMING, K. A. 1998. Long-term safety and effectiveness of iron-chelation therapy with deferiprone for thalassemia major. *N Engl J Med,* 339**,** 417-23.

PAIBOONSUKWONG, K., HIDER, R. C. & YU, Y. 2016. An open-label, single center and single dose study to assess safety tolerability and pharmacokinetics of CN128 in healthy volunteers. *In:* CENTER, T. R. (ed.). Thailand.

PAJOUHESH, H. & LENZ, G. R. 2005. Medicinal Chemical Properties of Successful Central Nervous System Drugs. *NeuroRx,* 2**,** 541-553.

PALACINO, J. J., SAGI, D., GOLDBERG, M. S., KRAUSS, S., MOTZ, C., WACKER, M., KLOSE, J. & SHEN, J. 2004. Mitochondrial dysfunction and oxidative damage in parkin-deficient mice. *J Biol Chem,* 279**,** 18614-22.

PÅLSSON-MCDERMOTT, E. M. & O'NEILL, L. A. J. 2004. Signal transduction by the lipopolysaccharide receptor, Toll-like receptor-4. *Immunology,* 113**,** 153-162.

PAN, G., GIRI, N. & ELMQUIST, W. F. 2007. Abcg2/Bcrp1 Mediates the Polarized Transport of Antiretroviral Nucleosides Abacavir and Zidovudine. *Drug Metabolism and Disposition,* 35**,** 1165-1173.

PAN, M. H., GHAI, G. & HO, C. T. 2008. Food bioactives apoptosis, and cancer. *Mol Nutr Food Res,* 52.

PAN, Y., SCANLON, M. J., OWADA, Y., YAMAMOTO, Y., PORTER, C. J. & NICOLAZZO, J. A. 2015. Fatty Acid-Binding Protein 5 Facilitates the Blood-Brain Barrier Transport of Docosahexaenoic Acid. *Mol Pharm,* 12**,** 4375-85.

PAN, Y.-H., SADER, K., POWELL, J. J., BLELOCH, A., GASS, M., TRINICK, J., WARLEY, A., LI, A., BRYDSON, R. & BROWN, A. 2009. 3D morphology of the human hepatic ferritin mineral core: New evidence for a subunit structure revealed by single particle analysis of HAADF-STEM images. *Journal of Structural Biology,* 166**,** 22-31.

PANG, K. S. 2003. Modeling of intestinal drug absorption: roles of transporters and metabolic enzymes (for the Gillette Review Series). *Drug Metab Dispos,* 31**,** 1507-19.

PANKRATZ, N. & FOROUD, T. 2007. Genetics of Parkinson disease. *Genet Med,* 9**,** 801-811.

PANOPOULOS, A., HARRAZ, M., ENGELHARDT, J. F. & ZANDI, E. 2005. Iron-mediated H2O2 production as a mechanism for cell type-specific inhibition of tumor necrosis factor alpha-induced but not interleukin-1beta-induced IkappaB kinase complex/nuclear factor-kappaB activation. *J Biol Chem,* 280**,** 2912-23.

PAPADEMETRIOU, I. T. & PORTER, T. 2015. Promising approaches to circumvent the blood-brain barrier: progress, pitfalls and clinical prospects in brain cancer. *Therapeutic delivery,* 6**,** 989-1016.

PARDRIDGE, W. M. 1983. Brain metabolism: a perspective from the blood-brain barrier. *Physiol Rev,* 63**,** 1481-535.

PARDRIDGE, W. M. 2002a. Drug and Gene Delivery to the Brain. *Neuron,* 36**,** 555-558.

PARDRIDGE, W. M. 2002b. Drug and gene targeting to the brain with molecular Trojan horses. *Nat Rev Drug Discov,* 1**,** 131-9.

PARDRIDGE, W. M. 2003. Blood-brain barrier drug targeting: the future of brain drug development. *Mol Interv,* 3**,** 90-105, 51.

PARDRIDGE, W. M. 2005. The Blood-Brain Barrier: Bottleneck in Brain Drug Development. *NeuroRx,* 2**,** 3-14.

PARDRIDGE, W. M. 2012. Drug transport across the blood–brain barrier. *Journal of Cerebral Blood Flow & Metabolism,* 32**,** 1959-1972.

PARDRIDGE, W. M., TRIGUERO, D., YANG, J. & CANCILLA, P. A. 1990. Comparison of in vitro and in vivo models of drug transcytosis through the blood-brain barrier. *J Pharmacol Exp Ther,* 253**,** 884-91.

PARIS-ROBIDAS, S., BROUARD, D., EMOND, V., PARENT, M. & CALON, F. 2016. Internalization of targeted quantum dots by brain capillary endothelial cells in vivo. *J Cereb Blood Flow Metab,* 36**,** 731-42.

PARKER, W. D., PARKS, J. K. & SWERDLOW, R. H. 2008. Complex I Deficiency in Parkinson's Disease Frontal Cortex. *Brain research,* 1189**,** 215-218.

PATLAK, C. S. & BLASBERG, R. G. 1985. Graphical evaluation of blood-to-brain transfer constants from multiple-time uptake data. Generalizations. *J Cereb Blood Flow Metab,* 5**,** 584-90.

PATLAK, C. S., BLASBERG, R. G. & FENSTERMACHER, J. D. 1983. Graphical evaluation of blood-to-brain transfer constants from multiple-time uptake data. *J Cereb Blood Flow Metab,* 3**,** 1-7.

PAVAN, B., DALPIAZ, A., CILIBERTI, N., BIONDI, C., MANFREDINI, S. & VERTUANI, S. 2008. Progress in drug delivery to the central nervous system by the prodrug approach. *Molecules,* 13**,** 1035-65.

PENG, J., MAO, X. O., STEVENSON, F. F., HSU, M. & ANDERSEN, J. K. 2004. The herbicide paraquat induces dopaminergic nigral apoptosis through sustained activation of the JNK pathway. *J Biol Chem,* 279**,** 32626-32.

PENTTINEN, A. M., SULEYMANOVA, I., ALBERT, K., ANTTILA, J., VOUTILAINEN, M. H. & AIRAVAARA, M. 2016. Characterization of a new low-dose 6-hydroxydopamine model of Parkinson's disease in rat. *J Neurosci Res,* 94**,** 318-28.

PERRY, T. L. & YONG, V. W. 1986. Idiopathic Parkinson's disease, progressive supranuclear palsy and glutathione metabolism in the substantia nigra of patients. *Neuroscience Letters,* 67**,** 269-274.

PETIT, A., KAWARAI, T., PAITEL, E., SANJO, N., MAJ, M., SCHEID, M., CHEN, F., GU, Y., HASEGAWA, H., SALEHI-RAD, S., WANG, L., ROGAEVA, E., FRASER, P., ROBINSON, B., ST GEORGE-HYSLOP, P. & TANDON, A. 2005. Wild-type PINK1 prevents basal and induced neuronal apoptosis, a protective effect abrogated by Parkinson disease-related mutations. *J Biol Chem,* 280**,** 34025-32.

PETROVITCH, H., ROSS, G. W., ABBOTT, R. D., SANDERSON, W. T., SHARP, D. S., TANNER, C. M., MASAKI, K. H., BLANCHETTE, P. L., POPPER, J. S., FOLEY, D., LAUNER, L. & WHITE, L. R. 2002. Plantation work and risk of Parkinson disease in a population-based longitudinal study. *Arch Neurol,* 59**,** 1787-92.

PETRUCELLI, L., O'FARRELL, C., LOCKHART, P. J., BAPTISTA, M., KEHOE, K., VINK, L., CHOI, P., WOLOZIN, B., FARRER, M., HARDY, J. & COOKSON, M. R. 2002. Parkin protects against the toxicity associated with mutant alpha-synuclein: proteasome dysfunction selectively affects catecholaminergic neurons. *Neuron,* 36**,** 1007-19.

PEURA, L., MALMIOJA, K., HUTTUNEN, K., LEPPANEN, J., HAMALAINEN, M., FORSBERG, M. M., GYNTHER, M., RAUTIO, J. & LAINE, K. 2013. Design, synthesis and brain uptake of LAT1-targeted amino acid prodrugs of dopamine. *Pharm Res,* 30**,** 2523-37.

PEURA, L., MALMIOJA, K., LAINE, K., LEPPANEN, J., GYNTHER, M., ISOTALO, A. & RAUTIO, J. 2011. Large amino acid transporter 1 (LAT1) prodrugs of valproic acid: new prodrug design ideas for central nervous system delivery. *Mol Pharm,* 8**,** 1857-66.

PFAFFEN, S., ABDULQADIR, R., LE BRUN, N. E. & MURPHY, M. E. 2013. Mechanism of ferrous iron binding and oxidation by ferritin from a pennate diatom. *J Biol Chem,* 288**,** 14917-25.

PINTO, E., SIGAUD-KUTNER, T. C. S., LEITÃO, M. A. S., OKAMOTO, O. K., MORSE, D. & COLEPICOLO, P. 2003. HEAVY METAL–INDUCED OXIDATIVE STRESS IN ALGAE1. *Journal of Phycology,* 39**,** 1008-1018.

PITT, J. J. 2009. Principles and Applications of Liquid Chromatography-Mass Spectrometry in Clinical Biochemistry. *The Clinical Biochemist Reviews,* 30**,** 19-34.

POGGIALI, E., CASSINERIO, E., ZANABONI, L. & CAPPELLINI, M. D. 2012. An update on iron chelation therapy. *Blood Transfusion,* 10**,** 411-422.

PONKA, P., BEAUMONT, C. & RICHARDSON, D. R. 1998. Function and regulation of transferrin and ferritin. *Seminars in hematology,* 35**,** 35-54.

POPA-WAGNER, A., MITRAN, S., SIVANESAN, S., CHANG, E. & BUGA, A.-M. 2013. ROS and Brain Diseases: The Good, the Bad, and the Ugly. *Oxidative Medicine and Cellular Longevity,* 2013**,** 14.

PORTER, J. B. 1996. Evaluation of new iron chelators for clinical use. *Acta Haematol,* 95**,** 13-25.

PORTER, J. B., ABEYSINGHE, R. D., HOYES, K. P., BARRA, C., HUEHNS, E. R., BROOKS, P. N., BLACKWELL, M. P., ARANETA, M., BRITTENHAM, G., SINGH, S. & ET AL. 1993. Contrasting interspecies efficacy and toxicology of 1,2-diethyl-3-hydroxypyridin-4-one, CP94, relates to differing metabolism of the iron chelating site. *Br J Haematol,* 85**,** 159-68.

PORTER, J. B., HOYES, K. P., ABEYSINGHE, R. D., BROOKS, P. N., HUEHNS, E. R. & HIDER, R. C. 1991. Comparison of the subacute toxicity and efficacy of 3-hydroxypyridin-4-one iron chelators in overloaded and nonoverloaded mice. *Blood,* 78**,** 2727-34.

PORTER, J. B., HUEHNS, E. R. & HIDER, R. C. 1989. The development of iron chelating drugs. *Bailliere's clinical haematology,* 2**,** 257-292.

PORTER, J. B., MORGAN, J., HOYES, K. P., BURKE, L. C., HUEHNS, E. R. & HIDER, R. C. 1990. Relative oral efficacy and acute toxicity of hydroxypyridin-4-one iron chelators in mice. *Blood,* 76**,** 2389-96.

PORTER, J. B., SINGH, S., HOYES, K. P., EPEMOLU, O., ABEYSINGHE, R. D. & HIDER, R. C. 1994. Lessons from preclinical and clinical studies with 1,2-diethyl-3-hydroxypyridin-4-one, CP94 and related compounds. *Adv Exp Med Biol,* 356**,** 361-70.

PRASAD, R., ATUL, KOLLA, V. K., LEGAC, J., SINGHAL, N., NAVALE, R., ROSENTHAL, P. J. & SIJWALI, P. S. 2013. Blocking Plasmodium falciparum development via dual inhibition of hemoglobin degradation and the ubiquitin proteasome system by MG132. *PLoS One,* 8**,** e73530.

PREMYSLOVA, M., XU, J., WANG, L., XIONG, H., NITIA-NOOTAN, T., DEOSARAN, E., PENG, C., CALLAGHAN, D., ZANG, W., RABADIA, V., FEENEY, C., WODZINSKA, J., SPINO, M. & CONNELLY, J. 2016. Neuroprotective Properties of Apo6856, a Novel Hydroxypyridinone Iron Chelator, in Alzheimer's Disease (P5.208). *Neurology,* 86.

PRESGRAVES, S. P., AHMED, T., BORWEGE, S. & JOYCE, J. N. 2004. Terminally differentiated SH-SY5Y cells provide a model system for studying neuroprotective effects of dopamine agonists. *Neurotox Res,* 5**,** 579-98.

PRESTON, J., AL-SARRAF, H. & SEGAL, M. 1995. Permeability of the developing blood-brain barrier to 14C-mannitol using the rat in situ brain perfusion technique. *Developmental Brain Research,* 87**,** 69-76.

PRIYADARSHI, A., KHUDER, S. A., SCHAUB, E. A. & PRIYADARSHI, S. S. 2001. Environmental risk factors and Parkinson's disease: a metaanalysis. *Environ Res,* 86**,** 122-7.

PRZEDBORSKI, S., LEVIVIER, M., JIANG, H., FERREIRA, M., JACKSON-LEWIS, V., DONALDSON, D. & TOGASAKI, D. M. 1995. Dose-dependent lesions of the dopaminergic nigrostriatal pathway induced by intrastriatal injection of 6-hydroxydopamine. *Neuroscience,* 67**,** 631-47.

PULICHERLA, K. K. & VERMA, M. K. 2015. Targeting Therapeutics Across the Blood Brain Barrier (BBB), Prerequisite Towards Thrombolytic Therapy for Cerebrovascular Disorders—an Overview and Advancements. *AAPS PharmSciTech,* 16**,** 223-233.

QIN, Y., FAN, W., CHEN, H., YAO, N., TANG, W., TANG, J., YUAN, W., KUAI, R., ZHANG, Z., WU, Y. & HE, Q. 2010. In vitro and in vivo investigation of glucose-mediated brain-targeting liposomes. *Journal of Drug Targeting,* 18**,** 536-549.

QUANQUAN, G., PING, L., YAZUO, Z., HUALEI, X., YUCAI, L. & XIAOJING, J. 2010. Pharmacokinetics and tissue distribution of deferiprone in rats. *Chinese Journal of Pharmacology and Toxicology***,** 59-63.

QUTUB, A. A. & HUNT, C. A. 2005. Glucose transport to the brain: A systems model. *Brain Research Reviews,* 49**,** 595-617.

RAFAT, C., FAKHOURI, F., RIBEIL, J.-A., DELARUE, R. & LE QUINTREC, M. 2009. Fanconi Syndrome Due to Deferasirox. *American Journal of Kidney Diseases,* 54**,** 931-934.

RAFI, S. B., HEARN, B. R., VEDANTHAM, P., JACOBSON, M. P. & RENSLO, A. R. 2012. Predicting and Improving the Membrane Permeability of Peptidic Small Molecules. *Journal of Medicinal Chemistry,* 55**,** 3163-3169.

RAICHLE, M. E. & GUSNARD, D. A. 2002. Appraising the brain's energy budget. *Proceedings of the National Academy of Sciences,* 99**,** 10237-10239.

RAJAGOPAL, S. 2005. Clozapine, agranulocytosis, and benign ethnic neutropenia. *Postgraduate Medical Journal,* 81**,** 545-546.

RAUSCH, W.-D., HIRATA, Y., NAGATSU, T., RIEDERER, P. & JELLINGER, K. 1988. Tyrosine Hydroxylase Activity in Caudate Nucleus from Parkinson's Disease: Effects of Iron and Phosphorylating Agents. Journal of Neurochemistry, 50, 202-208.

RAUTIO, J., LAINE, K., GYNTHER, M. & SAVOLAINEN, J. 2008. Prodrug approaches for CNS delivery. *Aaps j,* 10**,** 92-102.

RAVINA, B. M., FAGAN, S. C., HART, R. G., HOVINGA, C. A., MURPHY, D. D., DAWSON, T. M. & MARLER, J. R. 2003. Neuroprotective agents for clinical trials in Parkinson's disease: a systematic assessment. *Neurology,* 60**,** 1234-40.

REYES, A. M., BUSTAMANTE, F., RIVAS, C. I., ORTEGA, M., DONNET, C., ROSSI, J. P., FISCHBARG, J. & VERA, J. C. 2002. Nicotinamide is not a substrate of the facilitative hexose transporter GLUT1. *Biochemistry,* 41**,** 8075-81.

REYNOLDS, J. N. J. & WICKENS, J. R. 2000. Substantia nigra dopamine regulates synaptic plasticity and membrane potential fluctuations in the rat neostriatum, in vivo. *Neuroscience,* 99**,** 199-203.

REZNICHENKO, L., KALFON, L., AMIT, T., YOUDIM, M. B. & MANDEL, S. A. 2010. Low dosage of rasagiline and epigallocatechin gallate synergistically restored the nigrostriatal axis in MPTP-induced parkinsonism. *Neurodegener Dis,* 7**,** 219-31.

RILEY, B. E., LOUGHEED, J. C., CALLAWAY, K., VELASQUEZ, M., BRECHT, E., NGUYEN, L., SHALER, T., WALKER, D., YANG, Y., REGNSTROM, K., DIEP, L., ZHANG, Z., CHIOU, S., BOVA, M., ARTIS, D. R., YAO,

N., BAKER, J., YEDNOCK, T. & JOHNSTON, J. A. 2013. Structure and function of Parkin E3 ubiquitin ligase reveals aspects of RING and HECT ligases. *Nat Commun,* 4**,** 1982.

ROBINSON, T. E., MOCSARY, Z., CAMP, D. M. & WHISHAW, I. Q. 1994. Time course of recovery of extracellular dopamine following partial damage to the nigrostriatal dopamine system. *J Neurosci,* 14**,** 2687-96.

ROCHA, S., GOMES, D., LIMA, M., BRONZE-DA-ROCHA, E. & SANTOS-SILVA, A. 2015. Peroxiredoxin 2, glutathione peroxidase, and catalase in the cytosol and membrane of erythrocytes under H2O2-induced oxidative stress. *Free Radic Res,* 49**,** 990-1003.

ROCKWELL, P., YUAN, H., MAGNUSSON, R. & FIGUEIREDO-PEREIRA, M. E. 2000. Proteasome inhibition in neuronal cells induces a proinflammatory response manifested by upregulation of cyclooxygenase-2, its accumulation as ubiquitin conjugates, and production of the prostaglandin PGE(2). *Arch Biochem Biophys,* 374**,** 325-33.

RODRIGUES, R. W. P., GOMIDE, V. C. & CHADI, G. 2003. Striatal injection of 6-hydroxydopamine induces retrograde degeneration and glial activation in the nigrostriatal pathway. *Acta Cirurgica Brasileira,* 18**,** 272-282.

RODRIGUEZ-PALLARES, J., PARGA, J. A., MUNOZ, A., REY, P., GUERRA, M. J. & LABANDEIRA-GARCIA, J. L. 2007. Mechanism of 6-hydroxydopamine neurotoxicity: the role of NADPH oxidase and microglial activation in 6-hydroxydopamine-induced degeneration of dopaminergic neurons. *J Neurochem,* 103**,** 145-56.

ROEDTER, A., WINKLER, C., SAMII, M., WALTER, G. F., BRANDIS, A. & NIKKHAH, G. 2001. Comparison of unilateral and bilateral intrastriatal 6-hydroxydopamine-induced axon terminal lesions: evidence for interhemispheric functional coupling of the two nigrostriatal pathways. *J Comp Neurol,* 432**,** 217-29.

ROSARIO DE LA TORRE, M., CASADO, A., LÓPEZ-FERNÁNDEZ, M. E., CARRASCOSA, D., CASADO, M. C., VENARUCCI, D. & VENARUCCI, V. 1996. Human aging brain disorders: Role of antioxidant enzymes. *Neurochemical Research,* 21**,** 885-888.

ROY, S., PRESTON, J. E., HIDER, R. C. & MA, Y. M. 2010. Glucosylated Deferiprone and Its Brain Uptake: Implications for Developing Glucosylated Hydroxypyridinone Analogues Intended to Cross the Blood-Brain Barrier. *Journal of Medicinal Chemistry,* 53**,** 5886-5889.

RYU, J., ZHANG, R., HONG, B. H., YANG, E. J., KANG, K. A., CHOI, M., KIM, K. C., NOH, S. J., KIM, H. S., LEE, N. H., HYUN, J. W. & KIM, H. S. 2013. Phloroglucinol attenuates motor functional deficits in an animal model of Parkinson's disease by enhancing Nrf2 activity. *PLoS One,* 8**,** e71178.

SAHA, J. K., XIA, J., GRONDIN, J. M., ENGLE, S. K. & JAKUBOWSKI, J. A. 2005. Acute hyperglycemia induced by ketamine/xylazine anesthesia in rats: mechanisms and implications for preclinical models. *Exp Biol Med (Maywood),* 230**,** 777-84.

SAI, T., UCHIDA, K. & NAKAYAMA, H. 2013. Biochemical evaluation of the neurotoxicity of MPTP and MPP(+) in embryonic and newborn mice. J Toxicol Sci, 38, 445-58.

SAKURAI, K. & CEDERBAUM, A. I. 1998. Oxidative stress and cytotoxicity induced by ferric-nitrilotriacetate in HepG2 cells that express cytochrome P450 2E1. *Mol Pharmacol,* 54**,** 1024-35.

SALIBA, A. N., HARB, A. R. & TAHER, A. T. 2015. Iron chelation therapy in transfusion-dependent thalassemia patients: current strategies and future directions. *Journal of Blood Medicine,* 6**,** 197-209.

SAMMARCO, M. C., DITCH, S., BANERJEE, A. & GRABCZYK, E. 2008. Ferritin L and H subunits are differentially regulated on a post-transcriptional level. *J Biol Chem,* 283**,** 4578-87.

SAPORITO, M. S., THOMAS, B. A. & SCOTT, R. W. 2000. MPTP activates c-Jun NH(2)-terminal kinase (JNK) and its upstream regulatory kinase MKK4 in nigrostriatal neurons in vivo. *J Neurochem,* 75**,** 1200-8.

SAUERBECK, A., SCHONBERG, D. L., LAWS, J. L. & MCTIGUE, D. M. 2013. Systemic iron chelation results in limited functional and histological recovery after traumatic spinal cord injury in rats. *Experimental Neurology,* 248**,** 53-61.

SCHAPIRA, A. H. & JENNER, P. 2011. Etiology and pathogenesis of Parkinson's disease. *Mov Disord,* 26**,** 1049-55.

SCHAPIRA, A. H. 2009. Neuroprotection in Parkinson's disease. *Parkinsonism Relat Disord,* 15 Suppl 4**,** S41-3.

SCHAPIRA, A. H., COOPER, J. M., DEXTER, D., CLARK, J. B., JENNER, P. & MARSDEN, C. D. 1990. Mitochondrial complex I deficiency in Parkinson's disease. *J Neurochem,* 54**,** 823-7.

SCHLAG, M. G., HOPF, R. & REDL, H. 2000. Convulsive seizures following subdural application of fibrin sealant containing tranexamic acid in a rat model. *Neurosurgery,* 47**,** 1463-7.

SCHLOSSMACHER, M. G., TOMLINSON, J. J., SANTOS, G., SHUTINOSKI, B., BROWN, E. G., MANUEL, D. & MESTRE, T. 2017. Modelling idiopathic Parkinson disease as a complex illness can inform incidence rate in healthy adults: the P(R)EDIGT score. *The European Journal of Neuroscience,* 45**,** 175-191.

SCHNEIDER, C. A., RASBAND, W. S. & ELICEIRI, K. W. 2012. NIH Image to ImageJ: 25 years of image analysis. *Nat Meth,* 9**,** 671-675.

SELIG, R. A., MADAFIGLIO, J., HABER, M., NORRIS, M. D., WHITE, L. & STEWART, B. W. 1993. Ferritin production and desferrioxamine cytotoxicity in human neuroblastoma cell lines. *Anticancer Res,* 13**,** 721-5.

SELIG, R. A., WHITE, L., GRAMACHO, C., STERLING-LEVIS, K., FRASER, I. W. & NAIDOO, D. 1998. Failure of iron chelators to reduce tumor growth in human neuroblastoma xenografts. *Cancer Res,* 58**,** 473-8.

SEMCHUK, K. M., LOVE, E. J. & LEE, R. G. 1992. Parkinson's disease and exposure to agricultural work and pesticide chemicals. *Neurology,* 42**,** 1328-35.

SENA, L. A. & CHANDEL, N. S. 2012. Physiological roles of mitochondrial reactive oxygen species. *Molecular cell,* 48**,** 158-167.

SHACHAR, D. B., KAHANA, N., KAMPEL, V., WARSHAWSKY, A. & YOUDIM, M. B. H. 2004. Neuroprotection by a novel brain permeable iron chelator, VK-28, against 6-hydroxydopamine lession in rats. *Neuropharmacology,* 46**,** 254-263.

SHARMA, P., JHA, A. B., DUBEY, R. S. & PESSARAKLI, M. 2012. Reactive Oxygen Species, Oxidative Damage, and Antioxidative Defense Mechanism in Plants under Stressful Conditions. *Journal of Botany,* 2012**,** 26.

SHEIKH, S., SAFIA, HAQUE, E. & MIR, S. S. 2013. Neurodegenerative Diseases: Multifactorial Conformational Diseases and Their Therapeutic Interventions. *Journal of Neurodegenerative Diseases,* 2013**,** 8.

SHERER, T. B., KIM, J. H., BETARBET, R. & GREENAMYRE, J. T. 2003. Subcutaneous rotenone exposure causes highly selective dopaminergic degeneration and alpha-synuclein aggregation. *Exp Neurol,* 179**,** 9-16.

SHETH, S. 2014. Iron chelation: an update. *Curr Opin Hematol,* 21**,** 179-85.

SHI, Z., LU, Z., ZHAO, Y., WANG, Y., ZHAO-WILSON, X., GUAN, P., DUAN, X., CHANG, Y. Z. & ZHAO, B. 2013. Neuroprotective effects of aqueous extracts of Uncaria tomentosa: Insights from 6-OHDA induced cell damage and transgenic Caenorhabditis elegans model. *Neurochem Int,* 62**,** 940-7.

SHUCHMAN, M. 2011. FDA panel recommends approval of deferiprone. *CMAJ,* 183**,** E1159-60.

SIAN, J., DEXTER, D. T., LEES, A. J., DANIEL, S., AGID, Y., JAVOY-AGID, F., JENNER, P. & MARSDEN, C. D. 1994. Alterations in glutathione levels in Parkinson's disease and other neurodegenerative disorders affecting basal ganglia. *Ann Neurol,* 36**,** 348-55.

SIDDIQUI, M. R., ALOTHMAN, Z. A. & RAHMAN, N. 2017. Analytical techniques in pharmaceutical analysis: A review. *Arabian Journal of Chemistry,* 10, Supplement 1**,** S1409-S1421.

SILVA, A. H., FONSECA, F. N., PIMENTA, A. T., LIMA, M. S., SILVEIRA, E. R., VIANA, G. S., VASCONCELOS, S. M. & LEAL, L. K. 2016. Pharmacognostical Analysis and Protective Effect of Standardized Extract and Rizonic Acid from Erythrina velutina against 6-Hydroxydopamine-Induced Neurotoxicity in SH-SY5Y Cells. *Pharmacogn Mag,* 12**,** 307-312.

SIMOLA, N., MORELLI, M. & CARTA, A. R. 2007. The 6-Hydroxydopamine model of parkinson's disease. *Neurotoxicity Research,* 11**,** 151-167.

SINGH, S., CHOUDHURY, R., EPEMOLU, R. O. & HIDER, R. C. 1996. Metabolism and pharmacokinetics of 1-(2'-hydroxy-ethyl)- and 1-(3'-hydroxypropyl)-2-ethyl-3-hydroxypyridin-4-ones in the rat. *Eur J Drug Metab Pharmacokinet,* 21**,** 33-41.

SINGH, S., EPEMOLU, R. O., DOBBIN, P. S., TILBROOK, G. S., ELLIS, B. L., DAMANI, L. A. & HIDER, R. C. 1992. Urinary metabolic profiles in human and rat of 1,2-dimethyl- and 1,2-diethyl-substituted 3-hydroxypyridin-4-ones. *Drug Metabolism and Disposition,* 20**,** 256-261.

SKIBINSKI, G. & FINKBEINER, S. 2011. Drug discovery in Parkinson's disease-Update and developments in the use of cellular models. *Int J High Throughput Screen,* 2011**,** 15-25.

SMITH, D. A., DI, L. & KERNS, E. H. 2010. The effect of plasma protein binding on in vivo efficacy: misconceptions in drug discovery. *Nat Rev Drug Discov,* 9**,** 929-39.

SMITH, D., ARTURSSON, P., AVDEEF, A., DI, L., ECKER, G. F., FALLER, B., HOUSTON, J. B., KANSY, M., KERNS, E. H., KRAMER, S. D., LENNERNAS, H., VAN DE WATERBEEMD, H., SUGANO, K. & TESTA, B. 2014. Passive Lipoidal Diffusion and Carrier-Mediated Cell Uptake Are Both Important Mechanisms of Membrane Permeation in Drug Disposition. *Molecular Pharmaceutics,* 11**,** 1727-1738.

SMITH, M. P. & CASS, W. A. 2007. Oxidative stress and dopamine depletion in an intrastriatal 6-hydroxydopamine model of Parkinson's disease. *Neuroscience,* 144**,** 1057-1066.

SMITH, Q. R. & ALLEN, D. D. 2003. *In Situ* Brain Perfusion Technique. *In:* NAG, S. (ed.) *The Blood Brain Barrier: Biology and Research Protocols.* Totowa, NJ: Humana Press Inc.

SMITH, Q. R. 2000. Transport of glutamate and other amino acids at the blood-brain barrier. *J Nutr,* 130**,** 1016S-22S.

SMITH, Q. R. 2003. A Review of Blood-Brain Barrier Transport Techniques. *In:* NAG, S. (ed.) *The Blood-Brain Barrier: Biology and Research Protocols.* Totowa, NJ: Humana Press Inc.

SNYDER, H., MENSAH, K., THEISLER, C., LEE, J., MATOUSCHEK, A. & WOLOZIN, B. 2003. Aggregated and monomeric alpha-synuclein bind to the S6' proteasomal protein and inhibit proteasomal function. *J Biol Chem,* 278**,** 11753-9.

SOFIC, E., LANGE, K. W., JELLINGER, K. & RIEDERER, P. 1992. Reduced and oxidized glutathione in the substantia nigra of patients with Parkinson's disease. *Neurosci Lett,* 142**,** 128-30.

SOFIC, E., RIEDERER, P., HEINSEN, H., BECKMANN, H., REYNOLDS, G. P., HEBENSTREIT, G. & YOUDIM, M. B. 1988. Increased iron (III) and total iron content in post mortem substantia nigra of parkinsonian brain. *J Neural Transm,* 74**,** 199-205.

SOFRONIEW, M. V. 2015. Astrocyte barriers to neurotoxic inflammation. *Nat Rev Neurosci,* 16**,** 249-263.

SOMOGYI, M. 1948. Studies of arteriovenous differences in blood sugar; effect of alimentary hyperglycemia on the rate of extrahepatic glucose assimilation. *J Biol Chem,* 174**,** 189-200.

SOTO-OTERO, R., MENDEZ-ALVAREZ, E., HERMIDA-AMEIJEIRAS, A., MUNOZ-PATINO, A. M. & LABANDEIRA-GARCIA, J. L. 2000. Autoxidation and neurotoxicity of 6-hydroxydopamine in the presence of some antioxidants: potential implication in relation to the pathogenesis of Parkinson's disease. *J Neurochem,* 74**,** 1605-12.

SPINO, M., CONNELLY, J., TSANG, Y.-C., FRADETTE, C. & TRICTA, F. 2015. Deferiprone Pharmacokinetics with and without Iron Overload and in Special Patient Populations. *Blood,* 126**,** 3365-3365.

SRINIVASAN, B., KOLLI, A. R., ESCH, M. B., ABACI, H. E., SHULER, M. L. & HICKMAN, J. J. 2015. TEER measurement techniques for in vitro barrier model systems. *Journal of laboratory automation,* 20**,** 107-126.

STOICA, B. A. & FADEN, A. I. 2010. Cell death mechanisms and modulation in traumatic brain injury. *Neurotherapeutics,* 7**,** 3-12.

STORCH, A., KAFTAN, A., BURKHARDT, K. & SCHWARZ, J. 2000. 6-Hydroxydopamine toxicity towards human SH-SY5Y dopaminergic neuroblastoma cells: independent of mitochondrial energy metabolism. *J Neural Transm (Vienna),* 107**,** 281-93.

STORCH, A., LUDOLPH, A. C. & SCHWARZ, J. 2004. Dopamine transporter: involvement in selective dopaminergic neurotoxicity and degeneration. *J Neural Transm (Vienna),* 111**,** 1267-86.

SUBRAMANIAN, R. K., SIDHARTHAN, A., MANEKSH, D., RAMALINGAM, L., MANICKAM, A. S., KANTHAKUMAR, P. & SUBRAMANI, S. 2013. Normative data for arterial blood gas and electrolytes in anesthetized rats. *Indian J Pharmacol,* 45**,** 103-4.

SUGANO, K., KANSY, M., ARTURSSON, P., AVDEEF, A., BENDELS, S., DI, L., ECKER, G. F., FALLER, B., FISCHER, H., GEREBTZOFF, G., LENNERNAES, H. & SENNER, F. 2010. Coexistence of passive and carrier-mediated processes in drug transport. *Nature Reviews Drug Discovery,* 9**,** 597-614.

SULLIVAN, P. G., DRAGICEVIC, N. B., DENG, J. H., BAI, Y., DIMAYUGA, E., DING, Q., CHEN, Q., BRUCE-KELLER, A. J. & KELLER, J. N. 2004. Proteasome inhibition alters neural mitochondrial homeostasis and mitochondria turnover. *J Biol Chem,* 279**,** 20699-707.

SUMMERFIELD, S., READ, K., BEGLEY, D., OBRADOVIC, T., HIDALGO, I., COGGON, S., LEWIS, A., PORTER, R. & JEFFREY, P. 2007. Central nervous system drug disposition: the relationship between in situ brain permeability and brain free fraction. *Journal of Pharmacology and Experimental Therapeutics,* 322**,** 205-213.

SWIETACH, P., TIFFERT, T., MAURITZ, J. M., SEEAR, R., ESPOSITO, A., KAMINSKI, C. F., LEW, V. L. & VAUGHAN-JONES, R. D. 2010. Hydrogen ion dynamics in human red blood cells. *J Physiol,* 588**,** 4995-5014.

SYVANEN, S., LINDHE, O., PALNER, M., KORNUM, B. R., RAHMAN, O., LANGSTROM, B., KNUDSEN, G. M. & HAMMARLUND-UDENAES, M. 2009. Species differences in blood-brain barrier transport of three positron emission tomography radioligands with emphasis on P-glycoprotein transport. Drug Metab Dispos, 37, 635-43.

TABANOR, K., LEE, P., KIPTOO, P., CHOI, I.-Y., SHERRY, E. B., EAGLE, C. S., WILLIAMS, T. D. & SIAHAAN, T. J. 2016. Brain Delivery of Drug and MRI Contrast Agent: Detection and Quantitative Determination of Brain Deposition of CPT-Glu Using LC–MS/MS and Gd-DTPA Using Magnetic Resonance Imaging. *Molecular Pharmaceutics,* 13**,** 379-390.

TAGLIAFERRO, P. & BURKE, R. E. 2016. Retrograde Axonal Degeneration in Parkinson Disease. *Journal of Parkinson's Disease,* 6**,** 1-15.

TAKAI, N., NAKANISHI, H., TANABE, K., NISHIOKU, T., SUGIYAMA, T., FUJIWARA, M. & YAMAMOTO, K. 1998. Involvement of caspase-like proteinases in apoptosis of neuronal PC12 cells and primary cultured microglia induced by 6-hydroxydopamine. *J Neurosci Res,* 54**,** 214-22.

TAKAKURA, A. C., DOS SANTOS MOREIRA, T., DE LUCA, L. A., JR., RENZI, A. & MENANI, J. V. 2003. Central alpha(2) adrenergic receptors and cholinergic-induced salivation in rats. *Brain Res Bull,* 59**,** 383-6.

TAKASATO, Y., RAPOPORT, S. & SMITH, Q. 1984. An in situ brain perfusion technique to study cerebrovascular transport in the rat. *American Journal of Physiology,* 247**,** H484-H493.

TAM, T. F., LEUNG-TOUNG, R., WANG, Y. & ZHAO, Y. 2014. Fluorinated derivatives of deferiprone. Google Patents.

TAMAI, I. & TSUJI, A. 2000. Transporter-mediated permeation of drugs across the blood-brain barrier. *J Pharm Sci,* 89**,** 1371-88.

TATTON, N. A. & KISH, S. J. 1997. In situ detection of apoptotic nuclei in the substantia nigra compacta of 1-methyl-4-phenyl-1,2,3,6-tetrahydropyridine-treated mice using terminal deoxynucleotidyl transferase labelling and acridine orange staining. *Neuroscience,* 77**,** 1037-48.

TATTON, N. A. 2000. Increased caspase 3 and Bax immunoreactivity accompany nuclear GAPDH translocation and neuronal apoptosis in Parkinson's disease. *Exp Neurol,* 166**,** 29-43.

TATTON, N. A., MACLEAN-FRASER, A., TATTON, W. G., PERL, D. P. & OLANOW, C. W. 1998. A fluorescent double-labeling method to detect and confirm apoptotic nuclei in Parkinson's disease. *Ann Neurol,* 44**,** S142-8.

TEISMANN, P. & SCHULZ, J. B. 2004. Cellular pathology of Parkinson's disease: astrocytes, microglia and inflammation. *Cell Tissue Res,* 318**,** 149-61.

THUMA, P. E., OLIVIERI, N. F., MABEZA, G. F., BIEMBA, G., PARRY, D., ZULU, S., FASSOS, F. F., MCCLELLAND, R. A., KOREN, G., BRITTENHAM, G. M. & GORDEUK, V. R. 1998. Assessment of the effect of the oral iron chelator deferiprone on asymptomatic Plasmodium falciparum parasitemia in humans. *Am J Trop Med Hyg,* 58**,** 358-64.

TIETZ, S. & ENGELHARDT, B. 2015. Brain barriers: Crosstalk between complex tight junctions and adherens junctions. *J Cell Biol,* 209**,** 493-506.

TIEU, K. 2011. A Guide to Neurotoxic Animal Models of Parkinson's Disease. *Cold Spring Harbor Perspectives in Medicine:,* 1**,** a009316.

TIMOSHNIKOV, V. A., KOBZEVA, T. V., POLYAKOV, N. E. & KONTOGHIORGHES, G. J. 2015. Inhibition of Fe2+- and Fe3+- induced hydroxyl radical production by the iron-chelating drug deferiprone. *Free Radical Biology and Medicine,* 78**,** 118-122.

TOSATTO, L., ANDRIGHETTI, A. O., PLOTEGHER, N., ANTONINI, V., TESSARI, I., RICCI, L., BUBACCO, L. & DALLA SERRA, M. 2012. Alpha-synuclein pore forming activity upon membrane association. *Biochimica et Biophysica Acta (BBA) - Biomembranes,* 1818**,** 2876-2883.

TÓTH, M., HÄGGKVIST, J., VARRONE, A., FINNEMA, S. J., DOORDUIN, J., TOKUNAGA, M., HIGUCHI, M., GULYÁS, B. & HALLDIN, C. 2014. ABC transporter-dependent brain uptake of the 5-HT1B receptor radioligand [(11)C]AZ10419369: a comparative PET study in mouse, rat, and guinea pig. *EJNMMI research,* 4**,** 64.

TRICTA, F., UETRECHT, J., GALANELLO, R., CONNELLY, J., ROZOVA, A., SPINO, M. & PALMBLAD, J. 2016. Deferiprone-induced agranulocytosis: 20 years of clinical observations. *American Journal of Hematology,* 91**,** 1026-1031.

TRIGUERO, D., BUCIAK, J. & PARDRIDGE, W. 1990. Capillary depletion method for quantification of blood-brain barrier transport of circulating peptides and plasma proteins. *Journal of Neurochemistry,* 54**,** 1882-1888.

TRIMBLE, W. S. & GRINSTEIN, S. 2015. Barriers to the free diffusion of proteins and lipids in the plasma membrane. *J Cell Biol,* 208**,** 259-71.

TSINMAN, O., TSINMAN, K., SUN, N. & AVDEEF, A. 2011. Physicochemical selectivity of the BBB microenvironment governing passive diffusion--matching with a porcine brain lipid extract artificial membrane permeability model. *Pharm Res,* 28**,** 337-63.

TSUJIMOTO, Y. 1997. Apoptosis and necrosis: intracellular ATP level as a determinant for cell death modes. *Cell Death Differ,* 4**,** 429-34.

TURNER, A., RADBURN-SMITH, K., MUSHTAQ, A. & TAN, L. 2011. Storage and Handling Guidelines for Custom Peptides. *Current Protocols in Protein Science.* John Wiley & Sons, Inc.

TURRENS, J. F. 2003. Mitochondrial formation of reactive oxygen species. *J Physiol,* 552**,** 335-44.

U.S.-F.D.A. 2001. Guidance for Industry: Bioanalytical Method Validation. *In:* DEPARTMENT OF HEALTH AND HUMAN SERVICES, C. F. D. E. A. R. C., CENTER OF VETERINARY MEDICINE (CVM) (ed.).

UPADHYAY, R. K. 2014. Transendothelial Transport and Its Role in Therapeutics. *Int Sch Res Notices,* 2014**,** 309404.

URRUTIA, P. J., MENA, N. P. & NÚÑEZ, M. T. 2014. The interplay between iron accumulation, mitochondrial dysfunction, and inflammation during the execution step of neurodegenerative disorders. *Frontiers in Pharmacology,* 5**,** 38.

URRUTIA, P., AGUIRRE, P., ESPARZA, A., TAPIA, V., MENA, N. P., ARREDONDO, M., GONZALEZ-BILLAULT, C. & NUNEZ, M. T. 2013. Inflammation alters the expression of DMT1, FPN1 and hepcidin, and it causes iron accumulation in central nervous system cells. J Neurochem, 126, 541-9.

VAN DER BRUG, M. P., SINGLETON, A., GASSER, T. & LEWIS, P. A. 2015. Parkinson's disease: From human genetics to clinical trials. *Sci Transl Med,* 7**,** 205ps20.

VAN MEERLOO, J., KASPERS, G. J. & CLOOS, J. 2011. Cell sensitivity assays: the MTT assay. *Methods Mol Biol,* 731**,** 237-45.

VILA, M., JACKSON-LEWIS, V., VUKOSAVIC, S., DJALDETTI, R., LIBERATORE, G., OFFEN, D., KORSMEYER, S. J. & PRZEDBORSKI, S. 2001. Bax ablation prevents dopaminergic neurodegeneration in the 1-methyl- 4-phenyl-1,2,3,6-tetrahydropyridine mouse model of Parkinson's disease. *Proceedings of the National Academy of Sciences,* 98**,** 2837-2842.

VILLA, M., MUÑOZ, P., AHUMADA-CASTRO, U., PARIS, I., JIMÉNEZ, A., MARTÍNEZ, I., SEVILLA, F. & SEGURA-AGUILAR, J. 2013. One-Electron Reduction of 6-Hydroxydopamine Quinone is Essential in 6-Hydroxydopamine Neurotoxicity. *Neurotoxicity Research,* 24**,** 94-101.

VIREL, A., FAERGEMANN, E., ORADD, G. & STROMBERG, I. 2014a. Magnetic resonance imaging (MRI) to study striatal iron accumulation in a rat model of Parkinson's disease. *PLoS One,* 9**,** e112941.

VISANJI, N. P., BROOKS, P. L., HAZRATI, L.-N. & LANG, A. E. 2013. The prion hypothesis in Parkinson's disease: Braak to the future. *Acta Neuropathologica Communications,* 1**,** 2-2.

VISWANATH, V., WU, Y., BOONPLUEANG, R., CHEN, S., STEVENSON, F. F., YANTIRI, F., YANG, L., BEAL, M. F. & ANDERSEN, J. K. 2001. Caspase-9 activation results in downstream caspase-8 activation and bid cleavage in 1-methyl-4-phenyl-1,2,3,6-tetrahydropyridine-induced Parkinson's disease. *J Neurosci,* 21**,** 9519-28.

WAHEED, N., ALI, S. & BUTT, M. A. 2014. Comparison of deferiprone and deferrioxamine for the treatment of transfusional iron overload in children with beta thalassemia major. *J Ayub Med Coll Abbottabad,* 26**,** 297-300.

WAKABAYASHI, K., MORI, F. & TAKAHASHI, H. 2006. Progression patterns of neuronal loss and Lewy body pathology in the substantia nigra in Parkinson's disease. *Parkinsonism & Related Disorders,* 12**,** S92-S98.

WAKABAYASHI, K., TANJI, K., ODAGIRI, S., MIKI, Y., MORI, F. & TAKAHASHI, H. 2013. The Lewy body in Parkinson's disease and related neurodegenerative disorders. *Mol Neurobiol,* 47**,** 495-508.

WALDMEIER, P. C., BUCHLE, A. M. & STEULET, A. F. 1993. Inhibition of catechol-O-methyltransferase (COMT) as well as tyrosine and tryptophan hydroxylase by the orally active iron chelator, 1,2-dimethyl-3-hydroxypyridin-4-one (L1, CP20), in rat brain in vivo. *Biochem Pharmacol,* 45**,** 2417-24.

WALKER, M. D., DINELLE, K., KORNELSEN, R., LEE, A., FARRER, M. J., STOESSL, A. J. & SOSSI, V. 2013. Measuring dopaminergic function in the 6-OHDA-lesioned rat: a comparison of PET and microdialysis. *EJNMMI Res,* 3**,** 69.

WALKINSHAW, G. & WATERS, C. M. 1994. Neurotoxin-induced cell death in neuronal PC12 cells is mediated by induction of apoptosis. *Neuroscience,* 63**,** 975-87.

WALL, NICHOLAS R., DE LA PARRA, M., CALLAWAY, EDWARD M. & KREITZER, ANATOL C. 2013. Differential Innervation of Direct- and Indirect-Pathway Striatal Projection Neurons. *Neuron,* 79**,** 347-360.

WAN, H., REHNGREN, M., GIORDANETTO, F., BERGSTROM, F. & TUNEK, A. 2007. High-throughput screening of drug-brain tissue binding and in silico prediction for assessment of central nervous system drug delivery. *J Med Chem,* 50**,** 4606-15.

WAN, W., JIN, L., WANG, Z., WANG, L., FEI, G., YE, F., PAN, X., WANG, C. & ZHONG, C. 2017. Iron Deposition Leads to Neuronal α-Synuclein Pathology by Inducing Autophagy Dysfunction. *Frontiers in Neurology,* 8**,** 1.

WANG, J. & MALDONADO, M. A. 2006. The ubiquitin-proteasome system and its role in inflammatory and autoimmune diseases. *Cell Mol Immunol,* 3**,** 255-61.

WANG, J., BI, M. & XIE, J. 2015. Ceruloplasmin is Involved in the Nigral Iron Accumulation of 6-OHDA-Lesioned Rats. *Cell Mol Neurobiol,* 35**,** 661-8.

WANG, J., FILLEBEEN, C., CHEN, G., BIEDERBICK, A., LILL, R. & PANTOPOULOS, K. 2007. Iron-Dependent Degradation of Apo-IRP1 by the Ubiquitin-Proteasome Pathway. *Molecular and Cellular Biology,* 27**,** 2423-2430.

WANG, J., JIANG, H. & XIE, J. X. 2004. Time dependent effects of 6-OHDA lesions on iron level and neuronal loss in rat nigrostriatal system. *Neurochem Res,* 29**,** 2239-43.

WANG, J.-Y., ZHUANG, Q.-Q., ZHU, L.-B., ZHU, H., LI, T., LI, R., CHEN, S.-F., HUANG, C.-P., ZHANG, X. & ZHU, J.-H. 2016a. Meta-analysis of brain iron levels of Parkinson's disease patients determined by postmortem and MRI measurements. *Scientific Reports,* 6**,** 36669.

WANG, L., XU, S., XU, X. & CHAN, P. 2009. (-)-Epigallocatechin-3-Gallate protects SH-SY5Y cells against 6-OHDA-induced cell death through STAT3 activation. J Alzheimers Dis, 17, 295-304.

WANG, W., SHI, L., XIE, Y., MA, C., LI, W., SU, X., HUANG, S., CHEN, R., ZHU, Z., MAO, Z., HAN, Y. & LI, M. 2004. SP600125, a new JNK inhibitor, protects dopaminergic neurons in the MPTP model of Parkinson's disease. *Neurosci Res,* 48**,** 195-202.

WANG, Y. I., ABACI, H. E. & SHULER, M. L. 2017. Microfluidic blood-brain barrier model provides in vivo-like barrier properties for drug permeability screening. *Biotechnol Bioeng,* 114**,** 184-194.

WANG, Z., LUO, X.-G. & GAO, C. 2016b. Utility of susceptibility-weighted imaging in Parkinson's disease and atypical Parkinsonian disorders. *Translational Neurodegeneration,* 5**,** 17.

WARD, R. J., COLIVICCHI, M. A., ALLEN, R., SCHOL, F., LALLEMAND, F., DE WITTE, P., BALLINI, C., CORTE, L. D. & DEXTER, D. 2009. Neuro-inflammation induced in the hippocampus of 'binge drinking' rats may be mediated by elevated extracellular glutamate content. *J Neurochem,* 111**,** 1119-28.

WARNER, T. T. & SCHAPIRA, A. H. 2003. Genetic and environmental factors in the cause of Parkinson's disease. *Ann Neurol,* 53 Suppl 3**,** S16-23; discussion S23-5.

WEBER, J. T. 2015. Methodologies and limitations in the analysis of potential neuroprotective compounds derived from natural products. *New Horizons in Translational Medicine,* 2**,** 81-85.

WEISS, H. M., FRESNEAU, M., CAMENISCH, G. P., KRETZ, O. & GROSS, G. 2006. In vitro blood distribution and plasma protein binding of the iron chelator deferasirox (ICL670) and its iron complex Fe-[ICL670]2 for rat, marmoset, rabbit, mouse, dog, and human. *Drug Metab Dispos,* 34**,** 971-5.

WEST, G. J., UKI, J., HERSCHMAN, H. R. & SEEGER, R. C. 1977. Adrenergic, cholinergic, and inactive human neuroblastoma cell lines with the action-potential Na+ ionophore. *Cancer Res,* 37**,** 1372-6.

WEYNE, J., PANNIER, J. L., DEMEESTER, G. & LEUSEN, I. 1970. Bicarbonate and chloride of rat brain during infusion-induced changes in bicarbonate concentration of blood. *Pflugers Arch,* 320**,** 45-63.

WILLIAMS, S. K., GILLIS, J. F., MATTHEWS, M. A., WAGNER, R. C. & BITENSKY, M. W. 1980. Isolation and characterization of brain endothelial cells: morphology and enzyme activity. *J Neurochem,* 35**,** 374-81.

WINDBERGER, U., BARTHOLOVITSCH, A., PLASENZOTTI, R., KORAK, K. J. & HEINZE, G. 2003. Whole blood viscosity, plasma viscosity and erythrocyte aggregation in nine mammalian species: reference values and comparison of data. *Exp Physiol,* 88**,** 431-40.

WONG, A., YE, M., LEVY, A., ROTHSTEIN, J., BERGLES, D. & SEARSON, P. 2013. The blood-brain barrier: an engineering perspective. *Frontiers in Neuroengineering,* 6.

WOOD, J. C., KANG, B. P., THOMPSON, A., GIARDINA, P., HARMATZ, P., GLYNOS, T., PALEY, C. & COATES, T. D. 2010. The effect of deferasirox on cardiac iron in thalassemia major: impact of total body iron stores. *Blood,* 116**,** 537-43.

WORKMAN, D. G., TSATSANIS, A., LEWIS, F. W., BOYLE, J. P., MOUSADOUST, M., HETTIARACHCHI, N. T., HUNTER, M., PEERS, C. S., TETARD, D. & DUCE, J. A. 2015. Protection from neurodegeneration in the 6-hydroxydopamine (6-OHDA) model of Parkinson's with novel 1-hydroxypyridin-2-one metal chelators. *Metallomics,* 7**,** 867-76.

WU, D. C., JACKSON-LEWIS, V., VILA, M., TIEU, K., TEISMANN, P., VADSETH, C., CHOI, D. K., ISCHIROPOULOS, H. & PRZEDBORSKI, S. 2002. Blockade of microglial activation is neuroprotective in the 1-methyl-4-phenyl-1,2,3,6-tetrahydropyridine mouse model of Parkinson disease. *J Neurosci,* 22**,** 1763-71.

WU, X., CHEN, P. S., DALLAS, S., WILSON, B., BLOCK, M. L., WANG, C.-C., KINYAMU, H., LU, N., GAO, X., LENG, Y., CHUANG, D.-M., ZHANG, W., LU, R. B. & HONG, J.-S. 2008. Histone deacetylase inhibitors up-regulate astrocyte GDNF and BDNF gene transcription and protect dopaminergic neurons. *The international journal of neuropsychopharmacology / official scientific journal of the Collegium Internationale Neuropsychopharmacologicum (CINP),* 11**,** 1123-1134.

XICOY, H., WIERINGA, B. & MARTENS, G. J. M. 2017. The SH-SY5Y cell line in Parkinson's disease research: a systematic review. *Molecular Neurodegeneration,* 12**,** 10.

XIE, H. R., HU, L. S. & LI, G. Y. 2010a. SH-SY5Y human neuroblastoma cell line: in vitro cell model of dopaminergic neurons in Parkinson's disease. *Chin Med J (Engl),* 123**,** 1086-92.

XIE, W., LI, X., LI, C., ZHU, W., JANKOVIC, J. & LE, W. 2010b. Proteasome inhibition modeling nigral neuron degeneration in Parkinson's disease. *J Neurochem,* 115**,** 188-99.

XU, H.-D., WU, D., GU, J.-H., GE, J.-B., WU, J.-C., HAN, R., LIANG, Z.-Q. & QIN, Z.-H. 2013. The Pro-Survival Role of Autophagy Depends on Bcl-2 Under Nutrition Stress Conditions. *PLOS ONE,* 8**,** e63232.

XU, Q., KANTHASAMY, A. G., JIN, H. & REDDY, M. B. 2016. Hepcidin Plays a Key Role in 6-OHDA Induced Iron Overload and Apoptotic Cell Death in a Cell Culture Model of Parkinson's Disease. *Parkinsons Dis,* 2016**,** 8684130.

YAMADA, T., HASHIDA, K., TAKARADA-IEMATA, M., MATSUGO, S. & HORI, O. 2011. alpha-Lipoic acid (LA) enantiomers protect SH-SY5Y cells against glutathione depletion. *Neurochem Int,* 59**,** 1003-9.

YANG, L., MATTHEWS, R. T., SCHULZ, J. B., KLOCKGETHER, T., LIAO, A. W., MARTINOU, J. C., PENNEY, J. B., JR., HYMAN, B. T. & BEAL, M. F. 1998. 1-Methyl-4-phenyl-1,2,3,6-tetrahydropyride neurotoxicity is attenuated in mice overexpressing Bcl-2. *J Neurosci,* 18**,** 8145-52.

YAO, H., SADOSHIMA, S., OKADA, Y., IBAYASHI, S. & FUJISHIMA, M. 1990. Hindbrain ischemia produced by bilateral vertebral artery occlusion and moderate hypotension in spontaneously hypertensive rats. *Angiology,* 41**,** 848-54.

YASSIN, M. S., EKBLOM, J., XILINAS, M., GOTTFRIES, C. G. & ORELAND, L. 2000. Changes in uptake of vitamin B(12) and trace metals in brains of mice treated with clioquinol. *J Neurol Sci,* 173**,** 40-4.

YEON, J. A. & KIM, S. J. 2010. Neuroprotective Effect of Taurine against Oxidative Stress-Induced Damages in Neuronal Cells. *Biomolecules & Therapeutics,* 18**,** 24-31.

YLIKANGAS, H., MALMIOJA, K., PEURA, L., GYNTHER, M., NWACHUKWU, E. O., LEPPANEN, J., LAINE, K., RAUTIO, J., LAHTELA-KAKKONEN, M., HUTTUNEN, K. M. & POSO, A. 2014. Quantitative insight into the design of compounds recognized by the L-type amino acid transporter 1 (LAT1). *ChemMedChem,* 9**,** 2699-707.

YOU, L. H., LI, F., WANG, L., ZHAO, S. E., WANG, S. M., ZHANG, L. L., ZHANG, L. H., DUAN, X. L., YU, P. & CHANG, Y. Z. 2015. Brain iron accumulation exacerbates the pathogenesis of MPTP-induced Parkinson's disease. *Neuroscience,* 284**,** 234-246.

YOU, L. H., YAN, C. Z., ZHENG, B. J., CI, Y. Z., CHANG, S. Y., YU, P., GAO, G. F., LI, H. Y., DONG, T. Y. & CHANG, Y. Z. 2017. Astrocyte hepcidin is a key factor in LPS-induced neuronal apoptosis. Cell Death Dis, 8, e2676.

YOUDIM, M. B. H., GRÜNBLATT, E. & MANDEL, S. 1999. The Pivotal Role of Iron in NF-κB Activation and Nigrostriatal Dopaminergic Neurodegeneration: Prospects for Neuroprotection in Parkinson's Disease with Iron Chelators. *Annals of the New York Academy of Sciences,* 890**,** 7-25.

YOUDIM, M. B., FRIDKIN, M. & ZHENG, H. 2005. Bifunctional drug derivatives of MAO-B inhibitor rasagiline and iron chelator VK-28 as a more effective approach to treatment of brain ageing and ageing neurodegenerative diseases. *Mech Ageing Dev,* 126**,** 317-26.

YOUDIM, M. B., GASSEN, M., GROSS, A., MANDEL, S. & GRUNBLATT, E. 2000. Iron chelating, antioxidant and cytoprotective properties of dopamine receptor agonist; apomorphine. *J Neural Transm Suppl***,** 83-96.

YOUDIM, M. B., GRUNBLATT, E., LEVITES, Y., MAOR, G. & MANDEL, S. 2002. Early and late molecular events in neurodegeneration and neuroprotection in Parkinson's disease MPTP model as assessed by cDNA microarray; the role of iron. Neurotox Res, 4, 679-689.

ZAMARAEVA, M. V., SABIROV, R. Z., MAENO, E., ANDO-AKATSUKA, Y., BESSONOVA, S. V. & OKADA, Y. 2005. Cells die with increased cytosolic ATP during apoptosis: a bioluminescence study with intracellular luciferase. *Cell Death Differ,* 12**,** 1390-7.

ZECCA, L., TAMPELLINI, D., GERLACH, M., RIEDERER, P., FARIELLO, R. G. & SULZER, D. 2001. Substantia nigra neuromelanin: structure, synthesis, and molecular behaviour. *Molecular Pathology,* 54**,** 414-418.

ZECCA, L., YOUDIM, M. B. H., RIEDERER, P., CONNOR, J. R. & CRICHTON, R. R. 2004. Iron, brain ageing and neurodegenerative disorders. *Nat Rev Neurosci,* 5**,** 863-873.

ZENG, B. Y., BUKHATWA, S., HIKIMA, A., ROSE, S. & JENNER, P. 2006. Reproducible nigral cell loss after systemic proteasomal inhibitor administration to rats. *Ann Neurol,* 60**,** 248-52.

ZHANG, W., WANG, T., PEI, Z., MILLER, D. S., WU, X., BLOCK, M. L., WILSON, B., ZHANG, W., ZHOU, Y., HONG, J. S. & ZHANG, J. 2005. Aggregated alpha-synuclein activates microglia: a process leading to disease progression in Parkinson's disease. *Faseb j,* 19**,** 533-42.

ZHANG, X.-M., YIN, M. & ZHANG, M.-H. 2014. Cell-based assays for Parkinson's disease using differentiated human LUHMES cells. *Acta Pharmacol Sin,* 35**,** 945-956.

ZHANG, Y., HUO, M., ZHOU, J. & XIE, S. 2010. PKSolver: An add-in program for pharmacokinetic and pharmacodynamic data analysis in Microsoft Excel. *Comput Methods Programs Biomed,* 99**,** 306-14.

ZHANG, Z., ANDERSEN, A., SMITH, C., GRONDIN, R., GERHARDT, G. & GASH, D. 2000. Motor slowing and parkinsonian signs in aging rhesus monkeys mirror human aging. *J Gerontol A Biol Sci Med Sci,* 55**,** B473-80.

ZHENG, H., BLAT, D. & FRIDKIN, M. 2006. Novel neuroprotective neurotrophic NAP analogs targeting metal toxicity and oxidative stress: potential candidates for the control of neurodegenerative diseases. *J Neural Transm Suppl***,** 163-72.

ZHENG, H., GAL, S., WEINER, L. M., BAR-AM, O., WARSHAWSKY, A., FRIDKIN, M. & YOUDIM, M. B. 2005. Novel multifunctional neuroprotective iron chelator-monoamine oxidase inhibitor drugs for neurodegenerative diseases: in vitro studies on antioxidant activity, prevention of lipid peroxide formation and monoamine oxidase inhibition. *J Neurochem,* 95**,** 68-78.

ZHENG, P. P., ROMME, E., VAN DER SPEK, P. J., DIRVEN, C. M. F., WILLEMSEN, R. & KROS, J. M. 2010. Glut1/SLC2A1 Is Crucial for the Development of the Blood-Brain Barrier In Vivo. *Annals of Neurology,* 68**,** 835-844.

ZHOU, C., HUANG, Y., SHAO, Y., MAY, J., PROU, D., PERIER, C., DAUER, W., SCHON, E. A. & PRZEDBORSKI, S. 2008. The kinase domain of mitochondrial PINK1 faces the cytoplasm. *Proc Natl Acad Sci U S A,* 105**,** 12022-7.

ZHOU, F. M., LIANG, Y., SALAS, R., ZHANG, L., DE BIASI, M. & DANI, J. A. 2005. Corelease of dopamine and serotonin from striatal dopamine terminals. *Neuron,* 46**,** 65-74.

ZHOU, T., MA, Y., KONG, X. & HIDER, R. C. 2012. Design of iron chelators with therapeutic application. *Dalton Transactions,* 41**,** 6371-6389.

ZHU, W., XIE, W., PAN, T., XU, P., FRIDKIN, M., ZHENG, H., JANKOVIC, J., YOUDIM, M. B. & LE, W. 2007. Prevention and restoration of lactacystin-induced nigrostriatal dopamine neuron degeneration by novel brain-permeable iron chelators. *Faseb j,* 21**,** 3835-44.

ZHU, Y., WANG, B., TAO, K., YANG, H., WANG, Y., ZHOU, T., YANG, Y., YUAN, L., LIU, X. & DUAN, Y. 2017b. Iron accumulation and microglia activation contribute to substantia nigra hyperechogenicity in the 6-OHDA-induced rat model of Parkinson's disease. *Parkinsonism Relat Disord,* 36**,** 76-82.

ZHU, Y., WANG, B., TAO, K., YANG, H., WANG, Y., ZHOU, T., YANG, Y., YUAN, L., LIU, X. & DUAN, Y. 2017. Iron accumulation and microglia activation contribute to substantia nigra hyperechogenicity in the 6-OHDA-induced rat model of Parkinson's disease. *Parkinsonism Relat Disord,* 36**,** 76-82.

ZIGMOND, M. J., BERGER, T. W., GRACE, A. A. & STRICKER, E. M. 1989. Compensatory responses to nigrostriatal bundle injury. Studies with 6-hydroxydopamine in an animal model of parkinsonism. *Mol Chem Neuropathol,* 10**,** 185-200.

ZLOKOVIC, B. V. 2008. The blood-brain barrier in health and chronic neurodegenerative disorders. *Neuron,* 57**,** 178-201.

ZLOKOVIC, B. V., MACKIC, J. B., MCCOMB, J. G., WEISS, M. H., KAPLOWITZ, N. & KANNAN, R. 1994. Evidence for transcapillary transport of reduced glutathione in vascular perfused guinea-pig brain. *Biochem Biophys Res Commun,* 201**,** 402-8.

ZORZI, G., ZIBORDI, F., CHIAPPARINI, L., BERTINI, E., RUSSO, L., PIGA, A., LONGO, F., GARAVAGLIA, B., AQUINO, D., SAVOIARDO, M., SOLARI, A. & NARDOCCI, N. 2011. Iron-related MRI images in patients with pantothenate kinase-associated neurodegeneration (PKAN) treated with deferiprone: results of a phase II pilot trial. *Mov Disord,* 26**,** 1756-9.